University of Alberta

Accelerometer Configurations for Gyroscope-Free Inertial Navigation

by

Thomas Richard Williams 

A thesis submitted to the Faculty of Graduate Studies and Research in partial fulfillment of the requirements for the degree of **Doctor of Philosophy**.

Department of Mechanical Engineering

Edmonton, Alberta
Spring 2008

Your file Votre référence
ISBN: 978-0-494-45624-8
Our file Notre référence
ISBN: 978-0-494-45624-8

Abstract

The recent application of MEMs accelerometers in automobile airbag deployment systems has led to an increase in their quality and a decrease in cost. This has motivated researchers to consider these accelerometers for use in inexpensive motion sensing systems. This thesis is chiefly concerned with *Gyroscope-Free Inertial Navigation* (GFIN), which involves using configurations of accelerometers to determine the motion of the body to which they are attached.

The major contribution of the thesis is a thorough investigation of the geometrical requirements for accelerometer configurations that are to be used for GFIN. In the past, researchers have used many different types of configurations without showing how they arrived at a particular design or why it should be preferred over any other. Two special classes of configuration are studied in detail. The first is suitable for measuring planar motion, and the second is dignified in that it uses the smallest possible number of accelerometers for measuring spatial motion. General configurations are also studied, and some very interesting geometry is uncovered.

A secondary contribution of the thesis is less theoretical. The consequences of placing accelerometers without geometric precision are studied using simple error analysis and simulations. It is shown that even very small placement errors will likely lead to very poor performance, and consequently, that GFIN is only practical if additional, non-inertial measurements are available. Simulations indicate that a possible application of GFIN could be the robust tracking of the motion of parallel mechanisms.

Acknowledgements

Dr. Ken Fyfe - Thank-you for giving me the opportunity and the right mix of support and freedom to pursue research in an area that I find very interesting.

Dr. Don Raboud - Thank-you for your patience, insight and motivation in helping me to bring this thesis to fruition.

Jordana - Thank-you for your love and understanding, that has kept me almost entirely sane over the writing of this thesis.

My Parents - Thank-you for the support and the proof-reading. Without you, Mum, this thesis would be filled with split infinitives!

Creators of Free Software Everywhere - In particular, LaTeX, AUCTeX, Asymptote, GNU Octave, GNU Emacs and Gnuplot (the other Thomas Williams), and Linux in general.

Dr. Jochen Kuttler - Thank-you for confirming that I had indeed found a twisted cubic.

Table of Contents

List of Tables

List of Figures

Nomenclature

Geometry

$\mathbf{E}$	Three-dimensional Euclidean vector space.
$\mathbf{a}, \mathbf{b}, \ldots$	Vectors of $\mathbf{E}$.
$\mathscr{E}$	Three-dimensional affine point space, directed by $\mathbf{E}$.
$A, B, \ldots$	Points of $\mathscr{E}$.
$\langle A, B, C \rangle$	Affine subspace spanned by the points A, B and C.
$\langle \mathbf{a}, \mathbf{b}, \mathbf{c} \rangle$	Vector subspace spanned by the vectors $\mathbf{a}$, $\mathbf{b}$ and $\mathbf{c}$.
$\boldsymbol{a} \equiv \{\mathbf{a}_i\}_1^3$	Right-handed orthonormal basis of $\mathbf{E}$.
$[\boldsymbol{a}] \equiv \begin{bmatrix} \mathbf{a}_1 & \mathbf{a}_2 & \mathbf{a}_3 \end{bmatrix}^T$	3×1 matrix of the basis vectors of $\boldsymbol{a}$.
$[\mathbf{v}^{\boldsymbol{a}}]$	Component matrix of $\mathbf{v}$ in $\boldsymbol{a}$, i.e., $\mathbf{v} = [\boldsymbol{a}][\mathbf{v}^{\boldsymbol{a}}]$.
$[\boldsymbol{a}^{\boldsymbol{b}}]$	Basis matrix of $\boldsymbol{a}$ in $\boldsymbol{b}$, with i^{th} column $[\mathbf{a}_i^{\boldsymbol{b}}]$.
$\mathbf{a} \times \mathbf{b}$	Vector product.
$\mathbf{a} \cdot \mathbf{b}$	Scalar product.
$\mathcal{C}$	Affine frame with origin O_C, and basis, $\boldsymbol{c}$.
$\mathbf{r}_{B/A}$	Position vector of B relative to A.
$[\mathbf{r}_P^{\mathcal{C}}]$	Coordinate matrix of P in the frame, $\mathcal{C}$, $\mathbf{r}_{P/O_C} = [\boldsymbol{c}]^T[\mathbf{r}_P^{\mathcal{C}}]$.
$\text{skew}([\mathbf{v}^{\boldsymbol{a}}])$	3×3 skew-symmetric matrix such that $[\boldsymbol{a}]\text{skew}([\mathbf{v}^{\boldsymbol{a}}])[\mathbf{w}^{\boldsymbol{a}}] = \mathbf{v} \times \mathbf{w}$.
$\mathscr{L}(P, \mathbf{v})$	The line through the point, P, directed by the vector, $\mathbf{v}$.
$[\mathscr{L}(P, \mathbf{v})^{\mathcal{F}}]$	The Plücker coordinates of $\mathscr{L}(P, \mathbf{u})$ in the frame, $\mathcal{F}$.

Accelerometers

$\mathbf{s}_P$	The specific force vector at P.
$\mathsf{A}(P, \mathbf{u})$	An accelerometer at P directed by $\mathbf{u}$.
A_k	Equivalent to $\mathsf{A}(P_k, \mathbf{u}_k)$
$\langle\{\mathsf{A}_k\}_1^n\rangle$	Accelerometers generated by the set $\{\mathsf{A}_k\}_1^n$.
$\mathsf{a}(P, \mathbf{u})$	The measurement of $\mathsf{A}(P, \mathbf{u})$
a_k	The measurement of A_k
$[\mathbf{a}_n]$	The $n \times 1$ matrix of measurements of $\{\mathsf{A}_k\}_1^n$.
$\mathbf{g}$	Local gravity vector.
$[\mathsf{A}(P, \mathbf{u})^{\mathcal{B}}]$	The accelerometer description matrix, (ADM), of $\mathsf{A}(P, \mathbf{u})$ in the frame, $\mathcal{B}$.
$[\tilde{\mathsf{A}}(P, \mathbf{u})^{\mathcal{B}}]$	The alternative accelerometer description matrix, (ADM), of $\mathsf{A}(P, \mathbf{u})$ in the frame, $\mathcal{B}$.
$[\mathsf{C}_n^{\mathcal{B}}]$	The configuration matrix for the set $\{\mathsf{A}_k\}_1^n$ in $\mathcal{B}$.
$\langle\{\mathsf{A}_k\}_1^n\rangle$	The set of accelerometers generated by the set $\{\mathsf{A}_k\}_1^n$.
$\{D, d\}_n$	A constrained configuration of n accelerometers.

Acronyms

ADM	Accelerometer Description Matrix
AADM	Alternative Accelerometer Description Matrix
FCC	Full Constrained Configurations
GFIN	Gyroscope-Free Inertial Navigation
MEMs	Micro-electro-mechanical systems
KDE	Kinematic Differential Equations
SDIN	Strapdown Inertial Navigation
SFSM	Specific-Force State Matrix
MSFSM	Minimal Specific-Force State Matrix

Chapter 1

Introduction

While gyroscopic instruments had been used in maritime applications since around the turn of the 20^{th} Century and in aerospace applications since the 1930s, when accelerometers became available commercially [1], it was not until 1942 when these sensors were used together as components in an inertial navigation system (INS). This initial application was military; the $V2$ ballistic rocket developed by the Peennemünde group in Germany [2]. After World War II, military sponsored research into INS continued in the United States of America [3]. The first couple of decades of INS development focused on the use of a 'stable platform' in which a series of gimbals and the measurements of the gyroscopes are used to ensure that the orientation of accelerometers relative to inertial space is constant.

As computer and gyroscope technology advanced, another type of INS became realizable: *Strapdown Inertial Navigation* (SDIN). In SDIN, accelerometers and gyroscopes are 'strapped down' directly to the vehicle. The stable platform is replaced by adding burden to the navigation computer which integrates kinematic differential equations to find the current orientation of the vehicle and performs the required coordinate transformation calculations [4].

In 1967, a paper by Schuler et al. [5] heralded the beginning of another variant of INS, which has come to be called *Gyroscope Free Inertial Navigation* (GFIN). The abstract of the paper stated

> Inertial navigation systems usually use gyroscopes to sense angular motion and use accelerometers to sense linear acceleration. It is feasible, however, using only linear accelerometers as sensors, to determine both the angular velocity and the linear acceleration of a vehicle.

The paper presented a series of 5 accelerometer configurations that could be used for GFIN along with the associated equations relating the accelerometer measurements to the motion of the body to which they are attached. One of the configurations is illustrated in Fig 1.1. At the time of the paper's

publication, GFIN was essentially an academic curiosity. Over the following decades, however, researchers have written about and applied GFIN in many different situations. Interest grew in the early 1990s when the price of MEMs accelerometers of reasonable quality dropped considerably, due to their bulk manufacture for use in automobile air-bag deployment systems [1].

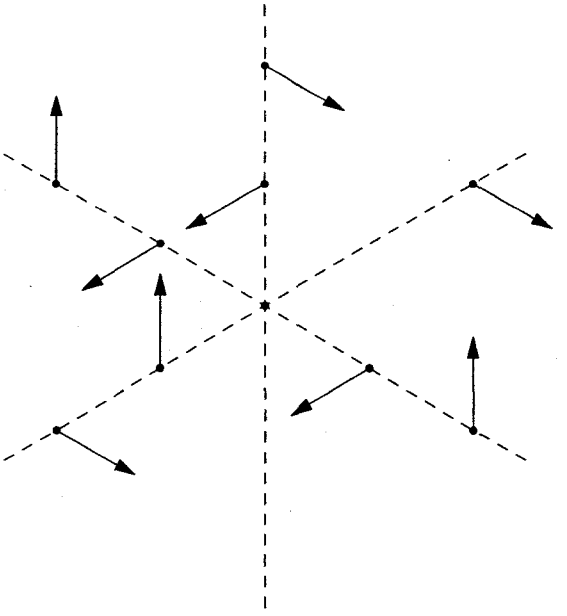

Figure 1.1: A 9-accelerometer configuration suggested by Schuler et al. [5]. Each arrow represents the location and sensitive direction of a single-axis accelerometer.

1.1 Two Major Themes in GFIN Research

Over the four decades since the introduction of the idea, two themes have been prevalent in the GFIN literature. The first of these is the number of different accelerometer configurations that have been proposed. It is generally accepted that 6 is the minimum number of accelerometers that can be used to determine the motion of a rigid body and various configurations have been presented using this minimum [6–9]. The literature also shows configurations using nine [10, 11], twelve [12–16], or even more accelerometers [17]. Even in the special case of planar motion, configurations ranging from three [18] to five [19, 20] accelerometers have been used. While most configurations designed for use in the case of general motion are, like that shown in Fig 1.1, based on a Cartesian coordinate system, there are some exceptions in which the accelerometers are located entirely in one plane [8, 21].

The wide range of proposed configurations is perhaps not surprising, given that the original paper on the topic presented 5 configurations itself. What is odd, however, is that there has been little theoretical work presented showing what geometrical conditions accelerometer configurations need to satisfy so that GFIN is possible. Further, some of the work that does exist is overly constrictive in the types of configurations that are considered [22], or is simply incorrect, because the mathematical reasoning employed is fallacious [23].

The second common feature in the presentation of GFIN research is, unfortunately, the poor results that have so far been obtained. In a paper introducing a six-accelerometer configuration that has proved to be popular, Chen et al. wrote [7]:

> The errors and error buildup rates are atrocious compared with the medium-accuracy gyro-based system.

The authors went on to state that the use of GFIN is only supported in applications with high angular rates or very short durations. These are, indeed, the characteristics of the motion in the applications where GFIN has been successful. Such applications include measuring the motion of an automobile crash-test dummy [11, 20, 24, 25], where the acceleration is very high and duration is only a few milliseconds. GFIN has also been successfully applied in human gait analysis [18, 19], using knowledge about the cyclical nature of the motion in the signal processing to prevent errors from accumulating. Aside from these two areas, in applications involving arbitrary motions for periods of more than a few seconds, GFIN yields very poor position and orientation estimates.

There are many reasons for the poor performance of GFIN compared to traditional SDIN. Some are specific to the configuration design that is employed. For example, in a general configuration of six accelerometers, a differential equation must be solved to find the angular velocity, and in some configuration designs this differential equation has been shown to be unstable [5, 26]. Numerical simulations have shown that a major contribution to error growth is *placement error*, i.e., the accelerometers of a configuration are not exactly where they are believed to be, or do not have exactly the intended direction [27, 28]. Placement errors can, in theory, be identified by calibration procedures in which known acceleration fields are generated by, for example, spinning the rigid body about a known axis at a known speed [29]. Once the placement errors are identified they can, again in theory, be compensated for [10, 30].

In a recent paper, Parsa et al. used numerical optimization to design an accelerometer configuration [31]. The performance index they chose was the condition number of the matrix relating the accelerometer measurements to the parameters describing the motion. Through minimizing the condition number

they theorized that the motion parameter estimates should be less sensitive to errors in the measurements. This paper is therefore associated with both themes discussed in this section, and, while interesting, shows that very fundamental questions regarding GFIN still need to be answered. Rather than having to resort to a numerical procedure to design a configuration with certain properties, it is desirable that the geometry of the problem be properly understood.

1.2 Thesis Outline

The main aim of this thesis is to obtain geometric results showing how accelerometer configurations should be designed so that GFIN is possible, and, further, how specific designs can lead to desirable properties. A secondary aim is to gain a more theoretical understanding of the propagation of errors due to accelerometer misplacement, and to show how GFIN can still be of use even in the face of such errors.

The majority of the thesis treats accelerometers as ideal geometric elements. Thus, in Chapter 2, the coordinates used to describe accelerometers are introduced, and their frame transformation rule is derived. This chapter also introduces the concepts of accelerometer dependence and generation; concepts that are used in the subsequent chapters. The basic GFIN algorithm is also described. It is shown that there are two GFIN paradigms, differentiated by the method by which angular velocity is determined from the accelerometer measurements. One uses a bare minimum of six accelerometers, and the other must use more, usually nine or twelve.

Chapter 3 is a thorough discussion of planar accelerometer configurations; configurations that are suitable for use when a body is undergoing planar motion. All configurations of dependent accelerometers are derived using algebra and geometry, so that a basic design strategy is obtained: it shows where accelerometers *cannot* be placed if the configuration is to be usable. Some investigation of the numerical properties of planar accelerometer configurations is also undertaken.

In Chapter 4, accelerometer generation and dependence is studied in the general case. Well known, but perhaps surprising, geometrical manifolds are involved in the statement of the results. It is shown, for instance, that if four accelerometers are located on a plane with coplanar directions, then there is a conic passing through the accelerometers, and a unique direction at each point of that conic, where another accelerometer cannot be placed if the five are to be independent.

The slightly esoteric results of Chapter 4 meet their foil in Chapter 5 where minimal accelerometer configurations, those using only six accelerometers to measure spatial motion, are studied. The geometrical requirements that must

be satisfied by the accelerometers are presented for the first time. A design procedure yielding minimal configurations with desirable properties is also presented. It is shown that a popular configuration, first presented by Chen et al. [7], can be obtained as a special case.

In Chapter 6, the world of geometric exactness is forgotten. The effect of accelerometer placement errors is analysed in the special case of planar motion. This is followed by supporting simulations using two configurations. Methods of determining and compensating for placement errors are discussed, and their efficacy is shown by simulation.

Chapter 7 presents a novel application of GFIN where the rapid growth of errors is not of great importance. The application is robust tracking of the motion of a Generalized Stewart-Gough Platform, (GSGP). The GSGP is a device capable of moving heavy loads with great precision [32]. The motion of the platform is controlled by altering the lengths of its six legs, and its position and orientation is generally determined using these lengths. Its kinematics are complicated by the fact that for a given set of six leg lengths, the platform may be in one of up to 40 assemblies. This is important not only when the platform is stationary, but also when its motion is being tracked using numerical methods, where divergence can occur. It is shown via simulations that GFIN can be used in conjunction with standard iterative methods to achieve promising results.

Chapter 8 summarizes the thesis, highlighting the important and novel aspects, and presents suggestions for future research.

Chapter 2

Accelerometers and Inertial Navigation

This chapter introduces basic theory on which the rest of the thesis depends. The concept of an ideal accelerometer is introduced in Section 2.1, and, in Section 2.2, its measurement is related to the 'acceleration state' of the body to which it is attached. This leads, in Section 2.3, to the definitions of *accelerometer independence*, and *generation* which are of prime importance in accelerometer configuration analysis and design. Some preliminary theory that is required in two subsequent chapters is introduced. Section 2.4 discusses how measurements obtained from an accelerometer configuration attached to a rigid body can be used to determine the motion of that body. The majority of the required algorithm is similar to that used in strapdown inertial navigation, which is therefore briefly reviewed.

2.1 Accelerometers

Consider a rigid frame[1], $\mathcal{B}$, and a particle, P, of mass, m, moving relative to an inertial frame, $\mathcal{F}$, as shown in Fig 2.1. The force required to act on P so that it is stationary relative to $\mathcal{B}$ is denoted by $m\mathbf{s}_P$, and $\mathbf{s}_P$ is referred to as the *specific force* [4]. Applying Newton's Second Law to the particle gives

$$m\,\mathbf{s}_P + m\,\mathbf{g} = m\,\mathbf{a}_P, \tag{2.1}$$

where $\mathbf{g}$ is the local gravity vector, and $\mathbf{a}_P$ is the acceleration of P as observed from $\mathcal{F}$. It follows that the specific force vector is related to the gravity and acceleration vectors by

$$\mathbf{s}_P = \mathbf{a}_P - \mathbf{g}. \tag{2.2}$$

[1]Refer to Appendix A for an explanation of the notation used for frames, bases, component matrices and coordinate matrices.

A consequence of this equation is that the specific force vectors at P and O_B, the origin of $\mathcal{B}$, can be related using the well known relationship between the acceleration vectors at two particles of a rigid body (see Kane and Levinson [33] for example):

$$\mathbf{s}_P = \mathbf{s}_{O_B} + \boldsymbol{\alpha} \times \mathbf{r}_{P/O_B} + \boldsymbol{\omega} \times (\boldsymbol{\omega} \times \mathbf{r}_{P/O_B}), \tag{2.3}$$

where $\boldsymbol{\omega}$ and $\boldsymbol{\alpha}$ are, respectively, the angular velocity and angular acceleration vectors of $\mathcal{B}$ as observed from $\mathcal{F}$.

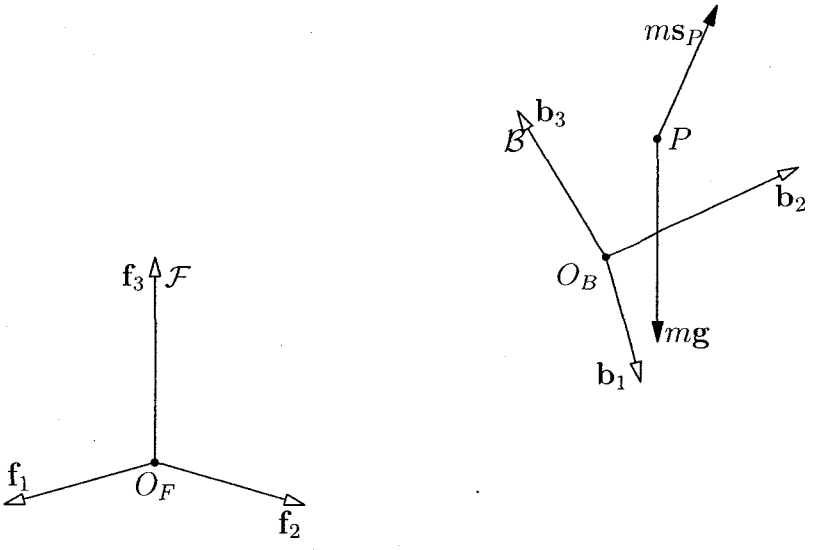

Figure 2.1: The force $m\mathbf{s}_P$ is that, other than the weight force, which must act on P so that it is stationary relative to the moving frame, $\mathcal{B}$.

Suppose now that the particle, P, is constrained in a frictionless guide so that it can move only in the direction of a unit vector, $\mathbf{u}$, described by the component matrix, $[\mathbf{u}^{\boldsymbol{b}}]$, that is constant in the moving basis, $\boldsymbol{b}$. Further, a transducer/actuator pair acts on the particle in the single direction of freedom, measuring and producing the force required to prevent motion of the particle relative to the guide. This is a highly idealized model of a *single-axis accelerometer*, $\mathsf{A}(P, \mathbf{u})$, a device that measures a component of the specific force at the particle, P, in the direction of the unit vector[2], $\mathbf{u}$. An approximate physical realization of the actuator/transducer pair preventing the motion of P comprises a spring-damper system to generate the force, and a means to measure the extension/compression of the spring. In MEMs accelerometers, a cantilevered silicon mass is prevented from deflecting by using a feedback

[2]More rigorous notation would employ the coordinate matrix of P in $\mathcal{B}$ and the component matrix of $\mathbf{u}$ in $\boldsymbol{b}$, since these are invariant, while the location of P and the direction of $\mathbf{u}$ vary as $\mathcal{B}$ moves through space.

system with capacitive sensing and actuation [4]. In the following, the word 'accelerometer' is regarded to mean 'single-axis accelerometer'.

Based upon the above description, the measurement, $\mathsf{a}(P, \mathbf{u})$, of the accelerometer, $\mathsf{A}(P, \mathbf{u})$, can be written in terms of component matrices[3] in the moving basis, $\boldsymbol{b}$, as

$$\mathsf{a}(P, \mathbf{u}) = [\mathbf{u}^{\boldsymbol{b}}]^T [\mathbf{s}_P^{\boldsymbol{b}}]. \tag{2.4}$$

Using Eq (2.3) to write the component matrix of $\mathbf{s}_P$ in terms of the component matrices of $\mathbf{s}_{O_B}$, $\boldsymbol{\omega}$, and $\boldsymbol{\alpha}$, and substituting into Eq (2.4) yields

$$\mathsf{a}(P, \mathbf{u}) = [\mathbf{u}^{\boldsymbol{b}}]^T [\mathbf{s}_{O_B}^{\boldsymbol{b}}] + [\mathbf{u}^{\boldsymbol{b}}]^T \mathrm{skew}([\boldsymbol{\alpha}^{\boldsymbol{b}}])[\mathbf{r}_P^{\mathcal{B}}] + [\mathbf{u}^{\boldsymbol{b}}]^T (\mathrm{skew}([\boldsymbol{\omega}^{\boldsymbol{b}}]))^2 [\mathbf{r}_P^{\mathcal{B}}]. \tag{2.5}$$

2.2 The Accelerometer Description Matrix

This section introduces a frame-specific matrix description of accelerometers and derives the relationship between the matrix description in two frames.

Equation (2.5) can be expanded and simplified as

$$\mathsf{a}(P, \mathbf{u}) = [\mathsf{A}(P, \mathbf{u})^{\mathcal{B}}][\mathbf{S}^{\mathcal{B}}], \tag{2.6}$$

where $[\mathsf{A}(P, \mathbf{u})^{\mathcal{B}}]$, referred to as the *Accelerometer Description Matrix*, (ADM) of $\mathsf{A}(P, \mathbf{u})$ in $\mathcal{B}$ is the following 1×12 matrix:

$$[\mathsf{A}(P, \mathbf{u})^{\mathcal{B}}] \stackrel{\text{def}}{=} [\mathbf{u}^{\boldsymbol{b}}]^T \left[[I]_3 \quad -\mathrm{skew}([\mathbf{r}_P^{\mathcal{B}}]) \quad \mathrm{sym}([\mathbf{r}_P^{\mathcal{B}}]) \quad -\mathrm{diag}([\mathbf{r}_P^{\mathcal{B}}]) \right], \tag{2.7}$$

with (letting $[\mathbf{v}]$ denote an arbitrary 3×1 matrix with i^{th} element v_i)

$$\mathrm{sym}([\mathbf{v}]) \stackrel{\text{def}}{=} \begin{bmatrix} 0 & v_3 & v_2 \\ v_3 & 0 & v_1 \\ v_2 & v_1 & 0 \end{bmatrix} \qquad \mathrm{diag}([\mathbf{v}]) \stackrel{\text{def}}{=} \begin{bmatrix} v_1 & 0 & 0 \\ 0 & v_2 & 0 \\ 0 & 0 & v_3 \end{bmatrix}, \tag{2.8}$$

and $[\mathbf{S}^{\mathcal{B}}]$, referred to as the *Specific-Force State Matrix*, (SFSM) is

$$[\mathbf{S}^{\mathcal{B}}] \stackrel{\text{def}}{=} \begin{bmatrix} [\mathbf{s}_{O_B}^{\boldsymbol{b}}] \\ [\boldsymbol{\alpha}^{\boldsymbol{b}}] \\ \mathrm{q}_{ij}([\boldsymbol{\omega}^{\boldsymbol{b}}]) \\ \mathrm{q}_{ii}([\boldsymbol{\omega}^{\boldsymbol{b}}]) \end{bmatrix}, \tag{2.9}$$

with

$$\mathrm{q}_{ij}([\mathbf{v}]) \stackrel{\text{def}}{=} \begin{bmatrix} v_2 v_3 \\ v_1 v_3 \\ v_1 v_2 \end{bmatrix} \qquad \mathrm{q}_{ii}([\mathbf{v}]) \stackrel{\text{def}}{=} \begin{bmatrix} v_2^2 + v_3^2 \\ v_1^2 + v_3^2 \\ v_1^2 + v_2^2 \end{bmatrix}. \tag{2.10}$$

Equations (2.6)–(2.10) make it clear that the measurement of an accelerometer depends

[3] See Appendix A for explanation of the notation.

- linearly upon the elements of $[\mathbf{s}^{\boldsymbol{b}}_{O_B}]$
- linearly upon the elements of $[\boldsymbol{\alpha}^{\boldsymbol{b}}]$
- quadratically upon the elements of $[\boldsymbol{\omega}^{\boldsymbol{b}}]$.

The coordinate transformation matrix that relates the ADM describing $\mathsf{A}(P, \mathbf{u})$ in two frames, $\mathcal{B}$ and $\mathcal{C}$, is presented here in two steps, as is shown schematically in Fig 2.2. First $[\mathsf{A}(P, \mathbf{u})^{\mathcal{B}}]$ is transformed, by a constant non-singular matrix, $[X]$, independent of the frame and the accelerometer, to another matrix, $[\tilde{\mathsf{A}}(P, \mathbf{u})^{\mathcal{B}}]$, with simpler structure. This latter matrix is used extensively in Chapter 4 and has a more straightforward coordinate transformation matrix.

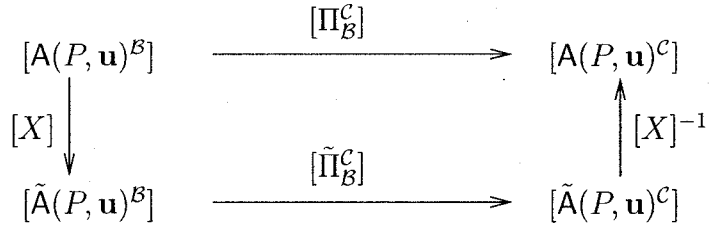

Figure 2.2: The frame transformation taking $[\mathsf{A}(P, \mathbf{u})^{\mathcal{B}}]$ to $[\mathsf{A}(P, \mathbf{u})^{\mathcal{C}}]$.

Using $r^{\mathcal{B}}_{P,i}$ to denote the i^{th} element of $[\mathbf{r}^{\mathcal{B}}_P]$, the 1×12 matrix

$$[\tilde{\mathsf{A}}(P, \mathbf{u})^{\mathcal{B}}] \stackrel{\text{def}}{=} \left[[\mathbf{u}^{\boldsymbol{b}}]^T \quad r^{\mathcal{B}}_{P,1}[\mathbf{u}^{\boldsymbol{b}}]^T \quad r^{\mathcal{B}}_{P,2}[\mathbf{u}^{\boldsymbol{b}}]^T \quad r^{\mathcal{B}}_{P,3}[\mathbf{u}^{\boldsymbol{b}}]^T \right], \tag{2.11}$$

is referred to as the *Alternative Accelerometer Description Matrix*, (AADM) of $\mathsf{A}(P, \mathbf{u})$ in $\mathcal{B}$. Using the Kronecker product (see Appendix C) the AADM can be written more compactly as

$$[\tilde{\mathsf{A}}(P, \mathbf{u})^{\mathcal{B}}] \stackrel{\text{def}}{=} \left[[\mathbf{u}^{\boldsymbol{b}}]^T \quad [\mathbf{r}^{\mathcal{B}}_P]^T \otimes [\mathbf{u}^{\boldsymbol{b}}]^T \right]. \tag{2.12}$$

The AADM and ADM of an accelerometer in the same frame are related by

$$[\mathsf{A}(P, \mathbf{u})^{\mathcal{B}}] = [\tilde{\mathsf{A}}(P, \mathbf{u})^{\mathcal{B}}][X] \tag{2.13}$$

where $[X]$ is a 12×12 matrix composed of three different numbers; 0, $+1$ and -1. The exact matrix is shown in Appendix B, and it is shown how the inverse, $[X]^{-1}$, can be expressed as the product of a diagonal matrix and $[X]^T$. The important point is that the inverse exists and that $[X]$ is independent of the frame in which the ADM and AADM are expressed.

With reference to Appendixes A and C and the definition of $[\tilde{\mathsf{A}}(P, \mathbf{u})^{\mathcal{B}}]$, it can be confirmed that

$$[\tilde{\mathsf{A}}(P, \mathbf{u})^{\mathcal{C}}] = [\tilde{\mathsf{A}}(P, \mathbf{u})^{\mathcal{B}}][\tilde{\Pi}^{\mathcal{C}}_{\mathcal{B}}], \tag{2.14}$$

where[4]

$$[\tilde{\Pi}^{\mathcal{C}}_{\mathcal{B}}] \stackrel{\text{def}}{=} \begin{bmatrix} [\boldsymbol{c}^{\boldsymbol{b}}] & [\mathbf{r}^{\mathcal{C}}_{O_{\mathcal{B}}}]^T \otimes [\boldsymbol{c}^{\boldsymbol{b}}] \\ [0]_{9\times 3} & [\boldsymbol{c}^{\boldsymbol{b}}] \otimes [\boldsymbol{c}^{\boldsymbol{b}}] \end{bmatrix}. \tag{2.15}$$

The determinant of this matrix can be evaluated by first exploiting its block structure:

$$\det[\tilde{\Pi}^{\mathcal{C}}_{\mathcal{B}}] = \det[\boldsymbol{c}^{\boldsymbol{b}}]\det([\boldsymbol{c}^{\boldsymbol{b}}] \otimes [\boldsymbol{c}^{\boldsymbol{b}}]),$$

and then using $\det[\boldsymbol{c}^{\boldsymbol{b}}] = 1$ and Eq (C.4), describing the determinant of a Kronecker product, to arrive at:

$$\det[\tilde{\Pi}^{\mathcal{C}}_{\mathcal{B}}] = \det([\boldsymbol{c}^{\boldsymbol{b}}])^7 = 1. \tag{2.16}$$

Referring to Fig 2.2 and Eqs (2.13) and (2.14) shows that the desired coordinate transformation rule is

$$[\mathsf{A}(P, \mathbf{u})^{\mathcal{C}}] = [\mathsf{A}(P, \mathbf{u})^{\mathcal{B}}][\Pi^{\mathcal{C}}_{\mathcal{B}}] \tag{2.17}$$

where

$$[\Pi^{\mathcal{C}}_{\mathcal{B}}] = [X]^{-1}[\tilde{\Pi}^{\mathcal{C}}_{\mathcal{B}}][X]. \tag{2.18}$$

The transformation matrix, $[\Pi^{\mathcal{C}}_{\mathcal{B}}]$, does not have a simple structure like $[\tilde{\Pi}^{\mathcal{C}}_{\mathcal{B}}]$, but, due to the form of Eq (2.19), it can be stated that, similar to the matrix from which it was derived:

$$\det[\Pi^{\mathcal{C}}_{\mathcal{B}}] = 1. \tag{2.19}$$

While $[\Pi^{\mathcal{C}}_{\mathcal{B}}]$ has a unit determinant, it is generally not an orthogonal matrix.

2.3 Accelerometer Independence

In the applications of interest in this thesis, a configuration of n accelerometers is attached to a single rigid body, represented here by the rigid frame, $\mathcal{B}$. The accelerometer, $\mathsf{A}(P_k, \mathbf{u}_k)$, is often denoted, in the interests of brevity, by A_k, and its measurement denoted by a_k.

According to Eq (2.6) the measurements of the configuration, $\{\mathsf{A}_k\}_1^n$, are related to the SFSM by

$$\begin{bmatrix} [\mathsf{A}_1^{\mathcal{B}}] \\ \vdots \\ [\mathsf{A}_n^{\mathcal{B}}] \end{bmatrix} [\mathbf{S}^{\mathcal{B}}] = \begin{bmatrix} \mathsf{a}_1 \\ \vdots \\ \mathsf{a}_n \end{bmatrix}, \tag{2.20}$$

or,

$$[\mathsf{C}^{\mathcal{B}}_n][\mathbf{S}^{\mathcal{B}}] = [\mathbf{a}_n]. \tag{2.21}$$

[4]Refer to Appendix A for the definition of the orientation matrix, $[\boldsymbol{c}^{\boldsymbol{b}}]$

where $[\mathbf{a}_n]$ denotes the $n \times 1$ matrix of accelerometer measurements and the $n \times 12$ matrix,

$$[\mathsf{C}_n^{\mathcal{B}}] \stackrel{\text{def}}{=} \begin{bmatrix} [\mathsf{A}_1^{\mathcal{B}}] \\ \vdots \\ [\mathsf{A}_n^{\mathcal{B}}] \end{bmatrix}, \tag{2.22}$$

is referred to as the *Configuration Matrix* for the configuration, $\{\mathsf{A}_k\}_1^n$, in $\mathcal{B}$. Since $[\mathbf{S}^{\mathcal{B}}]$ is a 12×1 matrix it is clear that to solve Eq (2.21) for $[\mathbf{S}^{\mathcal{B}}]$ in terms of $[\mathbf{a}_n]$, and thus to reveal the motion of $\mathcal{B}$ relative to $\mathcal{F}$, requires that

$$\text{rank}[\mathsf{C}_n^{\mathcal{B}}] = 12. \tag{2.23}$$

A necessary condition for $\text{rank}[\mathsf{C}_n^{\mathcal{B}}] = 12$ is that $n \geq 12$, but this is not sufficient, and motivates the following definition:

Definition 2.3.1. A configuration of n accelerometers, $\{\mathsf{A}_k\}_1^n$, is said to be dependent (independent) if their n ADMs in some frame, $\mathcal{B}$, are linearly dependent (independent).

As was shown in Section 2.2, the coordinate transformation matrix relating ADMs of the same accelerometer in different frames is non-singular. This means that if $[\mathsf{C}_n^{\mathcal{B}}]$ has rank m, the configuration has rank m matrix in every other frame, and, consequently, defining independence in terms of the ADMs in one frame is permissible. This also means that one is free to choose coordinate frames to simplify the analysis.

According to the definition, a 12 accelerometer configuration is independent if and only if the determinant of its configuration matrix is non-zero. The determinant of the configuration matrix is easily shown to be invariant to the choice of frame:

$$\det[\mathsf{C}_{12}^{\mathcal{B}}] = \det([\mathsf{C}_{12}^{\mathcal{C}}][\Pi_{\mathcal{C}}^{\mathcal{B}}]) = \det[\mathsf{C}_{12}^{\mathcal{C}}] \det[\Pi_{\mathcal{C}}^{\mathcal{B}}] = \det[\mathsf{C}_{12}^{\mathcal{C}}], \tag{2.24}$$

where Eq (2.19) was used. The fact that the determinant of the configuration matrix is invariant under a change of frame means that it is intrinsically associated with the configuration, rather than any particular set of coordinates used to describe it. As a scalar, it entails some combination of variables that physically describe the relative locations and directions of the accelerometers.

According to Definition 2.3.1, $n = 12$ independent accelerometers are required to solve Eq (2.21) for $[\mathbf{S}^{\mathcal{B}}]$. If $n > 12$, then the configuration is dependent, and if a subset of 12 accelerometers is independent, $n-12$ accelerometers can be removed without altering the 'knowledge' of $[\mathbf{S}^{\mathcal{B}}]$. It should be remarked that this assumes that the accelerometer measurements are perfect. If the measurements are 'noisy', for instance, then a dependent configuration of $n > 12$ accelerometers might be used to reduce the error in $[\mathbf{S}^{\mathcal{B}}]$ using least-squares

techniques. Calculating the (left) pseudo-inverse [34] of the configuration matrix, which is required for the least-square solution of Eq (2.21), requires that $[\mathsf{C}_n^{\mathcal{B}}]$ have rank 12, so the fact remains that some sub-configuration of 12 accelerometers must be independent.

Given that accelerometer independence is a frame invariant concept, in the following, the frame in which the ADM and SFSM are expressed is often not made explicit. As will be seen in the coming chapters, however, some numerical properties of accelerometer configurations are not frame invariant, so when it comes to the actual implementation of configurations, a definite frame must be chosen.

2.3.1 Accelerometer Generation

A useful concept that is closely related to accelerometer independence is that of *generation*:

Definition 2.3.2. An accelerometer, $\mathsf{A}(P, \mathbf{u})$, is said to be *generated* by the configuration, $\{\mathsf{A}_k\}_1^n$, if n scalars, $\{\lambda_k\}_1^n$ can be found such that

$$[\mathsf{A}(P, \mathbf{u})] = \sum_{k=1}^{n} \lambda_k [\mathsf{A}_k].$$

The set of all accelerometers generated by the configuration, $\{\mathsf{A}_k\}_1^n$, is denoted by $\langle\{\mathsf{A}_k\}_1^n\rangle$.

Remark 2.3.1. Choosing $\lambda_j = 1$ for some $1 \leq j \leq n$ and $\lambda_k = 0$ otherwise, shows that every accelerometer in the configuration is generated by that configuration. This is referred to as *trivial generation.*

Remark 2.3.2. The definitions of the ADM and of accelerometer generation show that

$$\mathsf{A}(P_g, \mathbf{u}_g) \in \langle\{\mathsf{A}_k\}_1^n\rangle \Leftrightarrow \mathsf{A}(P_g, -\mathbf{u}_g) \in \langle\{\mathsf{A}_k\}_1^n\rangle .$$

Further, if $\mathsf{A}_l \equiv \mathsf{A}(P_l, \mathbf{u}_l)$ for some $1 \leq l \leq n$ is replaced by $\mathsf{A}(P_l, -\mathbf{u}_l)$, the set of generated accelerometers is not changed; for any accelerometer that was generated, the same can be generated by the new set by switching the sign of λ_l. For these reasons the accelerometers, $\mathsf{A}(P, \mathbf{u})$ and $\mathsf{A}(P, -\mathbf{u})$, are regarded as identical and when considering a configuration of accelerometers, each of their directions can be switched for analytical convenience.

2.3.2 Identification of Dependent Configurations

The concept of accelerometer generation is a very useful tool in the identification of dependent configurations, as is now described. If $\{\mathsf{A}_k\}_1^n$ is independent,

and $\mathsf{A}(P, \mathbf{u}) \in \langle \{\mathsf{A}_k\}_1^n \rangle$ is added to it, the resulting $n+1$ accelerometer configuration is dependent. Conversely, if $\mathsf{A}(P, \mathbf{u}) \notin \langle \{\mathsf{A}_k\}_1^n \rangle$ is added to $\{\mathsf{A}_k\}_1^n$, the resulting configuration is independent. Combining these statements allows the 'shapes' of all possible dependent configurations to be identified in an incremental fashion, and, as a consequence, independent configurations are found simply as all those that are not dependent. While identifying independent configurations as all those that are not dependent might seem like a roundabout method, it is quicker than directly seeking independent configurations because they far outnumber the dependent configurations.

An iterative identification process has the following n^{th} step:

1. Find $\langle \{\mathsf{A}_k\}_1^n \rangle$: adding any of these to $\{\mathsf{A}_k\}_1^n$ results in a dependent configuration.

2. Add any $\mathsf{A}(P, \mathbf{u}) \notin \langle \{\mathsf{A}_k\}_1^n \rangle$ to the configuration to result in an independent configuration.

3. Set $n = n + 1$ and return to Step 1.

Starting with 1 accelerometer and following this process would eventually result in an independent configuration of 12 accelerometers.

2.4 Gyroscope-Free Inertial Navigation

The previous sections showed what information about the motion of a rigid body, $\mathcal{B}$, is contained in the measurement of a configuration of accelerometers attached to $\mathcal{B}$. The best that one can do using only accelerometers is to fully determine $[\mathbf{S}^{\mathcal{B}}]$, and, as shown in Section 2.3, this requires an independent configuration of 12 accelerometers.

This section discusses how a time history of $[\mathbf{S}^{\mathcal{B}}]$ can be used to calculate the motion of $\mathcal{B}$ relative to the inertial frame, $\mathcal{F}$. A large number of the required calculations are used in *Strapdown Inertial Navigation*, (SDIN) so the first two subsections review these briefly before addressing the additional part of the GFIN algorithm in Section 2.4.3.

2.4.1 Kinematic Differential Equations

The *Kinematic Differential Equations*, (KDEs) relate some representation of the velocity of a rigid body to the rate of change of some representation of the pose[5] of that body. Using different representations for the pose and velocity may result in equations that have a simpler form, or more desirable computational properties. Generally there are two different equations; one for the

[5]Position and orientation.

position and the other for orientation, and it is the orientation equation that has seen the most research [35]. Using dual quaternions, however, to represent pose, and a dual vector (screw) to represent the velocity, it is possible to combine the two KDEs into a single equation [36, 37].

Here, for simplicity, matrix representations of the pose and velocity are used. In particular, the pose of $\mathcal{B}$ relative to $\mathcal{F}$ is described by $[\mathbf{r}_{O_B}^{\mathcal{F}}]$, which describes the location of the origin of $\mathcal{B}$, and $[\boldsymbol{b}^{\boldsymbol{f}}]$, describing the orientation of $\boldsymbol{b}$ relative to $\boldsymbol{f}$. The velocity of $\mathcal{B}$ relative to $\mathcal{F}$ is represented by $[\mathbf{v}_{O_B}^{\boldsymbol{f}}]$ and $[\boldsymbol{\omega}^{\boldsymbol{b}}]$. The KDE relating $[\mathbf{v}_{O_B}^{\boldsymbol{f}}]$ and the rate of change of $[\mathbf{r}_{O_B}^{\mathcal{F}}]$ is trivial:

$$\frac{\mathrm{d}}{\mathrm{dt}}[\mathbf{r}_{O_B}^{\mathcal{F}}] = [\mathbf{v}_{O_B}^{\boldsymbol{f}}]. \tag{2.25}$$

The orientation KDE is [35]

$$\frac{\mathrm{d}}{\mathrm{dt}}[\boldsymbol{b}^{\boldsymbol{f}}] = [\boldsymbol{b}^{\boldsymbol{f}}]\mathrm{skew}([\boldsymbol{\omega}^{\boldsymbol{b}}]). \tag{2.26}$$

2.4.2 Strapdown Inertial Navigation

The SDIN algorithm transforms measurements obtained from a triad of gyroscopes attached (strapped-down) to $\mathcal{B}$, and a triad of accelerometers attached to $\mathcal{B}$ at O_B into a description of the current pose of $\mathcal{B}$ relative to $\mathcal{F}$. More precisely, the algorithm requires the following inputs:

- $[\boldsymbol{\omega}(t)^{\boldsymbol{b}}] \quad \forall t \in [t_0, t_c]$
- $[\mathbf{s}_{O_B}(t)^{\boldsymbol{b}}] \quad \forall t \in [t_0, t_c]$
- $[\boldsymbol{b}(t_0)^{\boldsymbol{f}}]$ and $[\mathbf{r}_{O_B}(t_0)^{\mathcal{F}}]$

and outputs $[\boldsymbol{b}(t_c)^{\boldsymbol{f}}]$ and $[\mathbf{r}_{O_B}(t_c)^{\mathcal{F}}]$. The algorithm requires numerous integration steps and these are shown below as exact integrals evaluated between t_0 and t_c. In reality the integrals would be evaluated numerically, and updated at each time step. Further, it is generally agreed that SDIN should use different rates of integration, a fast one for attitude update and another for the remaining integration processes [38, 39]. These details are beyond the scope of the current work.

The first part of the algorithm involves updating the orientation by integrating Eq (2.26):

$$[\boldsymbol{b}(t_c)^{\boldsymbol{f}}] = \int_{t_0}^{t_c} [\boldsymbol{b}(t)^{\boldsymbol{f}}]\mathrm{skew}([\boldsymbol{\omega}(t)^{\boldsymbol{b}}])dt. \tag{2.27}$$

This matrix is used to transform the specific force component matrix into fixed basis components and related to $[\mathbf{a}_{O_B}^{\boldsymbol{f}}]$ using Eq (2.2):

$$[\boldsymbol{b}^{\boldsymbol{f}}][\mathbf{s}_{O_B}^{\boldsymbol{b}}] = [\mathbf{s}_{O_B}^{\boldsymbol{f}}] = [\mathbf{a}_{O_B}^{\boldsymbol{f}}] - [\mathbf{g}^{\boldsymbol{f}}] \tag{2.28}$$

It is assumed that $[\mathbf{g}^{\boldsymbol{f}}]$, the component matrix of the local gravity vector in the inertial frame, is known to good accuracy. Next, since

$$[\mathbf{a}^{\boldsymbol{f}}_{O_B}] = \frac{\mathrm{d}}{\mathrm{dt}}[\mathbf{v}^{\boldsymbol{f}}_{O_B}]$$

it follows that

$$[\mathbf{v}_{O_B}(t_c)^{\boldsymbol{f}}] = \int_{t_0}^{t_c} ([\boldsymbol{b}(t)^{\boldsymbol{f}}][\mathbf{s}_{O_B}(t)^{\boldsymbol{b}}] + [\mathbf{g}^{\boldsymbol{f}}])dt + [\mathbf{v}_{O_B}(t_0)^{\boldsymbol{f}}] \tag{2.29}$$

after which $[\mathbf{r}_{O_B}(t_c)^{\mathcal{F}}]$ is obtained by integrating Eq (2.25):

$$[\mathbf{r}_{O_B}(t_c)^{\mathcal{F}}] = \int_{t_0}^{t_c} ([\mathbf{v}_{O_B}(t)^{\boldsymbol{f}}])dt + [\mathbf{r}_{O_B}(t_0)^{\mathcal{F}}]. \tag{2.30}$$

Important features of the SDIN algorithm as described here are the reliance upon integration and accurate initial conditions, and the coupling between the solutions for orientation and position. Numerical integration of erroneous measurements leads to divergence, and this is exacerbated if the initial conditions are not correct. A detailed error analysis of SDIN is beyond the scope of this work (refer to the book of Titterton and Weston [4]), but it is clear from Eqs (2.29) and (2.30) that erroneous calculation of the orientation will cause errors in the calculated position.

2.4.3 Calculating Angular Velocity

As described in the previous section, the SDIN algorithm requires time-histories of $[\mathbf{s}^{\boldsymbol{b}}_{O_B}]$ and $[\boldsymbol{\omega}^{\boldsymbol{b}}]$ as inputs. It was shown in Section 2.1 that only the former of these quantities can be obtained using accelerometers exclusively; further processing of the accelerometer measurements is required to calculate $[\boldsymbol{\omega}^{\boldsymbol{b}}]$ from elements of $[\mathbf{S}^{\mathcal{B}}]$. Once this processing is complete, the SDIN algorithm can be applied.

The simplest way to obtain $[\boldsymbol{\omega}^{\boldsymbol{b}}]$ from $[\mathbf{S}^{\mathcal{B}}]$ is to integrate $[\boldsymbol{\alpha}^{\boldsymbol{b}}]$, which *is* part of the SFSM:

$$[\boldsymbol{\omega}(t_c)^{\boldsymbol{b}}] = \int_{t_0}^{t_c} [\boldsymbol{\alpha}(t)^{\boldsymbol{b}}]dt + [\boldsymbol{\omega}(t_0)^{\boldsymbol{b}}]. \tag{2.31}$$

This basic method has been used by many researchers [7, 15, 18–20, 24, 27, 40, 41]. It has two potential downfalls: its dependence upon accurate knowledge of $[\boldsymbol{\omega}(t_0)^{\boldsymbol{b}}]$, and the tendency of the integral to diverge due to stochastic and/or deterministic errors in the matrix, $[\boldsymbol{\alpha}(t)^{\boldsymbol{b}}]$, that is calculated from the accelerometer measurements. This divergence means that the method is only suitable for very short durations as found, for example, in measuring the motion of a crash-test dummy at impact [20, 24, 40], which is generally measured

for less than half a second, or the motion of the human leg over a single step [18, 19]. In the latter case, and in others involving periodic motion, reasonable assumptions about the angular velocity at the beginning and the end of each period allow much of the divergence to be eliminated.

Other researchers have used the information about the *magnitude* of the elements of $[\boldsymbol{\omega}^b]$ that *is* available in the SFSM, in the forms of $q_{ii}([\boldsymbol{\omega}^b])$ and/or $q_{ij}([\boldsymbol{\omega}^b])$, to lessen the dependence upon integration. The simplest way to do this is to assume that the signs of the elements of $[\boldsymbol{\omega}^b]$ are known at some instant, t_i, and use $[\boldsymbol{\alpha}(t_i)^b]$ to propagate an estimate $[\boldsymbol{\omega}^b]$ to the next instant, t_{i+1}, by a numerical integration step. This estimate is used simply to determine the correct signs of $[\boldsymbol{\omega}(t_{i+1})^b]$; the magnitudes are obtained using $q_{ii}([\boldsymbol{\omega}^b])$ and/or $q_{ij}([\boldsymbol{\omega}^b])$. This method, which has been proposed, in essence, by many authors [13, 17, 22, 42], requires that the signs of the elements of $[\boldsymbol{\omega}(t_0)^b]$ be known. Zappa et al. [22] showed, using simple algebra, that knowledge of $q_{ij}([\boldsymbol{\omega}^b])$ alone is insufficient to determine the magnitudes of the components of angular velocity in a robust manner. For example, suppose

$$q_{ij}([\boldsymbol{\omega}^b]) = \begin{bmatrix} a \\ b \\ c \end{bmatrix},$$

then, since $bc = \omega_1^2\omega_2\omega_3$, $|\omega_1|$ can be calculated from

$$|\omega_1| = \sqrt{\frac{bc}{a}},$$

but if $a = 0$, which can occur if $\omega_2 = 0$, or $\omega_3 = 0$, then ω_1 cannot be determined. Knowledge of the elements of $q_{ii}([\boldsymbol{\omega}^b])$, is, on the other hand, always sufficient to determine the magnitudes of the elements $[\boldsymbol{\omega}^b]$.

The 'sign choosing' method just described, when applied using both $q_{ii}([\boldsymbol{\omega}^b])$ and $q_{ij}([\boldsymbol{\omega}^b])$, ignores the likelihood that the matrices will 'disagree' on the magnitudes of the elements of $[\boldsymbol{\omega}^b]$, due to errors in the accelerometer measurements. To counter this possibility, Parsa et al. [16, 31, 43] have proposed that a numerical method be used to find an estimate of $[\boldsymbol{\omega}^b]$ that minimizes the discrepancy. The authors suggest using the propagated estimate of the angular velocity obtained as discussed in the 'sign choosing' method as the initial guess for the numerical method.

Park et al. have proposed application of the Extended Kalman Filter [34] for the estimation of angular velocity [8, 10]. In the former paper they use an 'iterative' Extended Kalman Filter. This algorithm employs a predictive step and an iterative update step that has been proved by Bell and Cathey [44] to be equivalent to the Gauss-Newton method of optimization, so the approach, while more theoretically interesting, is very similar to the method used by Parsa et al.

2.4.4 Two GFIN Paradigms

The previous section showed how $[\boldsymbol{\omega}^b]$ can be estimated from accelerometer measurements, after which the SDIN algorithm can be applied. It was tacitly assumed that an independent configuration of 12 accelerometers was used, so that $[\mathbf{S}^{\mathcal{B}}]$ could be obtained as

$$[\mathbf{S}^{\mathcal{B}}] = [\mathsf{C}_{12}^{\mathcal{B}}]^{-1}[\mathbf{a}_{12}]. \tag{2.32}$$

The high-level flow chart of the GFIN algorithm up to the point where $[\boldsymbol{\omega}^b]$ and $[\mathbf{s}_{O_B}^b]$ are input SDIN algorithm is shown in in Fig 2.3.

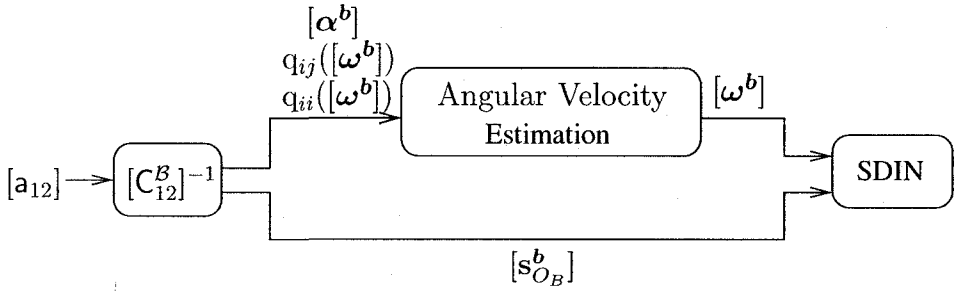

Figure 2.3: Flow chart showing the full GFIN algorithm up to the point of SDIN.

A different implementation of GFIN, referred to as *Minimal GFIN*, (MGFIN) is illustrated in Fig 2.4. It is based on the following partitioning and reorgainisation of Eq (2.21):

$$[\mathbf{M}_n^{\mathcal{B}}] \begin{bmatrix} [\mathbf{s}_{O_B}^b] \\ [\boldsymbol{\alpha}^b] \end{bmatrix} = [\mathbf{a}_n] - [\mathbf{Q}_n^{\mathcal{B}}] \begin{bmatrix} \mathsf{q}_{ij}([\boldsymbol{\omega}^b]) \\ \mathsf{q}_{ii}([\boldsymbol{\omega}^b]) \end{bmatrix}, \tag{2.33}$$

where $[\mathbf{M}_n^{\mathcal{B}}]$ and $[\mathbf{Q}_n^{\mathcal{B}}]$ are, respectively, the first and last six columns of the configuration matrix, $[\mathsf{C}_n^{\mathcal{B}}]$. The solution of Eq (2.33) requires a minimum of 6 accelerometers arranged so that $[\mathbf{M}_n^{\mathcal{B}}]$ is non-singular. In possession of such a configuration, which is referred to as a *minimal configuration*, Eq (2.33) can be solved for $[\boldsymbol{\alpha}^b]$ and $[\mathbf{s}_{O_B}^b]$ in terms of the accelerometer measurements and the quadratic combinations of $[\boldsymbol{\omega}^b]$. In general, the solution of $[\boldsymbol{\alpha}^b]$ will depend upon $\mathsf{q}_{ij}([\boldsymbol{\omega}^b])$ and $\mathsf{q}_{ii}([\boldsymbol{\omega}^b])$, and this gives rise to nonlinear differential equations. These differential equations and any other required manipulations to transform $[\mathbf{a}_n]$ into $[\boldsymbol{\alpha}^b]$ and $[\mathbf{s}_{O_B}^b]$ are the contents of the box marked 'Processing' in Fig 2.4.

MGFIN is generally less accurate than 'full' GFIN, as illustrated in Fig 2.3, for two reasons:

- the necessity of solving a nonlinear differential equation for $[\boldsymbol{\omega}^b]$.

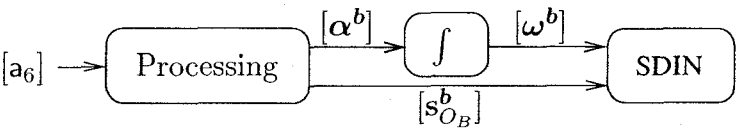

Figure 2.4: Flow chart showing the Minimal GFIN algorithm up to the point of SDIN.

- the propagation of errors in $[\boldsymbol{\omega}^b]$ into the estimate of $[\mathbf{s}^b_{O_B}]$.

The design of configurations to reduce or eliminate these drawbacks is discussed in Chapter 5.

2.4.5 Nine-Accelerometer Configurations

While this thesis is concerned mainly with *Minimal* and *Full* GFIN, respectively requiring six and at least twelve accelerometers, these are not the only alternatives. The most common alternative is to use nine accelerometers.

A nine-accelerometer configuration presented by Schuler et al. [5] was shown in Fig 1.1. This configuration allows the solution of $[\mathbf{s}^b_{O_B}]$ and $[\boldsymbol{\alpha}^b]$ in terms of $[\mathbf{a}_9]$. A configuration originally presented by Padgaonkar et al. [11], and since considered by many other researchers [40, 45, 46] is shown in Fig 2.5. Compared to a minimal configuration this shares the same benefits as Schuler's nine-accelerometer configuration:

- it is not necessary to solve a nonlinear differential equation for $[\boldsymbol{\omega}^b]$,
- the solution of $[\mathbf{s}^b_{O_B}]$ does not depend upon $[\boldsymbol{\omega}^b]$.

Both Park et al. [10] and Ding et al. [42] have proposed nine-accelerometer configurations obtained by adding three accelerometers to a popular minimal configuration originally presented by Chen et al. [7]. Chen's minimal configuration will be discussed in detail in Chapter 5. The proposed additions to the minimal configuration aim to improve the quality of the solutions for $[\boldsymbol{\omega}^b]$ and $[\mathbf{s}^b_{O_B}]$.

Finally, a configuration devised by Nusholtz [21] consisting of three triaxial accelerometers should be mentioned. Nusholtz used concepts from differential geometry of surfaces to explain the functioning of his configuration. Unfortunately the paper is riddled with typographical errors and omissions. One part of his algorithm requires the numerical differentiation of accelerometer measurements, a process that will magnify noise that will no doubt be present.

2.4.6 Regarding Frames

The discussion of SDIN in Section 2.4.2 is simpler than that typically found in the inertial navigation literature in that only two frames are studied: a body

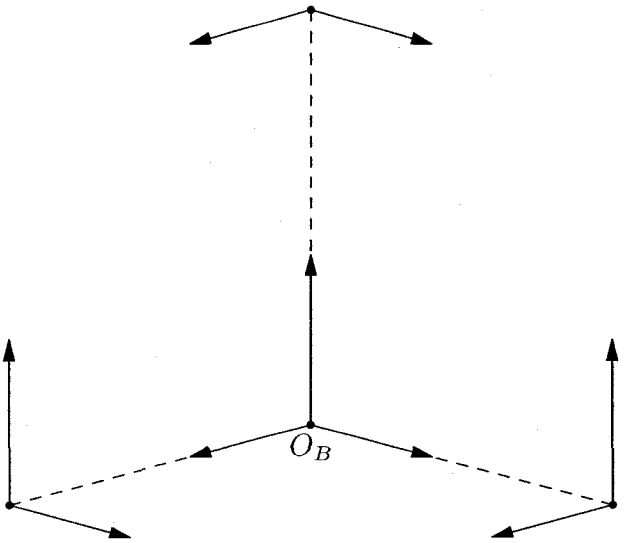

Figure 2.5: Padgaonkar's 9-accelerometer configuration.

frame and an inertial frame. In terrestrial applications of inertial navigation, one generally uses a series of frames, including one fixed in and rotating with the earth [4, 38]. The analytical details of these additional frames are not studied here because they are identical for SDIN and GFIN.

Further, in all the papers describing applications of GFIN that have been referenced above, one finds a similar two-frame approach, and what should be called a 'laboratory frame' is treated as an inertial frame. Without wanting to negatively foreshadow the coming results, the divergence of the GFIN solution due to accelerometer alignment errors and other error sources is generally much more significant than this mistreatment of frames.

2.5 Summary

This chapter has introduced a number of concepts and definitions that are used repeatedly in the thesis. Aside from the discussion of the GFIN algorithm, without which there would be little motivation for the analysis and use of accelerometer configurations, the most important aspects of this chapter are the definitions of the ADM and AADM, and, subsequently, accelerometer dependence and generation.

Chapter 3

Planar Accelerometer Configurations

This chapter is dedicated to elucidating the accelerometer configurations that can be used for GFIN in the special case where the rigid body to which the accelerometers are attached is undergoing planar motion relative to inertial space. Accelerometer configurations have been used for the analysis of planar motion chiefly in biomechanical applications such as gait analysis [18, 19] and measuring the motion of an automobile crash-testing dummy's head [20, 25].

Some of the results presented in this chapter have been published by the author [47] using a less rigorous approach. A more axiomatic approach was taken here to show the completeness and correctness of the results.

In Section 3.1 a reduced form of the ADM presented in Chapter 2 that is suitable for the case of planar motion is derived, along with its coordinate transformation law. Section 3.2 presents some necessary conditions for accelerometer generation. This is followed in Section 3.3 with a series of propositions regarding the geometry of accelerometer generation that are only applicable in the case of planar configurations. These propositions are then used to identify dependent planar configurations of 2, 3 and 4 accelerometers. Two examples of planar accelerometer configurations are presented in Section 3.4. They are mainly concerned with the numerical properties of configurations. Motivated by a recent paper by Parsa et al. [31] in which a numerical optimization procedure is used to minimize the condition number of a 12 accelerometer configuration, a planar configuration with optimal condition number is designed. It is shown that the condition number depends upon the choice of origin. Finally, in Section 3.5, the geometry of configurations that can be used for MGFIN in the case of planar motion is studied. For simplicity, and to highlight similarities, notation used in this chapter for 'planar quantities' is the same as that used in the spatial case in other chapters.

3.1 Planar Accelerometer Measurements

If the frame, $\mathcal{B}$, is undergoing planar motion relative to the inertial space then it can be assumed, without loss of generality, that the plane of motion passes through O_F and O_B, and that $\mathbf{f}_3 = \mathbf{b}_3$ is orthogonal to this plane, as is shown in Fig 3.1. When this choice of frames is made, the component matrices of $\boldsymbol{\alpha}$,

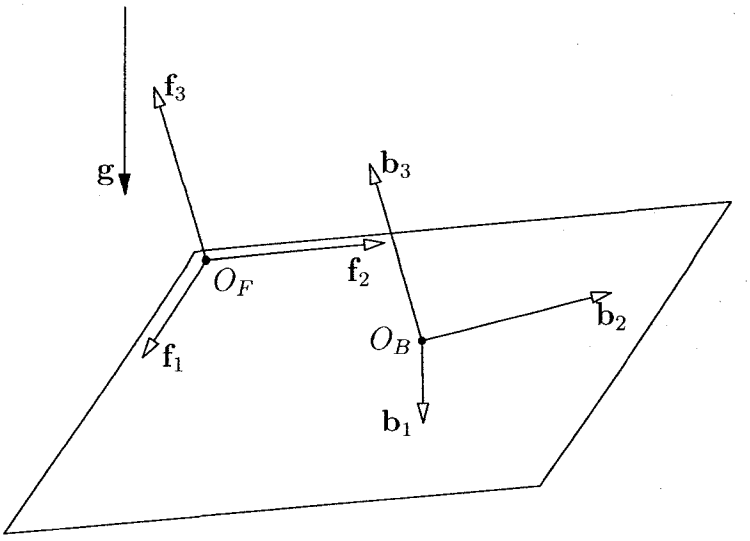

Figure 3.1: Frames used for planar motion.

$\boldsymbol{\omega}$ and $\mathbf{s}_{O_B}$ in $\boldsymbol{b}$ are

$$[\boldsymbol{\alpha}^{\boldsymbol{b}}] = \begin{bmatrix} 0 \\ 0 \\ \alpha \end{bmatrix}, \quad [\boldsymbol{\omega}^{\boldsymbol{b}}] = \begin{bmatrix} 0 \\ 0 \\ \omega \end{bmatrix}, \quad [\mathbf{s}^{\boldsymbol{b}}_{O_B}] = \begin{bmatrix} s_1 \\ s_2 \\ s_3 \end{bmatrix} = \begin{bmatrix} a_1 - g_1 \\ a_2 - g_2 \\ -g_3 \end{bmatrix}, \tag{3.1}$$

where g_i and a_i are, respectively, the i^{th} element of $[\mathbf{g}^{\boldsymbol{b}}]$ and $[\mathbf{a}^{\boldsymbol{b}}_{O_B}]$; $a_3 = 0$ due to the choice of frame. When these component matrices are substituted into the definition of the SFSM (Eq (2.9)), it is found that there are only 6 non-zero elements, and that two of them equal ω^2. Condensing the SFSM into the following 5×1 matrix:

$$[\mathbf{S}^{\mathcal{B}}] = \begin{bmatrix} a_1 - g_1 \\ a_2 - g_2 \\ -g_3 \\ \alpha \\ \omega^2 \end{bmatrix}, \tag{3.2}$$

and redefining the ADM so that $\mathsf{a}_k = [\mathsf{A}^{\mathcal{B}}_k][\mathbf{S}^{\mathcal{B}}]$ still holds gives

$$[\mathsf{A}^{\mathcal{B}}_k] = \begin{bmatrix} u_{k,1} & u_{k,2} & u_{k,3} & u_{k,2}r_{k,1} - u_{k,1}r_{k,2} & -u_{k,1}r_{k,1} - u_{k,2}r_{k,2} \end{bmatrix}, \tag{3.3}$$

where $u_{k,i}$ and $r_{k,i}$ are the i^{th} elements of $[\mathbf{u}_k^b]$ and $[\mathbf{r}_k^{\mathcal{B}}]$, respectively. The absence of $r_{k,3}$ from $[\mathsf{A}_k^{\mathcal{B}}]$ confirms what is intuitively expected: the measurements of the accelerometers, $\mathsf{A}(P, \mathbf{u})$ and $\mathsf{A}(P + \lambda \mathbf{b}_3, \mathbf{u})$, are identical, so, for simplicity, and without loss of generality, it is assumed that all accelerometers are located in the plane of motion, i.e., $r_{k,3} = 0$.

A further simplification is possible. Only the first two elements of $[\mathbf{s}_{O_B}^b]$ contain information about the motion of $\mathcal{B}$. The third element, $s_3 = -g_3$, is a constant, dependent only upon the included angle between the normal to the plane of motion and the local gravity vector. Since this scalar is not useful in calculating the motion of $\mathcal{B}$ relative to $\mathcal{F}$, there is no need to measure it. Reference to Eqs (3.2) and (3.3) shows that A_k is free of g_3 if $u_{k,3} = 0$, i.e., if the direction of the accelerometer is parallel to the plane of motion. In this chapter, therefore, *all accelerometers are assumed to be parallel to the plane of motion*, and whenever reference is made to accelerometers of 'all directions', this limitation is implied. This being the case, the SFSM and ADM become

$$[\mathbf{S}^{\mathcal{B}}] = \begin{bmatrix} s_1 \\ s_2 \\ \alpha \\ \omega^2 \end{bmatrix} \tag{3.4}$$

and

$$[\mathsf{A}_k^{\mathcal{B}}] = \begin{bmatrix} [\mathbf{u}_k^b]^T & [\mathbf{u}_k^b]^T[J][\mathbf{r}_k^{\mathcal{B}}] & -[\mathbf{u}_k^b]^T[\mathbf{r}_k^{\mathcal{B}}] \end{bmatrix}, \tag{3.5}$$

where here, and elsewhere in this chapter, except where noted, all component matrices are 2×1 and

$$[J] \stackrel{\text{def}}{=} \begin{bmatrix} 0 & -1 \\ 1 & 0 \end{bmatrix}. \tag{3.6}$$

Using the angles shown in Fig 3.2, the ADM can be written as

$$[\mathsf{A}_k^{\mathcal{B}}] = \begin{bmatrix} \cos\gamma_k & -\sin\gamma_k & \|\mathbf{r}_{P_k/O_B}\| \sin(\gamma_k - \phi_k) & \|\mathbf{r}_{P_k/O_B}\| \cos(\gamma_k - \phi_k) \end{bmatrix}. \tag{3.7}$$

If $\mathcal{C}$ is another frame with origin in the plane of motion and with $\mathbf{c}_3 = \mathbf{b}_3$, the transformation matrix relating $[\mathsf{A}_k^{\mathcal{B}}]$ to $[\mathsf{A}_k^{\mathcal{C}}]$, is

$$[\Pi_{\mathcal{B}}^{\mathcal{C}}] = \begin{bmatrix} [\boldsymbol{c}^b] & [\boldsymbol{c}^b]\begin{bmatrix} [J] & -[I]_2 \\ & [I]_2 \end{bmatrix}[\mathbf{r}_{O_B}^{\mathcal{C}}] \\ [0]_{2\times 1} & \end{bmatrix}, \tag{3.8}$$

where $[I]_2$ is the 2×2 identity matrix. This planar version of the coordinate transformation matrix has considerably simpler structure than that required in the spatial case (see Section 2.3), but they are similar in that they both have unit determinants. This means, again, that it is permissible to investigate the dependence of accelerometers using their ADMs in any frame. Since the ADM is a 1×4 matrix it follows that 4 is the maximum number of independent accelerometers in a planar configuration. The fact that $[\Pi_{\mathcal{B}}^{\mathcal{C}}]$ has a

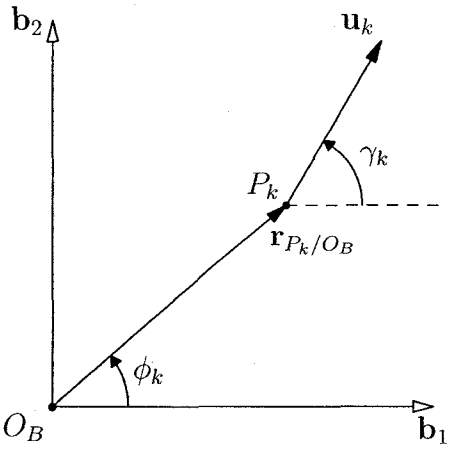

Figure 3.2: Angles used in the specification of an accelerometer of a planar configuration.

unit determinant means that the determinant of a four accelerometer planar configuration is invariant to the selection of the frame.

3.2 Accelerometer Generation - Preliminaries

Proposition 3.2.1. *A necessary condition for* $\mathsf{A}(P_g, \mathbf{u}_g)$ *to be generated by* $\{\mathsf{A}_k\}_1^n$ *is that* $\mathbf{u}_g \in \langle\{\mathbf{u}_k\}_1^n\rangle$.

Proof. Reference to Eq (2.7) and (3.5) shows that $[\mathbf{u}_k]$ is part of the spatial and planar ADMs, thus, in order that

$$[\mathsf{A}(P_g, \mathbf{u}_g)] = \sum_{k=1}^{n} \lambda_k [\mathsf{A}_k]$$

which is required if $\mathsf{A}(P_g, \mathbf{u}_g) \in \langle\{\mathsf{A}_k\}_1^n\rangle$, it is necessary that

$$[\mathbf{u}_g] = \sum_{k=1}^{n} \lambda_k [\mathbf{u}_k], \tag{3.9}$$

and this equation can be satisfied only if $\mathbf{u}_g \in \langle\{\mathbf{u}_k\}_1^n\rangle$. □

The dimension of the subspace of $\mathbf{E}$ that is spanned by the directions of $\{\mathsf{A}_k\}_1^n$ is denoted by d:

$$d \stackrel{\text{def}}{=} \dim \langle\{\mathbf{u}_k\}_1^n\rangle . \tag{3.10}$$

In the case of planar accelerometer configurations there are two possible values for d:

- $d = 1$, $\mathbf{u}_1 = \mathbf{u}_k$ for $k = 2, \ldots, n$.

- $d = 2$, $\{\mathbf{u}_k\}_1^n$ spans a plane of $\mathbf{E}$.

Equation (3.9) can be rewritten in matrix form as

$$[\mathbf{u}_g] = [\mathbf{U}_n][\boldsymbol{\lambda}], \tag{3.11}$$

where $[\mathbf{U}_n]$ is the matrix with k^{th} column, $[\mathbf{u}_k]$, and $[\boldsymbol{\lambda}]$ is the $n \times 1$ matrix with k^{th} element, λ_k. The rank of $[\mathbf{U}_n]$ is d, and the matrix therefore has a null-space of dimension, $z = n - d$. The general solution of Eq (3.11) can therefore be written as [48]

$$[\boldsymbol{\lambda}] = [\boldsymbol{\lambda}^*] + \sum_{k=d+1}^{n} \mu_k [\mathbf{z}_k], \tag{3.12}$$

where $[\boldsymbol{\lambda}^*]$ is a particular solution of Eq (3.11), $\{[\mathbf{z}_k]\}_{d+1}^n$, is a basis for the null-space of $[\mathbf{U}_n]$ and $\{\mu_k\}_{d+1}^n$ are arbitrary scalars. In the following, a particular solution, $[\boldsymbol{\lambda}^*]$, and null-space basis, $\{[\mathbf{z}_k]\}_{d+1}^n$ are identified.

Definition 3.2.1. A set of *principal accelerometers* from $\{\mathsf{A}_k\}_1^n$ is any set of d accelerometers with linearly independent directions, i.e., the directions of the principal accelerometers form a basis for $\langle\{\mathbf{u}_k\}_1^n\rangle$.

It is assumed in the following that the accelerometers have been numbered so that the first d accelerometers are a set of principal accelerometers.

Under the assumption regarding the numbering of accelerometers, the matrix, $[\mathbf{U}_d]$, consisting of the first d columns of $[\mathbf{U}_n]$, is, like $[\mathbf{U}_n]$, of rank d. Assuming $\mathbf{u}_g \in \langle\{\mathbf{u}_k\}_1^n\rangle$, i.e., the direction of the generated accelerometer is in the subspace spanned by the directions of the existing accelerometers, unique scalars, $\{\beta_{k,j}\}_{j=1}^d$, can be obtained from the solution of

$$[\mathbf{u}_k] = [\mathbf{U}_d] \begin{bmatrix} \beta_{k,1} \\ \vdots \\ \beta_{k,d} \end{bmatrix} \qquad k = 1, \ldots, n, g, \tag{3.13}$$

so that

$$[\mathbf{u}_k] = \sum_{j=1}^{d} \beta_{k,j} [\mathbf{u}_j] \qquad k = 1, \ldots, n, g. \tag{3.14}$$

The solutions for the scalars $\{\beta_{k,j}\}_{j=1}^d$ when $d = 1, 2$ are as follows for $k = d+1, \ldots, n, g$:

- $d = 1$: $\mathbf{u}_k = \mathbf{u}_1$, so

$$\beta_{k,1} = 1 \tag{3.15}$$

- $d = 2$: Assuming, without loss of generality, that the directions are in the plane spanned by $\mathbf{b}_1$ and $\mathbf{b}_2$, and letting γ_k denote the angle measured from $\mathbf{b}_1$ to $\mathbf{u}_k$ about $\mathbf{b}_3$, as shown in Fig 3.2, the two equations obtained by taking the scalar product of

$$\mathbf{u}_k = \beta_{k,1}\mathbf{u}_1 + \beta_{k,2}\mathbf{u}_2$$

with $\mathbf{u}_1$ and $\mathbf{u}_2$ can be solved for $\beta_{k,1}$ and $\beta_{k,2}$ as

$$\beta_{k,1} = \frac{\sin(\gamma_2 - \gamma_k)}{\sin(\gamma_2 - \gamma_1)} \quad \beta_{k,2} = \frac{\sin(\gamma_k - \gamma_1)}{\sin(\gamma_2 - \gamma_1)}. \tag{3.16}$$

Letting $[\boldsymbol{\beta}_k]$ denote the $n \times 1$ matrix with j^{th} element, $\beta_{k,j}$, and zeros elsewhere, Eq (3.13) shows that

$$[\mathbf{u}_k] = [\mathbf{U}_n][\boldsymbol{\beta}_k], \tag{3.17}$$

and, therefore, a particular solution of Eq (3.11) is

$$[\boldsymbol{\lambda}^*] = [\boldsymbol{\beta}_g]. \tag{3.18}$$

Equation (3.14) can be arranged as

$$\sum_{j=1}^{d} \beta_{k,j}[\mathbf{u}_j] - [\mathbf{u}_k] = [0] \qquad k > d. \tag{3.19}$$

Letting $[\mathbf{i}_k]$ denote the k^{th} column of the $n \times n$ identity matrix, Eq (3.19) indicates that the z, $n \times 1$ matrices,

$$[\mathbf{z}_k] \stackrel{\text{def}}{=} [\boldsymbol{\beta}_k] - [\mathbf{i}_k] \qquad k = d+1, \ldots, n, \tag{3.20}$$

all lie in the null-space of $[\mathbf{U}_n]$. Furthermore, the definition of $[\mathbf{z}_k]$ shows that the z matrices are linearly independent, and they therefore form a basis for the null-space of $[\mathbf{U}_m]$.

With reference to Eqs (3.12) and (3.18), the general solution of Eq (3.11) is

$$\lambda_k = \begin{cases} \beta_{g,k} + \sum_{j=d+1}^{n} \mu_j \beta_{j,k} & k \leq d \\ -\mu_k \qquad k > d, \end{cases} \tag{3.21}$$

where $\{\mu_k\}_{d+1}^{n}$ are arbitrary scalars.

3.3 Dependent Configuration Identification

The dependent configuration identification procedure that was outlined at the end of Section 2.3.2 is now applied for the case of planar configurations.

As previously mentioned, the largest possible number of independent accelerometers in a planar configuration is 4. In the following subsections therefore, starting with $n = 1$, $\langle\{\mathsf{A}_k\}_1^n\rangle$ is identified, and some $\mathsf{A}(P_{n+1}, \mathbf{u}_{n+1}) \notin \langle\{\mathsf{A}_k\}_1^n\rangle$ is added to the configuration. These steps are repeated until $n = 3$, at which point all types of dependent configurations are identified. The bulk of the analysis required for each n is common, and is now outlined in a collection of propositions.

For the purposes of dependence/generation analysis it is often useful in the following sections to rewrite $[\mathsf{A}_k]$ as

$$[\mathsf{A}_k] = \left[[\mathbf{u}_k]^T \quad ([\mathbf{N}_k][\mathbf{r}_k])^T\right], \tag{3.22}$$

where

$$[\mathbf{N}] \stackrel{\text{def}}{=} \left[[J] \quad -[I]_2\right][\mathbf{u}_k] = \begin{bmatrix} \sin\gamma_k & -\cos\gamma_k \\ -\cos\gamma_k & -\sin\gamma_k \end{bmatrix}. \tag{3.23}$$

A product of two of these matrices has a simple form:

$$[\mathbf{N}_k][\mathbf{N}_l] = \begin{bmatrix} \cos(\gamma_k - \gamma_l) & -\sin(\gamma_k - \gamma_l) \\ \sin(\gamma_k - \gamma_l) & \cos(\gamma_k - \gamma_l) \end{bmatrix} \equiv [\mathbf{R}(\gamma_k - \gamma_l)], \tag{3.24}$$

where $[\mathbf{R}(\gamma_k - \gamma_l)]$ is the matrix that effects a rotation through the angle $\gamma_k - \gamma_l$ in the plane. Equation (3.24) can be used to show that $[\mathbf{N}_k]$ is an involutory matrix, i.e., that

$$[\mathbf{N}_k]^{-1} = [\mathbf{N}_k]. \tag{3.25}$$

Proposition 3.3.1. *For any* $\mathbf{u}_g \in \langle\{\mathbf{u}_k\}_1^n\rangle$ *there exists a point,* P_g*, such that* $\mathsf{A}(P_g, \mathbf{u}_g) \in \langle\{\mathsf{A}_k\}_1^n\rangle$.

Proof. According the definition of generation (Definition 2.3.2) and the form of the ADM given in Eq (3.22), $\mathsf{A}(P_g, \mathbf{u}_g)$ is generated by the set $\{\mathsf{A}_k\}_1^n$ if and only if scalars $\{\lambda_k\}_1^n$ can be found such that

$$[\mathbf{u}_g] = \sum_{k=1}^{n} \lambda_k [\mathbf{u}_k] \tag{3.26}$$

and

$$[\mathbf{N}_g][\mathbf{r}_g] = \sum_{k=1}^{n} \lambda_k [\mathbf{N}_k][\mathbf{r}_k]. \tag{3.27}$$

When $\mathbf{u}_g \in \langle\{\mathbf{u}_k\}_1^n\rangle$, $\{\lambda_k\}_1^n$ can, as was shown in the previous section, always be found to satisfy Eq (3.26). Using the involutory property of $[\mathbf{N}_g]$, gives

$$[\mathbf{r}_g] = [\mathbf{N}_g] \sum_{k=1}^{n} \lambda_k [\mathbf{N}_k][\mathbf{r}_k], \tag{3.28}$$

which shows that $[\mathbf{r}_g]$, the coordinate matrix of P_g such that $\mathsf{A}(P_g, \mathbf{u}_g) \in \langle\{\mathsf{A}_k\}_1^n\rangle$, always exists. □

Substituting, from Eq (3.21), the general solution for $\{\lambda_k\}_1^n$ satisfying Eq (3.26), into Eq (3.28) gives an equation that can be written as

$$[\mathbf{r}_g] = [\mathbf{N}_g] \sum_{k=1}^{d} \beta_{g,k} [\mathbf{N}_k][\mathbf{r}_k] + \sum_{j=d+1}^{n} \mu_j [\mathbf{R}(\gamma_g - \gamma_j)] \left([\mathbf{N}_j] \sum_{k=1}^{d} \beta_{j,k} [\mathbf{N}_k][\mathbf{r}_k] - [\mathbf{r}_j] \right), \tag{3.29}$$

where Eq (3.24) has been used for simplification. Equation (3.29) is in a form that is open to interpretation. It can be stated immediately that:

Proposition 3.3.2. *If $n = d$ and $\mathbf{u}_g \in \langle\{\mathbf{u}_k\}_1^n\rangle$, then there is a* unique *point, P_g, such that $\mathsf{A}(P_g, \mathbf{u}_g) \in \langle\{\mathsf{A}_k\}_1^n\rangle$. This point is referred to as the* generated point *for the direction, $\mathbf{u}_g$, is denoted by $P_g(\mathbf{u}_g)$, and can be calculated using Eq* (3.29).

Definition 3.3.1. The unique point, $P^*(\mathbf{u})$, dignified by the property that $\mathsf{A}(P^*(\mathbf{u}), \mathbf{u})$ is generated by the *principal accelerometers* is referred to as the *principally generated point for the direction*, $\mathbf{u}$.

According to Eq (3.29) the coordinate matrix of $P^*(\mathbf{u}_g)$ is

$$[\mathbf{r}^*(\mathbf{u}_g)] = [\mathbf{N}_g] \sum_{k=1}^{d} \beta_{g,k} [\mathbf{N}_k][\mathbf{r}_k]. \tag{3.30}$$

Substituting Eq (3.30) into Eq (3.29) gives

$$[\mathbf{r}_g] = [\mathbf{r}^*(\mathbf{u}_g)] + \sum_{j=d+1}^{n} \mu_j [\mathbf{R}(\gamma_g - \gamma_j)]([\mathbf{r}^*(\mathbf{u}_j)] - [\mathbf{r}_j]). \tag{3.31}$$

Thus, it has been shown that:

Proposition 3.3.3. *If $n > d$ and $\mathbf{u}_g \in \langle\{\mathbf{u}_k\}_1^n\rangle$, the point, P_g, such that $\mathsf{A}(P_g, \mathbf{u}_g) \in \langle\{\mathsf{A}_k\}_1^n\rangle$ can lie anywhere in the affine subspace, referred to as the* generated affine subspace for the direction, $\mathbf{u}_g$, *through the point, $P^*(\mathbf{u}_g)$, that is directed by the Euclidean subspace spanned by the $n-d$ vectors with component matrices*

$$[\mathbf{R}(\gamma_g - \gamma_j)]([\mathbf{r}^*(\mathbf{u}_j)] - [\mathbf{r}_j]) \qquad j = d+1, \ldots, n.$$

The utility of this result is that one only ever needs to consider accelerometers generated by a principal set.

3.3.1 One Accelerometer

Obviously, when there is one accelerometer, $n = d = 1$, and generation is only possible[1] for $\mathbf{u}_g = \mathbf{u}_1$. Applying Proposition 3.3.2 shows that $P_g = P_1$, i.e., only trivial generation is possible.

Having identified the accelerometers generated by a single accelerometer, the conditions for the independence of two accelerometers can be stated.

Conditions for Independence of Two Accelerometers Two accelerometers are independent unless they are coincident and have the same direction.

3.3.2 Two Accelerometers

In this section it is assumed that the conditions for the independence of two accelerometers that were just presented are satisfied. This approach is repeated in the coming sections; the conditions for independence for n accelerometers are identified by studying the accelerometers generated by an independent $n-1$ accelerometer configuration.

When there are two accelerometers ($n = 2$) there are two distinct possibilities, they are parallel ($d = 1$) or their directions span the plane of motion ($d = 2$).

3.3.2.1 Parallel Accelerometers

Here, again, generation is only possible for $\mathbf{u}_g = \mathbf{u}_1 (= \mathbf{u}_2)$. Since $n > d$, Proposition 3.3.3 indicates that the generated affine subspace for the direction, $\mathbf{u}_1$, is the line through $P^*(\mathbf{u}_1) = P_1$ (according to Section 3.3.1) that is directed by the vector from P_2 to $P^*(\mathbf{u}_1) = P_1$. This can be stated compactly as

$$\langle \mathsf{A}(P_1, \mathbf{u}_1), \mathsf{A}(P_2, \mathbf{u}_1) \rangle = \mathsf{A}(\langle P_1, P_2 \rangle, \mathbf{u}_1), \tag{3.32}$$

[1]The condition $\mathbf{u}_g \in \langle \mathbf{u}_1 \rangle$ can be transformed in the strict equality using the switching of sense discussed at Remark 2.3.2.

where $\langle P_1, P_2 \rangle$ denotes the line through P_1 and P_2. In words: *a parallel pair of accelerometers generates all parallel accelerometers on the line through them.* This is illustrated in Fig 3.3.

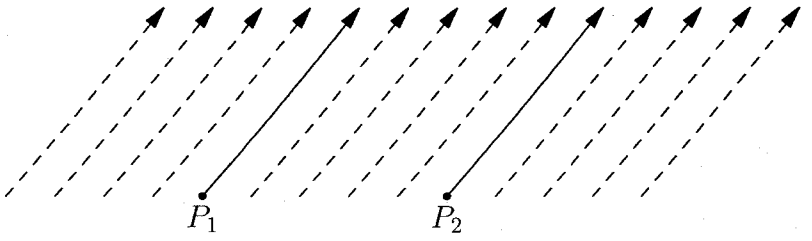

Figure 3.3: The accelerometers generated by a parallel pair.

3.3.2.2 Non-Parallel Accelerometers

When $\mathbf{u}_1 \neq \mathbf{u}_2$, $n = d = 2$, and Proposition 3.3.2 indicates that there is a unique generated point, $P_g(\mathbf{u}_g) = P_g(\gamma_g)$, for each $\mathbf{u}_g$, in the plane of motion and that this point has the coordinate matrix,

$$[\mathbf{r}_g(\gamma_g)] = \beta_{g,1}[\mathbf{R}(\gamma_g - \gamma_1)][\mathbf{r}_1] + \beta_{g,2}[\mathbf{R}(\gamma_g - \gamma_1)][\mathbf{r}_2], \tag{3.33}$$

where Eq (3.24) has been used to simplify the products $[\mathbf{N}_g][\mathbf{N}_k]$. The required algebra can be simplified by choosing the coordinate system such that

$$[\mathbf{r}_1] = -[\mathbf{r}_2] = \begin{bmatrix} h \\ 0 \end{bmatrix}, \tag{3.34}$$

where $2h$ is the distance between P_1 and P_2. Making this choice and substituting from Eq (3.16) for $\beta_{g,1}$ and $\beta_{g,2}$ shows that

$$[\mathbf{r}_g(\gamma_g)] = \frac{h}{\sin(\gamma_2 - \gamma_1)}[\mathbf{R}(2\gamma_g - \gamma_1 - \gamma_2)] \begin{bmatrix} 0 \\ 1 \end{bmatrix} + [\mathbf{r}_C] \tag{3.35}$$

where

$$[\mathbf{r}_C] = -\begin{bmatrix} 0 \\ h\cot(\gamma_2 - \gamma_1) \end{bmatrix}. \tag{3.36}$$

In this form it is clear that the locus of generated points, $P_g(\gamma_g)$, that is swept out for $\gamma_g \in [0, \pi)$, is a circle of radius $h/|\sin(\gamma_2 - \gamma_1)|$ that is centered at the point, C, with coordinate matrix, $[\mathbf{r}_C]$. If $\gamma_2 > \gamma_1$ then C is 'below' the line through P_1 and P_2, as is shown in Fig 3.4, otherwise it is 'above'. In the following, it is assumed that $\gamma_2 > \gamma_1$, but the details in the opposite case are simple modifications.

It follows from Eq (3.35) that

$$[\mathbf{r}_g(\gamma_g)] - [\mathbf{r}_C] = [\mathbf{R}(2(\gamma_g - \gamma_1))]([\mathbf{r}_g(\gamma_1)] - [\mathbf{r}_C]), \tag{3.37}$$

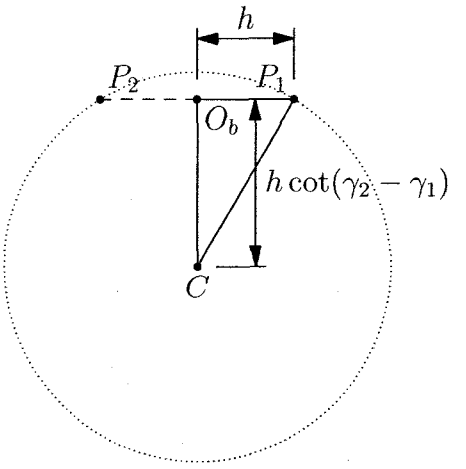

Figure 3.4: The relationship between P_1, P_2 and C when $\gamma_2 > \gamma_1$.

that is, $\angle P_1 C P_g(\gamma_g) = 2(\gamma_g - \gamma_1)$. Using a well-known theorem on angles measured between points on circles, if Q is any point on the circle, then [49]

$$\angle P_1 Q P_g(\gamma_g) = \frac{1}{2}\angle P_1 C P_g(\gamma_g) = \gamma_g - \gamma_1. \tag{3.38}$$

Let X denote the point on the circle that intersects the line through P_1 directed by $\mathbf{u}_1$. If this line is rotated about X by $\gamma_g - \gamma_1$, it will, according to Eq (3.38) pass through $P_g(\gamma_g)$. This realization leads to a simple method of identifying the dependent point for each accelerometer direction:

1. Extend the lines through P_1 and P_2 that are directed, respectively, by $\mathbf{u}_1$ and $\mathbf{u}_2$, to their point of intersection, X.

2. Draw the unique circle, Ψ, through P_1, P_2 and X.

3. The intersection of any line through X with Ψ, is the generated point for the accelerometer parallel to that line.

An example of this construction is shown in Fig 3.5.

It has been implicitly assumed that the distance, $2h$, between P_1 and P_2, is non-zero, but the analysis does not require this. Thus, when there are two coincident, non-parallel accelerometers, the circular distribution shrinks to a single point and the generation that occurs can be compactly stated as

$$\mathsf{A}(P_1, \langle \mathbf{u}_1, \mathbf{u}_2 \rangle) = \langle \mathsf{A}(P_1, \mathbf{u}_1), \mathsf{A}(P_1, \mathbf{u}_2) \rangle . \tag{3.39}$$

Thus, as is illustrated in Fig 3.6 *a pair of coincident accelerometers generate all accelerometers at that point with direction in the plane spanned by them.*

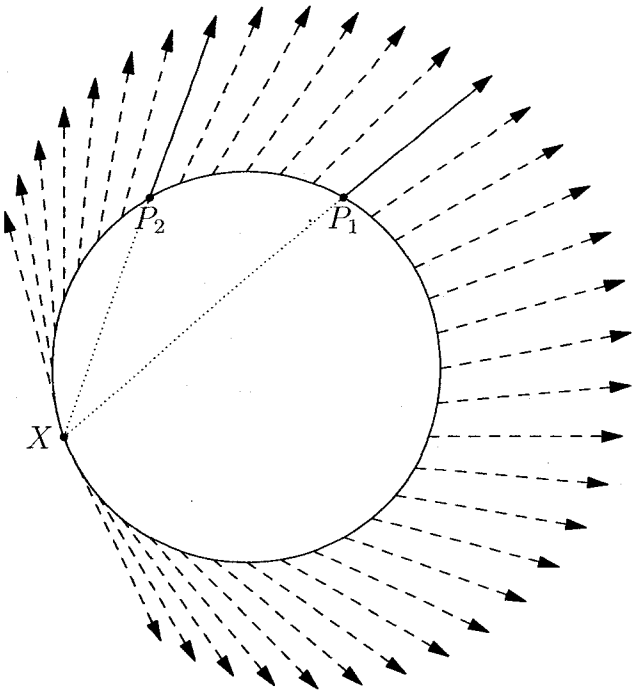

Figure 3.5: The accelerometers generated by a non-parallel, non-coincident pair.

Conditions for Independence of Three Accelerometers Assuming no 2 of the accelerometers are dependent, a configuration of 3 accelerometers involving

- a parallel pair is independent unless the third accelerometer is parallel to the first two *and* located on the line through them.
- a pair of non-parallel accelerometers is independent unless the lines drawn through the accelerometers parallel to their directions intersect at a single point, *and* there is a circle through the three accelerometers and the point of intersection.

Remark 3.3.1. The results obtained for the configuration of three accelerometers involving a parallel pair can be considered a special case of that involving non-parallel accelerometers by letting the radius of the circle and the point of intersection of the three lines tend to infinity. The parallel case could be referred to as 'projectively equivalent' to the general case [50].

3.3.3 Three Accelerometers

When $n = 3$, there are, again, two cases to consider: that where all accelerometers are parallel ($d = 1$) and that where they span the plane of motion ($d = 2$).

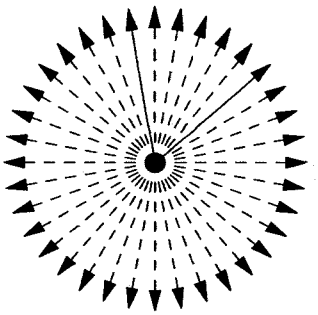

Figure 3.6: The accelerometers generated by a coincident non-parallel pair.

3.3.3.1 Parallel Accelerometers

According to the summary of Section 3.3.2.1, a configuration of 3 parallel accelerometers is independent if and only if there is no line through the accelerometers' locations, i.e., if $\langle P_1, P_2, P_3 \rangle$ is the plane of motion. Using Proposition 3.3.3, shows that the generated affine subspace in this case is that through $P^*(\mathbf{u}_1) = P_1$ directed by the vectors from P_2 to P_1 and from P_3 to P_1, thus:

$$\left\langle \{\mathsf{A}(P_i, \mathbf{u}_1)\}_1^3 \right\rangle = \mathsf{A}(\langle P_1, P_2, P_3 \rangle, \mathbf{u}_1) \tag{3.40}$$

In words: *three parallel accelerometers generate all parallel accelerometers on the plane through them.* This is shown in Fig 3.7

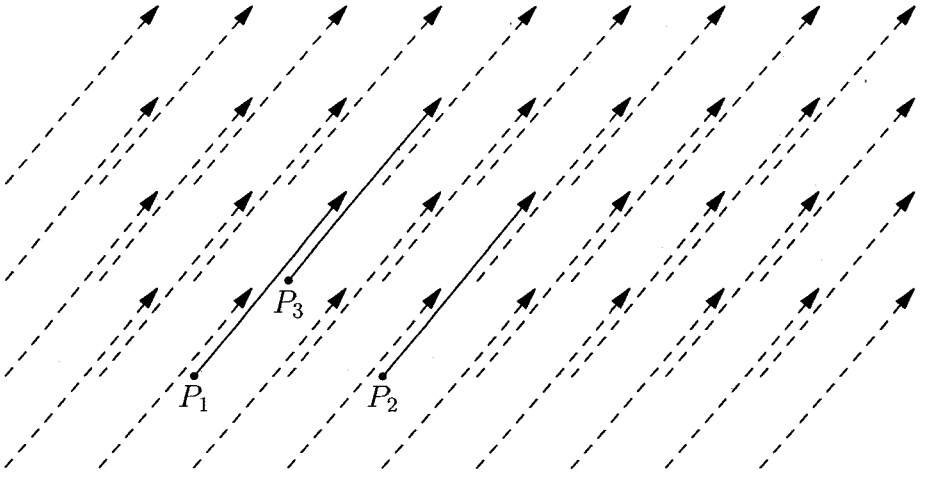

Figure 3.7: The accelerometers generated by three parallel accelerometers with no line through their locations.

3.3.3.2 Non-Parallel Accelerometers

Proposition 3.3.3 indicates that the generated affine subspace for the direction, $\mathbf{u}_g$, is the line through the principally generated point, $P^*(\mathbf{u}_g)$, directed by the vector obtained by rotating that from P_3 to $P^*(\mathbf{u}_3)$ through the angle, $\gamma_g - \gamma_3$. In particular, the generated affine subspace for the direction, $\mathbf{u}_3$, is the line through P_3 and $P^*(\mathbf{u}_3)$, as is shown in Fig 3.8. This line intersects the circle, Ψ, defined by the principal[2] accelerometers, at a point, F, referred to as the *focus.*

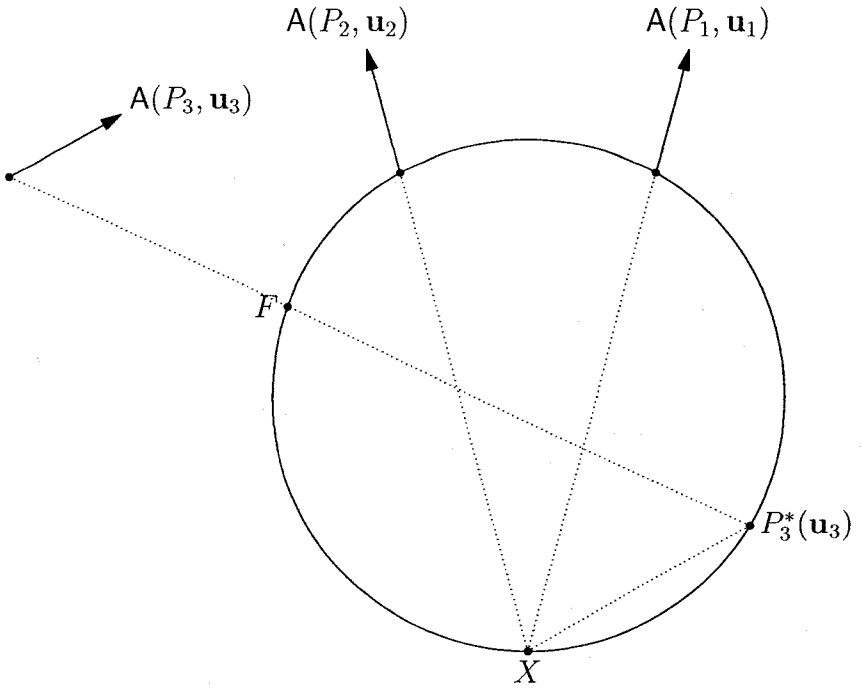

Figure 3.8: The construction for the focus, F

For any other direction, $\mathbf{u}_g$, the principally generated point (according to Section 3.3.2.2) satisfies

$$\angle P^*(\mathbf{u}_3) F P^*(\mathbf{u}_g) = \gamma_g - \gamma_3.$$

Since the generated affine subspace for the direction, $\mathbf{u}_g$, is parallel to the line obtained by rotating the vector from F to $P^*(\mathbf{u}_3)$ by $\gamma_g - \gamma_3$, it follows that the generated affine subspace for *every* $\mathbf{u}_g$ in the plane also passes through F, and the following construction for the generated affine subspaces is obtained:

[2]Recall from Definition 3.2.1 that the principal accelerometers are any d accelerometers with directions that span $\langle \{\mathbf{u}_k\}_1^n \rangle$; in this case a pair of non-parallel accelerometers, and that it is assumed that they are labelled as the first d accelerometers.

1. Choose two non-parallel accelerometer as the principal accelerometers and construct the circle of generated points, Ψ, as described in Section 3.3.2.2.

2. Draw the line through P_3 and $P^*(\mathbf{u}_3)$ and find the point of intersection, F of the line and Ψ.

3. Each line through F is the generated affine subspace for the direction for which the point of intersection of the line and Ψ, that is not F, is a principally generated point.

This is illustrated for a small number of choices of direction in Fig 3.9. When all possible directions are considered, the lines fill all of the plane. Since F is at the intersection of the generated affine subspaces for each direction it follows that F is a generated point for every direction, i.e., an accelerometer of any direction at F will yield a dependent configuration.

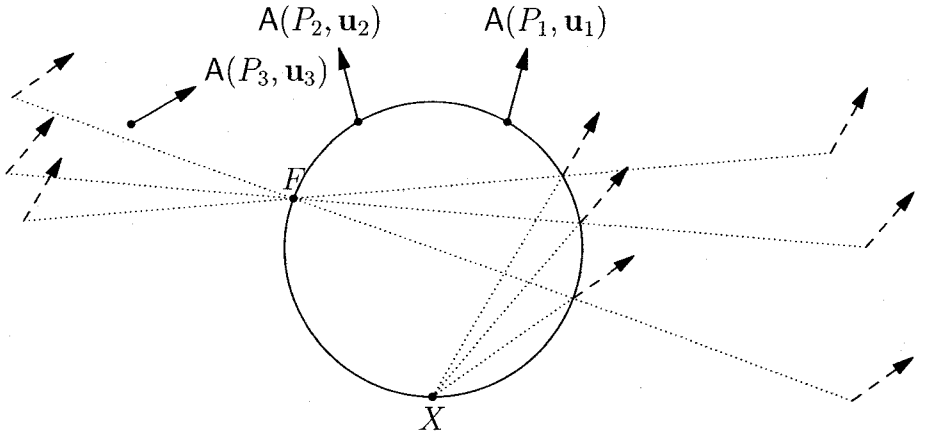

Figure 3.9: Some of the infinite number of accelerometers generated by three non-parallel accelerometers. Each possible line through F is the dependent subspace for a unique direction. The initial construction is taken from Fig 3.8.

A subtly different method of obtaining this result is of interest. This method starts in the same way; by finding the generated affine subspace for the direction, $\mathbf{u}_3$, and identifying the point, F. Then, since $F \in \langle P_3, P^*(\mathbf{u}_3)\rangle$, the results for the generation by a parallel pair indicate that

$$\mathsf{A}(F, \mathbf{u}_3) \in \langle \mathsf{A}(P_3, \mathbf{u}_3), \mathsf{A}(P^*(\mathbf{u}_3), \mathbf{u}_3)\rangle$$

and since

$$\mathsf{A}(P^*(\mathbf{u}_3), \mathbf{u}_3) \in \langle \{\mathsf{A}_k\}_1^n \rangle ,$$

it can be concluded that $\mathsf{A}(F, \mathbf{u}_3)$ is generated by the 3 accelerometers:

$$\mathsf{A}(F, \mathbf{u}_3) \in \left\langle \{\mathsf{A}_k\}_1^3 \right\rangle .$$

Now, F is the principally generated point for some direction, $\mathbf{u}_F \neq \mathbf{u}_3$, so, using the results regarding the generation of a coincident pair of accelerometers it is possible to generate any accelerometer at F:

$$\langle \mathsf{A}(F, \mathbf{u}_F), \mathsf{A}(F, \mathbf{u}_3) \rangle = \mathsf{A}(F, \langle \mathbf{u}_F, \mathbf{u}_3 \rangle).$$

Since $\mathsf{A}(F, \mathbf{u}_F)$ and $\mathsf{A}(F, \mathbf{u}_3)$ are both generated by $\{\mathsf{A}_k\}_1^3$, it follows that every accelerometer at F with coplanar direction is generated by $\{\mathsf{A}_k\}_1^3$:

$$\mathsf{A}(F, \mathbf{u}_g) \in \left\langle \{\mathsf{A}_k\}_1^3 \right\rangle \quad \forall \mathbf{u}_g \in \langle \mathbf{u}_F, \mathbf{u}_3 \rangle .$$

Finally, the affine subspace for any direction, $\mathbf{u}_g$, can be identified as the line through F and $P^*(\mathbf{u}_g)$ by again using the results of Section 3.3.2.1, i.e., those for the generation of parallel accelerometers.

Conditions for Independence of Four Accelerometers Assuming no 3 of the accelerometers are dependent, a configuration of 4 accelerometers involving

- 3 parallel accelerometers is independent unless the fourth accelerometer is also parallel, in which case the configuration is always dependent.
- at least 2 non-parallel accelerometers is independent unless the fourth accelerometer[3] lies on the line, L, obtained via the following construction:
  - a circle, Ψ, is drawn through the location of the principal accelerometers and the point of intersection, X, of the lines drawn through their locations parallel to their directions.
  - a point F on Ψ is found as the intersection of the line through the location of the third accelerometer and the point on Ψ that is, itself, the intersection of the line through X that is parallel to the third accelerometer.
  - the line L is obtained by rotating the line through F and the location of the third accelerometer about F through the angle between the directions of the third and fourth accelerometers.

[3]There is freedom in selecting which of the two non-principal accelerometers is the 'fourth'.

A special but important configuration of four accelerometers is that of two coincident pairs:

$$\{\mathsf{A}(P_A, \mathbf{u}_1), \mathsf{A}(P_A, \mathbf{u}_2), \mathsf{A}(P_B, \mathbf{u}_3), \mathsf{A}(P_B, \mathbf{u}_4)\}$$

with $\mathbf{u}_2 \neq \mathbf{u}_1$ and $\mathbf{u}_4 \neq \mathbf{u}_3$. This configuration is easily shown to be independent as long as $P_A \neq P_B$. Taking the accelerometers at P_A to be the principal accelerometers, leads to a circle, Ψ of zero radius at P_A, which is therefore equal to X and F. Rotating the line through $P_A = F$ and P_B by the angle $\gamma_4 - \gamma_3$ leads to a line that does not pass through P_B unless $\gamma_4 = \gamma_3$.

3.4 Examples

In this section two examples of planar configuration are presented. The first example illustrates planar configuration design using the results obtained using the previous section. The second example takes its motivation from the first and investigates the existence of configurations that are optimal in some sense.

3.4.1 First Example

The design process afforded by the results of Section 3.3 is incremental. At each step, one adds an accelerometer to an existing configuration so that the result is not dependent, i.e., so that it is not identical to any of the accelerometers generated by the existing configuration. As more accelerometers are added, the conditions that the next accelerometer must satisfy (or avoid) become more stringent.

The placement of the first accelerometer is completely arbitrary. Indeed since the independence of accelerometers is a geometric concept, the position and orientation of an accelerometer is meaningless until a second accelerometer is added. The only condition that the placement of the second accelerometer needs to satisfy is that it must not be identical to the first. In this particular example, the first two accelerometers are chosen to have orthogonal directions, as shown in Fig 3.10. This accelerometer pair generates a circular distribution of accelerometers, through X, P_1 and P_2. The generated accelerometer at the point, Q, diametrically opposite X is parallel to the line from X to Q. The independence of the 3 accelerometer configuration can therefore be ensured by placing an accelerometer at Q that is orthogonal to the line from X to Q, as is shown in Fig 3.10. Placing the third accelerometer on the circle makes F, the focus, coincide with P_3, and the generated affine subspace for each direction of accelerometer therefore passes through P_3. It is decided (mainly to keep the geometry simple) that the final accelerometer is to be placed at the intersection of two lines: that through P_2 and P_3 and that through X orthogonal to the line through X and P_3. Since the line through $F = P_3$ intersects the circle at

P_2, the generated accelerometer at the prospective location has the direction, $\mathbf{u}_2$. Thus, as long as the fourth accelerometer does not have the same direction as the second, the configuration will be independent, and it will be possible to solve the equation,

$$[\mathsf{C}_4][\mathbf{S}] = [\mathbf{a}_4], \tag{3.41}$$

for the SFSM, $[\mathbf{S}]$. Given the freedom in the choice of direction of the fourth

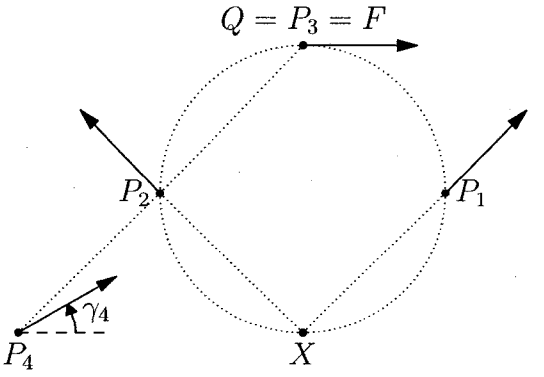

Figure 3.10: Three accelerometers, and the accelerometer generated by them at P_4.

accelerometer (regarding the rest of the accelerometers as fixed), one may wonder what the *best* choice is. Intuition suggests that choosing $\mathbf{u}_4$ so that it is orthogonal to the direction of the accelerometer generated at P_4 by $\{\mathsf{A}_k\}_1^3$ at that point will lead to an accelerometer that is 'maximally independent'. This intuition is confirmed in Fig 3.11, which shows the absolute value of determinant of $[\mathsf{C}_4]$ as a function of the direction of the fourth accelerometer. The determinant attains maximum magnitude at $\gamma_4 = \frac{\pi}{4}$, and is equal to 0 at $\gamma_4 = \frac{3\pi}{4} = \gamma_2$.

Maximizing the size of the determinant ensures that the matrix is 'far' from singular, but does not necessarily imply any robustness of the configuration, i.e., it does not show how much errors in the accelerometer measurements or configuration itself may be magnified in solving for the SFSM. A more appropriate measure is the *condition number* of the configuration matrix [51, 52]:

$$\kappa[\mathsf{C}_4^{\mathcal{B}}] \equiv \|[\mathsf{C}_4^{\mathcal{B}}]\|\|[\mathsf{C}_4^{\mathcal{B}}]^{-1}\|, \tag{3.42}$$

where $\|[\mathsf{C}_4^{\mathcal{B}}]\|$ denotes some matrix norm, here the *spectral norm*, i.e., the maximum singular value of $[\mathsf{C}_4^{\mathcal{B}}]$. Parsa et al. recently used the condition number of a 12 accelerometer spatial configuration as the cost function in an optimization algorithm [31].

The condition number, $\kappa[\mathsf{C}_4^{\mathcal{B}}]$, is useful because it establishes bounds [51] on the size of the error, $[\delta\mathbf{S}^{\mathcal{B}}]$, in the calculated SFSM, due to errors in the

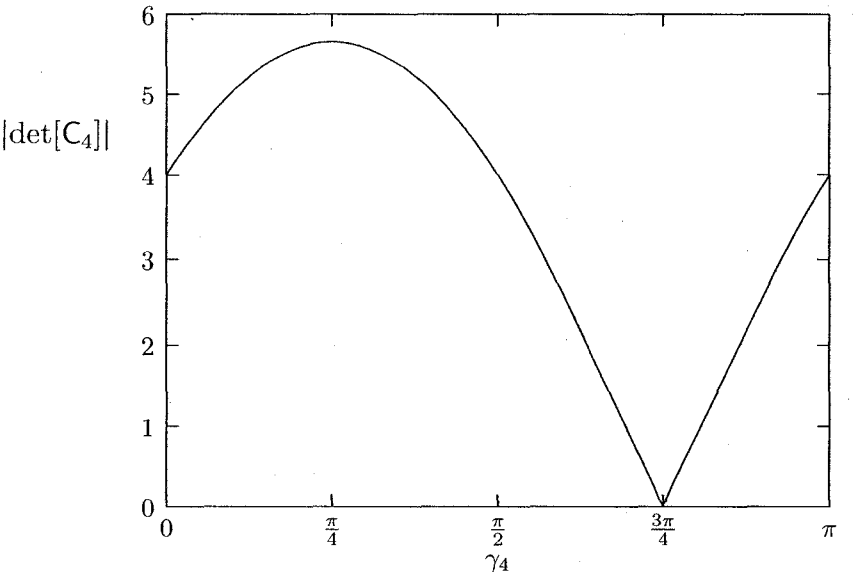

Figure 3.11: The absolute value of the determinant of $[\mathsf{C}_4]$ as a function of γ_4.

measurements $[\mathbf{a}_4]$, or errors in accelerometer configuration itself,

$$\frac{\|[\boldsymbol{\delta}\mathbf{S}^{\mathcal{B}}]\|}{\|[\mathbf{S}^{\mathcal{B}}]\|} \leq \kappa[\mathsf{C}_4^{\mathcal{B}}] \frac{\|\boldsymbol{\delta}[\mathbf{a}_4]\|}{\|[\mathbf{a}_4]\|} \tag{3.43}$$

$$\frac{\|[\boldsymbol{\delta}\mathbf{S}^{\mathcal{B}}]\|}{\|[\mathbf{S}^{\mathcal{B}}]\|} \leq \kappa[\mathsf{C}_4^{\mathcal{B}}] \frac{\|[\boldsymbol{\delta}\mathsf{C}_4^{\mathcal{B}}]\|}{\|[\mathsf{C}_4^{\mathcal{B}}]\|}. \tag{3.44}$$

Regardless of the norm used in the definition of the condition number, the smallest value it can achieve is unity:

$$\kappa[\mathsf{C}_4^{\mathcal{B}}] \geq 1. \tag{3.45}$$

If $\kappa[\mathsf{C}_4^{\mathcal{B}}] \approx 1$, the matrix is said to be *well-conditioned*, whereas if $\kappa[\mathsf{C}_4^{\mathcal{B}}]$ is 'large' it is said to be *ill-conditioned* and small errors in the accelerometer measurements or configuration can lead to large errors in the calculated SFSM.

It may have been noticed that the specification of the frame in which the configuration matrix is expressed has suddenly again been made explicit. This is not accidental. While the determinant of the configuration matrix is invariant to the choice of the frame, the same cannot be said of the singular value decomposition of a configuration matrix, and, hence, its condition number. Reference to Eq (3.8) shows that the ADM transformation matrix, $[\Pi_{\mathcal{B}}^{\mathcal{C}}]$, is an orthogonal matrix if and only if $O_B = O_C$, i.e., when the two frames share their origin. Under this condition, the singular values of $[\mathsf{C}_4^{\mathcal{B}}]$ are identical to those of

$$[\mathsf{C}_4^{\mathcal{C}}] = [\mathsf{C}_4^{\mathcal{B}}][\Pi_{\mathcal{B}}^{\mathcal{C}}],$$

so

$$\kappa[\mathsf{C}_4^{\mathcal{C}}] = \kappa[\mathsf{C}_4^{\mathcal{B}}] \qquad \text{if} \quad O_B = O_C. \tag{3.46}$$

What this means is that when specifying the condition number of a planar accelerometer configuration, one needs to specify the origin of the coordinate system used; the orientation of the basis is immaterial. This dependence of the condition number upon the origin of the frame will be further explored in the next example. Here for purposes of illustration, the origin is chosen at X. While there is 'little correlation' [52] between the determinant and the condition number, it is seen from Fig 3.12 that choosing the direction of the fourth accelerometer so that it is orthogonal to the generated accelerometer comes close to minimizing, $\kappa[\mathsf{C}_4^{\mathcal{B}}]$. The actual minimum occurs at $\gamma_4 \approx 39°$, 6° from the intuitively selected γ_4.

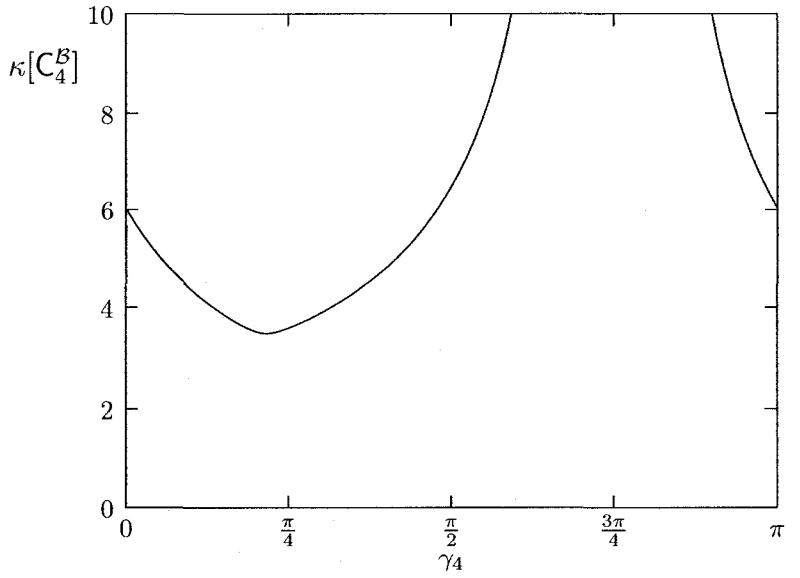

Figure 3.12: The condition number of $[\mathsf{C}_4^{\mathcal{B}}]$ with origin, X, as a function of γ_4.

3.4.2 Second Example

The consideration of the condition number in the previous example motivates one to wonder whether it is possible to design a configuration that is optimal in the sense that it has the smallest possible condition number, 1. Such a configuration should, theoretically, have the greatest robustness to measurement errors.

It is shown in Appendix D that if $[\mathsf{C}_4^{\mathcal{B}}]$ has unit condition number, then

$$[\mathsf{C}_4^{\mathcal{B}}][\mathsf{C}_4^{\mathcal{B}}]^T = \sigma^2[I]_4. \tag{3.47}$$

Equation (3.47) is a compact way of writing the following 10 conditions:

$$[\mathsf{A}_k^{\mathcal{B}}][\mathsf{A}_k^{\mathcal{B}}]^T = \sigma^2 \qquad k = 1, 2, 3, 4 \tag{3.48}$$

$$[\mathsf{A}_k^{\mathcal{B}}][\mathsf{A}_l^{\mathcal{B}}]^T = 0 \qquad k \neq l. \tag{3.49}$$

Referring to Eq (3.7), Eq (3.48) can be rewritten as

$$1 + \|\mathbf{r}_{P_k/O_B}\|^2 = \sigma^2 \qquad k = 1, 2, 3, 4, \tag{3.50}$$

thus, the four accelerometers must be chosen the same distance from O_B. For simplicity this distance is taken as 1 unit. Setting $\|\mathbf{r}_{P_k/O_B}\| = \|\mathbf{r}_{P_l/O_B}\| = 1$ in the equation obtained from substituting Eq (3.7) into Eq (3.49) gives

$$\cos(\gamma_k - \gamma_l) + \cos((\gamma_k - \phi_k) - (\gamma_l - \phi_l)) = 0 \qquad k \neq l. \tag{3.51}$$

This is a set of 6 nonlinear equations in 8 unknowns: $\{\phi_k\}_1^4$ and $\{\gamma_k\}_1^4$, the angles specifying the location and direction of the 4 accelerometers. Choosing ϕ_1 and γ_1 arbitrarily reduces the number of unknowns to the number of equations. These equations were solved numerically using GNU Octave's function, `fsolve.m` [53]. While the region of convergence was not analysed, the method did yield a solution with unit condition number for every initial condition that was tried.

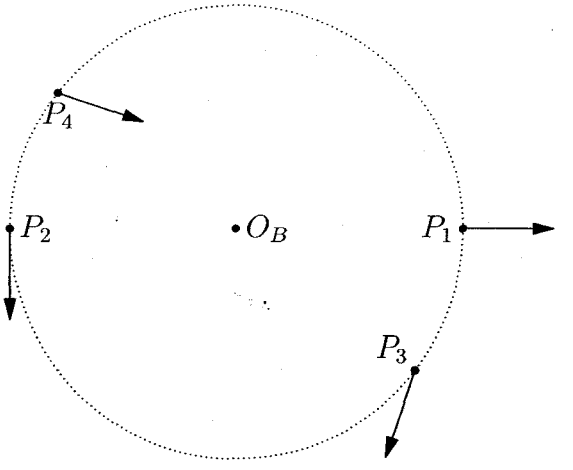

Figure 3.13: One configuration that has unit condition number with origin, O_B.

Figures 3.13 and 3.14 show two configurations obtained using this method. In the first design the angle measured from P_1 to P_3 is equal to that from P_2 to P_4, and the accelerometers are in two orthogonal pairs. The second design, consists of two coincident orthogonal pairs at diametrically opposite points. The orientation of the pair on the left is immaterial; if the accelerometers on

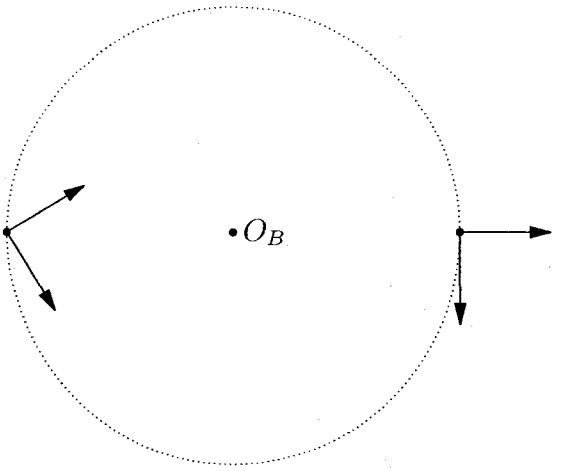

Figure 3.14: A biaxial configuration that has unit condition number with origin, O_B.

the left are rotated so that they are parallel to those on the right, the condition number is still unity.

Figure 3.15 shows the variation in the condition number of the configuration in Fig 3.14 as the origin is shifted across the unit circle along any diameter. Using the location of one of the biaxial accelerometers for the origin ($x = \pm 1$) results in a condition number of around 2.7, indicating that the possible 'error magnification' is nearly 3 times that when the origin is located at the center. Regardless of the location of O_B, the calculation for ω^2 and α is the same, so the explanation for the growth in the condition number must be associated with the calculation of the specific force at the origin. When the origin is at the midpoint, each of the four accelerometers makes an equal contribution to calculating the specific force, whereas when O_B is at one of the accelerometer locations, only two accelerometers are used. It is believed that this lack of symmetry in the calculation leads to the growth in condition number.

3.5 Minimal Planar Configurations

The focus of the last two sections has been the design of planar configurations of 4 accelerometers that can be used to obtain the SFSM in its entirety. Such configurations allow the 'full' GFIN algorithm described in Section 2.4.4 to be applied. That same section also discussed minimal GFIN, and the design of planar configurations for use with this algorithm is now considered.

The spatial MGFIN algorithm requires that 6 parameters be isolated from the measurements: the elements of $[\mathbf{s}^{\boldsymbol{b}}_{O_B}]$ and $[\boldsymbol{\alpha}^{\boldsymbol{b}}]$. In the case of planar motion these 6 elements are reduced to 3; the two elements of $[\mathbf{s}^{\boldsymbol{b}}_{O_B}]$ and α, and the

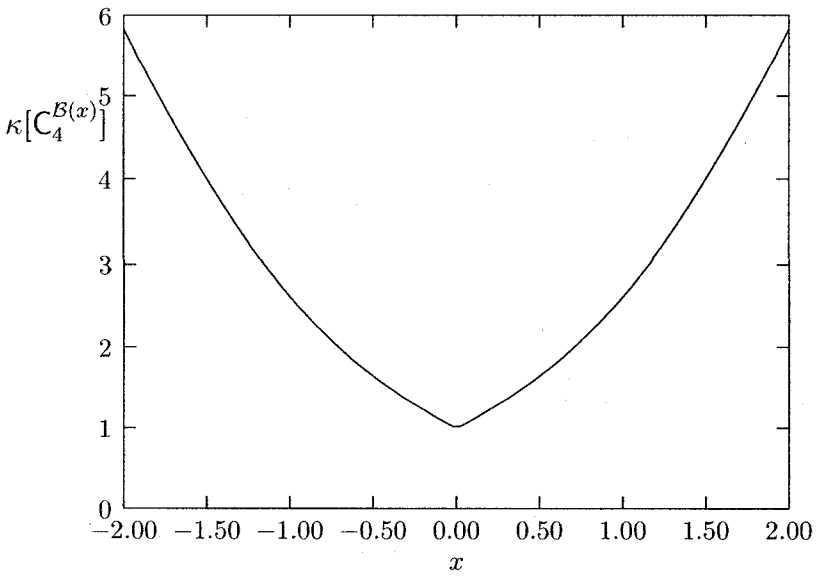

Figure 3.15: The condition number of the configuration in Fig 3.14 as a function of the location of the origin.

equivalent of Eq (2.33) is

$$[\mathbf{M}_n^{\mathcal{B}}] \begin{bmatrix} [\mathbf{s}_{O_B}^{\boldsymbol{b}}] \\ \alpha \end{bmatrix} = [\mathbf{a}_n] + [\mathbf{q}_n^{\mathcal{B}}]\omega^2, \tag{3.52}$$

where $[\mathbf{M}_n^{\mathcal{B}}]$ is an $n \times 3$ matrix with i^{th} row:

$$[\mathbf{m}_i^{\mathcal{B}}] = \left[[\mathbf{u}_i^{\boldsymbol{b}}]^T \quad [\mathbf{u}_i^{\boldsymbol{b}}]^T [J] [\mathbf{r}_i^{\mathcal{B}}] \right], \tag{3.53}$$

and $[\mathbf{q}_n^{\mathcal{B}}]$ is an $n \times 1$ matrix with i^{th} element

$$q_i^{\mathcal{B}} = [\mathbf{u}_1^{\boldsymbol{b}}]^T [\mathbf{r}_1^{\mathcal{B}}] = \mathbf{u}_i \cdot \mathbf{r}_{P_i/O_B}. \tag{3.54}$$

Given that there are 3 parameters of interest, 3 accelerometers are required for planar MGFIN, and they must be arranged so that the matrix, $[\mathbf{M}_3^{\mathcal{B}}]$, is non-singular. This requirement can be rephrased by using the following definition:

Definition 3.5.1. A set of n accelerometers is said to be *minimally independent* if the corresponding rows of $[\mathbf{M}_n^{\mathcal{B}}]$ are linearly independent.

Proposition 3.5.1. *Planar MGFIN requires* 3 *minimally independent accelerometers; such a set is referred to as a* minimal configuration.

The matrix relating $[\mathbf{m}_i^{\mathcal{B}}]$ and $[\mathbf{m}_i^{\mathcal{C}}]$ for some other frame[4], $\mathcal{C}$, is the upper-left 3×3 block of $[\Pi_{\mathcal{B}}^{\mathcal{C}}]$ as given in Eq (3.8). This 3×3 coordinate transformation

[4]Assumed, of course to be 'fitted' to the plane of motion in the same way as $\mathcal{B}$.

matrix is, like the matrix it was extracted from, of full rank (it has unit determinant), and this means that $\text{rank}[\mathbf{M}_n^{\mathcal{B}}] = \text{rank}[\mathbf{M}_n^{\mathcal{C}}]$ and, consequently, the concept of minimal independence is frame invariant. This also means that one is free to choose the frame to simplify the analysis of rank.

Since the minimal independence of accelerometers is defined in terms of the first three columns of the configuration matrix, it can be concluded that the minimal independence of a set of $n \leq 3$ accelerometers is a sufficient (not necessary) condition for the independence of the same set. More than 3 accelerometers are minimally dependent by definition. It should be noted, however, that the minimal dependence of $n \leq 3$ accelerometers does not imply the dependence of the same set.

The conditions under which *two* accelerometers are minimally dependent are studied first. A proposition summarising the result can be stated more compactly using the following definition:

Definition 3.5.2. The *line of the accelerometer*, $\mathsf{A}(P, \mathbf{u})$, is that passing through P directed by $\mathbf{u}$, $\mathscr{L}(P, \mathbf{u})$.

Proposition 3.5.2. *Two accelerometers are minimally dependent if and only if the lines of the accelerometers corresponding to them are identical.*

Proof. Two accelerometers are minimally dependent if some scalar, λ, can be found such that

$$[\mathbf{m}_1^{\mathcal{B}}] = \lambda[\mathbf{m}_2^{\mathcal{B}}].$$

Reference to Eq(3.53) shows that a necessary condition for this equality to hold is that

$$[\mathbf{u}_1^{\boldsymbol{b}}] = \lambda[\mathbf{u}_2^{\boldsymbol{b}}],$$

i.e., the accelerometers must have the same direction. Supposing that $\mathbf{u}_2 = \pm\mathbf{u}_1$, linear dependence requires that $\lambda = \pm 1$, i.e., $[\mathbf{m}_1^{\mathcal{B}}] = \pm[\mathbf{m}_2^{\mathcal{B}}]$, and the third element of this matrix equality is (regardless of the sign)

$$[\mathbf{u}_1^{\boldsymbol{b}}]^T[J][\mathbf{r}_1^{\mathcal{B}}] = [\mathbf{u}_1^{\boldsymbol{b}}]^T[J][\mathbf{r}_2^{\mathcal{B}}].$$

This equation can be rewritten as

$$[\mathbf{u}_1^{\boldsymbol{b}}]^T[J]([\mathbf{r}_1^{\mathcal{B}}] - [\mathbf{r}_2^{\mathcal{B}}]) = 0.$$

The null-space of $[\mathbf{u}_1^{\boldsymbol{b}}]^T[J]$ is one-dimensional and spanned by $[\mathbf{u}_1^{\boldsymbol{b}}]$, so the equality requires that

$$[\mathbf{r}_1^{\mathcal{B}}] + \mu[\mathbf{u}_1^{\boldsymbol{b}}] = [\mathbf{r}_2^{\mathcal{B}}]$$

showing that P_2 must lie on $\mathscr{L}(P_1, \mathbf{u}_1)$. Since it is also required that $\mathbf{u}_2 = \mathbf{u}_1$, the proposition has been proved. □

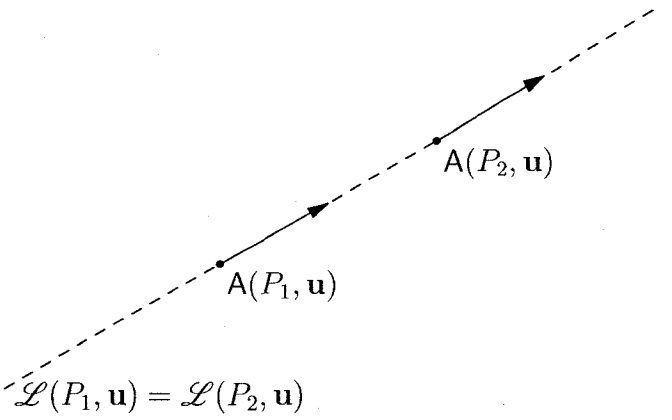

Figure 3.16: A pair of minimally dependent accelerometers.

Figure 3.16 shows two minimally dependent accelerometers. Since this pair is not coincident, they are independent.

Proposition 3.5.3. *Three accelerometers are minimally dependent if and only if one of the following conditions is satisfied*

- *the lines of the accelerometers are concurrent.*
- *the lines of the accelerometers are parallel.*

Proof. By definition, the 3 accelerometers are minimally dependent if and only if λ_1 and λ_2 can be found such that

$$\lambda_1[\mathbf{m}_1^{\mathcal{B}}] + \lambda_2[\mathbf{m}_2^{\mathcal{B}}] = [\mathbf{m}_3^{\mathcal{B}}]. \tag{3.55}$$

Reference to Eq (3.53) shows that a necessary condition for minimal dependence is that

$$\lambda_1[\mathbf{u}_1^{\boldsymbol{b}}] + \lambda_2[\mathbf{u}_2^{\boldsymbol{b}}] = [\mathbf{u}_3^{\boldsymbol{b}}]. \tag{3.56}$$

There are two distinct cases to consider; that where there is a pair of parallel accelerometers and that where there is not. The latter is considered first.

Assuming $\mathbf{u}_1 \neq \pm\mathbf{u}_2$, the lines, $\mathscr{L}(P_1, \mathbf{u}_1)$ and $\mathscr{L}(P_2, \mathbf{u}_2)$, must intersect. Taking, O_B, the origin of the coordinate system, to lie at this point of intersection, $[\mathbf{m}_1^{\mathcal{B}}]$ and $[\mathbf{m}_2^{\mathcal{B}}]$ become

$$[\mathbf{m}_1^{\mathcal{B}}] = \begin{bmatrix} [\mathbf{u}_1^{\boldsymbol{b}}]^T & 0 \end{bmatrix} \quad [\mathbf{m}_2^{\mathcal{B}}] = \begin{bmatrix} [\mathbf{u}_2^{\boldsymbol{b}}]^T & 0 \end{bmatrix}$$

so Eq (3.55) can only be satisfied if $[\mathbf{m}_3^{\mathcal{B}}]$ has a similar form, i.e., if

$$[\mathbf{u}_3^{\boldsymbol{b}}]^T[J][\mathbf{r}_3^{\mathcal{B}}] = 0.$$

Since the null-space of the matrix $[\mathbf{u}_3^{\boldsymbol{b}}]^T[J]$ is directed by $[\mathbf{u}_3^{\boldsymbol{b}}]$, dependence requires that $\mathbf{r}_{P_3/O_B} = \mu\mathbf{u}_3$, for some μ, i.e., that $\mathscr{L}(P_3, \mathbf{u}_3)$ passes through O_B, the point of intersection of the other two lines.

If $\mathbf{u}_1 = \mathbf{u}_2$, Eq (3.55) becomes

$$(\lambda_1 + \lambda_2)\mathbf{u}_1 = \mathbf{u}_3$$

which can only be satisfied if the third accelerometer is parallel to the first two. In fact, this can be seen to be a *sufficient* condition by choosing the basis, $\boldsymbol{b}$, so that $\mathbf{b}_1 = \mathbf{u}_1$, and the second column of $[\mathbf{M}_3^{\mathcal{B}}]$ is $[0]_{3\times 1}$, i.e., it is singular. □

The two conditions in this proposition are projectively equivalent, since parallel lines intersect at a point at infinity [50]. Figure 3.17 shows three minimally dependent accelerometers. According to the analysis in Section 3.3.3, this triple of accelerometers is dependent only if the circle through P_1, P_2 and P_3 also passes through the point of intersection of the lines of the accelerometers.

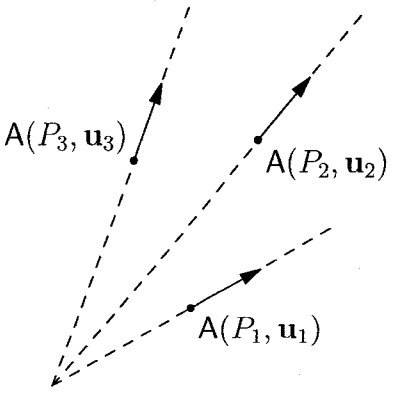

Figure 3.17: Three minimally dependent accelerometers.

In summary, any three accelerometers with lines that do not satisfy either of the conditions listed in Proposition 3.5.3 can be used for MGFIN. This conclusion could have been deduced more rapidly by a reader familiar with Plücker coordinates [54, 55], since the elements of $[\mathbf{m}_i^{\mathcal{B}}]$ are precisely the non-zero elements of the Plücker coordinates of the line $\mathscr{L}(P_i, \mathbf{u}_i)$.

3.5.1 Special Minimal Configurations

For an arbitrary minimal configuration, the solution of Eq (3.52) will require that a non-linear differential equation be solved for ω, since α will depend linearly upon ω^2. Reference to Eq (3.54) shows that the dependence of the i^{th} accelerometer measurement upon ω^2 can be removed by choosing $\mathbf{u}_i$ so that it is orthogonal to $\mathbf{r}_{P_i/O_B}$. Such an accelerometer is said to be *free* of ω^2. This concept of 'freedom' is, unlike independence and minimal independence, not frame-invariant. For example, if $\mathsf{A}(P_i, \mathbf{u}_i)$ is free of ω^2, i.e., $\mathbf{u}_i \cdot \mathbf{r}_{P_i/O_B} = 0$,

and O_b is shifted in any direction except parallel to $\mathbf{r}_{P_i/O_B}$, the freedom will be destroyed.

Definition 3.5.3. A minimally independent configuration of accelerometers all of which are free of ω^2 is a *special minimal configuration.*

It is clear that the equations required for the solution of MGFIN for a special minimal configuration are simpler than those for an arbitrary minimal configuration; α and $[\mathbf{s}^{\boldsymbol{b}}_{O_B}]$ are both obtained as linear combinations of the accelerometer measurements. This means that no nonlinear differential equation needs to be solved for ω, and $[\mathbf{s}^{\boldsymbol{b}}_{O_B}]$ does not depend upon the computed value of ω^2. One should therefore certainly prefer the use of a special minimal configuration, a symmetrical example of which is shown in Fig 3.18. The con-

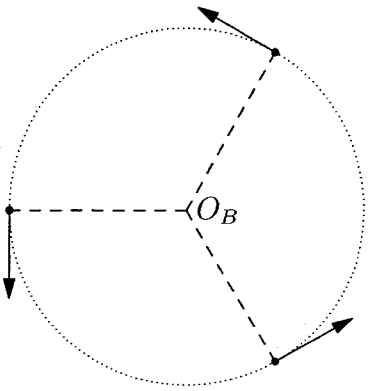

Figure 3.18: A planar special minimal configuration.

dition number of the configuration shown in Fig 3.18 is $\sqrt{2}$. It can be proved, by using the form of $[\mathbf{m}_i^{\mathcal{B}}]$ and the result proved in Appendix D, that it is impossible to design a minimal configuration (special or not) that has a unit condition number.

3.6 Summary

This chapter includes many important results. Among them are the identification of the dependent planar configurations and the specification of the geometrical requirements for minimal and special minimal configurations. These results allow the design of configurations of 3 and 4 accelerometers that can be used for GFIN. The brief investigation into the numerical properties of planar configurations and particularly the dependence of the condition number of a configuration upon the chosen origin are believed to be interesting.

Chapter 4

Spatial Accelerometer Configurations

This chapter is concerned with the investigation of the dependence of general accelerometer configurations. Since there are up to 12 independent accelerometers in a configuration, the analysis is considerably more complex than that for planar accelerometer configurations, as studied in the previous chapter, where there were only up to 4 independent accelerometers. The simple graphical constructions that were a feature of that chapter are replaced with descriptions of algebraic curves and surfaces associated with dependence. Given the large number of possible types of configuration of up to 12 accelerometers, this chapter cannot claim to be exhaustive in its presentation. A comparitively well-known problem that is similar to that at hand (in that it searches for dependencies between geometric elements) is the enumeration and description of 'screw systems' [55, 56]. These screw systems have applications in both statics and kinematics. There are a few key differences between the investigation of screw systems and that of sets of dependent accelerometers:

- there are 6 independent screws (as opposed to 12 independent accelerometers)
- the linear combination of screws is always another screw (this is not true for linear combinations of ADMs)
- a relationship between screw systems known as 'reciprocity' can be used so that screw systems 'generated' by $n > 3$ screws can be identified through knowledge of the systems of $6 - n$ screws (no such relationship has been identified for accelerometers)

Besides all these factors, the enumeration and description of the screw systems is certainly not a trivial task, and until recently, in the time-frame of screw theory at least, there was disagreement about whether all systems had been

described [57, 58]. The point is not that it is foreseen that the study of dependent accelerometer configurations is going to be as important as that of screw systems, but that this latter, 'smaller' problem has occupied very capable researchers over decades. Bearing this in mind, the main goals of this chapter are to identify groups of configurations sharing similar properties and to analyse the accelerometers generated by these configurations. As has been described in Chapters 2 and 3, the study of accelerometer generation is required for the identification of dependent configurations.

Section 4.1 summarises previous research on the independence of accelerometer configurations. Existing work is mainly concerned with ensuring the independence of a configuration capable of determining the entire SFSM. As is shown in that section, some of what has been reported in the literature is vague or incorrect. In Section 4.2 some general theory regarding accelerometer generation is presented. It is proved that if the directions of all the accelerometers in a configuration are rotated, then the accelerometers that the rotated configuration generates are exactly those obtained by rotating the directions of the accelerometers generated by the original configuration. The definition of a *constrained configuration* follows in Section 4.3. The constrained configurations are shown to be similar to vector subspaces in that if a linear combination of ADMs from a certain constrained configuration results in another ADM, it will describe an accelerometer in the same constrained configuration. A full constrained configuration is then introduced as a set of accelerometers that is loosely analogous to a basis in a vector subspace. Section 4.4 forms the most important part of the chapter. The accelerometers that are generated by the configurations obtained by successively removing accelerometers from full constrained configurations are studied and summarised.

4.1 Previous Work on Spatial Accelerometer Configurations

Few researchers have studied the conditions under which an accelerometer configuration is independent. When investigation has been done it is normally to prove that a certain configuration is independent, and therefore able to determine the SFSM. One common design of a 12 accelerometer configuration uses 4 non-coplanar triaxial accelerometers. This configuration was, it seems, first used by Kane et al. [14] in a biomechanical study of the forces exerted on a racket during tennis play. While this is not an application of GFIN, the requirement for the determination of the SFSM is the same. Hayes et al. have also used this configuration [13] in a study of human gait. The suggestion of the use of four or more triaxial accelerometers has become more common as accelerometers have become cheaper [15–17, 43]. These superabundant ac-

celerometers are, of course, not independent, but should improve the estimates of the SFSM if least squares techniques are used. That a set of four triaxial accelerometers is independent if and only if there is no plane through their locations is easy to prove, and follows from the fact that the specific force field is an affine vector field. Zappa et al. [22] offer a matrix based proof. Here it is proved using a simple vector approach and the fact that an accelerometer configuration is dependent if the measurements of some subset of accelerometers can always be written as a linear combination of the measurements of the remaining accelerometers. Each triaxial accelerometer essentially[1] yields a vector measurement of the specific force at that point. If triaxial accelerometers are located at P_i for $i = 1, \ldots, 4$, then the specific force vectors can be related by

$$\mathbf{s}_{P_j} - \mathbf{s}_{P_i} = \boldsymbol{\alpha} \times \mathbf{r}_{P_j/P_i} + \boldsymbol{\omega} \times (\boldsymbol{\omega} \times \mathbf{r}_{P_j/P_i}). \tag{4.1}$$

Suppose that P_1, P_2 and P_3 are collinear, then there exists λ such that $\mathbf{r}_{P_3/P_1} = \lambda \mathbf{r}_{P_2/P_1}$, and therefore,

$$\mathbf{s}_{P_3} - \mathbf{s}_{P_1} = \lambda(\boldsymbol{\alpha} \times \mathbf{r}_{P_2/P_1} + \boldsymbol{\omega} \times (\boldsymbol{\omega} \times \mathbf{r}_{P_2/P_1})) = \lambda(\mathbf{s}_{P_2} - \mathbf{s}_{P_1}),$$

i.e., the measurement of the triaxial accelerometer at P_3 can be written as a linear combination of those at P_1 and P_2. This proves that three triaxial accelerometers are not independent if they are collinear. If it is next assumed that the first three points are not collinear, but that the four points are coplanar, it is similarly proved that the specific force vector at P_4 can be written as a linear combination of the first three, proving that four triaxial accelerometers are dependent if they are located on a plane. Conversely, Eq (4.1) can be used to show that if the four points are not coplanar, then the specific force vector at any point in space can be written as a linear combination of $\mathbf{s}_{P_i}$ for $i = 1, \ldots, 4$.

Genin et al. [23], proposed a nine accelerometer configuration that they claimed would be able to determine the nine variables comprising $[\boldsymbol{\alpha}^b]$, $\mathrm{q}_{ij}([\boldsymbol{\omega}^b])$ and $\mathrm{q}_{ii}([\boldsymbol{\omega}^b])$. The configuration consisted of three sets of parallel accelerometers, with directions orthogonal to each other. Their reasoning, and conclusion, are erroneous, as is now demonstrated. Let $\mathsf{A}(P_j, \mathbf{e}_j)$ for $j = 1, 2, 3$, denote three parallel accelerometers. The authors took the differences $\mathsf{a}(P_2, \mathbf{e}_j) - \mathsf{a}(P_1, \mathbf{e}_j)$ and $\mathsf{a}(P_3, \mathbf{e}_j) - \mathsf{a}(P_1, \mathbf{e}_j)$ to obtain two equations that were linear in the nine variables to be determined. To this point, the method is sound. However, they then dictated that the difference, $\mathsf{a}(P_3, \mathbf{e}_j) - \mathsf{a}(P_1, \mathbf{e}_j)$, be evaluated, and assumed that the resulting equation would be linearly independent of the first two. They repeated these steps for $j = 1, 2, 3$, and assumed that the nine equations were independent, and hence capable of determining $[\boldsymbol{\alpha}^b]$, $\mathrm{q}_{ij}([\boldsymbol{\omega}^b])$

[1] It yields the component matrix in the basis defined by the directions of the accelerometers, but these are assumed to be known, so that the component matrices can all be transformed to a common basis.

and $q_{ii}([\boldsymbol{\omega}^b])$ whereas, as has just been shown, only six of the equations are linearly independent. It is also possible to see that their conclusion was wrong by another method that does not rely on the structure of their configuration. If $[\boldsymbol{\alpha}^b]$, $q_{ij}([\boldsymbol{\omega}^b])$ and $q_{ii}([\boldsymbol{\omega}^b])$ *can* be determined, and the accelerometer measurements at known positions with three different directions are known, then it is possible to calculate $[\mathbf{s}^b_{O_B}]$. Thus, by the authors' reasoning it is possible to determine twelve unknowns using nine equations.

Zappa et al. [22] reference Genin's paper without disputing its validity, but state that 12 (rather than 9) accelerometers are necessary to determine $[\mathbf{S}]$. They suggest two possible configurations for these twelve accelerometers. The first is the use of four triaxial accelerometers, referred to above. The second configuration consists of twelve accelerometers, divided into three equal groups of parallel accelerometers and positioned so that they are not on a plane.

Costello and Jitpraphai [17] consider the possibility of using three triaxial accelerometers in a plane. They note that while it is impossible to obtain all twelve elements of $[\mathbf{S}]$ as linear combinations of the accelerometer measurements, it is possible to find the magnitudes of the elements of $[\boldsymbol{\omega}^b]$ and $[\boldsymbol{\alpha}^b]$; the signs of the angular acceleration components are not available. They stated that this issue can be overcome through using more than three triaxial accelerometers, as discussed above. In their application, which was ballistics, they considered the use of configurations composed of dozens of triaxial accelerometers, using the superabundant data to improve accuracy.

This section has summarised most of the existing literature regarding the independence of accelerometer configurations. What has not been mentioned is a small number of papers that are concerned with minimal configurations, i.e., configuration for use with Minimal GFIN (refer to Section 2.4.4). This is discussed in the next chapter.

4.2 General Theory

According to Definition 2.3.2, $\mathsf{A}(P_g, \mathbf{u}_g)$ is generated by the configuration, $\{\mathsf{A}_k\}_1^n$, if and only if the ADM of the former can be written as a linear combination of the ADMs of the latter in the same frame:

$$\mathsf{A}(P_g, \mathbf{u}_g) \in \langle \{\mathsf{A}_k\}_1^n \rangle \Leftrightarrow [\mathsf{A}(P_g, \mathbf{u}_g)^{\mathcal{B}}] = \sum_{k=1}^{n} \lambda_k [\mathsf{A}_k^{\mathcal{B}}]. \tag{4.2}$$

Recall the AADM introduced in Section 2.2:

$$[\tilde{\mathsf{A}}(P_k, \mathbf{u}_k)^{\mathcal{B}}] = \begin{bmatrix} [\mathbf{u}_k^b]^T & [\mathbf{r}_k^{\mathcal{B}}]^T \otimes [\mathbf{u}_k^b]^T \end{bmatrix}. \tag{4.3}$$

The AADM was introduced principally for the purposes of deriving the coordinate transformation rule for the ADM, which was required to show that

defining independence in terms of the ADMs in one frame was sufficient. Since $[\tilde{\mathsf{A}}(P_k, \mathbf{u}_k)^{\mathcal{B}}]$ is related to $[\mathsf{A}(P_k, \mathbf{u}_k)^{\mathcal{B}}]$ by a non-singular transformation (the matrix $[X]$ given at Eq (B.1)), it follows that

$$[\tilde{\mathsf{A}}(P_g, \mathbf{u}_g)^{\mathcal{B}}] = \sum_{k=1}^{n} \lambda_k [\tilde{\mathsf{A}}_k^{\mathcal{B}}] \Leftrightarrow [\mathsf{A}(P_g, \mathbf{u}_g)^{\mathcal{B}}] = \sum_{k=1}^{n} \lambda_k [\mathsf{A}_k^{\mathcal{B}}]. \tag{4.4}$$

Combining Eqs (4.2) and (4.4) shows that generation can be defined in terms of the AADMs:

$$\mathsf{A}(P_g, \mathbf{u}_g) \in \langle \{\mathsf{A}_k\}_1^n \rangle \Leftrightarrow [\tilde{\mathsf{A}}(P_g, \mathbf{u}_g)^{\mathcal{B}}] = \sum_{k=1}^{n} \lambda_k [\tilde{\mathsf{A}}_k^{\mathcal{B}}]. \tag{4.5}$$

When using AADMs, the results regarding frame invariance still apply, i.e., the coordinate frame can be chosen to simplify the analysis without loss of generality. In addition, the following result is easily obtained using AADMs:

Proposition 4.2.1. *If* $\mathbf{R}$ *is a vector rotation, then*

$$\mathsf{A}(P_g, \mathbf{u}_g) = \sum_{k=1}^{n} \lambda_k \mathsf{A}(P_k, \mathbf{u}_k) \Leftrightarrow \mathsf{A}(P_g, \mathbf{R}(\mathbf{u}_g)) = \sum_{k=1}^{n} \lambda_k \mathsf{A}(P_k, \mathbf{R}(\mathbf{u}_k)). \tag{4.6}$$

Proof. Let $[\mathbf{R}^{\boldsymbol{b}}]$ denote the matrix of the rotation, $\mathbf{R}$, in the basis $\boldsymbol{b}$, then

$$[\mathbf{R}(\mathbf{u}_i)^{\boldsymbol{b}}] = [\mathbf{R}^{\boldsymbol{b}}][\mathbf{u}_i^{\boldsymbol{b}}]. \tag{4.7}$$

The definition of the AADM shows that

$$\begin{aligned} [\tilde{\mathsf{A}}(P_i, \mathbf{R}(\mathbf{u}_i))^{\mathcal{B}}] &= \left[[\mathbf{u}_i^{\boldsymbol{b}}]^T [\mathbf{R}^{\boldsymbol{b}}]^T \quad [\mathbf{r}_i^{\mathcal{B}}]^T \otimes ([\mathbf{u}_i^{\boldsymbol{b}}]^T [\mathbf{R}^{\boldsymbol{b}}])^T \right] \\ &= [\tilde{\mathsf{A}}(P_i, \mathbf{u}_i)^{\mathcal{B}}][I]_4 \otimes [\mathbf{R}^{\boldsymbol{b}}]^T. \end{aligned} \tag{4.8}$$

Consequently, if

$$[\tilde{\mathsf{A}}(P_g, \mathbf{R}(\mathbf{u}_g))^{\mathcal{B}}] = \sum_{k=1}^{n} \lambda_k [\tilde{\mathsf{A}}(P_k, \mathbf{R}(\mathbf{u}_k))^{\mathcal{B}}] \tag{4.9}$$

then, using Eq (4.8),

$$[\tilde{\mathsf{A}}(P_g, \mathbf{u}_g)^{\mathcal{B}}][I]_4 \otimes [\mathbf{R}^{\boldsymbol{b}}]^T = \left(\sum_{k=1}^{n} \lambda_k [\tilde{\mathsf{A}}(P_k, \mathbf{u}_k)^{\mathcal{B}}] \right) [I]_4 \otimes [\mathbf{R}^{\boldsymbol{b}}]^T$$

and since $[I]_4 \otimes [\mathbf{R}^{\boldsymbol{b}}]$ has an inverse:

$$([I]_4 \otimes [\mathbf{R}^{\boldsymbol{b}}]^T)^{-1} = ([I]_4 \otimes [\mathbf{R}^{\boldsymbol{b}}]),$$

post-multiplying Eq (4.9) by $([I]_4 \otimes [\mathbf{R}^b])$ shows that

$$[\tilde{\mathsf{A}}(P_g, \mathbf{u}_g)^{\mathcal{B}}] = \sum_{k=1}^{n} \lambda_k [\tilde{\mathsf{A}}(P_k, \mathbf{u}_k)^{\mathcal{B}}], \tag{4.10}$$

as required. That Eq (4.10) implies Eq (4.9) follows by post-multiplication of the former by $[I]_4 \otimes [\mathbf{R}^b]^T$. □

Remark 4.2.1. This proof only required that $\mathbf{R}$ is a non-singular vector function, but only rotations are considered in the following.

4.3 Constrained Configurations

Definition 4.3.1. A *constrained configuration*, $\{D, d\}$, is one in which the accelerometers are located at points spanning a D-dimensional affine subspace with directions spanning a d-dimensional vector subspace. A constrained configuration of n accelerometers is denoted by $\{D, d\}_n$.

Since there are 4 possible affine subspaces: the point ($D = 0$), line ($D = 1$), plane ($D = 2$) and $\mathscr{E}$ ($D = 3$), and vector subspaces of dimension 1, 2 and 3, there are 12 types of constrained configuration. These range from $\{0, 1\}$, a configuration of parallel accelerometers located at a single point, to $\{3, 3\}$, where the accelerometers are not located on any plane, and the directions span $\mathbf{E}$. The latter configuration is really constrained only by its required generality.

The description of constrained configurations is considerably simplified through the choice of the frame, $\mathcal{B}$, and through application of Proposition 4.2.1, which was proved in the previous section. First, the frame can always be selected so that an accelerometer belonging to a $\{D, d\}$ has a coordinate matrix with only D non-zero elements. In particular, when

- $D = 0$: $[\mathbf{r}_{P_k}^{\mathcal{B}}] = [0]_{3\times 1}$, i.e., the origin is chosen to coincide with all the accelerometers.
- $D = 1$: the line through the origin, O_B, directed by the vector, $\mathbf{b}_1$, is chosen to pass through all the accelerometers:

$$[\mathbf{r}_{P_k}^{\mathcal{B}}] = \begin{bmatrix} x_k \\ 0 \\ 0 \end{bmatrix},$$

- $D = 2$: the plane through the origin, O_B, spanned by $\mathbf{b}_1$ and $\mathbf{b}_2$, is chosen to pass through all the accelerometers.

$$[\mathbf{r}_{P_k}^{\mathcal{B}}] = \begin{bmatrix} x_k \\ y_k \\ 0 \end{bmatrix}.$$

No special orientation of the basis $\boldsymbol{b}$ is possible for $D = 3$, but it is assumed that for each value of D the origin, O_B, is chosen to coincide with P_1, the location of the 'first' accelerometer.

Using Proposition 4.2.1, the directions of the accelerometers in a constrained configuration can be rotated *en masse* so that when

- $d = 1$: the accelerometers are all parallel to $\mathbf{b}_1$:

$$[\mathbf{u}_k^{\boldsymbol{b}}] = \begin{bmatrix} 1 \\ 0 \\ 0 \end{bmatrix}$$

- $d = 2$: the accelerometers are in the plane spanned by $\mathbf{b}_1$ and $\mathbf{b}_2$:

$$[\mathbf{u}_k^{\boldsymbol{b}}] = \begin{bmatrix} \cos\gamma_k \\ \sin\gamma_k \\ 0 \end{bmatrix} = \begin{bmatrix} u_{k,1} \\ u_{k,2} \\ 0 \end{bmatrix}.$$

When $d = 3$ no rotation of the accelerometers will give them a simple description, but it is assumed without loss of generality that for each value of d, a rotation is chosen that takes $\mathbf{u}_1$ to $\mathbf{b}_1$, thus, in every case

$$[\mathbf{u}_1^{\boldsymbol{b}}] = \begin{bmatrix} 1 \\ 0 \\ 0 \end{bmatrix}. \tag{4.11}$$

When the frame is fitted to the points and the directions of the accelerometers are rotated in the way just outlined, the location and direction of each accelerometer in the constrained configuration, $\{D, d\}$, is described by $d + D$ scalars. It is now shown how these scalars relate to the AADM, which, in turn, shows how many independent accelerometers there are in each type of constrained configuration.

The coordinate matrices of P_k in $\mathcal{B}$ in each case can be described as the product of a $D \times 1$ and $3 \times D$ matrices:

$$[\mathbf{r}_{P_k}^{\mathcal{B}}] = [E_D][\mathbf{r}_{P_k}^{\mathcal{B}}]_D, \tag{4.12}$$

where $[\mathbf{r}_{P_k}^{\mathcal{B}}]_D$ is the $D \times 1$ matrix comprised of only the non-zero values of $[\mathbf{r}_{P_k}^{\mathcal{B}}]$ as outlined above:

$$[\mathbf{r}_{P_k}^{\mathcal{B}}]_1 = [x_k] \quad [\mathbf{r}_{P_k}^{\mathcal{B}}]_2 = \begin{bmatrix} x_k \\ y_k \end{bmatrix} \quad [\mathbf{r}_{P_k}^{\mathcal{B}}]_3 = \begin{bmatrix} x_k \\ y_k \\ z_k \end{bmatrix}, \tag{4.13}$$

and the matrix, $[E_D]$, is defined to be the $3 \times D$ matrix[2] comprised of the first D columns of the 3×3 identity matrix:

$$[E_1] = \begin{bmatrix} 1 \\ 0 \\ 0 \end{bmatrix} \quad [E_2] = \begin{bmatrix} 1 & 0 \\ 0 & 1 \\ 0 & 0 \end{bmatrix} \quad [E_3] = \begin{bmatrix} 1 & 0 & 0 \\ 0 & 1 & 0 \\ 0 & 0 & 1 \end{bmatrix}. \tag{4.14}$$

Similarly, $[\mathbf{u}_k^{\boldsymbol{b}}]$ can be written as

$$[\mathbf{u}_k^{\boldsymbol{b}}] = [E_d][\mathbf{u}_k^{\boldsymbol{b}}]_d, \tag{4.15}$$

with

$$[\mathbf{u}_k^{\boldsymbol{b}}]_1 = [1] \quad [\mathbf{u}_k^{\boldsymbol{b}}]_2 = \begin{bmatrix} u_{k,1} \\ u_{k,2} \end{bmatrix} \quad [\mathbf{u}_k^{\boldsymbol{b}}]_3 = \begin{bmatrix} u_{k,1} \\ u_{k,2} \\ u_{k,3} \end{bmatrix}. \tag{4.16}$$

Using Eqs (4.12) and (4.15) along with Eq (4.3) gives the following expression for the AADM of an accelerometer in the constrained configuration, $\{D, d\}$:

$$\begin{aligned} [\tilde{\mathsf{A}}(P_k, \mathbf{u}_k)^{\mathcal{B}}] &= \left[[\mathbf{u}_k^{\boldsymbol{b}}]^T \quad [\mathbf{r}_k^{\mathcal{B}}]^T \otimes [\mathbf{u}_k^{\boldsymbol{b}}]^T \right] \\ &= \left[[\mathbf{u}_k^{\boldsymbol{b}}]_d^T [E_d]^T \quad [\mathbf{r}_k^{\mathcal{B}}]_D^T [E_D]^T \otimes [\mathbf{u}_k^{\boldsymbol{b}}]_d^T [E_d]^T \right] \\ &= \left[[\mathbf{u}_k^{\boldsymbol{b}}]_d^T \quad [\mathbf{r}_k^{\mathcal{B}}]_D^T \otimes [\mathbf{u}_k^{\boldsymbol{b}}]_d^T \right] [Z_{(D,d)}], \end{aligned} \tag{4.17}$$

where

$$[Z_{(D,d)}] = \begin{bmatrix} 1 & [0]_{1\times 3} \\ [0]_{D\times 1} & [E_D]^T \end{bmatrix} \otimes [E_d]^T, \tag{4.18}$$

and Eq (C.3) was used to rearrange the Kronecker product in Eq (4.17). The transpose[3] of the $1 \times d(D+1)$ matrix in Eq (4.17) is denoted by

$$[\tilde{\mathsf{A}}(P_k, \mathbf{u}_k)^{\mathcal{B}}]_{(D,d)} \stackrel{\text{def}}{=} \begin{bmatrix} [\mathbf{u}_k^{\boldsymbol{b}}]_d \\ [\mathbf{r}_k^{\mathcal{B}}]_D \otimes [\mathbf{u}_k^{\boldsymbol{b}}]_d \end{bmatrix} \tag{4.19}$$

and referred to as the *Constrained* ADM (CADM). The *Alternative Configuration Matrix* (ACM) of a general n accelerometer configuration is the following $n \times 12$ matrix:

$$[\tilde{\mathsf{C}}_n^{\mathcal{B}}] \stackrel{\text{def}}{=} \begin{bmatrix} [\tilde{\mathsf{A}}(P_1, \mathbf{u}_1)^{\mathcal{B}}] \\ \vdots \\ [\tilde{\mathsf{A}}(P_n, \mathbf{u}_n)^{\mathcal{B}}] \end{bmatrix}. \tag{4.20}$$

The *Constrained* ACM, (CACM) of a configuration, $\{D, d\}_n$, is the $d(D+1) \times n$ matrix with k^{th} column equal to $[\tilde{\mathsf{A}}(P_k, \mathbf{u}_k)^{\mathcal{B}}]_{(D,d)}$:

$$[\tilde{\mathsf{C}}_n^{\mathcal{B}}]_{(D,d)} \stackrel{\text{def}}{=} \left[[\tilde{\mathsf{A}}(P_1, \mathbf{u}_1)^{\mathcal{B}}]_{(D,d)} \quad \cdots \quad [\tilde{\mathsf{A}}(P_n, \mathbf{u}_n)^{\mathcal{B}}]_{(D,d)} \right]. \tag{4.21}$$

[2] $[E]_0$ is regarded to have zero columns, as is $[\mathbf{r}_{P_k}^{\mathcal{B}}]_0$.

[3] The transpose is more useful in following sections.

According to Eq (4.17) the ACM and CACM of the configuration, $\{D,d\}_n$, are related by

$$[\tilde{\mathsf{C}}_n^{\mathcal{B}}] = [\tilde{\mathsf{C}}_n^{\mathcal{B}}]_{(D,d)}^T [Z_{(D,d)}]. \tag{4.22}$$

A result that is used repeatedly in the coming sections is

Proposition 4.3.1. *$\mathsf{A}(P_g, \mathbf{u}_g)$ is generated by $\{D,d\}_n$ if and only if $[\tilde{\mathsf{A}}(P_g,\mathbf{u}_g)^{\mathcal{B}}]$ lies in the column space of $[\tilde{\mathsf{C}}_n^{\mathcal{B}}]_{(D,d)}$.*

Proof. It was established in Section 4.2 that $\mathsf{A}(P_g,\mathbf{u}_g)$ is generated by $\{\mathsf{A}_k\}_1^n$ if and only if

$$[\tilde{\mathsf{A}}(P_g,\mathbf{u}_g)^{\mathcal{B}}] = \sum_{k=1}^{n} \lambda_k [\tilde{\mathsf{A}}(P_k,\mathbf{u}_k)^{\mathcal{B}}].$$

When the configuration is a constrained configuration, $\{D,d\}_n$, this condition can be rewritten, using Eq (4.17), as

$$[\tilde{\mathsf{A}}(P_g,\mathbf{u}_g)^{\mathcal{B}}]_{(D,d)}^T [Z_{(D,d)}] = \left(\sum_{k=1}^{n} \lambda_k [\tilde{\mathsf{A}}(P_k,\mathbf{u}_k)^{\mathcal{B}}]_{(D,d)}^T \right) [Z_{(D,d)}]. \tag{4.23}$$

The sum in this expression can be rewritten as a matrix product:

$$\sum_{k=1}^{n} \lambda_k [\tilde{\mathsf{A}}(P_k,\mathbf{u}_k)^{\mathcal{B}}]_{(D,d)}^T = [\boldsymbol{\lambda}]^T [\tilde{\mathsf{C}}_n^{\mathcal{B}}]_{(D,d)}^T,$$

where $[\boldsymbol{\lambda}]^T$ is a $1 \times n$ matrix with k^{th} element, λ_k. Eq (4.23) is then seen to be equivalent to

$$\left([\tilde{\mathsf{A}}(P_g,\mathbf{u}_g)^{\mathcal{B}}]_{(D,d)}^T - [\boldsymbol{\lambda}]^T [\tilde{\mathsf{C}}_n^{\mathcal{B}}]_{(D,d)}^T \right) [Z_{(D,d)}] = [0]_{1\times 12}. \tag{4.24}$$

The matrix, $[Z_{(D,d)}]$, is clearly of full row-rank, so Eq (4.24) can only hold if

$$[\tilde{\mathsf{A}}(P_g,\mathbf{u}_g)^{\mathcal{B}}]_{(D,d)} = [\tilde{\mathsf{C}}_n^{\mathcal{B}}]_{(D,d)} [\boldsymbol{\lambda}], \tag{4.25}$$

as was to be proved. □

A consequence of this result is that any accelerometer that is generated by a constrained configuration is part of that constrained configuration. The constrained configurations are, in this regard, similar to vector subspaces. They differ from vector subspaces in that not *every* linear combination of accelerometers, whether represented by an ADM, AADM or CADM, is another accelerometer.

Another consequence of the full row-rank of $[Z_{(D,d)}]$ is

Proposition 4.3.2. *There are a maximum of*

$$N_{(D,d)} = d(D+1) \tag{4.26}$$

independent accelerometers in $\{D, d\}$.

Proof. It follows from Eq (4.22) and the full row-rank of $[Z_{(D,d)}]$ that

$$\text{rank}[\tilde{\mathsf{C}}_n^{\mathcal{B}}] = \text{rank}[\tilde{\mathsf{C}}_n^{\mathcal{B}}]_{(D,d)}^T = \text{rank}[\tilde{\mathsf{C}}_n^{\mathcal{B}}]_{(D,d)}$$

The maximum rank of $[\tilde{\mathsf{C}}_n^{\mathcal{B}}]_{(D,d)}$ is $d(D+1)$, since the dimension of $[\tilde{\mathsf{C}}_n^{\mathcal{B}}]_{(D,d)}$ is $d(D+1) \times n$. □

This proposition establishes an upper bound on the number of independent accelerometers in $\{D, d\}$. It is easy to show that the bound can be achieved. Consider, for example, the case $D = d = 2$. Choosing orthogonal accelerometers at O_B, $O_B + \mathbf{b}_1$ and $O_B + \mathbf{b}_2$ gives the following ACM,

$$[\tilde{\mathsf{C}}_6^{\mathcal{B}}] = \begin{bmatrix} [E_2]^T & [0] & [0] & [0] \\ [E_2]^T & [E_2]^T & [0] & [0] \\ [E_2]^T & [0] & [E_2]^T & [0] \end{bmatrix},$$

which can be seen to be rank 6, by inspection.

Definition 4.3.2. An independent constrained configuration $\{D, d\}$ of $N_{(D,d)}$ accelerometers is referred to as a *Full Constrained Configuration*, (FCC).

If a constrained configuration is analogous to a vector subspace, then a FCC is analogous to a basis for that vector subspace; every accelerometer in the constrained configuration can be written as a unique linear combination of the accelerometers in the FCC. The number of accelerometers in each of the 12 possible FCCs are shown in Table 4.1. This table uses words and phrases, rather than values of D and d to describe each type of constrained configuration. To avoid the confusion that can arise when using words such as 'coplanar' that can describe both the directions and the locations of accelerometers, in the description of constrained configurations, the words: 'Parallel', 'Coplanar' and 'Spatial' are used to describe the *directions* of the accelerometers in a configuration for $d = 1, 2, 3$, respectively, while the phrases: 'At a point', 'On a line', 'On a plane' and 'Not on a plane' are used to describe the *locations* of accelerometers for $D = 0, 1, 2, 3$. The phrase 'planar accelerometer configuration' is reserved for the topic discussed in Chapter 3, i.e., configurations that are suitable for use when a body is undergoing planar motion.

The notion of a FCC establishes of a functional upper limit on the number of accelerometers for each constrained configuration. The minimum number of accelerometers in $\{D, d\}$ is $\max(D+1, d)$; with fewer than $D+1$ accelerometers

Table 4.1: The number of independent accelerometers in the various full constrained configurations.

	At a Point	On a Line	On a Plane	Not on a Plane
Parallel	1	2	3	4
Coplanar	2	4	6	8
Spatial	3	6	9	12

their locations cannot span a D-dimensional affine subspace, and with fewer than d, the directions cannot span a d-dimensional vector space. Table 4.2 lists the minimum number of accelerometers in each constrained configuration. Comparing Tables 4.1 and 4.2 shows that the configuration types $\{0, d\}$ and $\{D, 1\}$ are special in that the minimum possible number of accelerometers required is equal to the maximum number of independent accelerometers. The geometric conditions that the accelerometers must satisfy in these two simple cases can therefore be stated as

Table 4.2: The minimum number of accelerometers in the various constrained configurations.

	At a Point	On a Line	On a Plane	Not on a Plane
Parallel	1	2	3	4
Coplanar	2	2	3	4
Spatial	3	3	3	4

Proposition 4.3.3. *The d accelerometers of a FCC at a point are independent if and only if their directions are linearly independent.*

Proposition 4.3.4. *The $D+1$ accelerometers of a FCC of parallel accelerometers are independent if and only if the $D+1$ locations of the accelerometers span the D-dimensional subspace to which they are constrained.*

These results regarding parallel and coincident accelerometers can be seen as a generalization of those obtained when considering planar configurations, in Chapter 3. When $d > 1$ and/or $D > 0$, the results are not as intuitive, as will be seen in the following section.

4.4 Generation by Constrained Configurations

In this section, the accelerometers that are generated by constrained configurations obtained by successively removing accelerometers from the FCCs shown

in Table 4.3 are studied. Working 'backwards' from FCCs ensures that the configurations that are studied are independent. This is a more practical approach than building up from the smallest possible number in each constrained configuration, due to the vast number of special configurations that are possible.

Table 4.3: The FCCs with $d > 1$ and $D > 0$.

	On a Line	On a Plane	Not on a Plane
Coplanar	4	6	8
Spatial	6	9	12

The general method of analysis that is used in the following subsections is now outlined. It is based upon Proposition 4.3.1, i.e., finding constrained ADMs of accelerometers, $\mathsf{A}(P_g, \mathbf{u}_g)$, that lie in the column space of the constrained ACM. This is achieved using determinants; for each accelerometer that is removed from a configuration, one determinant must be evaluated. Each determinant gives rise to a linear relationship that must hold between the elements of the constrained ADM of a generated accelerometer.

In the case where the configuration is one accelerometer short of being a FCC, the method is obvious. If $[\mathsf{A}(P_g, \mathbf{u}_g)]_{(D,d)}$ is to lie in the column space of $[\tilde{\mathsf{C}}_{N_{(D,d)}-1}]_{(D,d)}$, the augmented matrix,

$$\left[[\tilde{\mathsf{C}}_{N_{(D,d)}-1}]_{(D,d)} \quad [\tilde{\mathsf{A}}(P_g, \mathbf{u}_g)]_{(D,d)}\right], \tag{4.27}$$

must be singular. Setting the determinant of the augmented matrix equal to zero gives one linear relationship that must hold between the elements of the constrained ADM.

When $m > 1$ accelerometers are removed from a FCC it can be ensured that $[\tilde{\mathsf{A}}(P_g, \mathbf{u}_g)]_{(D,d)}$ lies in the column space of $[\tilde{\mathsf{C}}_{N_{(D,d)}-m}]_{(D,d)}$ using m determinants as is now described. To ease notation, consider the equivalent problem of ensuring that $[\mathbf{x}]$, an $(n+m)\times 1$ matrix with i^{th} element, x_i, lies in the column-space of $[\mathbf{C}]$, an $(n+m)\times n$ matrix of rank n with i^{th} row, $[\mathbf{c}_i]$. Since $[\mathbf{C}]$ is of rank n, there exists at least one set of n rows that are linearly independent. Suppose for simplicity that the first n rows are such a set, and denote the square matrix formed by those rows as $[\mathbf{C}_{1:n}]$. Setting

$$\det \begin{bmatrix} [\mathbf{C}_{1:n}] & [\mathbf{x}_{1:n}] \\ [\mathbf{c}_{n+1}] & x_{n+1} \end{bmatrix} = 0, \tag{4.28}$$

results in a linear relationship involving the first $n+1$ components of $[\mathbf{x}]$ that must be satisfied if $[\mathbf{x}]$ is to lie in the column space of $[\mathbf{C}]$. Another $m-1$

equations can be obtained by setting the determinant of

$$\begin{bmatrix} [\mathbf{C}_{1:n}] & [\mathbf{x}_{1:n}] \\ [\mathbf{c}_{n+j}] & x_{n+j} \end{bmatrix} \tag{4.29}$$

equal to 0 for $j = 2, \ldots, m$. If the elements of $[\mathbf{x}]$ are chosen to satisfy the linear relationships arising from each of the m equations obtained from the determinants, then it will lie in the column space of $[\mathbf{C}]$, i.e., the augmented matrix will be of rank n. That these m conditions are sufficient can be made clearer by considering the row rank of the augmented matrix, $\left[[\mathbf{C}] \quad [\mathbf{x}]\right]$. If Eq (4.28) can be satisfied then the $(n+1)^{th}$ row of the augmented matrix can be written as a linear combination of the first n rows. Similarly, if Eq (4.29) is satisfied, then the $(n+j)^{th}$ row can also be written as linear combination of the first n rows for $j = 2, \ldots, m$. This, and the independence of the first n rows of $[\mathbf{C}]$, means that the rank of the augmented matrix is n, as required.

In the general argument just outlined, the column matrix, $[\mathbf{x}]$, was arbitrary except for its dimension. In the current application, the constrained ADM, for which $[\mathbf{x}]$ played a substitute in the preceding argument, has a definite structure. Two interpretations of each linear equation involving the elements of the CADM are possible.

Homogeneous Equations for $[\mathbf{u}_g]_d$ First, with reference to Eq (4.19), it is seen that each element of the CADM is linearly proportional to some element of $[\mathbf{u}]_d$: the first d elements are $u_{g,i}$ for $i = 1, \ldots, d$ and the remaining $d \cdot D$ elements are of the form $x_g u_{g,i}$, $y_g u_{g,i}$, and so on, depending upon the value of D. It follows that each equation arising from setting the determinant of the augmented matrix equal to zero can be written as a *homogeneous* equation:

$$[\mathbf{v}([\mathbf{r}_g]_D)]^T [\mathbf{u}]_d = 0, \tag{4.30}$$

where $[\mathbf{v}([\mathbf{r}_g]_D)]^T$ is a $1 \times d$ matrix, the elements of which depend *linearly* upon those of $[\mathbf{r}_g]_D$. In the case $D = 2$ each element of $[\mathbf{v}([\mathbf{r}_g]_D)]$ has the general form,

$$v_i(x_g, y_g) = v_{i,x} x_g + v_{i,y} y_g + v_{i,0}, \tag{4.31}$$

the important point being the presence of an additional scalar term, which is present regardless of the value of D.

When $d = 2$, i.e., the directions of the accelerometers in the configuration are coplanar, a single homogeneous equation of the form of Eq (4.30) generally means that for each P_g in the D-dimensional affine subspace under consideration there will be a unique direction of generation. This is because the 1×2 matrix pre-multiplying $[\mathbf{u}]_d$ has a one-dimensional null-space and the two elements of $[\mathbf{u}]_d$ are also constrained by the requirement that $u_{g,1}^2 + u_{g,2}^2 = 1$. When there are two equations of this form, i.e., when 2 accelerometers have

been removed from the FCC of type, $\{D, 2\}$, the following matrix equation can be written:

$$\begin{bmatrix} v_{1,1}([\mathbf{r}_g]_D) & v_{1,2}([\mathbf{r}_g]_D) \\ v_{2,1}([\mathbf{r}_g]_D) & v_{2,2}([\mathbf{r}_g]_D) \end{bmatrix} \begin{bmatrix} u_{i,1} \\ u_{i,2} \end{bmatrix} = \begin{bmatrix} 0 \\ 0 \end{bmatrix}. \tag{4.32}$$

This equation will have non-trivial solutions only if the 2×2 matrix is singular, i.e., if

$$v_{1,1}v_{2,2} - v_{1,2}v_{2,1} = 0. \tag{4.33}$$

This equation is quadratic in each element of $[\mathbf{r}_g]_D$. The locus of points satisfying Eq (4.32) are the only ones for which generation is possible. This assumes, and this assumption is made throughout this section, that the d^{th} linear function of $[\mathbf{r}_g]_D$, $v_{j,d}([\mathbf{r}_g]_D)$ that is obtained from the j^{th} determinant is both non-zero and not a multiple of $v_{k,d}([\mathbf{r}_g]_D)$ for some $k \neq j$. If this assumption is not satisfied, which is certainly a special situation depending upon the relative directions and locations of the accelerometers, Eq (4.33) is satisfied for all P_g in the D-dimensional affine subspace.

When $d = 3$, a single equation of the form given in Eq (4.30) generally means that at each P_g in the D-dimensional affine subspace, a *plane* of accelerometer directions can be generated. The matrix, $[v([\mathbf{r}_g]_D)]$ is the component matrix for the normal of this 'plane of generation' at P_g. When there are two homogeneous equations, assuming as above, that they are 'general', $\mathbf{u}_g$ must be orthogonal to two vectors, and this is enough to define it uniquely since $\mathbf{u}_g$ must be of unit magnitude. The direction of $\mathbf{u}_g$ can, in this case be found as the vector product of the normals, leading to an expression of the form

$$[\mathbf{u}_g] \sim \begin{bmatrix} v_{1,2}v_{2,3} - v_{1,3}v_{2,2} \\ v_{1,2}v_{2,3} - v_{1,3}v_{2,2} \\ v_{1,2}v_{2,3} - v_{1,3}v_{2,2} \end{bmatrix}. \tag{4.34}$$

Each element of this matrix is a quadratic function of the elements of $[\mathbf{r}_g]_D$. Note that even once two accelerometers have been removed from an FCC with $d = 3$ it should still be possible to generate accelerometers at every point of the D-dimensional affine subspace. Restrictions upon the locations of accelerometers appear when three accelerometers are removed. The three homogeneous equations can be written in matrix form as

$$\left[[\mathbf{v}_1([\mathbf{r}_g]_D)] \quad [\mathbf{v}_2([\mathbf{r}_g]_D)] \quad [\mathbf{v}_3([\mathbf{r}_g]_D)] \right]^T \begin{bmatrix} u_{g,1} \\ u_{g,2} \\ u_{g,3} \end{bmatrix} = \begin{bmatrix} 0 \\ 0 \\ 0 \end{bmatrix}. \tag{4.35}$$

Assuming the 'generality' described above, the determinant of the 3×3 matrix in this equation is only zero, and non-trivial solutions for $[\mathbf{u}]_3$ are only possible, on a certain locus, that for which a cubic in the elements of $[\mathbf{r}_g]_D$ is zero.

Even when the number of accelerometers removed from the FCC, which is equal to the number of homogeneous equations, is greater than d, generation is still sometimes possible. For instance, consider the case where three accelerometers have been removed and $d = 2$, i.e., the accelerometers have coplanar directions. The equations in this case are

$$\begin{bmatrix} \mathbf{v}_1([\mathbf{r}_g]_D) & \mathbf{v}_2([\mathbf{r}_g]_D) & \mathbf{v}_3([\mathbf{r}_g]_D) \end{bmatrix}^T \begin{bmatrix} u_{g,1} \\ u_{g,2} \end{bmatrix} = \begin{bmatrix} 0 \\ 0 \\ 0 \end{bmatrix}. \tag{4.36}$$

For generation to be possible $[\mathbf{r}_g]_D$ must be chosen so that the 3×2 matrix is rank deficient. One way to try to do this is to select $[\mathbf{r}_g]_D$ so that both of the following equalities hold:

$$\det \begin{bmatrix} \mathbf{v}_1([\mathbf{r}_g]_D)^T \\ \mathbf{v}_2([\mathbf{r}_g]_D)^T \end{bmatrix} = 0 \qquad \det \begin{bmatrix} \mathbf{v}_1([\mathbf{r}_g]_D)^T \\ \mathbf{v}_3([\mathbf{r}_g]_D)^T \end{bmatrix} = 0. \tag{4.37}$$

Each of these determinants is quadratic in the elements of $[\mathbf{r}_g]_D$, and setting each of them equal to zero describes two loci in the D-dimensional affine subspace. The intersection of the loci, if any exist, are the positions at which accelerometers can be generated. Only two determinants have to be evaluated in the case just described because when $[\mathbf{r}_g]_D$ is chosen so that $\mathbf{v}_j([\mathbf{r}_g]_D)$ is a multiple of $\mathbf{v}_1([\mathbf{r}_g]_D)$ for $j = 2, 3$ it is obvious that $\mathbf{v}_2([\mathbf{r}_g]_D)$ is a multiple of $\mathbf{v}_3([\mathbf{r}_g]_D)$, so the remaining determinant is automatically equal to zero.

Non-Homogeneous Equations for $[\mathbf{r}_g]_D$ No matter how many accelerometers have been removed from an FCC, if it is still to remain a constrained configuration it must have at least d independent accelerometers. This means that every determinant of the augmented matrix that needs to be evaluated will involve at least $d + 1$ rows, and, consequently (with reference to the form of the constrained ADM) will depend upon at least one element of $[\mathbf{r}_g]_D$. Thus each equation arising from setting a determinant of the augmented matrix to zero can be written as a *non-homogeneous* equation

$$[\mathbf{w}([\mathbf{u}]_d)][\mathbf{r}_g]_D = c([\mathbf{u}]_d), \tag{4.38}$$

where $[\mathbf{w}([\mathbf{u}]_d)]$ is a $1 \times D$ matrix the elements of which depend linearly upon the d elements of $[\mathbf{u}_g]_d$, and where $c([\mathbf{u}]_d)$ is a scalar function that also depends linearly upon $[\mathbf{u}_g]_d$. Unlike the function, v_i, shown in Eq (4.31), neither the D elemental functions comprising $[\mathbf{w}([\mathbf{u}]_d)]$ nor $c([\mathbf{u}]_d)$ has an additional constant term; every term in the function is proportional to some element of $[\mathbf{u}_g]_d$.

One equation of the form of Eq (4.38) generally constrains P_g to lie in some $D - 1$ dimensional subspace for each $\mathbf{u}_g$ in the d-dimensional subspace. This means, for instance, that (generally) if

- $D = 1$, there will be a point at which an accelerometer with a given direction is generated.
- $D = 2$, there will be a line along which accelerometers with a given direction are generated.
- $D = 3$, there will be a plane upon which accelerometers with a given direction are generated.

This section has described the general approach that is employed in the following subsections, where accelerometers are successively removed from the FCCs given in Table 4.3. As the above discussion has shown, many of the coming results are from the field of algebraic geometry. For this reason, repeated reference is made to a book on this subject by Semple and Kneebone [50].

4.4.1 FCC Minus 1

As described above, when one accelerometer is removed, it can be ensured that the constrained ADM of $\mathsf{A}(P_g, \mathbf{u}_g)$ lies in the column space of the constrained ACM by setting a single determinant of the augmented matrix equal to zero. The three simplest examples are used for illustrative purposes. The first example is $\{1, 2\}_3$, i.e., three independent accelerometers on a line with directions spanning a plane. This example is treated in more detail than those following it for two reasons: to underscore the ideas discussed in the previous section, and because its simplicity means that the products of terms are not unwieldy. The augmented matrix is

$$\left[[\tilde{\mathsf{C}}_3]_{(1,2)} \quad [\tilde{\mathsf{A}}(P_g, \mathbf{u}_g)]_{(1,2)}\right] = \begin{bmatrix} 1 & u_{2,1} & u_{3,1} & u_{g,1} \\ 0 & u_{2,2} & u_{3,2} & u_{g,2} \\ 0 & x_2 u_{2,1} & x_3 u_{3,1} & x_g u_{g,1} \\ 0 & x_2 u_{2,2} & x_3 u_{3,2} & x_g u_{g,2} \end{bmatrix}. \tag{4.39}$$

Setting the determinant of this matrix equal to zero gives the homogeneous equation for $u_{g,1}$ and $u_{g,2}$

$$\begin{bmatrix} v_1(x_g) & v_2(x_g) \end{bmatrix} \begin{bmatrix} u_{g,1} \\ u_{g,2} \end{bmatrix} = 0 \tag{4.40}$$

with

$$v_1(x_g) = x_g(x_2 - x_3)u_{2,2}u_{3,2} \tag{4.41}$$

$$v_2(x_g) = x_g(x_3 u_{2,2}u_{3,1} - x_2 u_{2,1}u_{3,2}) + x_2 x_3(u_{2,1}u_{3,2} - u_{3,1}u_{2,2}). \tag{4.42}$$

The non-homogeneous equation for x_g is

$$w(u_{g,1}, u_{g,2})x_g = c(u_{g,1}, u_{g,2}) \tag{4.43}$$

with

$$w(u_{g,1}, u_{g,2}) = (u_{g,2}(x_3 u_{2,2} u_{3,1} - x_2 u_{2,1} u_{3,2}) - u_{g,1}(x_3 - x_2) u_{2,2} u_{3,2}) \quad (4.44)$$

$$c(u_{g,1}, u_{g,2}) = u_{g,2} x_2 x_3 (u_{3,1} u_{2,2} - u_{2,1} u_{3,2}). \quad (4.45)$$

Letting

$$\tau_i = \frac{u_{i,2}}{u_{i,1}} = \tan \gamma_i, \quad (4.46)$$

where γ_i is the angle measured from $\mathbf{u}_1$ to $\mathbf{u}_i$, Eq (4.43) can be solved for x_g as

$$x_g = \frac{\tau_g x_2 x_3 (\tau_g - \tau_3)}{x_3 \tau_2 (\tau_g - \tau_3) - x_2 \tau_3 (\tau_g - \tau_2)} \quad (4.47)$$

which makes it clear that for every $\mathbf{u}_g$ there is a point P_g on the line such that $\mathsf{A}(P_g, \mathbf{u}_g)$ is generated by $\{1, 2\}_3$. By setting $\tau_g = 0$, and $\tau_g = \tan \gamma_k$ for $k = 2, 3, 4$, in Eq (4.47) it is easily seen that the accelerometers generated with directions parallel to $\mathbf{u}_k$ for $k = 1, 2, 3, 4$ are at P_k, i.e., they are trivially generated. There is a unique direction, specified by

$$\tau_g = \tau_2 \tau_3 \frac{x_3 - x_2}{x_3 \tau_2 - x_2 \tau_3}, \quad (4.48)$$

for which the denominator in Eq (4.47) is zero. The generated accelerometer with this direction is 'at infinity' along the line through the accelerometers. An example of the accelerometers generated by $\{1, 2\}_3$ is shown in Fig 4.1. In Figure 4.1, and in the discussion so far, it has been tacitly assumed that

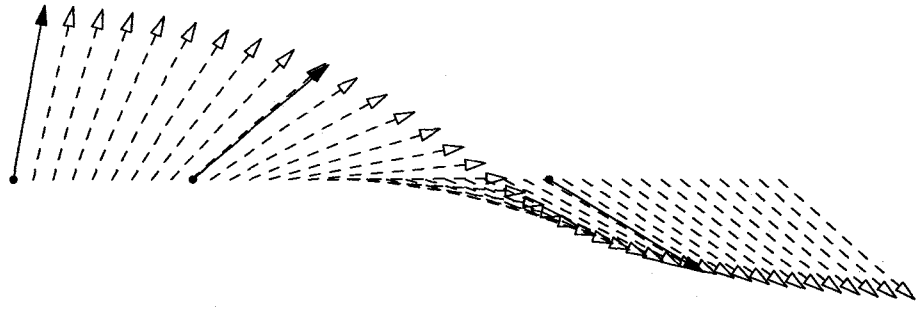

Figure 4.1: Accelerometers generated by $\{1, 2\}_3$.

none of the accelerometers of $\{1, 2\}_3$ is coincident or parallel. If there are two coincident accelerometers, say $P_3 = P_1$, then, since the coordinate system has been chosen such that $x_1 = 0$, Eq (4.40) becomes

$$x_g x_2 \tau_3 (\tau_2 - \tau_g) = 0. \quad (4.49)$$

Since $\tau_3 \neq 0$ (otherwise there would be a coincident parallel pair) this equation shows that generation is possible for $x_g \neq 0$ only if $\mathbf{u}_g = \mathbf{u}_2$, whereas if $x_g = 0$,

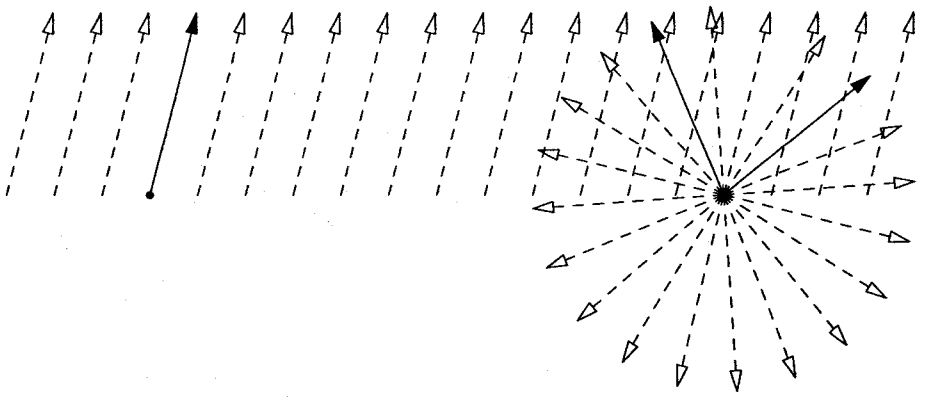

Figure 4.2: Accelerometers generated by $\{1,2\}_3$.

all directions can be generated. An example of this sort of generation is shown in Fig 4.2.

The second example is $\{1,3\}_5$; 5 independent accelerometers on a line with directions spanning $\mathbf{E}$. In this case, the homogeneous equation for $[\mathbf{u}_g]_3$ is

$$[\mathbf{v}(x_g)]^T[\mathbf{u}_g]_3 = 0. \tag{4.50}$$

As discussed above, $\mathbf{v}(x_g)$ is the normal to a plane of accelerometers that are generated at each point. In this case, the normal is a linear function of x_g. The fact that there is a plane of generated accelerometers at each point on the line reinforces what is intuitively obvious; there is a single infinity of directions, $\mathbf{u}_g$, such that the non-homogeneous equation for x_g,

$$w(u_{g,1}, u_{g,2}, u_{g,3})x_g = c(u_{g,1}, u_{g,2}, u_{g,3}), \tag{4.51}$$

will have the same solution, x_g. Effectively a double infinity of directions have been compacted onto a single infinity of points, a line. Some examples of the planes of accelerometers generated by $\{1,3\}_5$ are shown in Fig 4.3.

The final example is $\{2,2\}_5$; five independent accelerometers on a plane with coplanar directions. Setting the determinant of the 6×6 augmented matrix equal to zero gives rise to an homogeneous equation for $[\mathbf{u}_g]_2$ of the form:

$$[\mathbf{v}(x_g, y_g)]^T[\mathbf{u}_g]_2 = 0. \tag{4.52}$$

For each (x_g, y_g), $[\mathbf{u}_g]_2$ is uniquely[4] determined by this equation and the requirement that $\|\mathbf{u}_g\| = 1$. What Eq (4.52) indicates is that, generally, there is a unique direction of generation at each point in the plane. An exception occurs when the two elements of $[\mathbf{v}]$, which depend linearly upon x_g and y_g, are simultaneously zero. If this occurs at some point, P^*, then accelerometers

[4]Recall that the directions $\mathbf{u}_g$ and $-\mathbf{u}_g$ are considered to be identical.

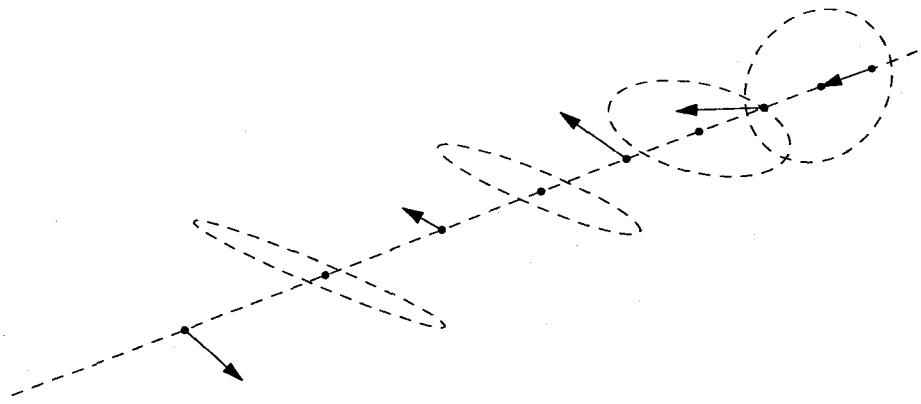

Figure 4.3: Some of the planes of accelerometers generated by $\{1,3\}_5$.

of all directions (in the plane) can be generated at that point. This can also be explained using the non-homogeneous equation for $[\mathbf{r}_g]_2$:

$$[\mathbf{w}(u_{g,1}, u_{g,2})][\mathbf{r}_g]_2 = c(u_{g,1}, u_{g,2}). \tag{4.53}$$

This equation shows that for each $\mathbf{u}_g$ there is a linear relationship between x_g and y_g, i.e., a line. This line, upon which accelerometers with the direction, $\mathbf{u}_g$, can be generated is denoted by $L(\mathbf{u}_g)$. It is obvious that $L(\mathbf{u}_k)$ must pass through P_k for $k = 1, \ldots, 5$. Two lines, $L(\mathbf{u}_a)$ and $L(\mathbf{u}_b)$, must either intersect or be parallel (intersect at infinity). If the lines do intersect, then generation of accelerometers of all directions (in the plane, since $d = 2$) is possible at the point of intersection. Referring back to Eq (4.52) it is now clear that the locus of points for which $v_1(x_g, y_g) = 0$ is $L(\mathbf{b}_1)$, and that for $v_2(x_g, y_g) = 0$ is $L(\mathbf{b}_2)$. Thus, if the lines, $L(\mathbf{b}_1)$ and $L(\mathbf{b}_2)$ intersect, $L(\mathbf{u}_g)$ passes through their intersection for each $\mathbf{u}_g \in \langle \mathbf{b}_1, \mathbf{b}_2 \rangle$. It is suggested that this is the general case; the parallelism of $L(\mathbf{b}_1)$ and $L(\mathbf{b}_2)$ requires

$$v_1(x_g, y_g) = \lambda v_2(x_g, y_g).$$

This condition is geometrically difficult to interpret given that each coefficient of v_i depends upon the relative directions and locations of 5 accelerometers. Figure 4.4 shows the lines along which the accelerometers in an example of $\{2,2\}_5$ are generated. The intersection of these lines is the one point in the plane at which it is not possible to place an accelerometer so that it is independent of the other 5.

These three examples, while being the simplest, have illustrated the important properties of configurations that are one shy of being full constrained configurations: generation of single directions along $D-1$ dimensional affine subspaces, and generation of accelerometers with directions spanning $d-1$ dimensional vector spaces at each point. The remaining three constrained configurations that are one accelerometer short of being FCCs: $\{2,3\}_8$, $\{3,2\}_7$

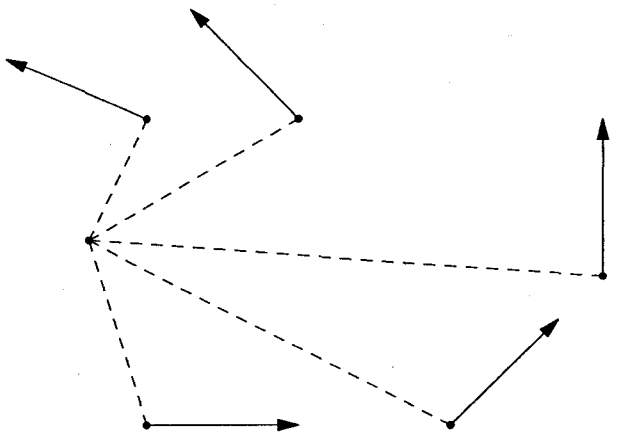

Figure 4.4: The lines along which the accelerometers of $\{2,2\}_5$ are generated.

and $\{3,3\}_{11}$ have similar properties. For example, $\{3,3\}_{11}$, will generate accelerometers of a given direction along a plane, and at each point will generate accelerometers with directions spanning a plane. Further, there will, in general be a unique point at which accelerometers of all direction are generated. This point is the generalization of the 'focus' that was important in the analysis of planar accelerometer configurations in Chapter 3.

4.4.2 FCC Minus 2

There are 6 types of constrained configuration that are obtained by removing 2 accelerometers from full constrained configurations with $d > 1$ and $D > 0$. They are listed in Table 4.4.

Table 4.4: The constrained configurations with $d > 1$ and $D > 0$ that are 2 accelerometers short of being FCCs.

	On a Line	On a Plane	Not on a Plane
Coplanar	2	4	6
Spatial	4	7	10

The simplest case is $\{1,2\}_2$; two non-parallel, non-coincident accelerometers. Firstly, the two homogeneous equations for $[\mathbf{u}_g]_2$ can be written as

$$\begin{bmatrix} v_{1,1}(x_g) & v_{1,2}(x_g) \\ v_{2,1}(x_g) & v_{2,2}(x_g) \end{bmatrix} \begin{bmatrix} u_{g,1} \\ u_{g,2} \end{bmatrix} = \begin{bmatrix} 0 \\ 0 \end{bmatrix}. \tag{4.54}$$

There can be non-trivial solutions for $u_{g,1}$ and $u_{g,2}$ only if the determinant of the 2×2 matrix is zero. The determinant is quadratic in x_g, implying that there

are only 2 values of x_g for which it is possible to generate an accelerometer. Since the configuration generates $\mathsf{A}(P_1, \mathbf{u}_1)$ and $\mathsf{A}(P_2, \mathbf{u}_2)$ trivially, it can be concluded that these are the only accelerometers generated by $\{1, 2\}_2$. A different argument leading to the same conclusion uses the non-homogeneous equations for x_g:

$$\begin{bmatrix} w_1(u_{g,1}, u_{g,2}) \\ w_2(u_{g,1}, u_{g,2}) \end{bmatrix} x_g = \begin{bmatrix} c_1(u_{g,1}, u_{g,2}) \\ c_2(u_{g,1}, u_{g,2}) \end{bmatrix}. \tag{4.55}$$

For these equations to be consistent the augmented matrix must be singular. The determinant of

$$\begin{bmatrix} w_1(u_{g,1}, u_{g,2}) & c_1(u_{g,1}, u_{g,2}) \\ w_2(u_{g,1}, u_{g,2}) & c_2(u_{g,1}, u_{g,2}) \end{bmatrix},$$

is quadratic in $u_{g,1}$ and $u_{g,2}$. According to Bezout's theorem, the locus for which the determinant is zero and the unit circle, $u_{g,1}^2 + u_{g,2}^2 = 1$, will have 4 intersections, since both are planar algebraic curves of the second order [49, 55]. These intersections will consist of two diametrically opposite pairs since $\mathbf{u}_g$ and $-\mathbf{u}_g$ are equivalent, and therefore only two intersections are meaningful, showing once again that only trivial generation is possible.

The next example, $\{2, 2\}_4$; 4 accelerometers on a plane with coplanar directions, is more interesting. The homogeneous equations of $[\mathbf{u}_g]_2$ obtained from taking 2 determinants of the 6×5 augmented matrix can be written as:

$$\begin{bmatrix} v_{1,1}(x_g, y_g) & v_{1,2}(x_g, y_g) \\ v_{2,1}(x_g, y_g) & v_{2,2}(x_g, y_g) \end{bmatrix} \begin{bmatrix} u_{g,1} \\ u_{g,2} \end{bmatrix} = \begin{bmatrix} 0 \\ 0 \end{bmatrix}. \tag{4.56}$$

Setting the determinant of the 2×2 matrix leads to the equation of a conic:

$$v_{1,1}(x_g, y_g) v_{2,2}(x_g, y_g) - v_{1,2}(x_g, y_g) v_{2,1}(x_g, y_g) = 0. \tag{4.57}$$

The independent configuration, $\{2, 2\}_4$, only generates accelerometers on the points of this conic. The identification of the conic is a non-trivial task. It is known that it must pass through the locations of the four accelerometers of the configuration, but there are, in general[5], an infinite number of conics that satisfy this requirement [59]. The non-homogeneous equations for $[\mathbf{r}_g]_2$:

$$\begin{bmatrix} w_{1,1}(u_{g,1}, u_{g,2}) & w_{1,2}(u_{g,1}, u_{g,2}) \\ w_{2,1}(u_{g,1}, u_{g,2}) & w_{2,2}(u_{g,1}, u_{g,2}) \end{bmatrix} \begin{bmatrix} x_g \\ y_g \end{bmatrix} = \begin{bmatrix} c_1(u_{g,1}, u_{g,2}) \\ c_2(u_{g,1}, u_{g,2}) \end{bmatrix}, \tag{4.58}$$

allow solution for the point, P_g, for which an accelerometer with direction, $\mathbf{u}_g$, is generated. In fact, since, as previously mentioned, each w_i and c_i depends solely upon $u_{g,1}$ and/or $u_{g,2}$, i.e., there is no additional constant term involved,

[5] Assuming no 3 of the points are collinear.

it is possible to divide each row the matrix equation in Eq (4.58) by $u_{g,1}$, say, to end up with

$$\begin{bmatrix} w'_{1,1}(\tau_g) & w'_{1,2}(\tau_g) \\ w'_{2,1}(\tau_g) & w'_{2,2}(\tau_g) \end{bmatrix} \begin{bmatrix} x_g \\ y_g \end{bmatrix} = \begin{bmatrix} c'_1(\tau_g) \\ c'_2(\tau_g) \end{bmatrix}, \tag{4.59}$$

where $w'_{i,j}$ and c'_i are linear functions of τ_g, the tangent of the angle, γ_g, measured from $\mathbf{u}_1$ to $\mathbf{u}_g$ as was used in the previous subsection. Using this approach it is possible to solve for x_g and y_g as rational functions of τ_g. An example of an elliptical distribution of generated accelerometers obtained using this method is shown in Fig 4.5. It is worthy of remark that the four accelerometers generating the ellipse are a subset of those pictured in Fig 4.4 and that the point of intersection indicated in that figure lies on the ellipse in Fig 4.5.

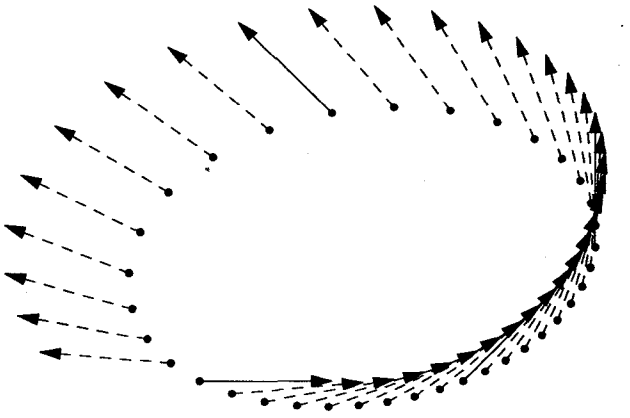

Figure 4.5: An ellipse of accelerometers generated by an example of $\{2,2\}_4$.

Following the same approach as above shows that the configuration, $\{3,2\}_6$; 6 independent accelerometers, not on a plane, with coplanar directions, also involves interesting geometry. Setting the determinant of the 2×2 matrix involved in the homogeneous equations for $[\mathbf{u}_g]_2$ equal to zero reveals that generation is only possible when P_g lies on some quadric. The requirement that the quadric pass through the 6 points $\{P_k\}_1^6$ is not enough to define it; a quadric is defined by 9 points [50]. One case that is obvious is two sets of 3 parallel accelerometers on two different planes. This configuration will yield the degenerate quadric that is the union of two planes. The two non-homogeneous equations for $[\mathbf{r}_g]_3$ imply that for each $[\mathbf{u}_g]_2$, there is a line of points P_g such that $\mathsf{A}(P_g, \mathbf{u}_g)$ is generated by $\{2,3\}_6$. Thus, it can be concluded that the quadric is generally also a ruled surface. This disqualifies some types of quadric, such as an hyperboloid of two sheets and an ellipsoid, from consideration.

When $d = 3$, satisfying the 2 homogeneous equations for $[\mathbf{u}_g]_3$ generally means that generation is possible in a single direction at each point in the D-dimensional affine subspace. The simplest case is $\{1,3\}_4$. This case was

discussed in general terms in Section 4.4. Translating to the current specific situation, it can be stated that a unique $\mathbf{u}_g$ is generated at each point, and that it is parallel to a vector with each element dependent quadratically upon x_g^2. The accelerometers generated along the line do not have *every* direction in $\mathbf{E}$. To see this, consider the 2 non-homogeneous equations for x_g:

$$\begin{bmatrix} w_1(u_{g,1}, u_{g,2}, u_{g,3}) \\ w_2(u_{g,1}, u_{g,2}, u_{g,3}) \end{bmatrix} x_g = \begin{bmatrix} c_1(u_{g,1}, u_{g,2}, u_{g,3}) \\ c_2(u_{g,1}, u_{g,2}, u_{g,3}) \end{bmatrix}. \tag{4.60}$$

These equations are consistent only if

$$\det \begin{bmatrix} w_1(u_{g,1}, u_{g,2}, u_{g,3}) & c_1(u_{g,1}, u_{g,2}, u_{g,3}) \\ w_2(u_{g,1}, u_{g,2}, u_{g,3}) & c_2(u_{g,1}, u_{g,2}, u_{g,3}) \end{bmatrix} = 0.$$

This requirement yields a quadric in terms of $u_{g,1}$, $u_{g,2}$ and $u_{g,3}$, that will intersect the unit sphere $u_{g,1}^2 + u_{g,2}^2 + u_{g,3}^2 = 1$ in a curve, indicating that only a single infinity of directions can be generated by $\{1,3\}_4$.

The other two configurations of the type under study with $d = 3$ are, as shown in Table 4.4, $\{2,3\}_7$ and $\{3,3\}_{10}$. In both cases the homogeneous equations for $[\mathbf{u}_g]_3$ mean that in general there is an accelerometer of a single direction generated at each point in the 2 and 3 dimensional affine subspaces. The non-homogeneous equations for $[\mathbf{r}_g]_D$ show that in the first case the accelerometers are generated at a single point while in the second they are generated along lines, suggesting the existence of a unique point at which accelerometers of all directions can be generated.

4.4.3 FCC Minus 3

Reference to Table 4.5 shows that there are only 5 types of constrained configurations to consider in this case. Further, two of the configurations, $\{2,2\}_3$ and $\{1,3\}_3$ have the minimum possible number of accelerometers allowable for constrained configurations of their types. Before considering the non-minimal cases it is quickly confirmed that $\{2,2\}_3$ and $\{1,3\}_3$ are only capable of trivial generation. In the first case, the consistency of the 3 non-homogeneous equations for $[\mathbf{r}_g]_2$ leads to a cubic in $u_{g,1}$ and $u_{g,2}$. Applying Bezout's theorem shows that this cubic will have 6 intersections with the unit circle, but, again these will appear in diametrically opposite pairs so that only three are meaningful. These meaningful intersections are at $[\mathbf{u}_k]_2$ for $k = 1,2,3$, so only trivial generation is possible. The configuration, $\{1,3\}_3$, is easier to dispense with. The determinant of the 3×3 matrix formed from the homogeneous equations for $[\mathbf{u}_g]_3$, is cubic in x_g, implying that generation is only possible for three values of x_g, and these must be $x_g = x_k$ for $k = 1,2,3$.

As shown in Table 4.5 the only configuration with $d = 2$ that remains to be considered is $\{3,2\}_5$; 5 accelerometers not on a plane, with coplanar directions.

Table 4.5: The constrained configurations with $d > 1$ and $D > 0$ that are 3 accelerometers short of being FCCs.

	On a Line	On a Plane	Not on a Plane
Coplanar	-	3	5
Spatial	3	6	9

The 3 homogeneous equations for the two elements of $[\mathbf{u}_g]_2$ are of the form

$$\begin{bmatrix} v_{1,1}(x_g, y_g, z_g) & v_{1,2}(x_g, y_g, z_g) \\ v_{2,1}(x_g, y_g, z_g) & v_{2,2}(x_g, y_g, z_g) \\ v_{3,1}(x_g, y_g, z_g) & v_{3,2}(x_g, y_g, z_g) \end{bmatrix} \begin{bmatrix} u_{g,1} \\ u_{g,2} \end{bmatrix} = \begin{bmatrix} 0 \\ 0 \\ 0 \end{bmatrix}. \tag{4.61}$$

As was discussed in Section 4.4, it can be ensured that the 3×2 matrix is rank deficient by setting 2 determinants equal to zero. Each of the determinants is a quadric, so this approach suggests that generation might be possible along a certain curve in $\mathscr{E}$; the intersection of two quadrics. The investigation is continued by turning to the non-homogeneous equations for $[\mathbf{r}_g]$, which are

$$\begin{bmatrix} w_{1,1}(u_{g,1}, u_{g,2}) & \cdots & w_{1,3}(u_{g,1}, u_{g,2}) \\ \vdots & \ddots & \vdots \\ w_{3,1}(u_{g,1}, u_{g,2}) & \cdots & w_{3,3}(u_{g,1}, u_{g,2}) \end{bmatrix} \begin{bmatrix} x_g \\ y_g \\ z_g \end{bmatrix} = \begin{bmatrix} c_1(u_{g,1}, u_{g,2}) \\ \vdots \\ c_3(u_{g,1}, u_{g,2}) \end{bmatrix}. \tag{4.62}$$

As in the analysis of $\{1,2\}_3$ and $\{2,2\}_4$, each equation can be divided by $u_{g,1}$ leading to 3 equations for x_g, y_g and z_g, in terms of $\tau_g = \tan\gamma_g$. Since each of the elements of the modified matrices is linear in τ_g, it is easy to see, using Cramer's rule, for example, that x_g, y_g and z_g can be expressed as rational functions of τ_g. The denominator of each function is the same cubic function of τ_g; it is equal to the determinant of the matrix. The numerator of each of the functions is a different cubic in τ_g. This rational structure and the fact that the curve must pass through 4 non-coplanar points allows the locus to be identified as a 'twisted cubic'. This identification also fits with the intersection of two quadrics suggested by the analysis of the homogeneous equations for $[\mathbf{u}_g]_2$, since a double infinity of quadrics pass through a given twisted cubic. Just as with the conics and quadrics that have been encountered so far, the requirement that the twisted cubic pass through the 5 points, $\{P_k\}_1^5$, is not sufficient to fully specify it because there is a unique twisted cubic through 6 (general) points in space [50]. It follows that the remaining freedom of the twisted cubic is some function of the relative directions of the accelerometers.

The two configurations with $d = 3$ that need to be considered are, $\{2,3\}_6$ and $\{3,3\}_9$. The accelerometers on the plane are considered first. The homo-

geneous equations for $[\mathbf{u}_g]_3$ are

$$\begin{bmatrix} v_{1,1}(x_g, y_g) & \cdots & v_{1,3}(x_g, y_g) \\ \vdots & \ddots & \vdots \\ v_{3,1}(x_g, y_g) & \cdots & v_{3,3}(x_g, y_g) \end{bmatrix} \begin{bmatrix} u_{g,1} \\ u_{g,2} \\ u_{g,3} \end{bmatrix} = \begin{bmatrix} 0 \\ 0 \\ 0 \end{bmatrix}. \tag{4.63}$$

Setting the determinant equal to zero shows that generation is only possible upon some cubic curve in the plane. There are 3 non-homogeneous equations for x_g and y_g. Taking the determinant of the augmented matrix leads to a cubic surface that will intersect the unit sphere, $u_{g,1}^2 + u_{g,2}^2 + u_{g,3}^2 = 1$ in a curve. It follows that a single infinity of directions are generated along the cubic curve in the plane.

As for $\{3,3\}_9$, setting the determinant of the 3 homogeneous equations for $[\mathbf{u}_g]_3$ equal to zero shows that generation is only possible on some cubic surface in $\mathscr{E}$. The non-homogeneous equations for $[\mathbf{r}_g]_D$ are of the form:

$$\begin{bmatrix} w_{1,1}(u_{g,1}, u_{g,2}, u_{g,3}) & \cdots & w_{1,3}(u_{g,1}, u_{g,2}, u_{g,3}) \\ \vdots & \ddots & \vdots \\ w_{3,1}(u_{g,1}, u_{g,2}, u_{g,3}) & \cdots & w_{3,3}(u_{g,1}, u_{g,2}, u_{g,3}) \end{bmatrix} \begin{bmatrix} x_g \\ y_g \\ z_g \end{bmatrix} = \begin{bmatrix} c_1(u_{g,1}, u_{g,2}, u_{g,3}) \\ \vdots \\ c_3(u_{g,1}, u_{g,2}, u_{g,3}) \end{bmatrix}. \tag{4.64}$$

The determinant of the 3×3 matrix is cubic in $u_{g,1}$, $u_{g,2}$ and $u_{g,3}$. Thus, the matrix will be singular for some single infinity of directions corresponding to the intersection of the cubic surface with the unit sphere, and, in general, generation will not be possible for these directions. The exception occurs when the 3×1 matrix on the right-hand side still lies in the column space. To determine whether or not this occurs requires knowledge of the actual coefficients.

4.4.4 FCC Minus 4 or More

The previous subsection showed that once three accelerometers have been removed there are only three types of constrained configuration that are still capable of non-trivial generation, $\{3,2\}$, $\{2,3\}$ and $\{3,3\}$. The configuration, $\{3,2\}_5$, was shown to generate along a twisted cubic, $\{2,3\}_6$, while the $\{2,3\}_6$ generates a single infinity of directions along a cubic curve and $\{3,3\}_9$ generates almost all directions on some cubic surface in $\mathscr{E}$. In this subsection accelerometers are removed from these configurations until they are no longer able to generate.

The configuration, $\{3,2\}_4$ is considered first. The four non-homogeneous equations for $[\mathbf{r}_g]_3$ are of the form,

$$\begin{bmatrix} w_{1,1}(u_{g,1},u_{g,2}) & \cdots & w_{1,3}(u_{g,1},u_{g,2}) \\ \vdots & \ddots & \vdots \\ w_{4,1}(u_{g,1},u_{g,2}) & \cdots & w_{4,3}(u_{g,1},u_{g,2}) \end{bmatrix} \begin{bmatrix} x_g \\ y_g \\ z_g \end{bmatrix} = \begin{bmatrix} c_1(u_{g,1},u_{g,2}) \\ \vdots \\ c_4(u_{g,1},u_{g,2}) \end{bmatrix}. \tag{4.65}$$

Forming the 4×4 augmented matrix and setting the determinant equal to zero gives rise to an equation of fourth order in $u_{g,1}$ and $u_{g,2}$. Bezout's theorem indicates that this equation will intersect the unit circle in 8 locations. As has been discussed above, these intersections will occur in diametrically opposite pairs. Thus, there are only four meaningful intersections, and these correspond to the four accelerometers, meaning that only trivial generation is possible.

The configuration, $\{2,3\}_5$, is now considered. There are 4 homogeneous equations for $[\mathbf{u}_g]$:

$$\begin{bmatrix} v_{1,1}(x_g,y_g) & \cdots & v_{1,3}(x_g,y_g) \\ \vdots & \ddots & \vdots \\ v_{4,1}(x_g,y_g) & \cdots & v_{4,3}(x_g,y_g) \end{bmatrix} \begin{bmatrix} u_{g,1} \\ u_{g,2} \\ u_{g,3} \end{bmatrix} = \begin{bmatrix} 0 \\ 0 \\ 0 \end{bmatrix}. \tag{4.66}$$

The 4×3 matrix is rank deficient if the determinants of the first 3 rows and last 3 rows are equal to zero. Each of these determinants describes cubics in the plane, so generation should only be possible at their intersection. Bezout's theorem suggests that there will be 9 intersections of these two cubics, where one would expect 5 since there are only 5 accelerometers. How to account for these 4 additional intersections remains to be seen. One possibility is that that some of the intersections have multiplicity, 2. It certainly seems, however, that $\{2,3\}_5$ is only capable of trivial generation.

The configuration, $\{3,3\}_8$, has homogeneous equations for $[\mathbf{u}_g]$ similar to those in Eq (4.66) with the exception that each element is a function of x_g, y_g and z_g. Setting the determinant of a matrix comprised of 3 rows equal to zero leads to a cubic surface in $\mathscr{E}$. The intersection of two cubic surfaces is a curve along which the configuration is able to generate. There are 4 non-homogeneous equations for $[\mathbf{r}_g]_3$, and the equations are only consistent if the 4×4 augmented matrix is singular. The determinant of the matrix is a cubic surface that will intersect the unit sphere in a curve. Thus, $\{3,3\}_8$ is able to generate accelerometers with a single infinity of directions along a single curve in space.

Based upon the results of the previous subsections it certainly seems that removing one more accelerometer from $\{3,3\}_8$ will result in a configuration, $\{3,3\}_7$ that is not able to generate. This configuration has 5 homogeneous equations for $[\mathbf{u}_g]_3$. To ensure that the 5×3 matrix is rank deficient requires that the determinants of 3 sets of 3×3 sub-matrices be equal to zero. Each

determinant leads to a cubic surface in $\mathscr{E}$. Three such surfaces will generally intersect in a finite number of points, indicating that $\{3,3\}_7$ is not able to generate. A similar conclusion is reached by considering the 5 non-homogeneous equations for $[\mathbf{r}_g]_3$.

4.4.5 Generation Summary

The results of the generation analysis of the previous four subsections are presented here in tabular form. Table 4.6 summarizes the results for configurations with coplanar directions, and Table 4.7 for those with spatial directions. In each of the tables it is taken for granted that the geometric loci that are involved pass through the existing accelerometers.

Table 4.6: The accelerometers generated by configurations of n accelerometers with coplanar directions.

n	At a Point	On a Line	On a Plane	Not on a Plane
2	All			
3		Single direction at each point on the line.		
4		All	Single direction at each point of a conic.	
5			Single direction at each point in the plane. Lines with common directions.	Single direction at each point of a twisted cubic.
6			All	Single direction at each point on a quadric that is also a ruled surface.
7				Single direction at each point of space. Planes with common directions.
8				All

Table 4.7: The accelerometers generated by configurations of n accelerometers with spatial directions.

n	At a Point	On a Line	On a Plane	Not on a Plane
3	All			
4		Single ∞ of directions along the line.		
5		Plane of directions at each point of the line.		
6		All	Single ∞ of directions on a cubic.	
7			Single direction at each point in the plane.	
8			Plane of directions at each point on the plane. Lines with common directions.	Single ∞ along the intersection of two cubic surfaces.
9			All	Single direction at each point on a cubic surface.
10				Single direction at each point in space. Common directions on lines.
11				Plane of directions at each point. Common directions on planes.
12				All

These tables show definite patterns and one skilled in the art of projective geometry might be able see even more. Consider for instance that the quadric surface and twisted cubic are the two manifolds in space that are analogous to the conic section.

Beyond the geometry, the point of the generation analysis is, of course, so that dependent configurations can be identified and avoided. For instance if one is looking to place accelerometers on a plane, these tables show that if the directions are coplanar, up to 3 can be placed arbitrarily after which a conic of accelerometers is generated. Placing a fourth accelerometer anywhere not on the conic leads to a pencil of lines along which accelerometers of each direction cannot be placed; one direction for each line of the pencil. It is not possible to position any independent accelerometer at the intersections of these lines if its direction is coplanar with the existing accelerometers. This distribution of generated accelerometers is similar to that encountered in Chapter 3 in the study of planar accelerometer configurations. The differences between the current case and that considered in Chapter 3 are that the circle has been replaced by a general conic and that 5 rather than 3 accelerometers are involved. Further, it is not possible to determine which of the infinite number of conics through the 4 accelerometers is required without recourse to calculations. Similar comments can be made regarding the positioning of independent accelerometers on lines and in space. Below a certain number of accelerometers the accelerometers can be placed without fear of dependence. Above another limit it is impossible to place an independent accelerometer, and between these, one must check that accelerometers do not lie on certain geometric manifolds and have certain directions.

4.5 Summary

The geometrical results presented in this chapter are entirely novel. Previous researchers have been content to prove the independence of certain configurations, rather than exploring the theory of accelerometer independence and generation as a topic in its own right.

It was not possible to be as definitive, or axiomatic, in the definitions of general accelerometer generation as it was in the case of planar accelerometer configurations considered in the previous chapter. This was because of the many special types of configurations that can arise. For example, a configuration with directions spanning $\mathbf{E}$ may be primarily composed of coplanar, or even parallel accelerometers, and this will no doubt change the 'shapes' of the accelerometers that are generated. More research needs to be done to uncover exactly how 'general' a configuration needs to be. It should be mentioned, however, that all configurations that were generated randomly using custom written code in GNU Octave, conformed with the presented results, leading

to conics, twisted cubics and so on. It might even be that the general results *do* hold even in the special cases, but degenerate forms of the geometric loci occur. For instance, one example of a degenerate conic is a pair of lines, and this can occur with two pairs of parallel accelerometers; certainly a special case of four coplanar accelerometers on a plane. This is certainly a fertile area for future research.

Chapter 5

Minimal Spatial Configurations

As was described in Section 2.4.4 there are two main types of GFIN; that where a full configuration of 12 (or more) accelerometers is used to determine the full specific force state, and that where 6 accelerometers are used to determine only the parameters that are strictly required to determine the motion of the body; the angular velocity $[\boldsymbol{\omega}^{\boldsymbol{b}}]$, and the specific force $[\mathbf{s}^{\boldsymbol{b}}_{O_B}]$. The latter method was referred to as Minimal GFIN (MGFIN). Six accelerometers that have been positioned so that they can be used for MGFIN are referred to as a *minimal configuration.* The analog of the minimal configuration for the case of planar motion was discussed in Section 3.5 where it was shown how 3 accelerometers can be used to determine the planar motion of a rigid body to which they are attached. This chapter is dedicated to the study of minimal configurations proper.

Section 5.1 gives a brief review of minimal configurations that have been presented in the literature. Next, in Section 5.2 the geometric conditions that accelerometers must satisfy in order to be part of a minimal configuration are stated. As was discussed in Section 2.4.4, general minimal configurations have two undesirable properties; the necessity to solve a nonlinear equation for $[\boldsymbol{\omega}^{\boldsymbol{b}}]$, and the fact that errors in the solution for $[\boldsymbol{\omega}^{\boldsymbol{b}}]$ can cause errors in the calculation of $[\mathbf{s}^{\boldsymbol{b}}_{O_B}]$. In Section 5.3 these difficulties are made explicit, and it is proved that it is impossible to design an 'ideal' minimal configuration that is free from both. In Section 5.4 it is shown how to design configurations in which the necessity to solve a nonlinear differential equation is removed, resulting in a type of configuration that is referred to as a *special minimal configuration.* Two examples of special minimal configurations are designed in Section 5.5.

5.1 Review of Minimal Configurations

Schuler et al., writing in 1967, were the first to present a minimal configuration [5]. The configuration, which is shown in Fig 5.1, required the integration of

a nonlinear differential equation for the angular velocity. The authors noted that the differential equation is unstable and so did not recommend its use.

In the Appendix of his paper on the use of accelerometers for the measurement of human gait, Morris presented a proof that 6 accelerometers can, in principle, be used to determine the motion of a rigid body [19]. He did not fully state the requirements regarding the orientations and positions of the accelerometers, saying that

> The only limitation on the points of measurements is that the measurement axes are orthogonal.

This is, on the one hand too restrictive in that non-orthogonal accelerometers can certainly be used, but also not precise enough, because it says nothing regarding the locations of the accelerometers; two triaxial accelerometers do not form a minimal configuration.

Padgaonkar et al. compared the use of a minimal configuration requiring the solution of a nonlinear differential equation for angular velocity and a 9-accelerometer configuration in which the angular acceleration is obtained as a linear combination of the accelerometer measurements [11]. Based upon the results of simulations, they noted that the minimal configuration was less stable than the 9-axis configuration. Liu offered analytical support to their findings [26]. Much more recently, Giansanti et al. compared Schuler's minimal configuration and the 9-accelerometer configurations used by Padgaonkar et al [27]. After conducting numerous simulations, involving the effects of various accelerometer errors, they concluded in favor of the minimal configuration, principally because of the effects of accelerometer positioning and orientation errors, the effects of which were more pronounced in the 9-accelerometer configuration.

A minimal configuration originally designed by Chen et al. has recently attracted a lot of attention in the literature [7]. This configuration, shown in Fig 5.2, is attractive because it does not require the integration of a nonlinear differential equation to obtain the angular velocity. Since the introduction of Chen's configuration, Tan et al. have written a series of papers considering various aspects of its use. They have presented a method by which accelerometer position and orientation errors can be identified by simple tests using a turntable, and proposed a method of accounting for these configuration errors [29, 41]. They have also considered the addition of a triaxial accelerometer to Chen's minimal configuration, and the use of an Extended Kalman Filter to estimate angular velocity using the resulting 9-accelerometer configuration [10]. Ding et al. have also presented a 9-accelerometer configuration resulting from the addition of sensors to Chen's configuration [42]. The proposed additional accelerometers are shown in Fig 5.2.

This review shows that minimal configurations have been of interest for over 40 years, both as stand-alone units, and, more recently, as a base upon

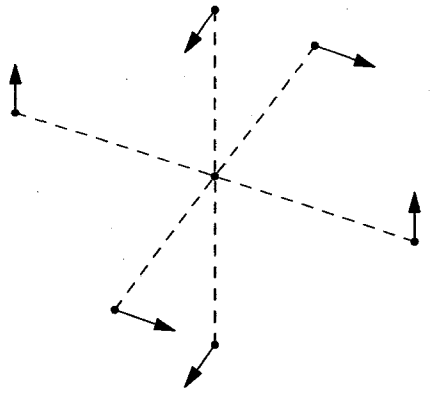

Figure 5.1: Schuler's minimal configuration, consisting of three parallel pairs of accelerometers, with orthogonal directions.

which other configurations can be built. Over these years, scant attention has been paid to the minimal configuration design problem. Tan et al. [29] have stated that in order for 6 accelerometers to form a minimal configuration, a certain 6×6 matrix must be non-singular, and that

> This condition is "almost surely" satisfied since the set of singular 6×6 matrices is a "measure zero" set in $R^{6\times 6}$.

Variations on this statement occur in the authors' other papers, but no geometric exploration of the conditions under which the matrix is singular was undertaken. Ding et al. [60] attempted to generalize Tan's result by saying that the rank of a certain $n \times 6$ matrix should be greater than or equal to 6. It is, however, impossible for the rank of any $n \times 6$ matrix to be greater than 6. Aside from this lack of geometric guidelines in the general case, there has been no indication in the literature about how accelerometers should be placed if one desires the configuration to have certain properties. Chief among the desirable properties of a minimal configuration is the avoidance of the necessity of solving a nonlinear differential equation for the angular velocity. Chen's configuration has this property, and this is probably the reason that it has received so much attention.

5.2 Geometry of Minimal Configurations

In Section 2.4.4 where the concept of MGFIN was introduced, the measurement equations of n accelerometers were written as

$$[\mathbf{M}_n^{\mathcal{B}}] \begin{bmatrix} [\mathbf{s}_{O_{\mathcal{B}}}^{b}] \\ [\boldsymbol{\alpha}^{b}] \end{bmatrix} = [\mathbf{a}_n] - [\mathbf{Q}_n^{\mathcal{B}}] \begin{bmatrix} \mathrm{q}_{ij}([\boldsymbol{\omega}^{b}]) \\ \mathrm{q}_{ii}([\boldsymbol{\omega}^{b}]) \end{bmatrix}. \tag{5.1}$$

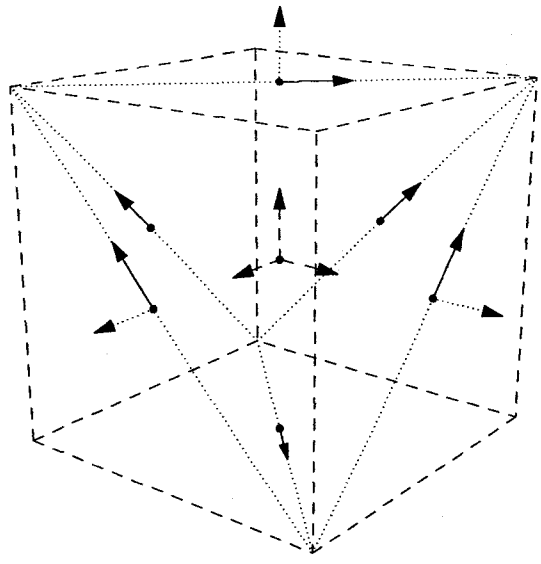

Figure 5.2: Chen's minimal configuration (solid arrows), with Tan's proposed addition of a triaxial accelerometer (dashed arrows), and Ding's addition of three accelerometers (dotted arrows).

In this equation the k^{th} row of $[\mathbf{M}_n^{\mathcal{B}}]$ is

$$[\mathbf{m}_k^{\mathcal{B}}] = \left[[\mathbf{u}_k^{\boldsymbol{b}}]^T \quad -[\mathbf{u}_k^{\boldsymbol{b}}]^T \text{skew}([\mathbf{r}_k^{\mathcal{B}}]) \right], \tag{5.2}$$

while the k^{th} row of $[\mathbf{Q}_6^{\mathcal{B}}]$ is

$$[\mathbf{q}_k^{\mathcal{B}}] = \left[[\mathbf{h}_k^{\mathcal{B}}] \quad [\mathbf{d}_k^{\mathcal{B}}] \right] \tag{5.3}$$

with

$$[\mathbf{h}_k^{\mathcal{B}}] = [\mathbf{u}_k^{\boldsymbol{b}}]^T \text{sym}([\mathbf{r}_{P_k}^{\mathcal{B}}]) \tag{5.4}$$

$$[\mathbf{d}_k^{\mathcal{B}}] = -[\mathbf{u}_k^{\boldsymbol{b}}]^T \text{diag}([\mathbf{r}_{P_k}^{\mathcal{B}}]). \tag{5.5}$$

Definition 5.2.1. A set of n accelerometers is *minimally independent* if the $n \times 6$ matrix, $[\mathbf{M}_n^{\mathcal{B}}]$, is of rank n, i.e., if the set of matrices, $\{[\mathbf{m}_k^{\mathcal{B}}]\}_{k=1}^n$ is linearly independent. A set of 6 minimally independent accelerometers is a *minimal configuration.*

The minimal independence of a set of accelerometers implies the independence of the same set, but the converse does not hold; minimal independence is a special sort of independence. Clearly, a configuration including 6 minimally independent accelerometers is required to solve Eq (5.1) for $[\mathbf{s}_{O_B}^{\boldsymbol{b}}]$ and $[\boldsymbol{\alpha}^{\boldsymbol{b}}]$.

In contrast to (full) independence as discussed in Chapter 4, minimal independence can be completely characterized using the results of line geometry. Recall Definition 3.5.2, used in the study of planar minimal configurations:

that the 'line of the accelerometer', $\mathsf{A}(P, \mathbf{u})$, is that through P directed by $\mathbf{u}$. This same definition is used here. The key result for interpreting the geometric requirements of the minimal independence of a set of accelerometers is:

Proposition 5.2.1. *A set of n accelerometers is minimally independent if and only if the lines of the accelerometers are linearly independent.*

Proof. The matrix, $[\mathbf{m}_k^{\mathcal{B}}]$, is composed of the Plücker coordinates [59, 61, 62] of the line of the accelerometer, A_k, in $\mathcal{B}$. Since a set of lines is linearly independent if the corresponding set of Plücker coordinates is independent (and vice versa) [59, 63], the result follows immediately. □

Fortuitously, the conditions under which sets of lines have linearly dependent Plücker coordinates has been studied at length because it has application in determining singularities of parallel platforms [32, 61, 64]. These references, and others, list the conditions under which a set of $2 \leq n \leq 6$ lines are linearly *dependent*. Rather than list all of the special cases for each $2 \leq n \leq 6$, a few simple results, some of which are needed in the following sections, are stated here.

- Two accelerometers are minimally dependent if and only if their lines are the same, i.e., if $\mathbf{u}_2 = \pm\mathbf{u}_1$, and the line of $\mathsf{A}(P_1, \mathbf{u}_1)$ includes P_2.
- Three accelerometers are minimally dependent (assuming no pair is minimally dependent) if the lines of the accelerometers are either parallel and coplanar, or coplanar and intersect at a finite point.

These results are exactly those that were obtained for planar minimal configurations. A more interesting case involves 4 accelerometers. Suppose that 3 accelerometers with skew lines have been placed and one seeks the positions and orientations that a fourth accelerometer *cannot* have if the resulting set is to be minimally independent. The lines that are linearly dependent on those of the first three accelerometers are a regulus; either a circular hyperboloid or a hyperbolic paraboloid, as shown in Fig 5.3. These are doubly ruled surfaces; there are two families of skew straight lines on each of them. If a fourth accelerometer is placed so that it is in the same set of rulings as the first three accelerometers, then the resulting configuration is minimally dependent, otherwise it is minimally independent.

The important point is that the geometrical conditions under which a set of lines is linearly dependent are well known, thus minimally independent configurations can be constructed by ensuring that the set of $2 \leq n \leq 6$ lines associated with the n accelerometers does not match any of the cases catalogued in the aforementioned references.

The geometrical description of a minimal configuration obtained using Proposition 5.2.1 is equivalent to the algebraic definition given by Tan [10,

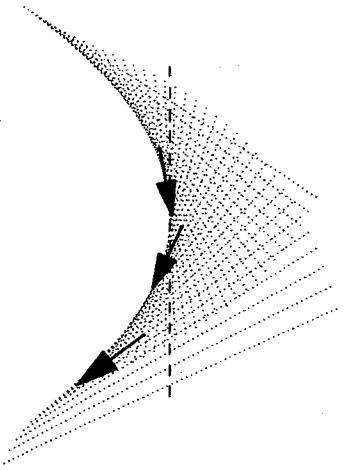

Figure 5.3: A hyperbolic paraboloid defined by the lines of three accelerometers. If a fourth accelerometer is located so that its line is a ruling (of the same family) on this surface, the resulting configuration will be minimally dependent.

29, 41], but here, rather than saying that almost all configurations of 6 accelerometers are minimally independent, specific geometric rules have been referred to.

5.3 Ideal Minimal Configurations

If $\{\mathsf{A}_k\}_1^6$ is a minimal configuration, Eq (5.1) can be solved for $[\mathbf{s}^{\boldsymbol{b}}_{O_B}]$ and $[\boldsymbol{\alpha}^{\boldsymbol{b}}]$ as

$$\begin{bmatrix}[\mathbf{s}^{\boldsymbol{b}}_{O_B}]\\ [\boldsymbol{\alpha}^{\boldsymbol{b}}]\end{bmatrix} = [\mathbf{M}_6^{\mathcal{B}}]^{-1}[\mathbf{a}_6] - [\mathbf{M}_6^{\mathcal{B}}]^{-1}[\mathbf{H}_6^{\mathcal{B}}]\mathrm{q}_{ij}([\boldsymbol{\omega}^{\boldsymbol{b}}]) - [\mathbf{M}_6^{\mathcal{B}}]^{-1}[\mathbf{D}_6^{\mathcal{B}}]\mathrm{q}_{ii}([\boldsymbol{\omega}^{\boldsymbol{b}}]), \quad (5.6)$$

where the k^{th} rows of the 6×3 matrices $[\mathbf{H}_6^{\mathcal{B}}]$ and $[\mathbf{D}_6^{\mathcal{B}}]$ are $[\mathbf{h}_k^{\mathcal{B}}]$ and $[\mathbf{d}_k^{\mathcal{B}}]$ as given at Eqs (5.4) and (5.5). To get more insight into the exact nature of these equations, the matrices pre-multiplying $[\mathbf{a}_6]$, $\mathrm{q}_{ij}([\boldsymbol{\omega}^{\boldsymbol{b}}])$ and $\mathrm{q}_{ii}([\boldsymbol{\omega}^{\boldsymbol{b}}])$ are all partitioned into 3×3 matrices:

$$\begin{bmatrix}[\mathbf{X}_{\mathbf{s}}^{\mathcal{B}}]\\ [\mathbf{X}_{\boldsymbol{\alpha}}^{\mathcal{B}}]\end{bmatrix} = [\mathbf{M}_6^{\mathcal{B}}]^{-1} \quad (5.7)$$

$$\begin{bmatrix}[\mathbf{Y}_{\mathbf{s}}^{\mathcal{B}}]\\ [\mathbf{Y}_{\boldsymbol{\alpha}}^{\mathcal{B}}]\end{bmatrix} = -[\mathbf{M}_6^{\mathcal{B}}]^{-1}[\mathbf{H}_6^{\mathcal{B}}] \quad (5.8)$$

$$\begin{bmatrix}[\mathbf{Z}_{\mathbf{s}}^{\mathcal{B}}]\\ [\mathbf{Z}_{\boldsymbol{\alpha}}^{\mathcal{B}}]\end{bmatrix} = -[\mathbf{M}_6^{\mathcal{B}}]^{-1}[\mathbf{D}_6^{\mathcal{B}}], \quad (5.9)$$

so that Eq (5.6) can be written as two separate equations:

$$[\mathbf{s}^{b}_{O_B}] = [\mathbf{X}^{\mathcal{B}}_{\mathbf{s}}][\mathbf{a}_6] + [\mathbf{Y}^{\mathcal{B}}_{\mathbf{s}}]\mathrm{q}_{ij}([\boldsymbol{\omega}^{b}]) + [\mathbf{Z}^{\mathcal{B}}_{\mathbf{s}}]\mathrm{q}_{ii}([\boldsymbol{\omega}^{b}]) \tag{5.10a}$$

$$[\boldsymbol{\alpha}^{b}] = [\mathbf{X}^{\mathcal{B}}_{\boldsymbol{\alpha}}][\mathbf{a}_6] + [\mathbf{Y}^{\mathcal{B}}_{\boldsymbol{\alpha}}]\mathrm{q}_{ij}([\boldsymbol{\omega}^{b}]) + [\mathbf{Z}^{\mathcal{B}}_{\boldsymbol{\alpha}}]\mathrm{q}_{ii}([\boldsymbol{\omega}^{b}]). \tag{5.10b}$$

Clearly, unless

- $[\mathbf{Y}^{\mathcal{B}}_{\boldsymbol{\alpha}}] = [\mathbf{Z}^{\mathcal{B}}_{\boldsymbol{\alpha}}] = [0]_{3\times 3}$, a nonlinear differential equation must be solved for $[\boldsymbol{\omega}^{b}]$.
- $[\mathbf{Y}^{\mathcal{B}}_{\mathbf{s}}] = [\mathbf{Z}^{\mathcal{B}}_{\mathbf{s}}] = [0]_{3\times 3}$, errors in the calculation of $[\boldsymbol{\omega}^{b}]$ will cause errors in the calculation of $[\mathbf{s}^{b}_{O_B}]$.

These conditions are far from ideal. Small errors in the initial conditions and accelerometer measurements will quickly lead to divergence in the calculation of $[\boldsymbol{\omega}^{b}]$. To have these errors propagate into the 'position part' of the algorithm only makes matters worse. Clearly then, the *ideal* minimal configuration has

$$[\mathbf{Y}^{\mathcal{B}}_{\boldsymbol{\alpha}}] = [\mathbf{Z}^{\mathcal{B}}_{\boldsymbol{\alpha}}] = [\mathbf{Y}^{\mathcal{B}}_{\mathbf{s}}] = [\mathbf{Z}^{\mathcal{B}}_{\mathbf{s}}] = [0]_{3\times 3} \tag{5.11}$$

so that Eqs (5.10a) and (5.10b) become

$$[\mathbf{s}^{b}_{O_B}] = [\mathbf{X}^{\mathcal{B}}_{\mathbf{s}}][\mathbf{a}_6] \tag{5.12a}$$

$$[\boldsymbol{\alpha}^{b}] = [\mathbf{X}^{\mathcal{B}}_{\boldsymbol{\alpha}}][\mathbf{a}_6]. \tag{5.12b}$$

The possibility of designing such an ideal configuration is now investigated.

Since $[\mathbf{M}^{\mathcal{B}}_6]^{-1}$ is non-singular, Eqs (5.7) and (5.8) show that Eq (5.11) can occur only if

$$[\mathbf{H}^{\mathcal{B}}_6] = [\mathbf{D}^{\mathcal{B}}_6] = [0]_{6\times 6}. \tag{5.13}$$

With reference to Eqs (5.4) and (5.5), this requires that

$$[\mathbf{h}^{\mathcal{B}}_k] = \quad [\mathbf{u}^{b}_k]^T \mathrm{sym}([\mathbf{r}^{\mathcal{B}}_{P_k}]) = [0] \qquad k = 1, \ldots 6 \tag{5.14a}$$

$$[\mathbf{d}^{\mathcal{B}}_k] = -[\mathbf{u}^{b}_k]^T \mathrm{diag}([\mathbf{r}^{\mathcal{B}}_{P_k}]) = [0] \qquad k = 1, \ldots 6 \tag{5.14b}$$

An accelerometer satisfying Eq (5.14a) is said to be free of $\mathrm{q}_{ij}([\boldsymbol{\omega}^{b}])$, since, with reference to Eq (5.1), its measurement is not affected by $\mathrm{q}_{ij}([\boldsymbol{\omega}^{b}])$. Similarly, an accelerometer satisfying Eq (5.14b) is said to be free of $\mathrm{q}_{ii}([\boldsymbol{\omega}^{b}])$. The ideal minimal configuration thus requires that all 6 accelerometers be chosen so that they are free of $\mathrm{q}_{ij}([\boldsymbol{\omega}^{b}])$ *and* $\mathrm{q}_{ii}([\boldsymbol{\omega}^{b}])$.

Conditions for Freedom From $\mathrm{q}_{ij}([\boldsymbol{\omega}^{b}])$**:** Taking the transpose of Eq (5.14a) and using the symmetry of $\mathrm{sym}([\mathbf{r}^{\mathcal{B}}_{P_k}])$ gives

$$[\mathbf{h}^{\mathcal{B}}_k]^T = \mathrm{sym}([\mathbf{r}^{\mathcal{B}}_{P_k}])[\mathbf{u}^{b}_k] = [0], \tag{5.15}$$

indicating that A_k is free of $\mathrm{q}_{ij}([\boldsymbol{\omega}^b])$ only if $[\mathbf{u}_k^b]$ lies in the null-space of $\mathrm{sym}([\mathbf{r}_{P_k}^{\mathcal{B}}])$. The determinant of $\mathrm{sym}([\mathbf{r}_{P_k}^{\mathcal{B}}])$ is $2r_{k,1}r_{k,2}r_{k,3}$, meaning that the matrix is only rank-deficient if P_k lies on a coordinate plane (or axis) of the body frame, $\mathcal{B}$. With the exception of the origin, O_B, of the frame, where $\mathrm{sym}([\mathbf{r}_{P_k}^{\mathcal{B}}]) = [0]$, the rank of $\mathrm{sym}([\mathbf{r}_{P_k}^{\mathcal{B}}])$ is 2 whenever P_k is on a coordinate plane or axis. The single dimension of the null-space means that when P_k is on a coordinate plane (or axis) there is a unique choice for $[\mathbf{u}_k^b]$ (down to a sign) such that $[\mathbf{h}_k^{\mathcal{B}}] = [0]$, i.e., A_k is free of $\mathrm{q}_{ij}([\boldsymbol{\omega}^b])$. Explicitly calculating the null-space leads the conclusion that A_k (with $P_k \neq O_B$) is free of $\mathrm{q}_{ij}([\boldsymbol{\omega}^b])$ if and only if

- P_k is on a coordinate plane of $\mathcal{B}$ and $\mathbf{u}_k$ is parallel to the vector obtained by reflecting $\mathbf{r}_{P_k/O_B}$ in either of the axes of that plane, *or*
- P_k is on a coordinate axis of $\mathcal{B}$, and $\mathbf{u}_k$ is parallel to that axis.

The second case can be seen as a special case of the first. Accelerometers satisfying these conditions are shown in Fig 5.4.

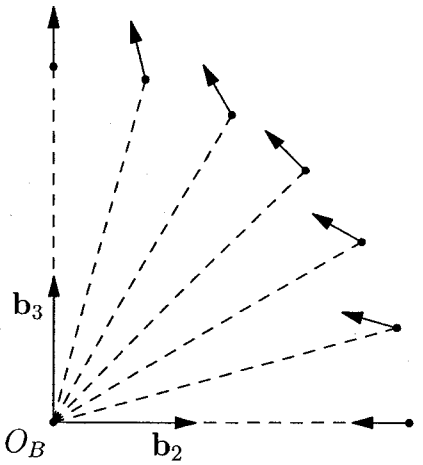

Figure 5.4: A sampling of accelerometers in the '23' plane of $\mathcal{B}$ that are free of $\mathrm{q}_{ij}([\boldsymbol{\omega}^b])$.

Conditions for Freedom From $\mathrm{q}_{ii}([\boldsymbol{\omega}^b])$: Since $\mathrm{diag}([\mathbf{r}_{P_k}^{\mathcal{B}}])$ is a symmetrical matrix Eq (5.14b) is satisfied if

$$[\mathbf{d}_k^{\mathcal{B}}]^T = -\mathrm{diag}([\mathbf{r}_{P_k}^{\mathcal{B}}])[\mathbf{u}_k^b] = [0], \tag{5.16}$$

i.e., if $[\mathbf{u}_k^b]$ lies in the null-space of $\mathrm{diag}([\mathbf{r}_{P_k}^{\mathcal{B}}])$. Similar to $\mathrm{sym}([\mathbf{r}_{P_k}^{\mathcal{B}}])$, $\mathrm{diag}([\mathbf{r}_{P_k}^{\mathcal{B}}])$ has full-rank if and only if each element of $[\mathbf{r}_{P_k}^{\mathcal{B}}]$ is non-zero. If exactly one element is zero, meaning that P_k lies on a coordinate plane, the matrix has rank, 2, and if two elements are zero, which occurs when P_k is on a coordinate

axis, it has rank, 1. Geometrically, the null-space of the matrix in each case is such that A_k (with $P_k \neq O_B$) is free of $\mathrm{q}_{ii}([\boldsymbol{\omega}^b])$ if and only if

- P_k is on a coordinate plane of $\mathcal{B}$ and $\mathbf{u}_k$ is orthogonal to that plane, *or*
- P_k is on a coordinate axis of $\mathcal{B}$ and $\mathbf{u}_k$ is orthogonal to that axis.

Accelerometers that are free of $\mathrm{q}_{ii}([\boldsymbol{\omega}^b])$ are important in this chapter, so to make discussion involving them more readable, some terminology is introduced. As shown in Fig 5.5, a Type A_i accelerometer is located on the i^{th} axis of $\mathcal{B}$ and directed orthogonal to it, while a Type P_{ij} accelerometer is located on the ij plane of $\mathcal{B}$ and directed orthogonal to it.

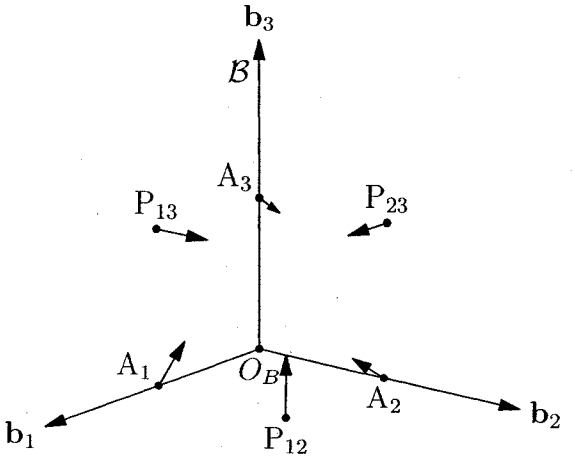

Figure 5.5: The types of accelerometer placement that are free of $\mathrm{q}_{ii}([\boldsymbol{\omega}^b])$.

Figures 5.4 and 5.5 show that, with the exception of O_B where $\mathrm{diag}([\mathbf{r}^{\mathcal{B}}_{P_k}]) = \mathrm{sym}([\mathbf{r}^{\mathcal{B}}_{P_k}]) = [0]_{3\times 3}$, the geometric requirements on the placement of an accelerometer to be free of $\mathrm{q}_{ij}([\boldsymbol{\omega}^b])$ and $\mathrm{q}_{ii}([\boldsymbol{\omega}^b])$ are mutually exclusive. Since it is impossible to locate 6 independent accelerometers at a single point it can be concluded that it is not possible to design an ideal minimal configuration, i.e., one such that $[\mathbf{s}^b_{O_B}]$ and $[\boldsymbol{\alpha}^b]$ can be determined as in Eqs (5.12a) and (5.12b).

It is important to note that the freedom of an accelerometer from $\mathrm{q}_{ij}([\boldsymbol{\omega}^b])$ or $\mathrm{q}_{ii}([\boldsymbol{\omega}^b])$ is a frame specific property. Generally, if the frame, $\mathcal{B}$ is rotated or translated while the accelerometers remain stationary, the geometric conditions for freedom will be lost. It is because of this frame specificity that the superscripts, $\mathcal{B}$ and $\boldsymbol{b}$, are used for all quantities in this chapter.

5.4 Special Minimal Configurations

Having conceded that the ideal minimal configuration is impossible, attention is turned to the design of minimal configurations for which it is not necessary

to solve a nonlinear differential equation for $[\boldsymbol{\omega}^{\boldsymbol{b}}]$, but the coupling between $[\mathbf{s}^{\boldsymbol{b}}_{O_B}]$ and $[\boldsymbol{\omega}^{\boldsymbol{b}}]$ remains.

Definition 5.4.1. A minimal configuration with $[\mathbf{Y}^{\mathcal{B}}_{\boldsymbol{\alpha}}] = [\mathbf{Z}^{\mathcal{B}}_{\boldsymbol{\alpha}}] = [0]_{3\times 3}$ is referred to as a *special minimal configuration.*

Equations (5.8) and (5.2) show that the following relationship must exist for a special minimal configuration:

$$[\mathbf{H}^{\mathcal{B}}_6] = -[\mathbf{M}^{\mathcal{B}}_6]\begin{bmatrix}[\mathbf{Y}^{\mathcal{B}}_{\mathbf{s}}]\\ [0]_{3\times 3}\end{bmatrix} = \begin{bmatrix}[\mathbf{u}^{\boldsymbol{b}}_1]^T[\mathbf{Y}^{\mathcal{B}}_{\mathbf{s}}]\\ \vdots \\ [\mathbf{u}^{\boldsymbol{b}}_6]^T[\mathbf{Y}^{\mathcal{B}}_{\mathbf{s}}]\end{bmatrix}. \tag{5.17}$$

Recalling the definition of $[\mathbf{h}^{\boldsymbol{b}}_k]$ from Eq (5.4) then leads to the following series of constraint equations:

$$-[\mathbf{Y}^{\mathcal{B}}_{\mathbf{s}}]^T[\mathbf{u}^{\boldsymbol{b}}_k] = \mathrm{sym}([\mathbf{r}^{\mathcal{B}}_{P_k}])[\mathbf{u}^{\boldsymbol{b}}_k] \qquad k = 1,\ldots,6. \tag{5.18}$$

Performing similar steps for $[\mathbf{D}^{\mathcal{B}}_6]$ and $[\mathbf{Z}^{\mathcal{B}}_{\boldsymbol{\alpha}}]$ gives

$$[\mathbf{Z}^{\mathcal{B}}_{\boldsymbol{\alpha}}]^T[\mathbf{u}^{\boldsymbol{b}}_k] = \mathrm{diag}([\mathbf{r}^{\mathcal{B}}_{P_k}])[\mathbf{u}^{\boldsymbol{b}}_k] \qquad k = 1,\ldots,6. \tag{5.19}$$

Using

$$\mathrm{diag}([\mathbf{r}^{\mathcal{B}}_{P_k}])[\mathbf{u}^{\boldsymbol{b}}_k] = \mathrm{diag}([\mathbf{u}^{\boldsymbol{b}}_k])[\mathbf{r}^{\mathcal{B}}_{P_k}] \quad \mathrm{sym}([\mathbf{r}^{\mathcal{B}}_{P_k}])[\mathbf{u}^{\boldsymbol{b}}_k] = \mathrm{sym}([\mathbf{u}^{\boldsymbol{b}}_k])[\mathbf{r}^{\mathcal{B}}_{P_k}],$$

Equations (5.18) and (5.19) can be combined in matrix form as

$$\begin{bmatrix}\mathrm{sym}([\mathbf{u}^{\boldsymbol{b}}_k])\\ \mathrm{diag}([\mathbf{u}^{\boldsymbol{b}}_k])\end{bmatrix}[\mathbf{r}^{\mathcal{B}}_{P_k}] = \begin{bmatrix}-[\mathbf{Y}^{\mathcal{B}}_{\mathbf{s}}]^T\\ [\mathbf{Z}^{\mathcal{B}}_{\mathbf{s}}]^T\end{bmatrix}[\mathbf{u}^{\boldsymbol{b}}_k] \qquad k = 1,\ldots,6. \tag{5.20}$$

This set of equations can be used for the purpose of designing special minimal accelerometer configurations.

Proposition 5.4.1. *An accelerometer with a given direction can either not be part of a special minimal configuration or can be placed at a unique location.*

Proof. The 3×6 matrix,

$$\begin{bmatrix}\mathrm{sym}([\mathbf{u}^{\boldsymbol{b}}_k])\\ \mathrm{diag}([\mathbf{u}^{\boldsymbol{b}}_k])\end{bmatrix} = \begin{bmatrix} 0 & u_{k,3} & u_{k,2}\\ u_{k,3} & 0 & u_{k,1}\\ u_{k,2} & u_{k,1} & 0\\ u_{k,1} & 0 & 0\\ 0 & u_{k,2} & 0\\ 0 & 0 & u_{k,3}\end{bmatrix}, \tag{5.21}$$

which appears in Eq (5.20) is, by inspection, of full-rank whenever $\|\mathbf{u}_k\| \neq 0$. Equation (5.20) has a unique solution for $[\mathbf{r}_{P_k}^{\mathcal{B}}]$ if

$$\begin{bmatrix} -[\mathbf{Y}_{\mathbf{s}}^{\mathcal{B}}]^T \\ [\mathbf{Z}_{\mathbf{s}}^{\mathcal{B}}]^T \end{bmatrix} [\mathbf{u}_k^{\boldsymbol{b}}]$$

lies in the column-space of the matrix in Eq (5.21), and no solution exists otherwise. □

This proposition has an important corollary:

Corollary 5.4.1. Parallel accelerometers cannot be used in special minimal configurations.

5.5 Two Design Examples

In this section, two special minimal configurations are designed. Both configurations are constructed entirely of accelerometers that are free of $\mathrm{q}_{ii}([\boldsymbol{\omega}^{\boldsymbol{b}}])$. This has two advantages:

- It makes the design process simpler by removing degrees of freedom from the selection of accelerometer placements.
- It makes the resulting equation for $[\mathbf{s}_{O_B}^{\boldsymbol{b}}]$, (Eq (5.10a)), simpler, since $[\mathbf{Z}_{\mathbf{s}}^{\mathcal{B}}] = [0]_{3\times 3}$.

When Type P and A accelerometer placements are used, Eqs (5.20), the equations used for the design of special minimal configurations can be simplified to

$$\mathrm{sym}[\mathbf{u}_k^{\boldsymbol{b}}][\mathbf{r}_{P_k}^{\mathcal{B}}] = [\Xi][\mathbf{u}_k^{\boldsymbol{b}}] \qquad k = 1, \ldots, 6, \tag{5.22}$$

where for simplicity, $[\Xi] = -[\mathbf{Y}_{\mathbf{s}}^{\mathcal{B}}]^T$. The 'bottom' 3 equations for each k simply state that $[0]_{3\times 1} = [0]_{3\times 1}$, so can be omitted.

Each accelerometer placement introduces constraints upon the elements of $[\Xi]$. For example, a Type A_1 placement has $[\mathbf{u}_k^{\boldsymbol{b}}]^T = \begin{bmatrix} 0 & \cos\theta & \sin\theta \end{bmatrix}$ and $[\mathbf{r}_{P_k}^{\mathcal{B}}]^T = \begin{bmatrix} r_{k,1} & 0 & 0 \end{bmatrix}$ so Eq (5.22) becomes

$$\begin{bmatrix} 0 \\ r_{k,1}\sin\theta \\ r_{k,1}\cos\theta \end{bmatrix} = \begin{bmatrix} \xi_{1,2}\cos\theta + \xi_{1,3}\sin\theta \\ \xi_{2,2}\cos\theta + \xi_{2,3}\sin\theta \\ \xi_{3,2}\cos\theta + \xi_{3,3}\sin\theta \end{bmatrix}, \tag{5.23}$$

where $\xi_{i,j}$ is the element of $[\Xi]$ in the i^{th} row and j^{th} column. The constraint equations for each Type P and A placement are summarized in Table 5.1. Given that each accelerometer placement introduces 3 constraint equations and $[\Xi]$ has but 9 elements, there must be some dependence between the equations;

9 scalars cannot satisfy 18 independent equations. Indeed, $[\Xi]$ is specified once 3 accelerometers with linearly independent constraints have been placed, after which the remaining accelerometer placements must be chosen to satisfy the constraints.

In the two designs that are now presented the constraints on $[\Xi]$ introduced by accelerometer placements are introduced symbolically and the resulting equations are then solved so that Eq (5.22) is satisfied. It should be noted that this design strategy does not of itself ensure that the resulting configuration is minimally independent. After the design is complete, one must check that the result is a minimal configuration.

Table 5.1: The constraints on the elements of $[\Xi]$ introduced by the special placements that are free of $\mathrm{q}_{ii}([\boldsymbol{\omega}^b])$, where $s_k = \sin\theta_k$ and $c_k = \cos\theta_k$.

Type	Constraints
P_{12}	$\xi_{1,3} = r_{k,2}$ $\xi_{2,3} = r_{k,1}$ $\xi_{3,3} = 0$
P_{13}	$\xi_{1,2} = r_{k,3}$ $\xi_{2,2} = 0$ $\xi_{3,2} = r_{k,1}$
P_{23}	$\xi_{1,1} = 0$ $\xi_{2,1} = r_{k,3}$ $\xi_{3,1} = r_{k,2}$
A_1	$\xi_{1,2}c_k + \xi_{1,3}s_k = 0$ $\xi_{2,2}c_k + \xi_{2,3}s_k = r_{k,1}s_k$ $\xi_{3,2}c_k + \xi_{3,3}s_k = r_{k,1}c_k$
A_2	$\xi_{1,1}s_k + \xi_{1,3}c_k = r_{k,2}c_k$ $\xi_{2,1}s_k + \xi_{2,3}c_k = 0$ $\xi_{3,1}s_k + \xi_{3,3}c_k = r_{k,2}s_k$
A_3	$\xi_{1,1}c_k + \xi_{1,2}s_k = r_{k,3}s_k$ $\xi_{2,1}c_k + \xi_{2,2}s_k = r_{k,3}c_k$ $\xi_{3,1}c_k + \xi_{3,2}s_k = 0$

5.5.1 Three Axial and Three Planar Placements

The first design uses one of each kind of accelerometer placement that is free of $\mathrm{q}_{ij}([\boldsymbol{\omega}^b])$. The general 'shape' of the configuration and the numbers of the accelerometers are shown in Fig 5.6.

Applying the constraints associated with the first 3 accelerometer placements, which are of type Type P_{23}, P_{13} and P_{12} respectively, gives $[\Xi]$ the

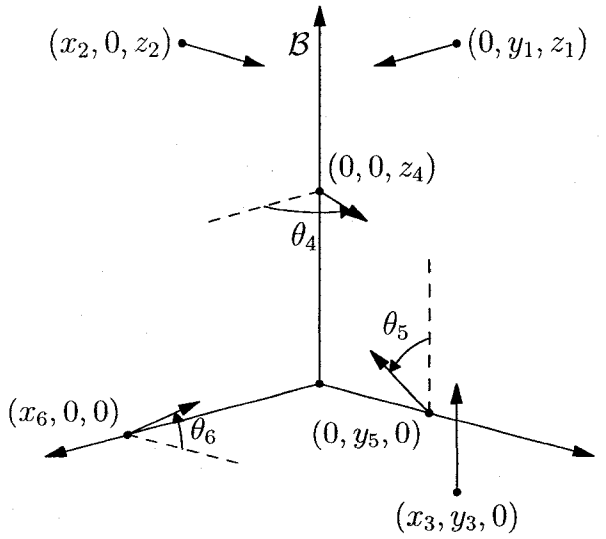

Figure 5.6: The numbering scheme of the accelerometer placements used in the first special minimal configuration design.

following form:

$$[\Xi] = \begin{bmatrix} 0 & z_2 & y_3 \\ z_1 & 0 & x_3 \\ y_1 & x_2 & 0 \end{bmatrix}. \tag{5.24}$$

The fourth accelerometer is of Type A_3 and, taking Eq (5.24) into account, introduces the following constraints:

$$z_2 \sin\theta_4 = z_4 \sin\theta_4 \tag{5.25a}$$
$$z_1 \cos\theta_4 = z_4 \cos\theta_4 \tag{5.25b}$$
$$y_1 \cos\theta_4 + x_2 \sin\theta_4 = 0. \tag{5.25c}$$

An implicit constraint is that $\theta_4 \neq 0$, since otherwise the Type A_3 accelerometer would be parallel to the Type P_{23} accelerometer, and parallel accelerometers cannot appear in special minimal configurations. Taking this angle constraint into consideration, Eq (5.24) shows that

$$z_1 = z_2 = z_4 \tag{5.26a}$$
$$y_1 = -x_2 \tan\theta_4. \tag{5.26b}$$

Proceeding similarly for the remaining two accelerometers shows that the locations of the 6 accelerometers are described by 3 scalars:

$$x \equiv x_2 = x_3 = x_6 \quad y \equiv y_1 = y_3 = y_5 \quad z \equiv z_1 = z_2 = z_4, \tag{5.27}$$

and these 3 scalars must satisfy the following three constraints involving the

angles describing the directions of the Type A placements:

$$x = -z \tan\theta_5 \tag{5.28a}$$
$$y = -x \tan\theta_4 \tag{5.28b}$$
$$z = -y \tan\theta_6. \tag{5.28c}$$

Combining these 3 equations gives

$$\tan\theta_4 \tan\theta_5 \tan\theta_6 = -1. \tag{5.29}$$

The angles, θ_i for $i = 4, 5, 6$ must be chosen to satisfy this equation. After this, the *relative* magnitudes of x, y and z can be determined. For example x can be taken as unity, after which Eqs (5.28) give $y = -\tan\theta_4$ and $z = -\tan^{-1}\theta_6$. All other solutions for x, y and z are scalar multiples of these solutions, which simply means that the 'scale' of the configuration is free.

Equation (5.29) shows that there are two degrees of freedom in the selection of θ_i for $i = 4, 5, 6$. There is therefore a double infinity of special minimal configurations in which one of each type of special placement is used. If configurations obtained by scaling are regarded as different, then this should be increased to a triple infinity. One particular configuration obtained using this method; that with $\theta_4 = \theta_5 = -\frac{\pi}{4}$, and hence $\theta_6 = -\frac{\pi}{4}$ is shown in Fig 5.7. This configuration is particularly simple because $x = y = z$ and $\theta_4 = \theta_5 = \theta_6$. It can be confirmed that this configuration is a minimal configuration, i.e., the six accelerometers are minimally independent.

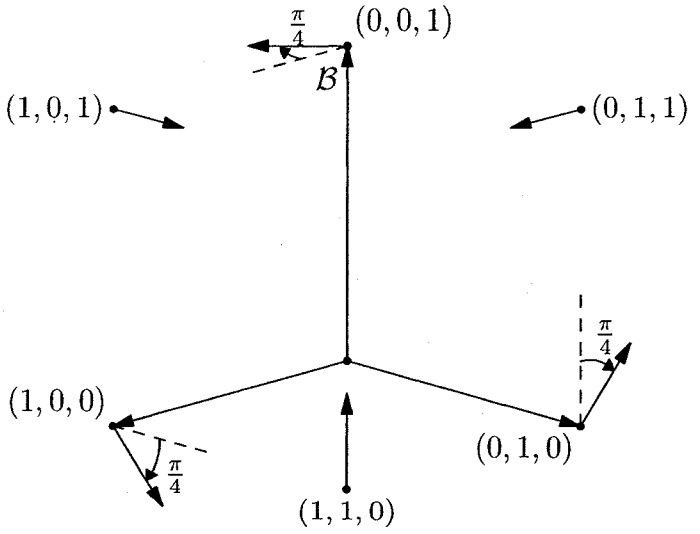

Figure 5.7: A special minimal configuration obtained using one of each type of axial (A) and planar (P) placement.

5.5.2 Six Axial Placements - Chen's Configuration

This design uses two of each type of axial placement. A general configuration with these placements, showing how the accelerometers are numbered in this discussion is shown in Fig 5.8.

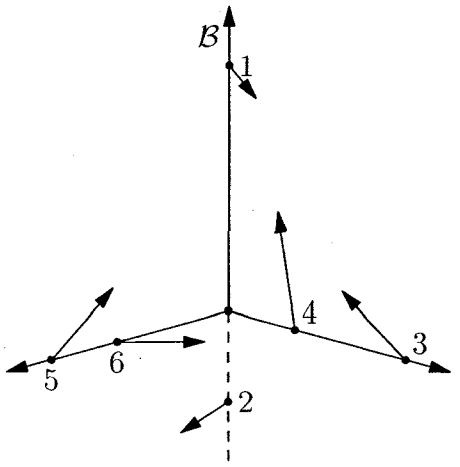

Figure 5.8: The numbering of the accelerometer placements used in the second special minimal configuration design.

According to Table 5.1, the two Type A_3 accelerometers introduce the following constraints to the elements of $[\Xi]$:

$$\begin{bmatrix} \cos\theta_1 & \sin\theta_1 \\ \cos\theta_2 & \sin\theta_2 \end{bmatrix} \begin{bmatrix} \xi_{1,1} \\ \xi_{1,2} \end{bmatrix} = \begin{bmatrix} z_1 \sin\theta_1 \\ z_2 \sin\theta_2 \end{bmatrix} \tag{5.30a}$$

$$\begin{bmatrix} \cos\theta_1 & \sin\theta_1 \\ \cos\theta_2 & \sin\theta_2 \end{bmatrix} \begin{bmatrix} \xi_{2,1} \\ \xi_{2,2} \end{bmatrix} = \begin{bmatrix} z_1 \cos\theta_1 \\ z_2 \cos\theta_2 \end{bmatrix} \tag{5.30b}$$

$$\begin{bmatrix} \cos\theta_1 & \sin\theta_1 \\ \cos\theta_2 & \sin\theta_2 \end{bmatrix} \begin{bmatrix} \xi_{1,3} \\ \xi_{2,3} \end{bmatrix} = \begin{bmatrix} 0 \\ 0 \end{bmatrix}. \tag{5.30c}$$

The determinant of the 2×2 matrix involved in each of these equations is $\sin(\theta_2 - \theta_1)$, which is non-zero for $\theta_2 \neq \theta_1$. This inequality must hold because it has been established that parallel accelerometers cannot be used in special minimal configurations. The solutions of Eqs (5.30) are found to be

$$\begin{bmatrix} \xi_{1,1} \\ \xi_{2,1} \end{bmatrix} = \frac{1}{\sin(\theta_2 - \theta_1)} \begin{bmatrix} (z_1 - z_2)\sin\theta_1 \sin\theta_2 \\ z_2 \cos\theta_1 \sin\theta_2 - z_1 \sin\theta_1 \cos\theta_2 \end{bmatrix} \tag{5.31a}$$

$$\begin{bmatrix} \xi_{2,1} \\ \xi_{2,2} \end{bmatrix} = \frac{1}{\sin(\theta_2 - \theta_1)} \begin{bmatrix} z_1 \cos\theta_1 \sin\theta_2 - z_2 \sin\theta_1 \cos\theta_2 \\ (z_2 - z_1)\cos\theta_2 \cos\theta_1 \end{bmatrix} \tag{5.31b}$$

$$\begin{bmatrix} \xi_{3,1} \\ \xi_{3,2} \end{bmatrix} = \begin{bmatrix} 0 \\ 0 \end{bmatrix}. \tag{5.31c}$$

It is important to note that $\xi_{3,1} = \xi_{3,2} = 0$. If this analysis is repeated for the other four accelerometers shown in Fig 5.8, it is found that

$$\xi_{i,j} = 0 \qquad i \neq j, \tag{5.32}$$

i.e., $[\Xi]$ is a diagonal matrix. Now, Eqs (5.30) show that $\xi_{1,2} = \xi_{2,1} = 0$ only if

$$\begin{bmatrix} \sin\theta_1 \cos\theta_2 & \cos\theta_1 \sin\theta_2 \\ \cos\theta_1 \sin\theta_2 & \sin\theta_1 \cos\theta_2 \end{bmatrix} \begin{bmatrix} z_1 \\ z_2 \end{bmatrix} = \begin{bmatrix} 0 \\ 0 \end{bmatrix}. \tag{5.33}$$

In order that there be non-zero solutions for z_1 and z_2, the 2×2 matrix must be singular, i.e., its determinant must be zero:

$$\sin^2\theta_1 \cos^2\theta_2 - \cos^2\theta_1 \sin^2\theta_2 = 0.$$

Writing $1 - \cos^2\theta_i$ for $\sin^2\theta_i$ shows that

$$\cos^2\theta_1 = \cos^2\theta_2.$$

Now, θ_2 cannot be equal to θ_1, because then the accelerometers would be parallel. Thus, θ_2 is taken to equal $-\theta_1$. Substituting $\theta_2 = -\theta_1$ into Eq (5.33) it is found that the solutions for z_1 and z_2 are of the form, $z_2 = -z_1$. Defining $\theta_A = \theta_1$ and $z_A = z_1$ the first two accelerometers must have the relative configuration shown in Fig 5.9. Since accelerometers at the same point with opposite directions are identified, the geometric relationship between the two accelerometers can be described as a binary rotation about either of the axes that they are *not* mounted on. In the following, such a pair of accelerometers is referred to as a *binary rotation pair*. An important point to note is that the *pairs* described by (z_A, θ_A) and $(-z_A, -\theta_A)$ are identical.

Repeating the analysis for the Type A_1 and Type A_2 placements shows that each pair of accelerometers is a binary rotation pair. These pairs are parameterized by (y_B, θ_B) and (x_C, θ_C) just as the first pair are parameterized by (z_A, θ_A).

So far only the off-diagonal elements of $[\Xi]$, and the conditions that must hold in order to make them all zero have been used. Each pair of accelerometers also introduces two equations involving two of the diagonal elements of $[\Xi]$. These equations can be written as

$$\xi_{1,1} = z_A \tan\theta_A = y_C \cot\theta_C \tag{5.34a}$$

$$\xi_{2,2} = x_B \tan\theta_B = z_A \cot\theta_A \tag{5.34b}$$

$$\xi_{3,3} = y_C \tan\theta_C = x_B \cot\theta_B. \tag{5.34c}$$

These equalities can be combined to yield the following equation constraining the directions of the accelerometers:

$$\tan^2\theta_A \tan^2\theta_B \tan^2\theta_C = 1. \tag{5.35}$$

Just as in the previous design, there are two degrees of freedom in the selection of the directions of the accelerometers after which only the scale of the configuration is unknown. For example, say θ_A and θ_B are chosen, then $\tan^2\theta_C$ can be obtained from Eq (5.35). If θ_C is taken to be the angle in the range[1] $0 < \theta_C < \frac{\pi}{2}$ with the required value of $\tan^2\theta_C$, then setting $z_A = \lambda$, Eq (5.34) can be used to find x_B and y_C as

$$z_A = \lambda \qquad x_B = \lambda\frac{\cot\theta_A}{\tan\theta_B} \qquad y_C = \lambda\frac{\tan\theta_A}{\cot\theta_C}. \tag{5.36}$$

Beyond showing that there is freedom in the choice of the scale of the configuration, Eq (5.36) shows that if θ_C is taken to be in the range $-\frac{\pi}{2} < \theta_C < 0$, then the sign of y_C is switched relative to the solution obtained when $0 < \theta_C < \frac{\pi}{2}$. The equivalence of the binary rotation pairs described by (y_C, θ_C) and $(-y_C, -\theta_C)$ shows that it does not matter which solution is used for θ_C.

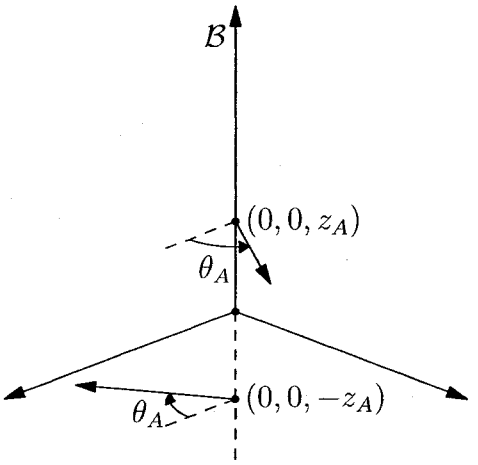

Figure 5.9: A binary rotation pair of accelerometers.

A configuration designed using this method is now illustrated; that obtained using $\theta_A = \theta_B = -\frac{\pi}{4}$. Scaling the configuration by taking $z_A = 1$, Eq (5.36) shows that $x_B = 1$, so the first four accelerometers are fixed. Next, using Eq (5.35), it is found that $\tan^2\theta_C = 1$. If θ_C is taken as $-\frac{\pi}{4}$, then Eq (5.36) indicates that $y_C = 1$. The configuration thus obtained is that first proposed by Chen et al. [7] without discussion of how it was obtained. It has now been shown that this popular configuration, which was shown in Fig 5.2, is a particular case of a special minimal configuration with two Type A_X, two Type A_Y and two Type A_Z placements. The appealing aspect of this design is its symmetry; each of the angles, θ_A, θ_B and θ_C, and each of the distances, x_A, y_C and z_B is identical.

[1]The strict inequalities are used because if $\theta_C = 0$ or $\frac{\pi}{2}$, then the binary rotation pair of accelerometers would be parallel.

5.6 Summary

This chapter has, for the first time, presented the geometric conditions that a set of 6 accelerometers must satisfy in order that it be a minimal configuration, i.e., that it be possible to determine the motion of a rigid body that the configuration is attached to. These geometric conditions were obtained by realizing that a certain 6×6 matrix that is required to be non-singular was comprised of the Plücker coordinates of lines drawn through the locations of the accelerometers in the directions of their sensitive axes. The results on the linear dependence of lines obtained by previous researchers in geometry and parallel robotics were then adopted to show when accelerometers are minimally dependent. Designing a configuration using these geometric rules would be an incremental affair. The first accelerometer could be placed anywhere, after which the second accelerometer must be placed so that two lines of the accelerometers are not identical. The locations and directions that a third accelerometer may not have are dependent upon the configuration of the first two. If the lines of the first two accelerometers intersected, for example, then the third must be placed so that it is not part of the planar pencil of lines through the point of intersection, and so forth. Following this procedure of placing an accelerometer so it is not minimally dependent upon the existing accelerometers will eventually lead to a minimal configuration. Generally, the resulting minimal configuration would require that a non-linear differential equation be solved for the angular velocity, since the angular acceleration would be expressed in terms of the accelerometer measurements and quadratic combinations of the elements of the angular velocity vector.

Two other contributions of this chapter were proving that it is impossible to design a minimal configuration in which the angular acceleration and specific force are both equal *solely* to linear combinations of accelerometer measurements, and presenting a design methodology for 'special minimal configurations'; those for which the first goal is achieved.

Chapter 6

GFIN Performance

The previous chapters have treated accelerometers as geometric elements and have shown how they should be arranged so that GFIN is possible, and, in the case of special minimal configurations, how to arrange them so that the configurations have desirable properties. In this chapter accelerometers are still treated as perfect, but the reality of errors in their arrangement is allowed.

Section 6.1 discusses GFIN error analysis in general; a topic that has not seen much treatment in the literature. This is followed in Section 6.2 by the analysis of the effects of placement errors in a simple planar accelerometer configuration. The errors are followed through the calculation of ω, either by integration of α, or by taking the square root of ω^2, both of which are available as linear combinations of accelerometer measurements. The analysis stops at the angular velocity, because beyond that the many treatments of SDIN error analysis can be used. Following this brief analytical study are some simulations showing the effects of placement errors in simple situations. Two different configurations are studied; a planar configuration, and Chen's cubic configuration (see Section 5.5.2). The results of the analytical treatment of placement errors are used to explain the appearance of some of the results for the planar configuration. Ways in which placement errors can be measured are discussed in Section 6.4, and methods of compensating for them are presented.

6.1 Error Analysis

There is a large amount of literature on the error analysis of SDIN [4, 65]. The result of such analysis is a set of differential equations that can be used to simulate the error propagation in a navigation system. In addition to erroneous initial conditions, error analysis focuses on the characteristics of the gyroscopes and accelerometers, such as bias and/or drift. Reference to Section 2.4 shows that the major difference between traditional SDIN and GFIN is the use of accelerometers in the determination of angular velocity. Consequently,

theoretical treatments of the error analysis of GFIN should be focused on the errors encountered in estimating angular velocity from accelerometer measurements. Beyond this point, the propagation through to orientation and position errors is algorithmic.

The most comprehensive report on the errors encountered during GFIN is a recent paper by Giansanti et al. [27]. In this paper, the authors used repeated computer simulations to compare the use of two accelerometer configurations, one minimal, but not 'special' six-accelerometer configuration, and the other, Padgaonkar's 9-accelerometer configuration [11], which is illustrated in Fig 2.5. They considered five different sources of error, three of which, sensitivity, bias and noise, are accelerometer specific, and the final two, location and orientation errors, which depend upon the installation of the accelerometer. For the motions that they considered, they found that the most significant sources of error were bias and orientation. They concluded that even with very small orientation and bias errors, that are 'hardly achievable' in practice, the two configurations were entirely unsuitable for determination of position and orientation, even over short periods of time. For example, in a simulation in which the accelerometer configurations were stationary in the local gravity field, and perfect apart from orientation errors of the order of 0.1°, a position error of around 0.4m arose after 4s for both configurations. The data sheets of MEMs accelerometers produced by Analog Devices, perhaps the largest manufacturer of such sensors, state that the orientation of the accelerometers within the 'chip' may be in error by up to 1°, so, without careful calibration, an orientation error of 0.1° is certainly possible [66]. A closely related error source is cross-axis sensitivity, in which an accelerometer with direction, $\mathbf{u}$, is slightly sensitive to specific force components orthogonal to $\mathbf{u}$. Analog Devices accelerometers typically have a cross axis sensitivity of 2%. Chen et al, while not performing any simulations, calculated that if a configuration was built using their 'cube design' (illustrated in Fig 5.2) with a 0.2m edge, and the accelerometers had a bias error of only $10\mu g$, that after 10s, there would be a 4 m position error [7]. To put the size of this bias error in context; if accelerometers with $+/-5$g range are used, then sensing an acceleration as small as 10μg would require a 20 bit A/D converter.

6.2 Planar Placement Error Analysis

In this section, the effects of placement errors on a planar accelerometer configuration are studied. Planar motion is studied, because it makes the analysis much simpler and provides insight the corresponding results in the spatial case, where the expressions become prohibitively complex. The expressions that are derived are used to explain some results obtained using simulations in Section 6.3.

If an accelerometer is believed to be $\mathsf{A}(P, \mathbf{u})$, but is really at point, P', with direction, $\mathbf{u}'$, then the measurement, $\mathsf{a}(P', \mathbf{u}')$, will generally be different from $\mathsf{a}(P, \mathbf{u})$. The difference between the actual and the expected measurements is referred to as the *model discrepancy.* An expression relating the placement errors to the model discrepancy is derived in this section. First however some assumptions must be outlined.

It is assumed that the plane of motion includes the local gravity vector, as is shown in Fig 6.1. As long as the plane of motion is known precisely, this assumption does not lessen the generality of the analysis, it merely makes the notation simpler. In the more general case, one would first have to find the projection of $\mathbf{g}$ onto the plane of motion.

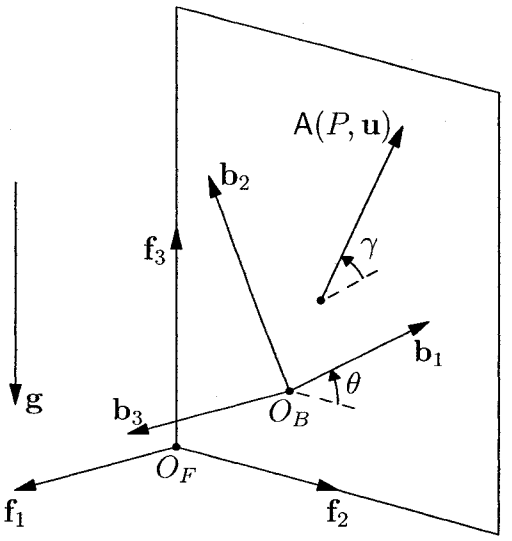

Figure 6.1: For the error analysis the plane of motion is assumed to include the gravity vector.

The second assumption is that even in its 'misplaced' state, the accelerometer, $\mathsf{A}(P', \mathbf{u}')$, is still parallel to the plane of motion. If the motion is entirely planar, locating P out of the plane of motion will have no effect, but if $\mathbf{u}'$ has some component orthogonal to the plane of motion it will cause an effect equivalent to a reduction in accelerometer sensitivity.

Since $\boldsymbol{\alpha} = \alpha \mathbf{b}_3$ and $\boldsymbol{\omega} = \omega \mathbf{b}_3$, the specific force vectors at any two points, P and Q, in the plane of motion are related by

$$\mathbf{s}_Q = \mathbf{s}_P + \alpha \mathbf{b}_3 \times \mathbf{r}_{Q/P} - \omega^2 \mathbf{r}_{Q/P}. \tag{6.1}$$

In particular, for the points, P and P' shown in Fig 6.2,

$$\mathbf{s}_{P'} = \mathbf{s}_P + \alpha \mathbf{b}_3 \times \boldsymbol{\delta}\mathbf{r} - \omega^2 \boldsymbol{\delta}\mathbf{r}. \tag{6.2}$$

This equation is true regardless of the magnitude of $\boldsymbol{\delta}\mathbf{r}$.

The unit vectors, $\mathbf{u}$ and $\mathbf{u}'$, shown in Fig 6.2, are related by

$$\mathbf{u}' = \cos(\delta\gamma)\mathbf{u} + \sin(\delta\gamma)\mathbf{b}_3 \times \mathbf{u}. \tag{6.3}$$

If $\delta\gamma$ is small enough that $\cos(\delta\gamma) \approx 1$ and $\sin(\delta\gamma) \approx \delta\gamma$, then the following approximation can be used

$$\mathbf{u}' = \mathbf{u} + \delta\gamma\mathbf{b}_3 \times \mathbf{u}. \tag{6.4}$$

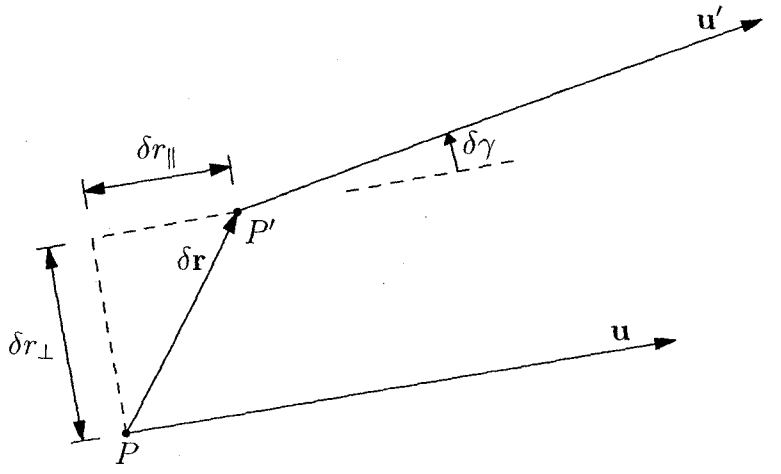

Figure 6.2: The geometry of $\mathsf{A}(P, \mathbf{u})$ and $\mathsf{A}(P', \mathbf{u}')$.

Using Eqs (6.2) and (6.4), the measurements of the accelerometers $\mathsf{A}(P, \mathbf{u})$ and $\mathsf{A}(P', \mathbf{u}')$ can be related by

$$\begin{aligned}
\mathsf{a}(P', \mathbf{u}') &= \mathbf{u}' \cdot \mathbf{s}_{P'} \\
&= (\mathbf{u} + \delta\gamma\mathbf{b}_3 \times \mathbf{u}) \cdot (\mathbf{s}_P + \alpha\mathbf{b}_3 \times \boldsymbol{\delta}\mathbf{r} - \omega^2\boldsymbol{\delta}\mathbf{r}) \\
&= \mathsf{a}(P, \mathbf{u}) + \delta\gamma\mathsf{a}(P, \mathbf{b}_3 \times \mathbf{u}) \\
&\quad + (\delta\gamma\delta r_{\parallel} - \delta r_{\perp})\alpha - (\delta r_{\parallel} + \delta\gamma\delta r_{\perp})\omega^2,
\end{aligned} \tag{6.5}$$

where, as shown in Fig 6.2, $\delta r_{\parallel}$ and $\delta r_{\perp}$ are the components of $\boldsymbol{\delta}\mathbf{r}$ in the directions of $\mathbf{u}$ and $\mathbf{b}_3 \times \mathbf{u}$, respectively. Assuming that the products of $\delta\gamma$ with $\delta r_{\perp}$ and $\delta r_{\parallel}$ are negligible gives the following simplified expression for the difference between the observed and expected accelerometer measurements due to placement error

$$\mathsf{a}(P', \mathbf{u}') - \mathsf{a}(P, \mathbf{u}) = \delta\gamma\mathsf{a}(P, \mathbf{b}_3 \times \mathbf{u}) - \delta r_{\perp}\alpha - \delta r_{\parallel}\omega^2. \tag{6.6}$$

Equation (6.6) shows the relationship between orientation and *cross-axis sensitivity*. If $\mathsf{A}(P, \mathbf{u})$, has a cross-axis sensitivity of $n\%$ then, in the absence

of all other forms of error, its measurement will be

$$\mathsf{a}(P, \mathbf{u}) + \frac{n}{100}\mathsf{a}(P, \mathbf{b}_3 \times \mathbf{u}).$$

Thus, cross-axis sensitivity of $n\%$ corresponds to an orientation error of $\frac{n}{100}$rad. As an example, accelerometers offered by Analog Devices typically have a cross-axis sensitivity of 2% [66], which corresponds to an orientation error of $0.02\text{rad} \approx 1.1°$.

6.2.1 Errors in Angular Velocity

As has been mentioned above, the major difference between GFIN and SDIN is that in GFIN, angular velocity is calculated from accelerometer measurements, rather than using gyroscopes. Given that SDIN error analysis is a mature field, it follows that error analysis of GFIN should focus on this difference. A suitable error model for the determination of angular velocity could then be incorporated into the SDIN error analysis.

Consider two parallel accelerometers, $\mathsf{A}(P, \mathbf{u})$ and $\mathsf{A}(Q, \mathbf{u})$. Using Eq (6.1) shows that the difference of the measurements depends linearly upon α and ω^2:

$$\mathsf{a}(Q, \mathbf{u}) - \mathsf{a}(P, \mathbf{u}) = \alpha \mathbf{u} \cdot \mathbf{b}_3 \times \mathbf{r}_{Q/P} - \omega^2 \mathbf{u} \cdot \mathbf{r}_{Q/P}. \tag{6.7}$$

If the vector separating the accelerometers is chosen so that the coefficient of α is zero, then ω^2 can be calculated as the difference of two accelerometers, and vice versa. This is now made more explicit.

If, $\mathbf{r}_{Q/P} = l\mathbf{u} \times \mathbf{b}_3$, then

$$\alpha = \frac{\mathsf{a}(Q, \mathbf{u}) - \mathsf{a}(P, \mathbf{u})}{l}. \tag{6.8}$$

If, $\mathbf{r}_{Q/P} = -l\mathbf{u}$, then, according to Eq (6.7),

$$\omega^2 = \frac{\mathsf{a}(Q, \mathbf{u}) - \mathsf{a}(P, \mathbf{u})}{l}. \tag{6.9}$$

These configurations are shown in Fig 6.3.

If accelerometers, $\mathsf{A}(P', \mathbf{u}')$ and $\mathsf{A}(Q', \mathbf{u}')$ are used, while they are modelled as $\mathsf{A}(P, \mathbf{u})$ and $\mathsf{A}(Q, \mathbf{u})$, the computations for α and ω^2 will be in error. The results of these computations are denoted by

$$\alpha' = \alpha + \delta\alpha \tag{6.10}$$

$$(\omega^2)' = \omega^2 + \delta(\omega^2). \tag{6.11}$$

If $\mathbf{r}_{P'/P} = \mathbf{r}_{Q'/Q}$ and the directions of the misconfigured accelerometers are identical, then no error will result in the computation of α or ω^2; it is the

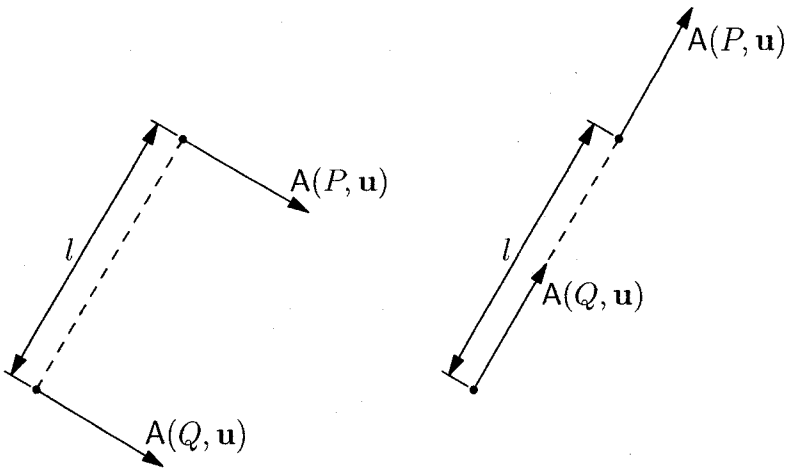

Figure 6.3: Pairs of accelerometers, the differences of the measurements of which can be used to find α (left) and ω^2(right).

difference in the location and orientation errors that is important. For this reason, in the following, it is assumed that $\mathsf{A}(Q, \mathbf{u})$ is placed correctly while the accelerometer, thought to be at P and directed by $\mathbf{u}$, $\mathsf{A}(P, \mathbf{u})$, is actually $\mathsf{A}(P', \mathbf{u}')$. While this step is justified, it should be noted that $\delta\gamma$, $\delta r_\perp$ and $\delta r_\parallel$ in this case actually denote the difference in placement errors, so may be up to twice the magnitude of the errors associated with a single accelerometer.

In the following two sections, expressions for $\delta\alpha$ and $\delta(\omega^2)$ are derived. These expressions, however, are not the desired goals. The expressions that are sought are the errors incurred in the calculation of ω and $|\omega|$ from integration of α' and taking the square-root of $(\omega^2)'$.

6.2.1.1 Error in α

From the above discussion, the erroneous calculation of α from misconfigured accelerometers is

$$\alpha' = \frac{\mathsf{a}(Q, \mathbf{u}) - \mathsf{a}(P', \mathbf{u}')}{l} = \frac{\mathsf{a}(Q, \mathbf{u}) - \mathsf{a}(P, \mathbf{u})}{l} + \frac{\mathsf{a}(P, \mathbf{u}) - \mathsf{a}(P', \mathbf{u}')}{l}$$

so, the error in the calculation of α is

$$\delta\alpha = \frac{\mathsf{a}(P, \mathbf{u}) - \mathsf{a}(P', \mathbf{u}')}{l}, \tag{6.12}$$

or, using Eq (6.6)

$$\delta\alpha = -\frac{\delta\gamma}{l}\mathsf{a}(P, \mathbf{b}_3 \times \mathbf{u}) + \frac{\delta r_\perp}{l}\alpha + \frac{\delta r_\parallel}{l}\omega^2. \tag{6.13}$$

Two points should be noted regarding this relationship. As was discussed above, the placement errors ascribed to $\mathsf{A}(P, \mathbf{u})$ are actually the difference of placement errors, so up to twice the expected values for location and orientation errors should be used. Secondly, and more significantly, the distance, l, between the accelerometers is, in applications, typically a few centimeters. Assuming a generous spacing of $l = 0.1\text{m}$, $\delta\alpha$ may be up to twenty times as large as $\mathsf{a}(P, \mathbf{u}) - \mathsf{a}(P', \mathbf{u}')$.

If α' is integrated from perfectly known initial conditions, the result is related to ω by

$$\int_0^t \alpha'(\tau)\mathrm{d}\tau = \int_0^t (\alpha(\tau) + \delta\alpha)\mathrm{d}\tau = \omega(t) + \delta_1\omega(t),$$

where,

$$\delta_1\omega(t) \stackrel{\text{def}}{=} \int_0^t \delta\alpha(\tau)\mathrm{d}\tau. \tag{6.14}$$

Substituting Eq (6.13) into Eq (6.14) gives

$$\delta_1\omega(t) = -\frac{\delta\gamma}{l}\int_0^t \mathsf{a}(Q, \mathbf{b}_3 \times \mathbf{u})\mathrm{d}\tau + \frac{\delta r_\perp}{l}(\omega(t) - \omega(0)) + \frac{\delta r_\parallel}{l}\int_0^t \omega^2\mathrm{d}\tau. \tag{6.15}$$

The relative contributions from each of the terms depends upon the motion, but some general comments can be made:

- The first term, which is due to (relative) misalignment, is proportional to the integral of the measurement of a perfect accelerometer at P directed away from Q. This is the only term of the three that may be non-zero when the body has been stationary over the time interval $[0, t]$.

- The second term is due to the component of the relative location error in the direction of the line through P and Q. It is interesting because it is zero whenever $\omega(t) = \omega(0)$. This may often be the case for cyclical motion, such as human gait; the contribution due to this term will have the same period as the motion.

- The final term is due to the component of the relative location error perpendicular to the line through P and Q. The integral in this term increases monotonically.

Equation (6.15) shows how placement errors of particular signs and magnitudes cause error in the estimation of ω. For example, if $\delta r_\perp > 0$, which means that the accelerometers are further apart than they are supposed to be, the difference of the accelerometer measurements is divided by a number that is smaller than it should be, and, consequently, α is overestimated.

6.2.1.2 Error in ω^2

If the accelerometers, $\mathsf{A}(P, \mathbf{u})$ and $\mathsf{A}(Q, \mathbf{u})$ are thought to be arranged as in the configuration in the right of Fig 6.3, but the former is slightly misplaced, then, similar to the development preceding Eq (6.12);

$$\delta(\omega^2) = \frac{\mathsf{a}(P, \mathbf{u}) - \mathsf{a}(P', \mathbf{u}')}{l},$$

or, in terms of the placement errors,

$$\delta(\omega^2) = -\frac{\delta\gamma}{l}\mathsf{a}(P, \mathbf{b}_3 \times \mathbf{u}) + \frac{\delta r_\perp}{l}\alpha + \frac{\delta r_\parallel}{l}\omega^2. \tag{6.16}$$

Let $\delta_2|\omega|$ be the error in the estimate of $|\omega|$ obtained by taking the square-root of $(\omega^2)' = \omega^2 + \delta(\omega^2)$, i.e.,

$$\sqrt{\omega^2 + \delta(\omega^2)} \stackrel{\text{def}}{=} |\omega| + \delta_2|\omega|. \tag{6.17}$$

In determining a relationship between $\delta_2|\omega|$ and $\delta(\omega^2)$, there are three cases to consider:

Case 1: $\omega^2 + \delta(\omega^2) < 0$ When realistic placement errors are assumed, this can only occur when $\omega \approx 0$. In this case no useful estimate of $|\omega|$ can be obtained, so $\delta_2|\omega|$ is left undefined.

Case 2: $\omega = 0, \delta(\omega^2) > 0$ Reference to Eq (6.17) shows that in this case

$$\delta_2|\omega| = \sqrt{\delta(\omega^2)}, \tag{6.18}$$

so, for $\delta(\omega^2) \ll 1$, the error in the estimate of $|\omega|$ will be greater than that in the measurement, $(\omega^2)'$.

Case 3: $\omega \neq 0, \omega^2 + \delta(\omega^2) > 0$ In this case, which is most likely to occur, a relationship between $\delta_2|\omega|$ and $\delta(\omega^2)$ can be obtained using an iteration of the Babylonian approximation [67] to the square root in Eq (6.17):

$$\sqrt{\omega^2 + \delta(\omega^2)} \approx \frac{1}{2}\left(|\omega| + \frac{\omega^2 + \delta(\omega^2)}{|\omega|}\right) = |\omega| + \frac{\delta(\omega^2)}{2|\omega|}. \tag{6.19}$$

The quality of this approximation depends upon the relative sizes of $\delta(\omega^2)$ and ω^2. Beyond $\omega^2 = 3\delta(\omega^2)$, the approximation is very good. Substituting Eq (6.19) into Eq (6.17) yields

$$\delta_2|\omega| = \frac{\delta(\omega^2)}{2|\omega|}. \tag{6.20}$$

Equation (6.16) can be substituted into Eqs (6.18) and (6.20) for the cases $\omega = 0$ and $\omega \neq 0$ to find relationships between the placement error and $\delta_2|\omega|$. In the latter case it is found that

$$\delta_2|\omega| = -\frac{\delta\gamma}{2l|\omega|}\mathsf{a}(Q, \mathbf{b}_3 \times \mathbf{u}) + \frac{\delta r_\perp}{l}\frac{\alpha}{2|\omega|} + \frac{\delta r_\parallel}{l}\frac{\omega^2}{|\omega|}. \tag{6.21}$$

Thus, while, Eq (6.20) suggests that as $|\omega|$ increases, the error in the estimate of $|\omega|$ should decrease, once it is realized that the $\delta(\omega^2)$ has a term that is proportional to ω^2, it is seen that $\delta_2|\omega|$ may actually increase linearly with $|\omega|$.

The basic error analysis just discussed is used to interpret results in the next section.

6.3 Performance

This section presents examples showing the performance of two accelerometer configurations in the face of placement errors of realistic size. The first example is a static test, where the configuration is maintained at some angle relative to gravity. This means that the only specific force that the accelerometers measure is that due to gravity. The second example uses the pendulum shown in Fig 6.4, which is released with zero angular velocity at $\theta_0 = \frac{\pi}{2}$. The equations of motion of the pendulum, which was modelled as a slender rod with length $L = 1$m, and mass, 1kg, were integrated using GNU Octave's `lsode.m` solver [53]. The perfect measurements of the accelerometers were calculated after the simulation, and used as inputs to the algorithms which are described below. In all cases it was assumed that the exact initial conditions were used, since the aim is to focus on the effects of placement errors.

Two different configurations were used; a planar configuration of two bi-axial accelerometers separated, in the perfect case, by $l = 0.1$m, as shown attached to the pendulum in Fig 6.4, and Chen's special minimal cubic configuration (shown in Fig 5.2) with a side of 0.1m.

6.3.1 Planar Configuration

The i^{th} step of the GFIN algorithm used with the measurements of the configuration displayed in Fig 6.4 is

1. Calculate the angular acceleration by the difference of two parallel accelerometers:
$$\alpha(t_i) = \frac{\mathsf{a}(O_B, \mathbf{b}_1)(t_i) - \mathsf{a}(P, \mathbf{b}_1)(t_i)}{l} \tag{6.22}$$

2. Integrate over the sample period to update angular velocity, here, using trapezoidal integration:

$$\omega(t_i) = \omega(t_{i-1}) + \frac{\Delta t}{2}(\alpha(t_{i-1}) + \alpha(t_i)). \tag{6.23}$$

3. Integrate again to find $\theta(t_i)$, the angle of the pendulum (and the configuration):

$$\theta(t_i) = \theta(t_{i-1}) + \frac{\Delta t}{2}(\omega(t_{i-1}) + \omega(t_i)). \tag{6.24}$$

4. Resolve the measurements of the biaxial pair at O_B into the stationary frame, and account for gravity:

$$[\mathbf{a}_{O_B}(t_i)^{\boldsymbol{f}}] = [\mathbf{R}(\theta(t_i))] \begin{bmatrix} \mathsf{a}(O_B, \mathbf{b}_1)(t_i) \\ \mathsf{a}(O_B, \mathbf{b}_2)(t_i) \end{bmatrix} + [\mathbf{g}^{\boldsymbol{f}}]. \tag{6.25}$$

5. Integrate the computed acceleration to get velocity (again using trapezoidal rule):

$$[\mathbf{v}_{O_B}(t_i)^{\boldsymbol{f}}] = [\mathbf{v}_{O_B}(t_{i-1})^{\boldsymbol{f}}] + \frac{\Delta t}{2}([\mathbf{a}_{O_B}(t_{i-1})^{\boldsymbol{f}}] + [\mathbf{a}_{O_B}(t_i)^{\boldsymbol{f}}]). \tag{6.26}$$

6. Integrate again to get position:

$$[\mathbf{r}_{O_B}(t_i)^{\mathcal{F}}] = [\mathbf{r}_{O_B}(t_{i-1})^{\mathcal{F}}] + \frac{\Delta t}{2}([\mathbf{v}_{O_B}(t_{i-1})^{\boldsymbol{f}}] + [\mathbf{v}_{O_B}(t_i)^{\boldsymbol{f}}]). \tag{6.27}$$

The sample period used was 0.01s, which is short compared to the dynamics of the situation, since the period of the pendulum is around 2s. A small amount of error due to the use of the simple trapezoidal integration method was observed; after 10s of pendulum motion the position error was 14cm.

In the simulations that follow, the biaxial accelerometer at O_B is assumed to be perfectly placed, while both the other accelerometers are rotated by $\delta\gamma$, and displaced by $\boldsymbol{\delta r} = \delta r_1 \mathbf{b}_1 + \delta r_2 \mathbf{b}_2$. With these configuration errors the misplaced accelerometers remain orthogonal and coincident. In the notation of the previous sections, the location errors, δr_1 and δr_2, correspond to $\delta r_\parallel$ and $\delta r_\perp$ for the accelerometer nominally parallel to $\mathbf{b}_1$, and $-\delta r_\perp$ and $\delta r_\parallel$ for the other accelerometer of the pair. While some development is made leaving $\delta\gamma$ and δr_i symbolic, when they need real values, those shown in Table 6.1 are used. These are smaller than the maximal errors that Giansanti and Maccioni stated were possible using an automated 'pick-and-place' machine, which were $\delta\gamma = 0.06°$ and $\delta r = 0.5$mm [28].

While ω^2 is not used in the simple algorithm described above, the errors in its calculation from the difference of the nominally collinear accelerometers are included. Indeed, the errors in the angular velocity estimates are what is of importance, but translating them into position errors makes more intuitive sense, as it will be seen that small angular velocity errors can be associated with very poor GFIN performance.

Table 6.1: Placement errors used in simulations involving the planar accelerometer configuration shown in Fig 6.4.

$\delta\gamma$	δr_1	δr_2
0.05°	0.1mm	0.1mm

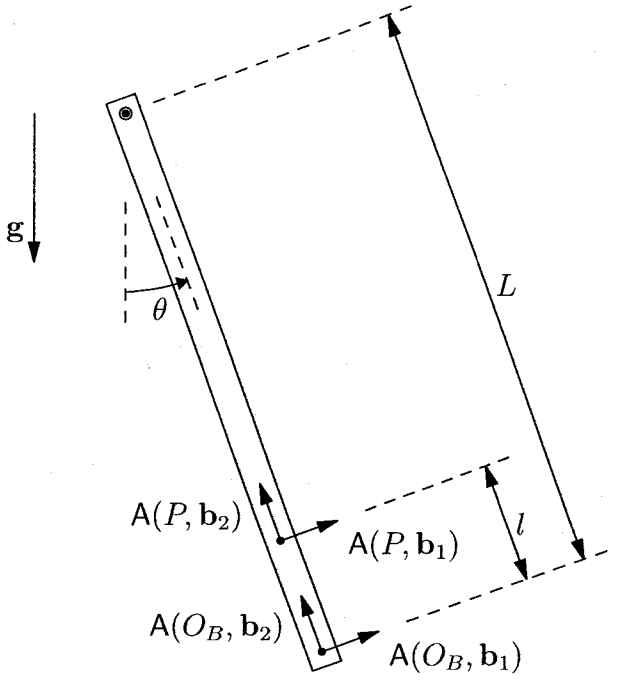

Figure 6.4: Two biaxial accelerometers attached to a pendulum.

6.3.1.1 Static Case

Equation (6.15) shows that when $\omega = \alpha = 0$, and $\mathbf{u} = \mathbf{b}_1$,

$$\delta_1\omega(t) = -\frac{\delta\gamma}{l}\int_0^t \mathsf{a}(P, \mathbf{b}_2)\mathrm{d}\tau,$$

so the error is independent of location errors. In the static case, $\mathbf{s}_P = \mathbf{s}_{O_B} = -\mathbf{g} = g(\sin\theta\mathbf{b}_1 + \cos\theta\mathbf{b}_2)\mathrm{m/s}^2$ with $g = 9.81\ \mathrm{m/s}^2$ so

$$\mathsf{a}(P, \mathbf{b}_2) = \mathbf{b}_2 \cdot \mathbf{s}_Q = -g\cos\theta$$

and

$$\delta_1\omega(t) = -gt\frac{\delta\gamma}{l}\cos\theta.$$

The error, $\delta_1\omega(t)$, is seen to be a linear function of time with coefficient depending on the orientation of the accelerometers relative to $\mathbf{g}$. The coefficient is largest when the accelerometers are orthogonal to $\mathbf{g}$, i.e., when $\theta = 0$. If $\theta = 0$, $\delta\gamma = 0.05° \approx 9 \cdot 10^{-4}$rad, and $l = 0.1$m then,

$$\delta_1\omega(t) \approx -0.09t\ \mathrm{rad/s}.$$

The negative sign in this expression can be explained as follows; the accelerometer at P' is rotated by $\delta\gamma$ so that it is measuring $g\delta\gamma$, while the accelerometer at O_B is measuring 0. The difference of these measurements suggests α is negative, and hence $\delta\omega$ becomes more negative over time. The error in the GFIN estimate of θ is the time integral of $\delta_1\omega$, and is therefore quadratic. For the case discussed above,

$$\delta\theta \approx -0.045t^2\ \mathrm{rad},$$

so that after 10s, $\delta\theta \approx -4.5$rad. These theoretical predictions were confirmed almost exactly by simulation. While this certainly seems like a rapid divergence in the angle, it is interesting to examine the effect on the GFIN solution for the position of the tip of the pendulum. Figure 6.5 shows the time evolution of this solution in the case where $\theta = 0$ and $\delta\gamma = 0.05°$. It is seen that the error in position is almost zero until around 1.5s, after which time the errors in position grow rapidly. The approximate error in θ at $t = 1.5$s is 6°.

The error in the estimate of $|\omega|$ obtained from taking the square-root of $(\omega^2)'$ is not dependent upon time, since no integration is required. Equation (6.16) shows that for $\mathbf{u} = \mathbf{b}_2$, and $\alpha = \omega = 0$,

$$\delta(\omega^2) = \frac{\delta\gamma}{l}\mathsf{a}(P, \mathbf{b}_1) = -\frac{\delta\gamma}{l}\mathbf{g} \cdot \mathbf{b}_1 = g\frac{\delta\gamma}{l}\sin\theta.$$

Since $\omega = 0$, the discussion in Section 6.2.1.2 suggests that

$$\delta_2|\omega| = \sqrt{|\delta(\omega^2)|}.$$

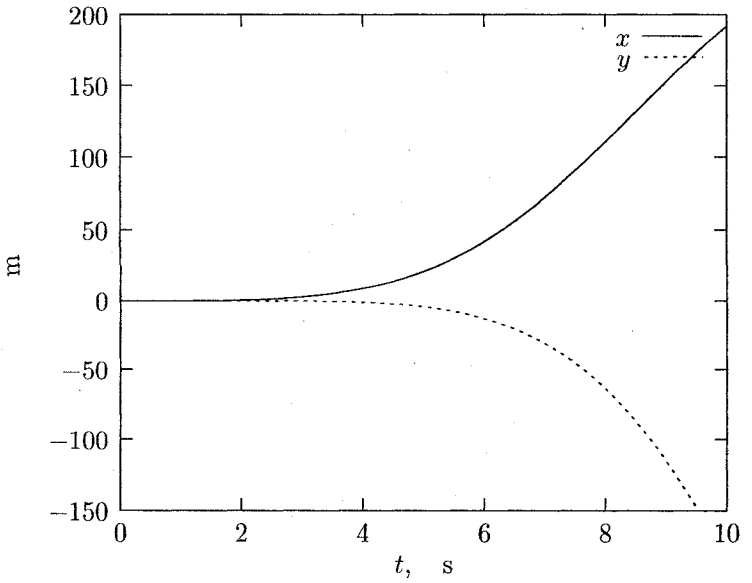

Figure 6.5: The planar GFIN computed position in the static case with $\theta = 0$ and $\delta\gamma = 0.05°$

The maximum value of $\delta_2|\omega|$ occurs when $\theta = \frac{\pi}{2}$. While the maximal error in ω^2 occurs when the pendulum is held horizontal, and the maximal error in α occurs when the pendulum is vertical, this is not an important difference. It is possible to choose the two axes for the measurement of ω^2 to be parallel to $\mathbf{b}_1$, and if this were done, the maximal error would occur when $\theta = 0$, i.e., when the pendulum was vertical. A more important difference is that $\delta_2|\omega|$ is, for the static case, constant, while $\delta_1\omega$ is a linear function of time.

6.3.1.2 Dynamic Case

When the pendulum to which the accelerometers are attached is allowed to swing, the accelerometer location errors have an effect. Noting that

$$\mathsf{a}(P, \mathbf{b}_2) = \omega^2(L - l) + g\cos\theta,$$

Eq (6.13) shows that

$$\delta\alpha = -\frac{\delta\gamma}{l}(\omega^2(L - l) + g\cos\theta) + \frac{\delta r_2}{l}\alpha + \frac{\delta r_1}{l}\omega^2. \tag{6.28}$$

For the pendulum under study, with the given initial conditions of $\omega_0 = 0$ and $\theta_0 = \frac{\pi}{2}$,

$$\alpha = -\frac{3}{2}g\sin\theta$$
$$\omega^2 = 3g\cos\theta.$$

Substituting these expressions, along with $L - l = 0.9\text{m}$, into Eq (6.28) gives

$$\delta\alpha = -\frac{\delta\gamma}{l}3.7g\cos\theta - \frac{\delta r_2}{l}\frac{3}{2}g\sin\theta + \frac{\delta r_1}{l}3g\cos\theta. \tag{6.29}$$

The contributions to $\delta\alpha$ due to $\delta\gamma$ and δr_1 are in phase, with maxima when the pendulum is vertical, while that due to δr_1 has maximum magnitudes when the pendulum is horizontal. For the contributions due to $\delta\gamma$ and δr_1 to be of similar magnitude requires that the numerical value of $\delta\gamma$, measured in radians, be similar to δr_1, measured in meters. For example, if $\delta\gamma = 0.05°$, then δr_1 would have to be around 1mm. Whereas 0.05° is a small orientation error, 1mm is a large location error, and this suggests, in agreement with the simulations of Giansanti et al. [27], that if the accelerometers of a configuration are placed with reasonable care, it is likely that orientation errors will be more problematic. The same conclusion can be reached when comparing the contributions to $\delta\alpha$ due to $\delta\gamma$ and δr_2, except in this case, for the contributions to be of similar magnitude, it is necessary that $\delta r_2 \approx 2\delta\gamma$ (where, again, the approximate equality is only concerned with the magnitude δr_2 in **m** and $\delta\gamma in \text{rad}$).

Figure 6.6 shows the dependence of $\delta\alpha$ on θ for the case with conditions described by Table 6.1. The plot was generated using the GFIN simulation, but matches that predicted by Eq (6.29). For larger placement errors, the agreement would not be as good, since the second order terms that were assumed to be negligible would become significant. The error has maximum magnitude when the pendulum is vertical. Reference to Eq (6.29) shows that the slight asymmetry evident in the figure is due to δr_2 term.

In the static case, $\delta(\omega^2)$ was constant and independent of the location errors. In the dynamic case neither of these statements is true. Using similar calculation as for Eq (6.29) shows that

$$\delta(\omega^2) = -\frac{\delta\gamma}{l}0.35g\sin\theta + \frac{\delta r_1}{l}\frac{3}{2}g\sin\theta + \frac{\delta r_2}{l}3g\cos\theta. \tag{6.30}$$

It is seen that for the contributions to $\delta(\omega^2)$ due to $\delta\gamma$, δr_1 and δr_2 to be of similar magnitude, requires the numerical value of $\delta\gamma$, measured in radians, be, respectively, 5 and 10 times greater than the values of δr_1 and δr_2, measured in meters. For example, if $\delta\gamma = 0.1°$, having $\delta r_1 \approx 0.35\text{mm}$ and $\delta r_2 \approx 0.2\text{mm}$ will lead to roughly equal contributions. These numbers indicate that the estimate of ω^2 is more sensitive to accelerometer location errors than that of α. Reference to Eqs (6.13) and (6.16) shows that the sensitivity to orientation errors in the estimates of α and ω^2 is proportional to the magnitude of the components of specific force orthogonal to the accelerometers used in the calculations. This component is greater for the accelerometers used to estimate α than it is for those used to estimate ω^2, while the sensitivity of $\delta\alpha$ and $\delta(\omega^2)$

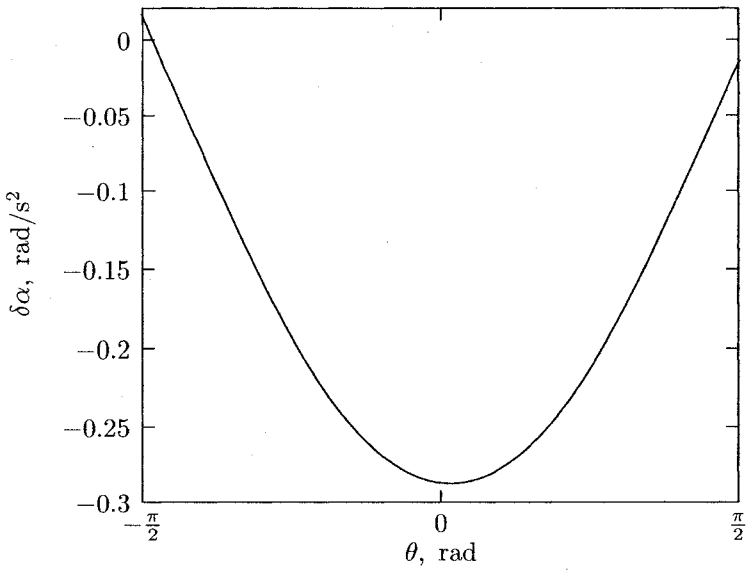

Figure 6.6: The dependence of $\delta\alpha$ on the angle of the pendulum, θ, for the case described by Table 6.1.

to δr_1 and δr_2 is similar, meaning that, relatively speaking, location errors are more important in the estimation of (ω^2). This is only true for the particular configuration used here. It is possible to use accelerometers parallel to $\mathbf{b}_1$ to estimate ω^2, in which case the error characteristics would be similar to those used here to estimate α. Figure 6.7 shows the dependence of $\delta(\omega^2)$ on θ for the placement errors detailed in Table 6.1. Figure 6.8 shows the θ-dependence of $\delta_2|\omega| = \sqrt{(\omega^2)'} - |\omega|$. Note the large errors at $\theta = \pm\frac{\pi}{2}$, which, with reference to Section 6.2.1.2 occur because $\omega = 0$ at those points.

Figure 6.9 shows the divergence of the GFIN solution for the position of the tip of the pendulum for the same case over the same period. The GFIN solution tracks reasonably well for about half the first period of the pendulum, after which it diverges. It is clear that even over short periods of time, small placement errors are problematic. Figure 6.10 shows the errors in the GFIN calculation of the tip of the pendulum when each of the placement errors in Table 6.1 is applied in turn. The dominance of the misalignment error is seen once again. Note also that the contribution due to δr_2 is periodic, as was predicted in Section 6.2.1.1 for $\delta\alpha$.

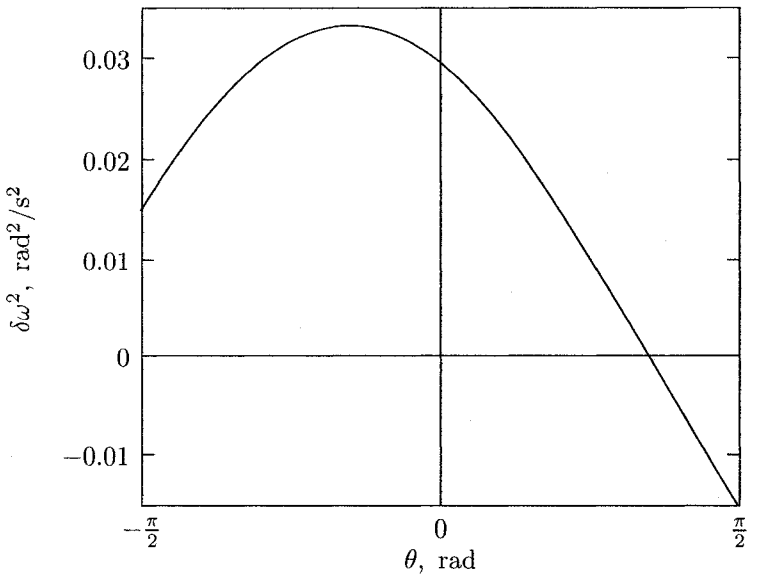

Figure 6.7: The error in the estimate of ω^2 as a function of θ for the case described by Table 6.1.

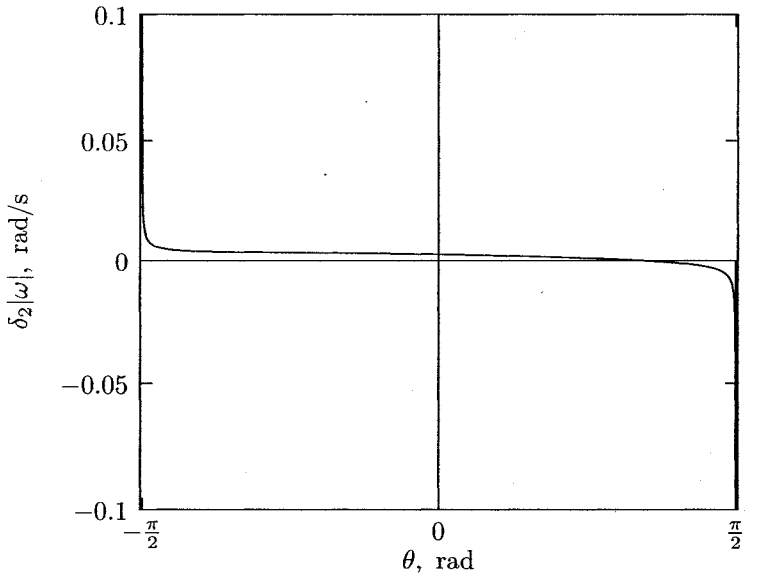

Figure 6.8: The error in the calculation of $|\omega|$ when taking the square root of $(\omega^2)'$.

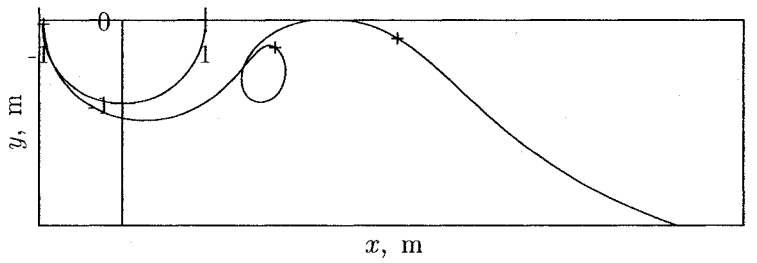

Figure 6.9: The GFIN solution for the location of the tip of the pendulum for the case described by Table 6.1 for the first 3.5s; each + denotes 1s.

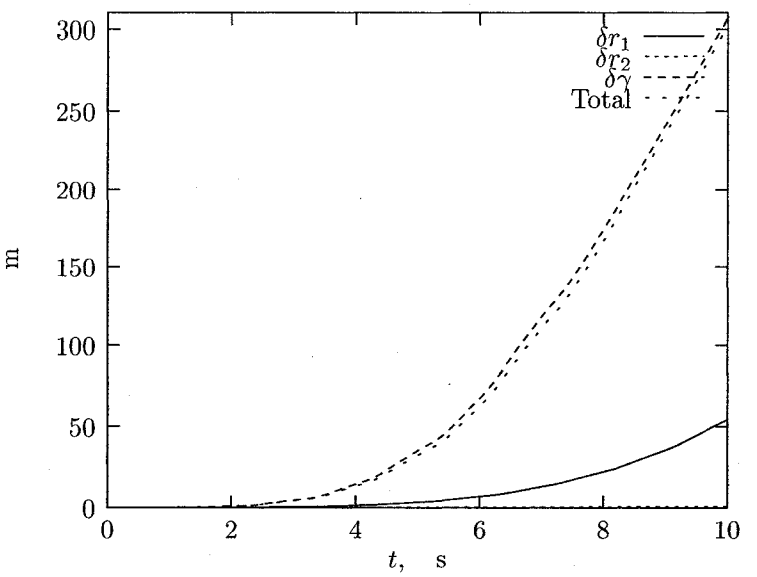

Figure 6.10: The evolution of the magnitude of the position error due to the various placement errors in Table 6.1.

6.3.2 Special Minimal Configuration

The GFIN algorithm used for Chen's configuration is a little more complex than that used for the planar configuration, so is only described verbally. At the i^{th} time step:

1. Calculate angular acceleration as the linear combination of accelerometer measurements.
2. Integrate angular acceleration over Δt to get the angular velocity at t_i.
3. Integrate the orientation kinematic differential equation over Δt to find the current position.
4. Using the updated orientation and angular velocity, calculate the specific force at O_B (refer to Section 5.4.).
5. Transform the calculated specific force at O_B into fixed frame coordinates and account for gravity to find $[\mathbf{a}_{O_B}(t_i)^{\boldsymbol{f}}]$.
6. Integrate $[\mathbf{a}_{O_B}(t_i)^{\boldsymbol{f}}]$ over Δt to find $[\mathbf{v}_{O_B}(t_i)^{\boldsymbol{f}}]$.
7. Integrate $[\mathbf{v}_{O_B}(t_i)^{\boldsymbol{f}}]$ over Δt to find $[\mathbf{r}_{O_B}(t_i)^{\mathcal{F}}]$.

The orientation kinematic differential equation that was used was that for Euler parameters [68], and it was integrated using a second order Runge Kutta method [69]. With no placement errors, this algorithm actually performed slightly better than the planar accelerometer algorithm described in Section 6.3.1, accruing a position error of less than 6 cm over 10s of simulation. This is likely due to the improved integration method.

Each of the accelerometers in the configuration was displaced and rotated by the angles shown in Table 6.2. They were rotated about vectors orthogonal to their directions. There is not enough information in the table to replicate the misplaced configuration exactly, but it does show the small sizes of placement errors considered. The perturbed locations and directions are fully described in Appendix E. Placement errors of these magnitudes could easily occur even during careful assembly.

Table 6.2: Placement errors used in simulations involving Chen's configuration.

	1	2	3	4	5	6
$\delta\gamma$ (°)	0.057	0.086	0.028	0.046	0.057	0.086
δr (mm)	0.29	0.11	0.50	0.23	0.10	0.16

6.3.2.1 Static Case

When using Chen's configuration in the static case with the placement errors in Table 6.2 a position error of around 340m is accrued after only 10 s. Figure 6.11 shows the components of angular velocity calculated using the configuration over this period. While each component should be zero, the same linear growth that was seen when using the planar accelerometer configuration is evident.

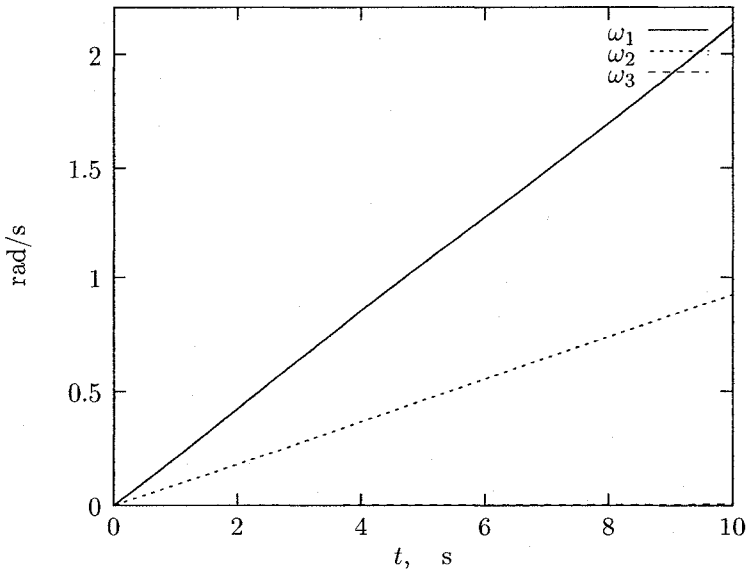

Figure 6.11: The errors in the estimates of angular velocity obtained from the special configuration when stationary.

6.3.2.2 Dynamic Case

Figures 6.12 and 6.13 show, respectively, the errors in the estimate of the angular velocity[1] and position using Chen's configuration with the placement errors of Table 6.2. For reference, the basis of the configuration is oriented so that $\mathbf{b}_1$ is in the direction of the actual angular velocity, while $\mathbf{b}_3$ is directed along the pendulum[2]. Thus the smallest component in Fig 6.11 is mistakenly sensed rotation about the length of the pendulum. Figure 6.13 shows that the solution for the position is effective only for about 1s. It is interesting to note that at this time the errors in the angular velocity are still relatively small; each component is less than 0.5rad/s while at $t = 0.5$s, the angular velocity has a magnitude of nearly 6rad/s.

[1] $\delta\omega_i$ is the calculated value of ω_i minus the true value of ω_i.

[2] This is different from the convention used for the planar configuration.

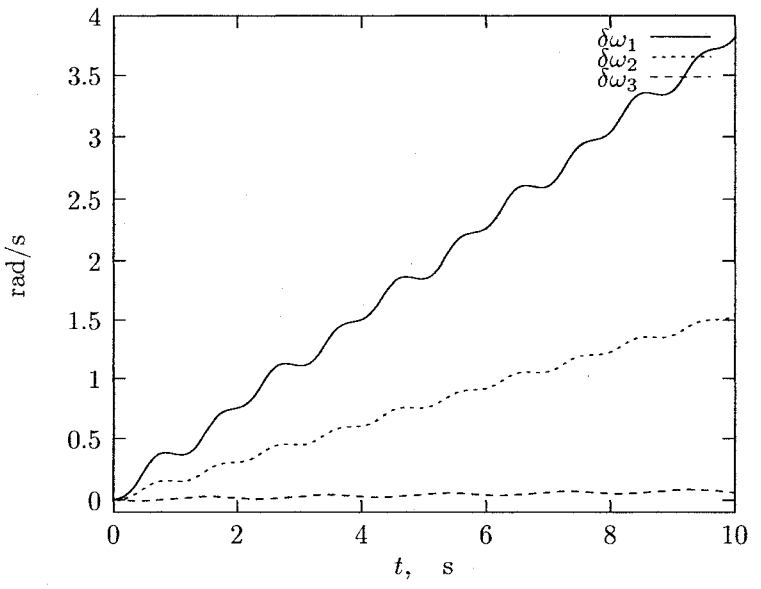

Figure 6.12: The errors in the estimates of angular velocity obtained from the special configuration.

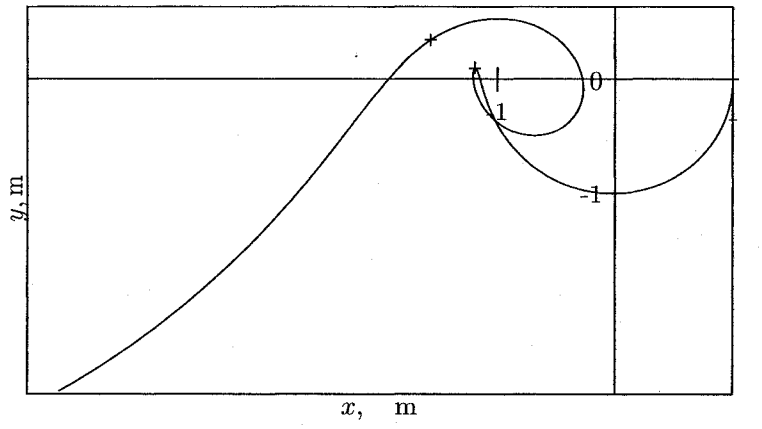

Figure 6.13: The evolution of the solution for the location of the tip of the pendulum using Chen's configuration, over 2.5s.

6.4 Calibration and Compensation

The preceding subsections have shown that very small placement errors lead to rapid divergence of the GFIN solution, even when perfect accelerometers and perfect initial conditions are assumed. Having established that the situation is bad, the question of what can be done to limit the rate of divergence is now addressed.

A prerequisite for compensating for the placement errors is that they be identified using a calibration process. Numerous authors have discussed calibration of accelerometers in which misalignment errors, bias and sensitivity are determined using carefully controlled static tests where the specific force each accelerometer measures is due only to gravity at a known angle [29, 31, 70]. There is an IEEE standard prescribing such calibration procedures [71]. Tests in which the accelerometer configuration is attached to a turntable with known and constant angular velocity at precise positions and orientations have been proposed for the determination of accelerometer locations [29, 70].

Recently an ingenious accelerometer configuration calibration method has been proposed by Parsa et al. [16, 43]. This method is specifically for a configuration of four (or more) triaxial accelerometers attached at non-coplanar locations. It is assumed that the directions of the accelerometers within each triple are mutually orthogonal, and that location errors of the accelerometers are negligible. Further, it is implicitly assumed that the bias and sensitivity of the accelerometers have already been determined by another method. What the method does allow is the determination of the orientation of each triaxial accelerometer. While this method certainly has a limited range of application, it is interesting because it does not require that the configuration undergo precise motion. The basic idea is that the supposed orientations of the triaxial accelerometers are incrementally changed so that the measurements correspond to a rigid-body acceleration field. Generalization of this method to relax the assumption of accelerometer orthogonality, and to allow determination of bias, sensitivity and location would be an interesting exercise. A possible shortcoming of the method that has not been discussed by the authors, but seems intuitively true, is that the method cannot uniquely determine the orientation of each triaxial accelerometer. If a solution is found for each triaxial accelerometer, then another solution can be found by rotating each accelerometer by the same angle about the same axis. A corresponding situation would hold if the method was generalized to allow calculation of location; upon solving for the orientations and locations of each accelerometer, another solution could be obtained by imparting the same displacement to each accelerometer. This, it seems, is the price to be paid for the convenience of not requiring specialized testing apparatus.

At this point it is difficult to say definitively how accurate the identification of misplacement errors can be. Most methods have only been used

in simulation where effects such as quantization error have not been considered. In a recent paper involving tests with actual accelerometers, rather than simulations, Parsa et al [31] stated that they were able to:

> reduce the estimated angular errors of the accelerometers from about 2° to...below 8.9×10^{-6}°...

This seems, on the one hand, to be a very large initial *estimated* angle and a very small final angle. In the following sections less stringent assumptions are made about the calibration procedure; it is assumed that following the calibration procedure, the effective placement errors, i.e., the difference between the model and the reality, have been reduced by an order of magnitude. Details are included in the following sections, where, for brevity, only the dynamic case it studied.

6.4.1 Planar Configuration

If the placement errors are identified exactly, then there is no compensation scheme, *per se*, that is required for the planar configuration; the model simply needs to be updated. In the algorithm described in Section 6.3.1 only steps 1 and 4 are different. In the first case the measurements of all four accelerometers are used to determine $\alpha(t_i)$, and in the second, all four are again used to determine the specific force at O_B. Exactly what linear combinations of the measurements are required is prescribed by the inverse of the 4×4 configuration matrix, as described in Chapter 3.

When simulations were run assuming perfect identification of the placement errors, the performance was exactly as if there was no placement error. This is true up to a limit. If the placement errors are so large that the configuration matrix becomes singular, or changes other properties of the configuration, such as the condition number, then differences will be noted.

Figure 6.14 shows the calculated position of the tip of the pendulum when, after the calibration procedure, angular and position discrepancies between the model and reality of magnitude, 0.001° and 0.03mm remain.

6.4.2 Special Configuration

As shown in Chapter 5 a minimal special configuration is only 'special' because of the particular locations and directions of the accelerometers. When the accelerometers are subject to placement errors, the configuration loses its status and becomes a 'regular' minimal configuration. This demotion means, in real terms, that a non-linear differential equation must be solved for the angular velocity. It also means that the equation for the specific force at O_B will become 'more' dependent upon the angular velocity. For instance, when

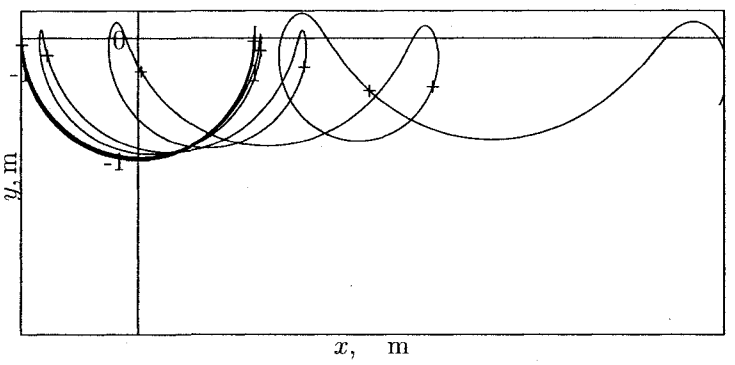

Figure 6.14: The calculated position of the tip of the pendulum using the planar configuration with wrongly identified placement errors.

the accelerometers of Chen's configuration are placed perfectly $[\mathbf{s}^{\boldsymbol{b}}_{O_B}]$ is a linear combination of the accelerometer measurements and $\mathrm{q}_{ij}([\boldsymbol{\omega}^{\boldsymbol{b}}])$, but after placement errors it will *also* generally depend upon $\mathrm{q}_{ii}([\boldsymbol{\omega}^{\boldsymbol{b}}])$. Thus, the algorithm shown in Section 6.3.2 will generally need modification at steps 1 and 5.

Tan et al. [41] have proposed a compensation scheme that processes the actual measurements of a minimal configuration and gives the measurements of a special configuration, after which the simpler algorithm can be applied. A simple derivation of the scheme is presented here using the notation of Chapter 5. The quantities associated with the 'ideal' configuration are denoted by the subscript, I, while those associated with the real configuration (subject to placement errors) have the subscript, R. According to Eq (5.1) the measurements of the two configurations satisfy

$$[\mathbf{M}_I]\begin{bmatrix}[\mathbf{s}_{O_B}]\\ [\boldsymbol{\alpha}]\end{bmatrix} = [\mathbf{a}_I] - [\mathbf{Q}_I]\begin{bmatrix}\mathrm{q}_{ij}([\boldsymbol{\omega}])\\ \mathrm{q}_{ii}([\boldsymbol{\omega}])\end{bmatrix} \tag{6.31}$$

and

$$[\mathbf{M}_R]\begin{bmatrix}[\mathbf{s}_{O_B}]\\ [\boldsymbol{\alpha}]\end{bmatrix} = [\mathbf{a}_R] - [\mathbf{Q}_R]\begin{bmatrix}\mathrm{q}_{ij}([\boldsymbol{\omega}])\\ \mathrm{q}_{ii}([\boldsymbol{\omega}])\end{bmatrix}. \tag{6.32}$$

Assuming that $[\mathbf{M}_R]$ is non-singular (it is already known that $[\mathbf{M}_I]$ is non-singular), pre-multiplying Eq (6.31) by $[\mathbf{M}_I]^{-1}$ and Eq (6.32) by $[\mathbf{M}_R]^{-1}$, and equating the results leads to

$$[\mathbf{a}_I] = [\mathbf{M}_I][\mathbf{M}_R]^{-1}[\mathbf{a}_R] + ([\mathbf{Q}_I] - [\mathbf{M}_I][\mathbf{M}_R]^{-1}[\mathbf{Q}_R])\begin{bmatrix}\mathrm{q}_{ij}([\boldsymbol{\omega}])\\ \mathrm{q}_{ii}([\boldsymbol{\omega}])\end{bmatrix}, \tag{6.33}$$

showing that the measurement of the ideal configuration can be written as a linear combination of the real measurements and some function of the angular velocity. There is an obvious problem with this procedure: the angular velocity at t_i needs to be known before the angular acceleration at the same instant

can be found. The authors suggested simply using the angular velocity at the previous time-step. How well this method performs will depend upon the magnitudes of the placement errors and the motion itself. If angular velocity changes appreciably over a time step, then the processed measurements will be in error.

Table 6.3 describes the assumed magnitudes of the location and direction errors remaining after a calibration. The locations and directions calculated using the assumed calibration produced are fully described in Appendix E. In the simulations the difference between the performance of Tan's compensation scheme and integration of the nonlinear differential equation were negligible. Figure 6.15 shows the estimated pendulum tip position calculated using both methods over the first 4 seconds of simulation. It is clear that regardless of whether the true nonlinear approach or Tan's compensation method is used, poor position estimates will be obtained. Figure 6.16, on the other hand, shows that the angular velocity estimates obtained are comparatively good; over short periods at least.

Table 6.3: Assumed placement error residuals after calibration of Chen's configuration.

	1	2	3	4	5	6
$\delta\gamma$ $(\times 10^{-3\circ})$	1.14	5.73	0.573	0.572	5.73	0.565
δr (mm)	0.025	0.014	0.075	0.050	0.056	0.058

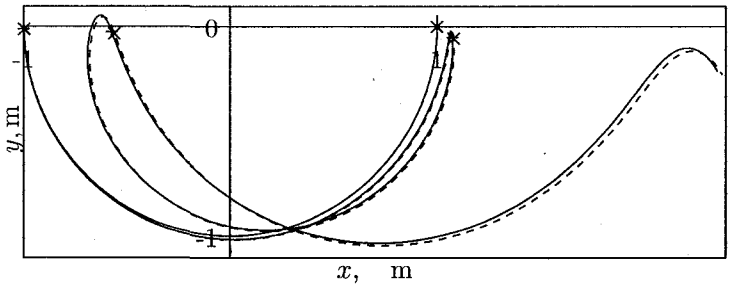

Figure 6.15: The estimated position of the tip of the pendulum using the true nonlinear approach and Tan's compensation are practically indistinguishable.

6.5 Summary

The results of this chapter are certainly not encouraging. Ideal accelerometers have been assumed, along with perfect initial conditions and small placement

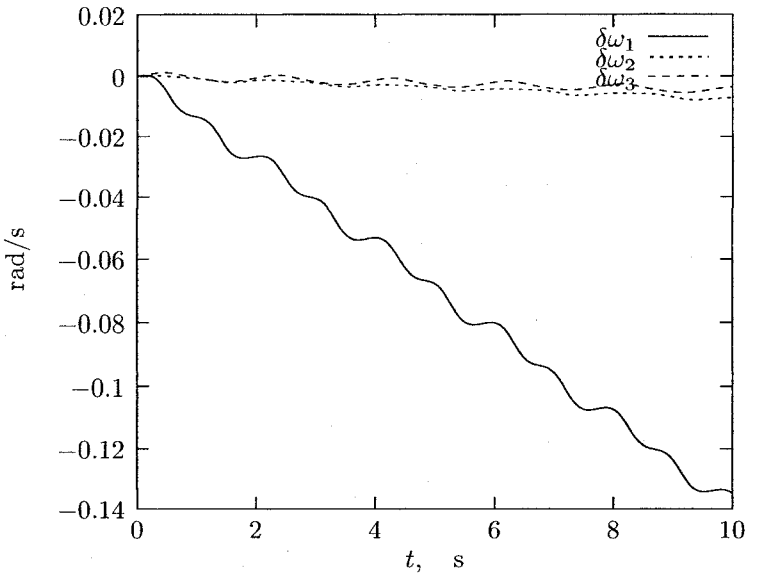

Figure 6.16: The error in the estimate of angular velocity using Tan's compensation method.

errors, and yet the results are very poor. After a few seconds the GFIN position estimate can be in error by many meters.

It would be satisfying if it were possible to present definite results relating the magnitudes of placement errors to GFIN performance, saying, for example, that placing accelerometers within certain tolerances could always guarantee the GFIN position estimate to be within a certain distance of truth after a certain time. The analysis in this chapter has shown that this is not possible, because the way each placement error affects the GFIN solution is motion dependent. It is believed that numerical simulations specific to the motions that are likely to be encountered in the application are the only way that likely bounds upon GFIN errors can be obtained.

While not considered here, the estimate of ω^2 that can be obtained using a planar accelerometer configuration can be used to limit the growth in the estimation error for ω. Parsa et al. have presented a method using a full 12 accelerometer configuration that illustrates how this can be done [15, 16, 31]. Essentially, the angular velocity is integrated forward using the angular acceleration estimate, after which a numerical method is used to refine the estimate so that it comes close to satisfying $\mathrm{q}_{ij}([\boldsymbol{\omega}^b])$ and $\mathrm{q}_{ii}([\boldsymbol{\omega}^b])$. This method was not considered here because this thesis is more concerned with designs of configurations, and if one is going to use 12 accelerometers, the obvious solution, and one that will likely minimize placement errors, is to use 4 triaxial accelerometers. Unfortunately the special minimal configurations, which are more interesting in the context of this thesis, have been shown to be very sensitive to place-

ment errors. It can be concluded that to use special configurations one must either have an application with very short durations, or use some additional information to prevent error accumulation.

Chapter 7

Application of GFIN to Kinematics of Stewart-Gough Platforms

The previous chapter illustrated the poor performance that can be expected from GFIN even in the most benign circumstances; ideal sensor characteristics, perfectly known initial conditions and small placement errors. This chapter presents an interesting application of GFIN where the rapid divergence of the solution will not usually be problematic. The application is in the kinematics of Generalized Stewart-Gough Platforms (GSGPs). A GSGP is a mechanism composed of two bodies; a fixed base, $\mathcal{F}$, and a moving platform, $\mathcal{B}$, see Fig 7.1. The two bodies are connected by six linear actuators, commonly referred to as *legs*. Each leg is connected to the base at a point, referred to as an *ankle point*, via a universal joint, and to the platform at a *hip point* via a spherical joint[1]. The platform pose (position and orientation) is controlled by altering the lengths of the legs. GSGPs, and parallel mechanisms in general, are attractive because they can be used to manipulate large payloads very accurately [32, 72]. Some background on the kinematics of GSGPs is presented in Section 7.1. As is discussed there, the solution to the *direct kinematics problem* (DKP), in which the pose of $\mathcal{B}$ relative to $\mathcal{F}$ is determined, has been a subject of intense research over the past decades. This brief chapter presents an application involving the DKP that utilizes GFIN. It is more of a proof of concept than a full investigation, because the latter would require more realistic models of accelerometers to be used. The preliminary results, however, are promising. The application is put into the context of GSGP literature by a reasonably complete literature review in Section 7.1. This is followed by an explanation of the various GSGP kinematics problems in Section 7.2. Results

[1] A universal joint is used instead of another spherical joint so that the legs are prevented from rotating about their own lengths.

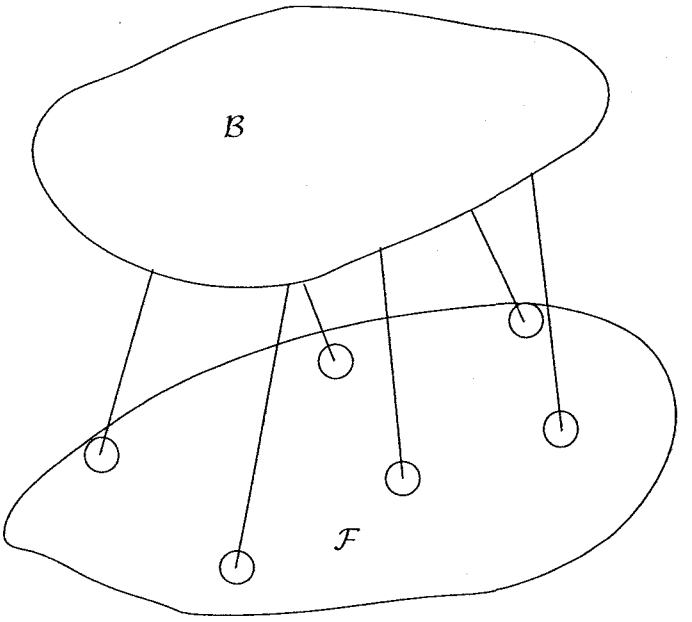

Figure 7.1: A sketch of a GSGP.

of simulations using the 'misplaced' special configuration applied in Chapter 6 follow in Section 7.3.

7.1 GSGP Kinematics Background

The *inverse kinematics problem* (IKP) for a GSGP consists of finding the lengths of each of the six legs from the pose of the platform. This problem is simple, and for any given pose of the platform there is a unique set of leg lengths. In contrast, the forward or *direct kinematics problem* (DKP) which consists of finding the pose of the platform from the six leg lengths, has been the subject of intense research over the past couple of decades [72]. What makes the DKP interesting is that for a given set of six leg lengths, it may be possible to assemble the platform with multiple poses. Each such pose is referred to as an *assembly*. In 1993, it was established by both Lazard and Mourrain, who used algebraic geometry, that for a given set of leg lengths there may be up to forty assemblies [32]. Having established this limit, a method by which all the assemblies of a GSGP for a given set of leg-lengths could be found was sought. In 1996 Husty, derived a 40^{th} order univariate polynomial, the roots of which could be used to identify the assemblies [73]. While Husty's derivation of the polynomial of minimal order was a celebrated milestone in the direct kinematics of GSGPs, it was not useful for calculating the pose of the platform in real-time. There are two reasons for this. First, the formation and subsequent solution of the polynomial posed a considerable computational

burden. Second, even after the polynomial was formed and solved there was no method to identify the *actual* pose of the platform from the other possible assemblies.

Two different avenues have been pursued in addressing the problem of multiple assemblies. First, iterative numerical methods have been used to find the pose 'near' to some known initial pose. Most of these numerical methods are based upon the velocity kinematics of the GSGP, i.e., the relationship between the rate of change of the leg lengths and the velocity of the platform, and the differences between them are subtle [74–77]. Some methods that are sufficiently different to warrant attention are now briefly described.

First is a method due to Innocenti and Parenti-Castelli [78] who proposed a numerical scheme in which the orientation of the platform is solved for, after which the position is directly determined. This method relies on a fact that will be discussed further in the following sections: that (generally) there can be only one assembly for a given set of leg lengths *and* platform orientation. A related, more rigorous scheme that was limited to particular platform architectures, was proposed by Egner [79]. Algorithms involving two phases have been presented by Wang and Chen [80] and Wang and Oen [81]. The first phase of the latter method is an optimization problem. Each leg is treated as a linear spring, and the platform as a collection of six point-masses connected by massless rigid rods. The estimated position of the platform is updated to minimize the resultant force and moment acting on it due to the extension or compression of these elastic legs. After the optimal solution is found, which requires the solution of a 32^{nd} order polynomial, the algorithm switches to a Newton-Raphson, (NR) scheme. The purported advantage of two stage schemes is that they reduce the dependence of the convergence of the traditional iterative schemes on a good initial estimate. Techniques from estimation theory have also been proposed for the direct kinematics problem. Jung and Lee suggested the use of a Kalman filter for estimating the rates of change of the leg lengths using discrete observations of the lengths [82]. In a more rigorous paper, Kang, Kim and Lee designed an estimator for the direct kinematics problem using a full dynamic model of the platform [83]. The estimator was designed to be robust with respect to errors in the model. Most recently, Fasse and Wavering have proposed the use of an Extended Kalman Filter for the solution of the direct kinematics problem of a GSGP [84].

If an iterative method converges, it will find *one* possible assembly of the platform for a given set of leg lengths, but there is no guarantee that this is the *actual* assembly of the platform. Numerous authors have shown how additional sensors can be used so that the measurements they provide, in combination with the leg lengths, mean that the actual assembly is the only possible solution. The sensors that have been utilized are either angular sensors, such as rotary potentiometers, used to measure the angle of a universal joint at the

base, or additional linear sensors, which can take the form of an unactuated leg. As a general rule, the more additional sensors that are used, the easier the direct kinematics problem becomes [85]. For example, Parenti-Castelli and Di Gregorio proposed the use of a single additional linear measurement, but this method was not feasible for real-time applications since it required the formation and solution of two high order polynomials. Cheok et al. presented some more practical approaches using linear sensors [86]. One of their methods involved using three additional linear measurements from different points on the base to a single point on the platform, so that the location of that point could be found by triangulation. After this, the orientation of the platform was obtained solving linear equations. While additional linear sensors are attractive in that they can be added to an existing platform, they have the disadvantage that they can limit the workspace of the platform. Angular sensors have exactly complementary characteristics. Parenti-Castelli and Di Gregorio presented a scheme capable of determining the actual assembly in real-time using two angular sensors [87]. Baron and Angeles considered the many different possibilities for the use of angular sensors and supported the use of redundant sensors so that the effects of measurement errors could be reduced in a least-squares fashion [88]. In a closely related paper, the same authors discussed the conditions under which the direct kinematics problem can be decoupled into two problems; one for the orientation of the platform, and the other for its position [89]. Merlet provides a tabular summary of the number of configurations that are possible for given platform architecture and distribution of angular sensors [32].

A small number of researchers have mentioned the possibility of using accelerometers for the real-time solution of the DKP. Jung and Lee, who were cited above for proposing the use of a Kalman filter for the estimation of the rate of change of leg-lengths from discrete measurements of the same, mentioned in passing that three accelerometers could be attached to the platform 'for measuring linear velocity' [82]. The suggested benefit of the addition of accelerometers was that it made part of the iterative solution for the platform kinematics unnecessary. It is inferred that the accelerometers will somehow yield perfect velocity information; something that is unachievable. Fasse and Wavering, in a paper primarily concerned with the presentation of a 15-state Extended Kalman filter for the solution of the DKP, noted that gyroscopes and accelerometers could be attached to the platform, but that they were not required [84]. The example they provide does not show the use of accelerometers. The team of Gao, Webb and Gindy has produced a series of papers concerning accelerometers attached to GSGPs in general [90–92]. In the first paper, they are concerned with using accelerometers to measure the extension of each leg, although they mention that the ultimate goal is to use a traditional strapdown system of a triaxial accelerometer and three gyroscopes to

determine the pose of the platform. In the most recent paper, they discuss the use of a Kalman filter, but the description is not clear.

7.2 Platform Kinematics

With reference to Fig 7.2, let the 6 ankle points be denoted by $\{A_i\}_0^5$, with coordinate matrices $[\mathbf{r}_{A_i}^{\mathcal{F}}]$ in the fixed frame, the origin of which is chosen so that $O_F = A_0$. Similarly, the coordinate matrices of the hip points, $\{H_i\}_0^5$, in $\mathcal{B}$, are $[\mathbf{r}_{H_i}^{\mathcal{B}}]$, and $O_B = H_0$.

The coordinate matrix of the i^{th} hip point, H_i, in $\mathcal{F}$ can be calculated from

$$[\mathbf{r}_{H_i}^{\mathcal{F}}] = [\boldsymbol{b}^{\boldsymbol{f}}][\mathbf{r}_{H_i}^{\mathcal{B}}] + [\mathbf{r}_{O_B}^{\mathcal{F}}], \tag{7.1}$$

where (refer to Appendix A), $[\boldsymbol{b}^{\boldsymbol{f}}]$ is the orientation matrix of $\boldsymbol{b}$ in $\boldsymbol{f}$. The two matrices, $[\boldsymbol{b}^{\boldsymbol{f}}]$ and $[\mathbf{r}_{O_B}^{\mathcal{F}}]$, describe the pose of $\mathcal{B}$ relative to $\mathcal{F}$. For brevity, these two matrices, or any other representation of the pose are denoted by $\mathcal{B}^{\mathcal{F}}$.

The i^{th} *leg vector* is that from the i^{th} ankle point to the i^{th} hip point:

$$\mathbf{l}_i \stackrel{\text{def}}{=} \mathbf{r}_{H_i/A_i}. \tag{7.2}$$

Using Eq (7.1) the component matrix of the i^{th} leg vector in $\boldsymbol{f}$ is

$$[\mathbf{l}_i^{\boldsymbol{f}}] = [\boldsymbol{b}^{\boldsymbol{f}}][\mathbf{r}_{H_i}^{\mathcal{B}}] + [\mathbf{r}_{O_B}^{\mathcal{F}}] - [\mathbf{r}_{A_i}^{\mathcal{F}}]. \tag{7.3}$$

In particular, due to the aforementioned choice of origins,

$$[\mathbf{l}_0^{\boldsymbol{f}}] = [\mathbf{r}_{O_B}^{\mathcal{F}}]. \tag{7.4}$$

The length of the i^{th} leg vector is denoted by l_i. Using Eq (7.3) shows that

$$\begin{aligned} l_i^2 = {} & [\mathbf{r}_{H_i}^{\mathcal{B}}]^T[\mathbf{r}_{H_i}^{\mathcal{B}}] + [\mathbf{r}_{A_i}^{\mathcal{F}}]^T[\mathbf{r}_{A_i}^{\mathcal{F}}] + [\mathbf{r}_{O_B}^{\mathcal{F}}]^T[\mathbf{r}_{O_B}^{\mathcal{F}}] \\ & - 2[\mathbf{r}_{H_i}^{\mathcal{B}}]^T[\boldsymbol{b}^{\boldsymbol{f}}]^T[\mathbf{r}_{A_i}^{\mathcal{F}}] + 2([\boldsymbol{b}^{\boldsymbol{f}}][\mathbf{r}_{H_i}^{\mathcal{B}}] - [\mathbf{r}_{A_i}^{\mathcal{F}}])^T[\mathbf{r}_{O_B}^{\mathcal{F}}]. \end{aligned} \tag{7.5}$$

This equation is the solution to the IKP; the leg-lengths can be calculated from the description of the pose of the platform $\mathcal{B}^{\mathcal{F}}$, which, recall, can be specified by $[\boldsymbol{b}^{\boldsymbol{f}}]$ and $[\mathbf{r}_{O_B}^{\mathcal{F}}]$.

The DKP consists of finding $\mathcal{B}^{\mathcal{F}}$ from the leg-lengths $\{l_k\}_0^5$, and, possibly, some information from additional sensors. As was mentioned in Section 7.1 there can be up to 40 different assemblies of the platform for a given set of leg-lengths. The most important assembly is the *actual* pose of the platform. The length of the i^{th} leg when the platform has some pose, $\mathcal{B}^{\mathcal{F}}$, is denoted by $L_i(\mathcal{B}^{\mathcal{F}})$, thus, the DKP can be stated as finding $\mathcal{B}^{\mathcal{F}}$ such that

$$L_i^2(\mathcal{B}^{\mathcal{F}}) - l_i^2 = 0 \qquad i = 0, \ldots, 5. \tag{7.6}$$

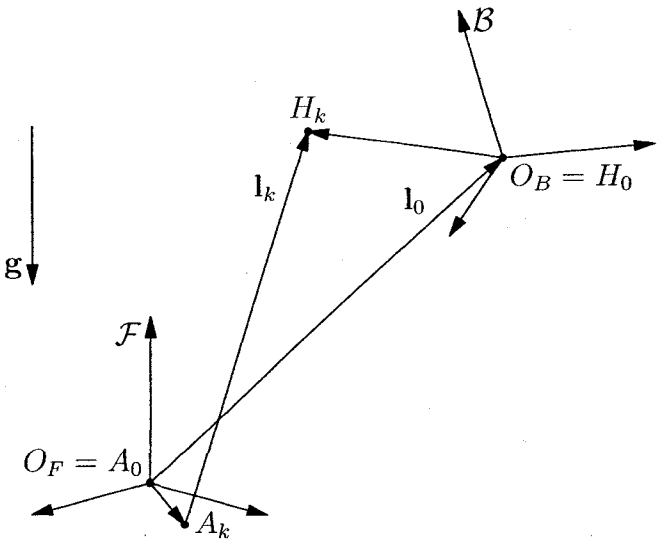

Figure 7.2: The relationship between the leg vectors, $\mathbf{l}_0$ and $\mathbf{l}_k$.

The *Inverse Velocity Problem* (IVP) involves finding the rates of change of the leg-lengths from a description of the velocity of the platform. Let $\mathbf{n}_i$ denote the unit vector along the i^{th} leg vector, i.e., $\mathbf{l}_i = l_i\mathbf{n}_i$. The derivative of $\mathbf{l}_i$ as observed from $\boldsymbol{f}$ is

$$\frac{\mathrm{d}^{\boldsymbol{f}}}{\mathrm{d}t}\mathbf{l}_i = \dot{l}_i\mathbf{n}_i + l_i\frac{\mathrm{d}^{\boldsymbol{f}}}{\mathrm{d}t}\mathbf{n}_i. \tag{7.7}$$

Also, since $\mathbf{l}_i = \mathbf{r}_{H_i/A_i}$ and A_i is a fixed point,

$$\frac{\mathrm{d}^{\boldsymbol{f}}}{\mathrm{d}t}\mathbf{l}_i = \mathbf{v}_{H_i}, \tag{7.8}$$

where $\mathbf{v}_{H_i}$ is the velocity of H_i relative to $\mathcal{F}$. Noting that the derivative of a unit vector is always orthogonal to the unit vector itself, equating the two expressions for the derivative of $\mathbf{l}_i$ and taking the scalar product of both sides with $\mathbf{n}_i$ shows that

$$\dot{l}_i = \mathbf{n}_i \cdot \mathbf{v}_{H_i}. \tag{7.9}$$

Letting $\boldsymbol{\omega}$ denote the angular velocity of $\mathcal{B}$ relative to $\mathcal{F}$, $\mathbf{v}_{H_i}$ can be written as

$$\mathbf{v}_{H_i} = \mathbf{v}_{O_B} + \boldsymbol{\omega} \times \mathbf{r}_{H_i/O_B}, \tag{7.10}$$

and substituting this into Eq (7.9) gives

$$\dot{l}_i = \mathbf{n}_i \cdot \mathbf{v}_{O_B} + \mathbf{n}_i \cdot \boldsymbol{\omega} \times \mathbf{r}_{H_i/O_B}. \tag{7.11}$$

This expression can be profitably rewritten in terms of component matrices as

$$\dot{l}_i = [\mathbf{L}_i^{\mathcal{B}}][\mathbf{V}^{\mathcal{B}}] \tag{7.12}$$

where

$$[\mathbf{L}_i^{\mathcal{B}}] = \begin{bmatrix} [\mathbf{n}_i^b]^T & -[\mathbf{n}_i^b]^T \text{skew}([\mathbf{r}_{H_i}^{\mathcal{B}}]) \end{bmatrix} \tag{7.13}$$

and

$$[\mathbf{V}^{\mathcal{B}}] = \begin{bmatrix} [\mathbf{v}_{O_B}^{\mathcal{B}}] \\ [\boldsymbol{\omega}^b] \end{bmatrix}. \tag{7.14}$$

The matrix, $[\mathbf{L}_i^{\mathcal{B}}]$ is seen to be comprised of the Plücker coordinates of the line through the i^{th} leg relative to $\mathcal{B}$, while $[\mathbf{V}^{\mathcal{B}}]$ fully describes the velocity of $\mathcal{B}$ relative to $\mathcal{F}$. The latter matrix, or that obtained by switching the order of the constituent matrices is sometimes known as the 'velocity motor' [93]. If Eq (7.12) is written for each leg the result is

$$[\dot{\boldsymbol{l}}] = [\mathbf{J}]^{-1}[\mathbf{V}^{\mathcal{B}}], \tag{7.15}$$

where $[J]^{-1}$ is a 6×6 matrix, the i^{th} row of which is $[\mathbf{L}_i^{\mathcal{B}}]$. Merlet refers to this matrix as the inverse Jacobian matrix [32]. Equation (7.15) is the solution to the IVP. The *Forward Velocity Problem*, (FVP) can be solved as long as $[\mathbf{J}]^{-1}$ is non-singular:

$$[\mathbf{V}^{\mathcal{B}}] = [\mathbf{J}][\dot{\boldsymbol{l}}]. \tag{7.16}$$

7.3 Robust Tracking of the Motion of a GSGP Using GFIN

A number of exotic numerical schemes for the solution of the DKP were discussed in Section 7.1. Here a standard technique, based on that used by Sugimoto [74] is applied. Sugimoto referred to it as an implementation of the Newton-Raphson method, but authors proposing essentially the same algorithm have called it successive approximation [76]. The method is based upon the IKP and the FVP and is easily understood with reference to Fig 7.3.

The inputs to the algorithm are the measured leg lengths, $[\boldsymbol{l}]$, and an initial estimate of the pose. The IKP is used to calculate the leg-lengths, denoted by $[L]$ in Figure 7.3, for the estimated pose, and these are compared to the actual lengths. If they are within a specified tolerance, the algorithm is finished and the initial guess is used as the pose. Under the assumption that the estimated pose is close to the true pose, the column matrix with k^{th} element $l_k - L_k$ will be roughly equal to a scaled version of some velocity matrix, as given in Eq (7.14). Using the solution of the FVP in Eq (7.16), the scaled velocity matrix corresponding to the leg length discrepancy is calculated and the pose is updated using some approximate version of kinematic differential equations. In possession of the new pose update, the algorithm begins again and iterates until either the difference in leg-lengths is small enough, i.e., it converges, or the method fails. It is important to note that part of the algorithm involves

the solution of the FVP, which, as mentioned above, requires that the Jacobian be non-singular.

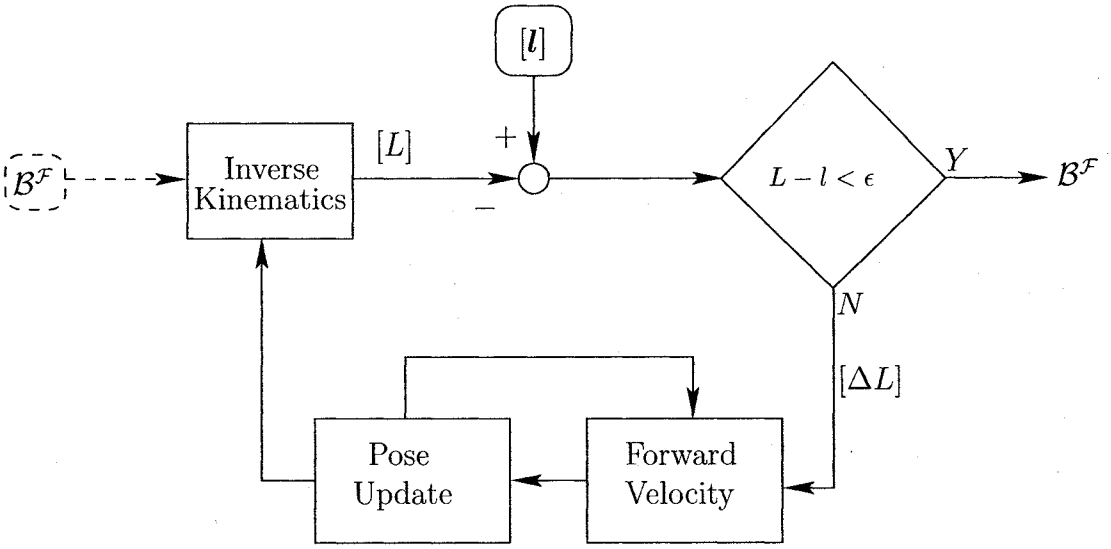

Figure 7.3: The Newton-Raphson method for the solution of the DKP.

7.3.1 Example

The geometry of the platform that is used for simulation purposes is shown in Table 7.1. It is a scaled version of a platform studied by Dasgupta and Mruthyunjaya [94]. All dimensions are taken to be in m.

k	$[\mathbf{r}_{A_k}^{\mathcal{F}}]^T$	$[\mathbf{r}_{P_k}^{\mathcal{B}}]^T$
0	$[0 \quad 0 \quad 0]$	$[0 \quad 0 \quad 0]$
1	$[0.6 \quad -0.3 \quad 0]$	$[0.5 \quad -0.2 \quad 0]$
2	$[0.9 \quad 0.3 \quad 0]$	$[0.5 \quad 0 \quad 0]$
3	$[1 \quad 1.2 \quad 0]$	$[0.5 \quad 0.5 \quad 0]$
4	$[5 \quad 1.33 \quad 0]$	$[0.2 \quad 0.7 \quad 0]$
5	$[0 \quad 1 \quad 0]$	$[0 \quad 0.5 \quad 0]$

Table 7.1: The geometry of the SGSP under study.

The orientation of the platform is described using Bryant angles [68] as

continuous functions of time:

$$\theta_1(t) = 0.5\cos 3t - 0.5 \tag{7.17a}$$

$$\theta_2(t) = -\frac{\pi}{2}\cos 4t + \frac{\pi}{2} \tag{7.17b}$$

$$\theta_3(t) = \frac{\pi}{3}\cos 2t - \frac{\pi}{3} \tag{7.17c}$$

The position of the platform is described by the following coordinate matrix:

$$[\mathbf{r}_{O_M}(t)^{\mathcal{F}}] = \begin{bmatrix} 0.4\cos 5t + .4 \\ 0.6\cos 4t + .6 \\ \cos 6t + 1.5 \end{bmatrix} \tag{7.18}$$

Using these functions allows the kinematics of the platform to be calculated exactly, and used for comparative purposes. The functions describing the position and orientation were chosen so that the velocity would be zero at $t = 0$, which is likely the case in application; the GSGP would be turned on, the current pose calculated, and then operation would begin. A sampling period of $\Delta T = 0.005$s was used for the simulations.

Figure 7.4 shows a result obtained when running the simulation using the Newton-Raphson method described in Section 7.3. The trace indicates the computed position of $O_B = H_0$. Figure 7.5 shows the error in this calculated position. It shows that the platform is tracked well until around $t = 2$s. The fact that the algorithm still converges after it leaves the true solution means that it has found another platform assembly. After approximately 0.5s the true pose is found again. Figure 7.5 shows that the algorithm 'loses track' in this manner 5 times over the 10s simulation period. This failure is not a result of a badly coded algorithm. It has been noted by a number of authors [32, 95] that numerical methods can lead to the wrong solution. This normally happens in the vicinity of a singularity; a point where the Jacobian of the platform loses rank. This was confirmed to be the case here. The condition number of the inverse Jacobian at around $t = 2.0$s shows a spike, indicating that the matrix, and hence the platform, are close to singularity.

So far the described method is 'classical'; a standard treatment of the numerical solution of the DKP. It is seen that this method has a shortcoming in that while the method may converge, it may converge to the wrong solution. Jakobovič and Budin proposed some extrapolation procedures to overcome this problem [95]. Based upon the results of the previous chapter it seems an ideal application for a special minimal configuration. Such a configuration attached to the moving platform could have two benefits:

- It could provide velocity estimates of the platform useful for control purposes.

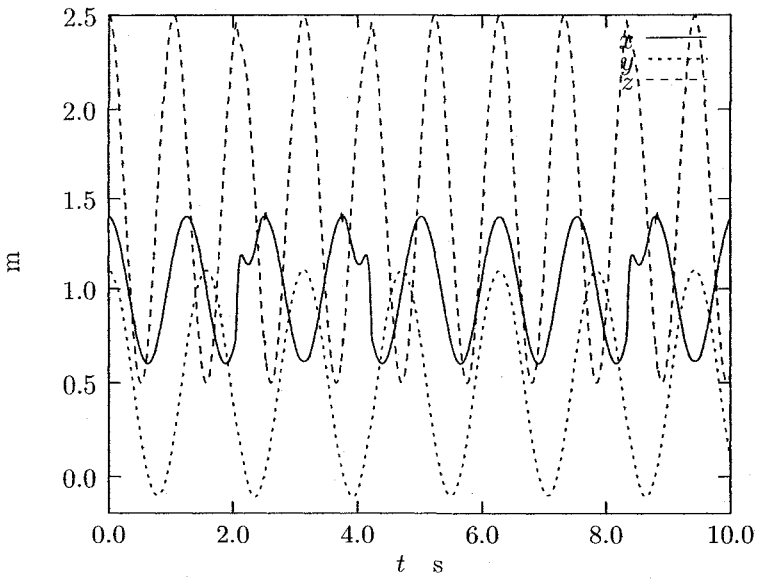

Figure 7.4: The position of O_B as calculated by the Newton-Raphson algorithm.

- It could help to 'drive' the solution of the platform through areas that are close to singularities.

This application is likely to succeed because:

- Position and orientation information that is *normally* very reliable is available from the Newton-Raphson algorithm.
- The GFIN pose solution would only be required for short durations when the platform is close to a singularity, which are normally to be avoided.

The proposed algorithm is simple and has the following typical time step, which is illustrated in Fig 7.6:

1. Implement the GFIN algorithm as described in Section 6.3.2 to get a new estimate of the platform pose.
2. Check the condition number of the Jacobian of the platform in the estimated pose. If it is large, indicating that the platform is close to a singularity, return to step 1, otherwise;
3. Use the GFIN calculated pose as the initial estimate for the NR algorithm.
4. Use the NR calculated pose in the GFIN algorithm at the next step.

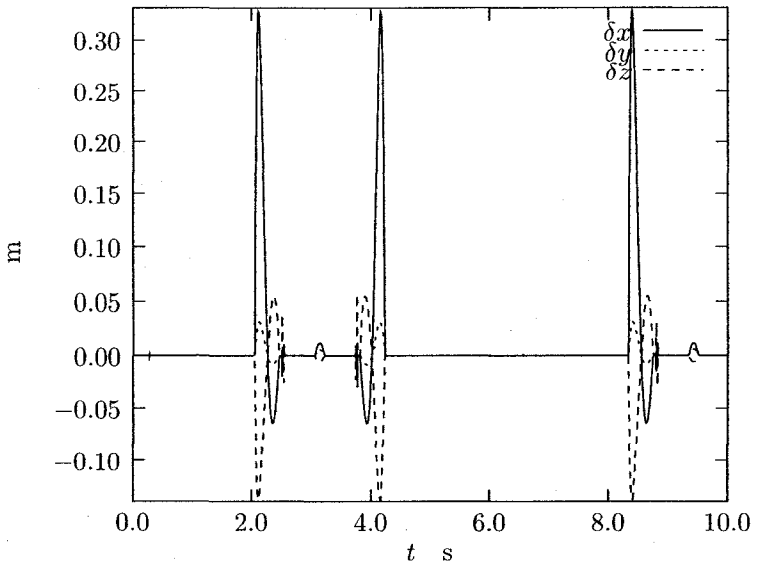

Figure 7.5: The error in the position of O_B as calculated by the Newton-Raphson algorithm.

A series of figures is now used to illustrate the performance of this algorithm. The accelerometer configuration used is again Chen's special minimal configuration. It is assumed to have the partly estimated placement errors described in Section 6.4.2.

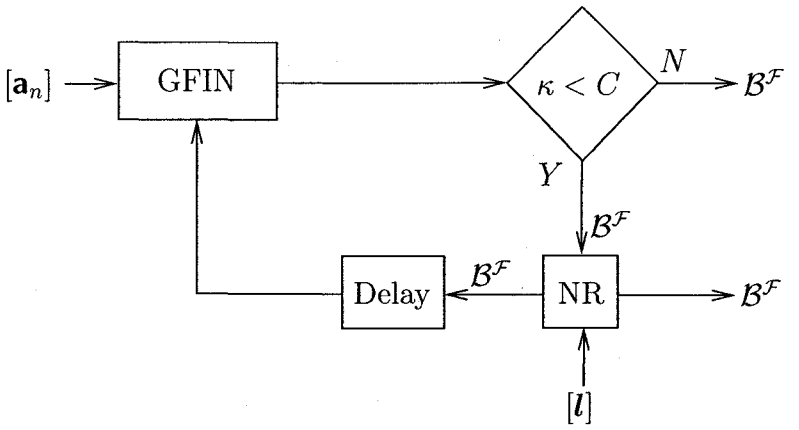

Figure 7.6: The proposed combination of GFIN and NR for the solution of the FKP of the GSGP.

Figure 7.7 shows the errors in the position estimate obtained using the accelerometer configuration alone, i.e., without using the Newton-Raphson solution based on the leg-lengths. The drift in the solution that was seen in Chapter 6 is in evidence here.

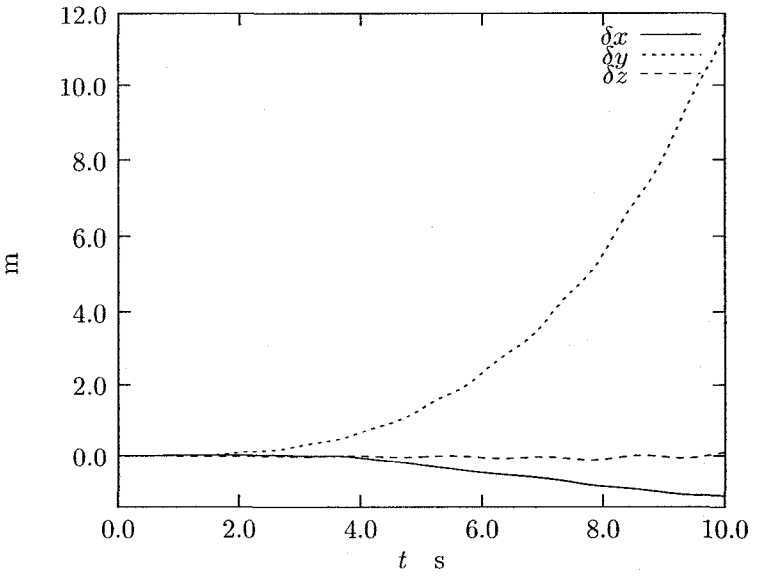

Figure 7.7: The error in the position of O_B as calculated by GFIN alone.

Figure 7.8 shows the position estimate obtained using the combination of GFIN and NR described above. The threshold for the condition number of the Jacobian was taken at 2000 for this particular example. It shows, as was hoped, that using the inertial solution when close to a singularity prevents the wrong solution track from being followed. The method could be refined, however. As is shown in Fig 7.9, there are small discontinuities in the calculation of the position when the NR algorithm is switched on and off. Figure 7.10 shows the periods over which GFIN is used exclusively. The discontinuities that occur when the algorithm switches from NR/GFIN to GFIN exclusively, could likely be overcome using some estimation scheme in which the NR solution is weighted rather than ignored completely. Another possible improvement to the method would be to use the time history of the reliably calculated pose to estimate velocity. This estimate could then be used to reset the GFIN algorithm periodically. While further simulations and modifications of the basic approach led to good results, to fully ascertain whether this is a viable application for GFIN would require a more realistic model be used for both the accelerometers and the motion of the GSGP.

7.4 Summary

As this chapter has shown, the tracking of the motion of a GSGP is an application that shows promise as an area where GFIN, even a special minimal configuration with placement errors, may be practical. The NR and GFIN algorithms complement each other well. On one hand, GFIN can be used to

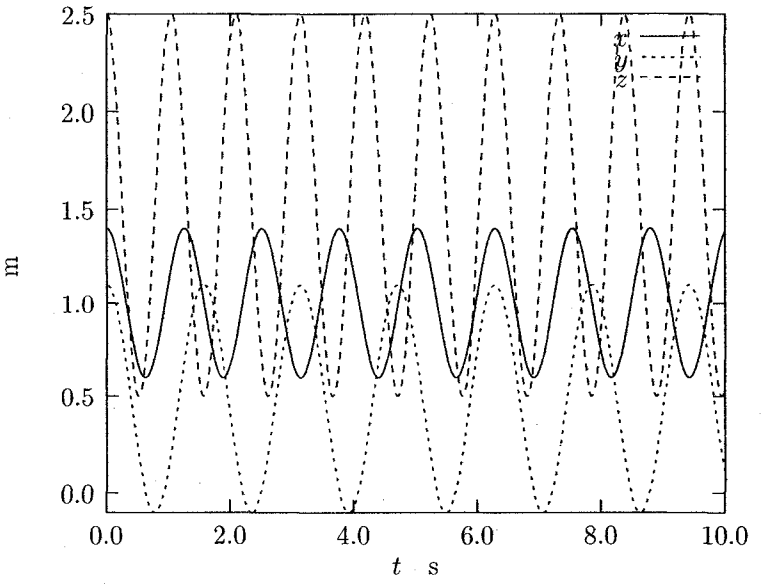

Figure 7.8: The position of O_B as calculated by the combination of Newton-Raphson and GFIN.

give a good starting estimate for NR, and can function without NR when close to a singularity. On the other hand, the position and orientation information that is available from NR can be used to prevent the drift of the GFIN estimate. While it appears promising, there is little point further developing the algorithm using ideal sensor characteristics and simulated motion; it would benefit more from experimental investigation.

It is mentioned in passing that the author investigated the use of accelerometer measurements when the platform is stationary. The development is not included here because it is not strictly an application of GFIN. It was established, however, that using the measurement of the local gravity vector obtained from accelerometers attached to the stationary platform, one could, assuming that the component matrix of the gravity vector was known in the fixed frame, limit the number of assemblies to 4, down from 40 without the accelerometer measurements. Such an application could be of interest if one was already using accelerometers for the robust tracking application described in this chapter.

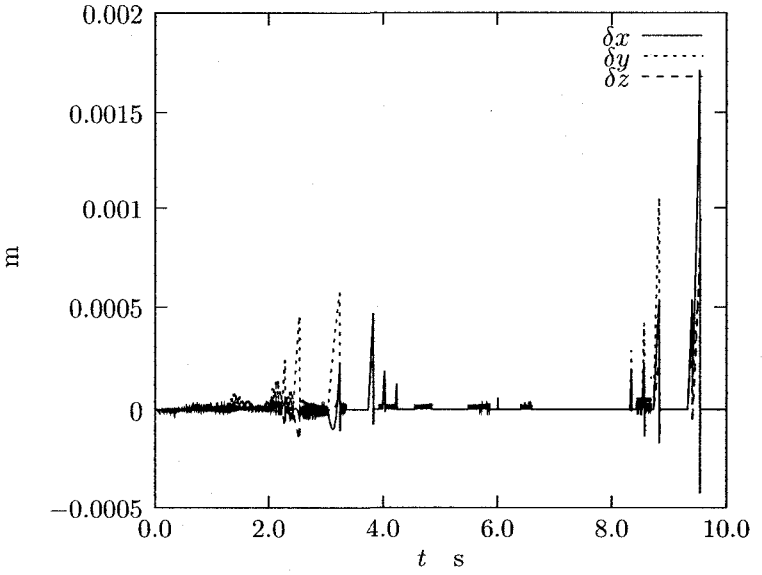

Figure 7.9: The error in the calculation of the position of O_B as calculated by the combination of Newton-Raphson and GFIN.

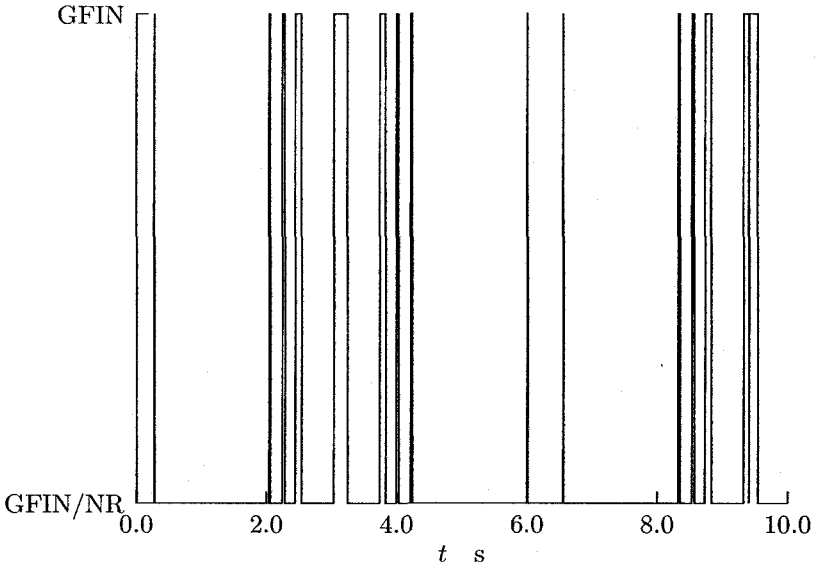

Figure 7.10: The periods over which GFIN is used alone (high) and in combination with NR (low).

Chapter 8

Conclusions and Recommendations

This chapter serves three purposes. It summarizes the main ideas of the thesis, and why they were studied. The novel contributions of this thesis are then outlined and, finally, recommendations for further research are given.

8.1 Summary

Motivated by the vast array of different accelerometer configurations that have been proposed for use with GFIN over the last four decades without justification for their particular designs, the main aim of this thesis was to investigate the geometry of such configurations; to find how they must be arranged so that GFIN is possible and to understand how the arrangement can lead to various properties, desirable and otherwise.

When designing an accelerometer configuration, the most basic demand that is made of each accelerometer is that it yield some information about the motion of the body that is not available from the rest of the configuration. This was formalized in this thesis using the concept of accelerometer dependence which was defined in terms of the linear dependence of matrices of coordinates, (ADMs), used to describe each accelerometer. The frame transformation rule for ADMs was derived and it was confirmed that if the ADMs were linearly dependent in one frame they were dependent in all frames, confirming that the definition of dependence is meaningful. Without recourse to the definition of the ADM and even linear dependence, a set of accelerometers can be stated to be dependent if the measurement of one of the accelerometers can be written as a constant linear combination of the other accelerometers, regardless of the motion.

A concept that is intimately related to accelerometer dependence is accelerometer generation; the accelerometers generated by a configuration are

exactly the accelerometers that are dependent upon the configuration. Accelerometer generation is important in the theory of configuration design. Starting with an independent configuration, one determines accelerometers that are generated and places an additional accelerometer accordingly, (i.e. so that the resulting configuration is independent). The process can be repeated until the maximum number of independent accelerometers have been placed. In this thesis geometric constructions for the accelerometers generated by all planar accelerometer configurations were given. Some numerical properties of these configurations were also explored. It was shown, for instance, that it is possible to design a planar configuration with unit condition number, but that the condition number is not invariant to the choice of frame used to describe the locations of the accelerometers. The accelerometers generated by general spatial accelerometer configurations of up to 12 accelerometers were also described. This investigation uncovered some very interesting geometrical results. In possession of these results it is possible, at least in the planar case, to incrementally build an independent accelerometer configuration without ever having to check for numerical dependence. The complexity of the geometry in the spatial case means that this would be difficult.

A class of accelerometer configurations referred to as minimal configurations, because they use the minimum possible number of accelerometers to measure spatial motion were studied. The accelerometer placement necessary for the configuration to function was described. Further, it was shown how 'special minimal configurations' can be designed so that the configurations have a desirable property; freedom from the requirement of solving a non-linear differential equation for the angular velocity.

A secondary aim of the thesis was to address, or at least investigate the consequences of, incorrect accelerometer placement within a configuration. It was shown using analytical arguments and corroborating simulations that even very small placement errors lead to terrible performance. For example a misalignment error of 0.05° could lead to a position error of hundreds of metres within 10s for a simple application. The special minimal configurations are particularly sensitive to placement errors because they lose their defining property.

A novel application of GFIN that might still be practical, even in the presence of placement errors, was briefly investigated. It was proposed that special minimal configurations could be used to aid in tracking the motion of a GSGP. Preliminary results are promising.

Thus, this thesis can be briefly summarized as showing how accelerometers should be arranged so that GFIN is possible, and what will occur, inevitably, when they are not arranged precisely. The concept of GFIN was essentially an academic exercise when it was first introduced 40 years ago. The lower cost, improved performance and smaller size of accelerometers have made that

exercise into a reality, albeit not a pleasant one. Hopefully, in the not too distant future, improved manufacturing techniques will make near precise accelerometer configurations possible and some of the geometrical results in this thesis will be able to be elevated from intriguing to useful.

8.2 Contributions

This thesis makes a number of novel contributions. Those that are considered the most important are:

- Formal definitions of accelerometer dependence and generation.
- The full solution of the planar accelerometer configurations dependence problem.
- Investigation of numerical properties of planar accelerometer configurations.
- The definition of constrained accelerometer configurations, and the geometrical identification of the general dependent constrained configurations.
- The presentation of the geometrical requirements that must be satisfied by a minimal accelerometer configurations, and a design methodology for special minimal configurations.
- A semi-analytical treatment of accelerometer placement errors with supporting simulations.
- The identification of the tracking of the motion of a Stewart-Gough Platform as a potential application for GFIN.

8.3 Recommendations for Further Research

During the process of writing this thesis, the following areas were seen as potentially fruitful, but lack of time and/or equipment and their remoteness from the main goal of the research meant that they were not pursued.

8.3.1 Minimal Configurations

A possible direction for future research is the enumeration of the different types of special minimal configuration and the comparison of their performance in the face of realistic configuration and sensor errors. Such a comparison could also consider the possibility of minimal configurations in which a non-linear

differential equation must be solved for the angular velocity but the solution of the specific force is independent of angular velocity.

8.3.2 Condition Number Properties

It was established that the condition number of an accelerometer configuration is not frame invariant, but it would be interesting to know whether designing a configuration so that it has a minimum condition number in one frame will guarantee this in any other frame. Also, simulations or experiments validating the theoretical predictions of performance would be of value.

8.3.3 Dependence Geometry

A lot of work remains to be done in the geometry of accelerometer dependence. This is, perhaps, work that is more suitable for a geometer, who could likely see links between the various cases and establish theorems that would unify the results.

8.3.4 Calibration and Compensation

In this thesis, accelerometers were treated as ideal and perfectly known, apart from their location and orientation. Modern accelerometers have good linear characteristics, so the major assumptions that were made were that the bias and gain of each accelerometer were known exactly. In reality, these sensor properties must be established by a process of calibration. A calibration procedure that simultaneously determines the bias, gain and configuration errors of every accelerometer in a configuration would be very useful. Further, accelerometers are often calibrated using gravity tests, and it would be interesting to know what accuracy it is possible to achieve using this method. Once the accelerometer configuration errors have been obtained by a calibration method, some means of compensation must be used. If full 12-accelerometer configurations are used, this is an area where estimation theory could be useful.

8.3.5 Platform Kinematics

Simple simulations showed that GFIN could be of use in tracking the motion of a GSGP. More work, most likely in the form of experiments, needs to be done to determine if this is true.

Appendix A

Bases and Frames

This appendix summarises some of the notation and concepts required particularly in Chapter 2.

A.1 Orthonormal Bases

An orthonormal basis $(\boldsymbol{a}, \boldsymbol{b}, \ldots)$ of the Euclidean space, $\mathbf{E}$, is a set of three mutually perpendicular unit vectors. One basis, $\boldsymbol{f}$, is defined to be *fixed*, all others may be rotating relative to it.

The 3×1 matrix of the basis-vectors of a basis, $\boldsymbol{a}$ is denoted by

$$[\boldsymbol{a}] = \begin{bmatrix} \mathbf{a}_1 \\ \mathbf{a}_2 \\ \mathbf{a}_3 \end{bmatrix}. \tag{A.1}$$

Similar matrices of unit vectors have been used by (among others) Hughes [96], who referred to them as *vectrices*. The 'orthonormality' of $\boldsymbol{a}$ can be stated by the following matrix equation:

$$[\boldsymbol{a}] \cdot [\boldsymbol{a}]^T = [I]_3, \tag{A.2}$$

where $[I]_3$ is the 3×3 identity matrix. The basis, $\boldsymbol{a}$, is *right-handed* if

$$[\boldsymbol{a}] \times [\boldsymbol{a}]^T = \begin{bmatrix} \mathbf{0} & \mathbf{a}_3 & -\mathbf{a}_2 \\ -\mathbf{a}_3 & \mathbf{0} & \mathbf{a}_1 \\ \mathbf{a}_2 & -\mathbf{a}_1 & \mathbf{0} \end{bmatrix} \equiv -\text{skew}(\boldsymbol{a}), \tag{A.3}$$

where, for a 3×1 matrix, $[\mathbf{v}]$ with i^{th} element, v_i:

$$\text{skew}([\mathbf{v}]) = \begin{bmatrix} 0 & -v_3 & v_2 \\ v_3 & 0 & -v_1 \\ -v_2 & v_1 & 0 \end{bmatrix}. \tag{A.4}$$

This matrix has, besides its obvious skew-symmetry, the property that for any 3×1 matrix, $[\mathbf{w}]$,

$$\text{skew}([\mathbf{v}])[\mathbf{w}] = -\text{skew}([\mathbf{w}])[\mathbf{v}]. \tag{A.5}$$

In this thesis all bases are assumed to be orthonormal and right-handed.

The *component matrix* of an arbitrary vector, $\mathbf{v}$, in $\boldsymbol{a}$ is the 3×1 matrix, $[\mathbf{v}^{\boldsymbol{a}}]$, satisfying

$$\mathbf{v} = [\boldsymbol{a}]^T[\mathbf{v}^{\boldsymbol{a}}] = [\mathbf{v}^{\boldsymbol{a}}]^T[\boldsymbol{a}]. \tag{A.6}$$

Using Eq (A.2) shows that the component matrix can be calculated as

$$[\mathbf{v}^{\boldsymbol{a}}] = [\boldsymbol{a}] \cdot \mathbf{v}. \tag{A.7}$$

The scalar product of two vectors, can be calculated using their component matrices:

$$\mathbf{v} \cdot \mathbf{w} = [\mathbf{v}^{\boldsymbol{a}}]^T[\boldsymbol{a}] \cdot [\boldsymbol{a}]^T[\mathbf{w}^{\boldsymbol{a}}] = [\mathbf{v}^{\boldsymbol{a}}]^T[\mathbf{w}^{\boldsymbol{a}}]. \tag{A.8}$$

The vector product can also be calculated using component matrices:

$$\begin{aligned} \mathbf{v} \times \mathbf{w} &= [\mathbf{v}^{\boldsymbol{a}}]^T[\boldsymbol{a}] \times [\boldsymbol{a}]^T[\mathbf{w}^{\boldsymbol{a}}] \\ &= -[\mathbf{v}^{\boldsymbol{a}}]^T\text{skew}(\boldsymbol{a})[\mathbf{w}^{\boldsymbol{a}}] \qquad \text{(A.9)} \\ &= [\boldsymbol{a}]\text{skew}([\mathbf{v}^{\boldsymbol{a}}])[\mathbf{w}^{\boldsymbol{a}}], \qquad \text{(A.10)} \end{aligned}$$

where Eqs (A.3) and (A.5) were used.

The *orientation matrix* of $\boldsymbol{b}$ in $\boldsymbol{a}$, is the 3×3 matrix with i^{th} column equal to $[\mathbf{b}_i^{\boldsymbol{a}}]$:

$$[\boldsymbol{b}^{\boldsymbol{a}}] = [\boldsymbol{a}] \cdot [\boldsymbol{b}]^T = \left[[\mathbf{b}_1^{\boldsymbol{a}}] \quad [\mathbf{b}_2^{\boldsymbol{a}}] \quad [\mathbf{b}_3^{\boldsymbol{a}}] \right]. \tag{A.11}$$

Operating on the left-hand side of $\mathbf{v} = [\boldsymbol{b}]^T[\mathbf{v}^{\boldsymbol{b}}]$ with $[\boldsymbol{a}]\cdot$, shows that

$$[\mathbf{v}^{\boldsymbol{a}}] = [\boldsymbol{b}^{\boldsymbol{a}}][\mathbf{v}^{\boldsymbol{b}}] \tag{A.12}$$

i.e., the orientation matrix of $\boldsymbol{b}$ in $\boldsymbol{a}$ serves to transform the component matrix of a vector in $\boldsymbol{b}$ to that of the same vector in $\boldsymbol{a}$. The orientation matrix has the following properties:

$$\det[\boldsymbol{b}^{\boldsymbol{a}}] = 1 \tag{A.13}$$

$$[\boldsymbol{b}^{\boldsymbol{a}}]^{-1} = [\boldsymbol{a}^{\boldsymbol{b}}] = [\boldsymbol{b}^{\boldsymbol{a}}]^T. \tag{A.14}$$

A.2 Frames

A *frame* in $\mathscr{E}$, $(\mathcal{A}, \mathcal{B}, \ldots)$ is the collection of a point $(O_A, O_B, \ldots)$, the *origin*, and a basis of $\mathbf{E}$, $(\boldsymbol{a}, \boldsymbol{b}, \ldots)$. The frame, $\mathcal{F}$, is regarded as fixed, inertial when necessary, and all other frames may move relative to it. Each frame may be visualized as a rigid wire frame.

The *coordinate matrix* of a point, $P \in \mathscr{E}$, in $\mathcal{A}$, is the component matrix in $\boldsymbol{a}$, of the vector, $\mathbf{r}_{P/O_A}$ from O_A to P. It is denoted by $[\mathbf{r}_P^{\mathcal{A}}]$, i.e.,

$$[\mathbf{r}_P^{\mathcal{A}}] \equiv [\boldsymbol{a}] \cdot \mathbf{r}_{P/O_A}. \tag{A.15}$$

Chasles' identity [49] states that

$$\mathbf{r}_{P/O_A} = \mathbf{r}_{P/O_B} + \mathbf{r}_{O_B/O_A}.$$

This can be written in terms of coordinate matrices as

$$[\boldsymbol{a}]^T[\mathbf{r}_P^{\mathcal{A}}] = [\boldsymbol{b}]^T[\mathbf{r}_P^{\mathcal{B}}] + [\boldsymbol{a}]^T[\mathbf{r}_{O_B}^{\mathcal{A}}]$$

and operating from the left with $[\boldsymbol{a}]\cdot$ gives the following relationship between the coordinate matrices of P in $\mathcal{A}$ and $\mathcal{B}$:

$$[\mathbf{r}_P^{\mathcal{A}}] = [\boldsymbol{b}^{\boldsymbol{a}}][\mathbf{r}_P^{\mathcal{B}}] + [\mathbf{r}_{O_B}^{\mathcal{A}}]. \tag{A.16}$$

Appendix B

The ADM to AADM Transformation Matrix

The matrix, $[X]$ appearing in Eq (2.13), that transforms the AADM of an accelerometer in some frame to the ADM of the same accelerometer in the same frame, is

$$[X] = \begin{bmatrix} 1 & 0 & 0 & 0 & 0 & 0 & 0 & 0 & 0 & 0 & 0 & 0 \\ 0 & 1 & 0 & 0 & 0 & 0 & 0 & 0 & 0 & 0 & 0 & 0 \\ 0 & 0 & 1 & 0 & 0 & 0 & 0 & 0 & 0 & 0 & 0 & 0 \\ 0 & 0 & 0 & 0 & 0 & 0 & 0 & 0 & 0 & -1 & 0 & 0 \\ 0 & 0 & 0 & 0 & 0 & 1 & 0 & 0 & 1 & 0 & 0 & 0 \\ 0 & 0 & 0 & 0 & -1 & 0 & 0 & 1 & 0 & 0 & 0 & 0 \\ 0 & 0 & 0 & 0 & 0 & -1 & 0 & 0 & 1 & 0 & 0 & 0 \\ 0 & 0 & 0 & 0 & 0 & 0 & 0 & 0 & 0 & 0 & -1 & 0 \\ 0 & 0 & 0 & 1 & 0 & 0 & 1 & 0 & 0 & 0 & 0 & 0 \\ 0 & 0 & 0 & 0 & 1 & 0 & 0 & 1 & 0 & 0 & 0 & 0 \\ 0 & 0 & 0 & -1 & 0 & 0 & 1 & 0 & 0 & 0 & 0 & 0 \\ 0 & 0 & 0 & 0 & 0 & 0 & 0 & 0 & 0 & 0 & 0 & -1 \end{bmatrix}. \tag{B.1}$$

It can be confirmed by calculation that

$$\det[X] = 8.$$

The product of $[X]$ with its transpose is a diagonal matrix. This leads to the following expression for $[X]^{-1}$:

$$[X]^{-1} = \frac{1}{2}\text{diag}([2 \quad 2 \quad 2 \quad 2 \quad 1 \quad 1 \quad 1 \quad 2 \quad 1 \quad 1 \quad 1 \quad 2])[X]^T. \tag{B.2}$$

Appendix C

The Kronecker Product

This appendix gives the definition of the Kronecker product [51, 97], also known as the direct or tensor product [98] of matrices and lists the small number of properties that are required for the work in the thesis.

For any matrix $[A]$ with elements $a_{i,j}$, and any matrix, $[B]$, the Kronecker product is defined as

$$[A] \otimes [B] = \begin{bmatrix} a_{1,1}[B] & \cdots & a_{1,n}[B] \\ \vdots & \ddots & \vdots \\ a_{m,1}[B] & \cdots & a_{m,n}[B] \end{bmatrix}. \tag{C.1}$$

The Kronecker product is distributive and associative, and also has the following properties (in the second relationship it is assumed that the matrices have suitable dimensions):

$$([A] \otimes [B])^T = [A]^T \otimes [B]^T \tag{C.2}$$

$$([A] \otimes [B])([C] \otimes [D]) = ([A][C]) \otimes ([B][D]). \tag{C.3}$$

Finally, if $[A]$ is an $m \times m$ matrix and $[B]$ is an $n \times n$ matrix, then

$$\det([A] \otimes [B]) = \det([A])^n \det([B])^m. \tag{C.4}$$

Appendix D

Requirement for Unit Condition Number

This appendix shows that an $n \times n$ matrix, $[A]$, has a unit condition number if $[A][A]^T$ is a positive scalar multiple of the $n \times n$ identity matrix. A similar result is proved by Angeles [12] using a different method. He refers to matrices with this property as 'isotropic matrices'.

If $[A]$ is a real $n \times n$ matrix, then its singular value decomposition is [52]:

$$[A] = [U][\Sigma][V]^T \tag{D.1}$$

where $[U]$ and $[V]$ are real orthogonal $n \times n$ matrices,

$$[\Sigma] = \text{diag}([\sigma_1, \ldots, \sigma_n]), \tag{D.2}$$

where $\sigma_1 \geq \sigma_2 \geq \ldots \sigma_n \geq 0$ are the singular values of $[A]$. The number of non-zero singular values of $[A]$ is equal to the rank of $[A]$.

The condition number of $[A]$ is

$$\kappa[A] = \frac{\sigma_1}{\sigma_n}. \tag{D.3}$$

Clearly the minimum possible condition number is 1, and this requires that the matrix be of full rank and that all the singular values be equal, i.e., that

$$[\Sigma] = \sigma[I]_n, \tag{D.4}$$

for some $\sigma > 0$ in which case

$$\begin{aligned} [A][A]^T &= [U][\Sigma][V]^T[V][\Sigma][U]^T \\ &= [U][\Sigma]^2[U]^T \\ &= [U]\sigma^2[I]_n[U]^T \\ &= \sigma^2[U][U]^T \\ &= \sigma^2[I]_n. \end{aligned} \tag{D.5}$$

Appendix E

Placement Errors in Simulations

In Section 6.3.2, the six accelerometers of Chen's special configuration were subjected to placement errors. In that chapter, only the magnitude of the location and direction errors were described. Here the perturbed locations and directions of the accelerometers are recorded so that the simulations can be reproduced. The locations of the six accelerometers can be described by the following 3×6 matrix, the k^{th} column of which is the coordinate matrix of the k^{th} accelerometer in the frame, $\mathcal{B}$, as described in Section 5.5.2:

$$\begin{bmatrix} -0.00025 & 0.00005 & -0.05050 & 0.04980 & 0.00010 & 0.00005 \\ 0.00000 & -0.05010 & 0.00000 & 0.00010 & 0.05000 & 0.00000 \\ -0.05015 & 0.00000 & 0.00000 & 0.00005 & 0.00000 & 0.04985 \end{bmatrix}, \quad \text{(E.1)}$$

where the dimensions are meters. For comparison, without location errors the matrix is

$$\begin{bmatrix} 0 & 0 & -0.05 & 0.05 & 0 & 0 \\ 0 & -0.05 & 0 & 0 & 0.05 & 0 \\ -0.05 & 0 & 0 & 00 & 0 & 0.05 \end{bmatrix}. \quad \text{(E.2)}$$

The directions of the six accelerometers in the perturbed configuration can be described by the 3×6 matrix:

$$\begin{bmatrix} 0.70751 & 0.70772 & 0.00000 & 0.00000 & -0.70670 & -0.70649 \\ 0.70670 & 0.00122 & 0.70675 & -0.70767 & -0.00082 & 0.70772 \\ 0.00082 & 0.70649 & 0.70746 & 0.70654 & 0.70751 & -0.00122 \end{bmatrix}, \quad \text{(E.3)}$$

where the k^{th} column is the component matrix of $\mathbf{u}_k$ in the aforementioned basis. For comparison, without orientation errors, the matrix is

$$\begin{bmatrix} 0.70711 & 0.70711 & 0.00000 & 0.00000 & -0.70711 & -0.70711 \\ 0.70711 & 0.00000 & 0.70711 & -0.70711 & 0.00000 & 0.70711 \\ 0.00000 & 0.70711 & 0.70711 & 0.70711 & 0.70711 & 0.00000 \end{bmatrix}. \quad \text{(E.4)}$$

In Section 6.4.2, when it is assumed that some calibration routine has allowed imperfect estimates of the accelerometer locations and directions to be obtained, the position and direction matrices used are

$$\begin{bmatrix} -0.000255 & 0.000060 & -0.050575 & 0.049750 & 0.000075 & 0.000080 \\ 0.000000 & -0.050110 & 0.000000 & 0.000105 & 0.050050 & 0.000005 \\ -0.050175 & 0.000000 & 0.000000 & 0.000051 & 0.000000 & 0.049900 \end{bmatrix} \tag{E.5}$$

and

$$\begin{bmatrix} 0.70752 & 0.70776 & 0.00000 & 0.00000 & -0.70666 & -0.70649 \\ 0.70669 & 0.00131 & 0.70675 & -0.70768 & -0.00090 & 0.70772 \\ 0.00083 & 0.70645 & 0.70747 & 0.70653 & 0.70756 & -0.00123 \end{bmatrix} \tag{E.6}$$

respectively. These same values were used for the simulations in Chapter 7.

References

[1] P.L. Walter. The history of the accelerometer. *Sound and Vibration*, pages 84–92, January 2007.

[2] W. Wrigley. History of inertial navigation. *Navigation*, 24(1):1–6, 1977.

[3] C.S. Draper, W. Wrigley, and J. Hovorka. *Inertial Guidance.* Pergamon Press, 1960.

[4] D.H. Titterton and J.L. Weston. *Strapdown Inertial Navigation Technology.* Peter Peregrinus Ltd, 1997.

[5] A.R. Schuler, A. Grammatikos, and K.A. Fegley. Measuring rotational motion with linear accelerometers. *IEEE Transactions on Aerospace and Electronic Systems*, 3(3):465–472, May 1967.

[6] W.T. Ang, P.K. Khosla, and C.N. Riviere. Design of all-accelerometer inertial measurement unit for tremor sensing in hand-held microsurgical unit. In *Proceedings of the 2003 IEEE International Conference on Robotics and Automation*, pages 1781–1786, September 2003.

[7] J-H. Chen, S-C. Lee, and D.B. DeBra. Gyroscope free strapdown inertial measurement unit by six linear accelerometers. *Journal of Guidance, Control, and Dynamics*, 17(2):286–290, 1994.

[8] T-L. Chen and S. Park. MEMS SoC: observer-based coplanar gyro-free inertial measurement unit. *Journal of Micromechanics and Microengineering*, 15:1664–1673, 2005.

[9] F. Di Puccio and P. Forte. Identification of the 3D vibratory motion of a rigid body by accelerometer measurements. *Shock and Vibration*, 11:281–293, 2004.

[10] S. Park, C-W. Tan, and J. Park. A scheme for improving the performance of a gyroscope-free inertial measurement unit. *Sensors and Actuators, A*, 121:410–420, 2005.

[11] A.J. Padgaonkar, K.W. Krieger, and A.I. King. Measurement of angular acceleration of a rigid body using linear accelerometers. *Journal of Applied Mechanics*, pages 552–556, 1975.

[12] J. Angeles. *Fundamentals of robotic mechanical systems: theory, methods and algorithms.* Springer, 2003.

[13] W.C. Hayes, J.D. Gran, M.L. Nagurka, J.M. Feldman, and C. Oatis. Leg motion analysis during gait by multiaxial accelerometry: Theoretical foundations and preliminary validations. *IEEE Transactions on Aerospace and Electronic Systems*, 105:283–289, August 1983.

[14] T.R. Kane, W.C. Hayes, and J.D. Priest. Experimental determination of forces exerted in tennis play. *Biomechanics IV*, pages 898–904, 1974.

[15] K. Parsa, J. Angeles, and A.K. Misra. Pose-and-twist estimation of a rigid body using accelerometers. *Proceedings of the 2001 International Conference on Robotics and Automation*, pages 2873–2878, 2001.

[16] K. Parsa, J. Angeles, and A.K. Misra. Rigid-body pose and twist estimation using an accelerometer array. *Archive of Applied Mechanics*, 74:223–236, 2004.

[17] M. Costello and T. Jitpraphai. Determining angular velocity and angular acceleration of projectiles using triaxial acceleration measurements. *Journal of Spacecraft and Rockets*, 39(1):73–80, 2002.

[18] K.R. Fyfe, J.K. Rooney, and K.W. Fyfe. Motion analysis system. US Patent #6513381, 2003.

[19] J.R.W. Morris. Accelerometry-a technique for the measurement of human body movements. *Journal of Biomechanics*, 6:729–736, 1973.

[20] R.T. Shea and D.C. Viano. Computing body segment trajectories in the Hybrid III dummy using linear accelerometer data. *Journal of Biomechanical Engineering*, 116:37–43, 1994.

[21] G.S. Nusholtz. Geometric methods in determining rigid-body dynamics. *Experimental Mechanics*, pages 153–158, June 1993.

[22] B. Zappa, G. Legnani, A.J. van den Bogert, and R. Adamini. On the number and placement of accelerometers for angular velocity and acceleration determination. *Journal of Dynamic Systems, Measurement and Control*, 123:552–554, September 2001.

[23] J. Genin, J. Hong, and W. Xu. Accelerometer placement for angular velocity determination. *Journal of Dynamical Systems, Measurement, and Contol*, 119(474-477), 1997.

[24] N.K. Mital and A.I. King. Computation of rigid-body rotation in three-dimensional space from body-fixed linear acceleration measurements. *Journal of Applied Mechanics*, 46:925–930, December 1979.

[25] G.S. Nusholtz and R. Molinaro. Force deflection curves for air bag response. *Experimental Techniques*, pages 33–35, 1991.

[26] Y.K. Liu. Discussion: Measurement of angular acceleration of a rigid body using linear accelerometers. *Journal of Applied Mechanics*, pages 377–378, June 1976.

[27] D. Giansanti, V. Macellari, G. Maccioni, and A. Cappozzo. Is it feasible to reconstruct body segment 3-D position and orientation using accelerometric data? *IEEE Transactions on Biomedical Engineering*, 50(4):476–483, April 2003.

[28] D. Giansanti and G. Maccioni. Comparison of three different kinematic sensor assemblies for locomotion studies. *Physiological Measurement*, 26:689–705, 2005.

[29] C-W. Tan, S. Park, K. Mostov, and P. Varaiya. Design of gyrosope-free navigation systems. *2001 IEEE Intelligent Systems Conference Proceedings*, pages 286–291, 2001.

[30] C-Y. Hung, C-M. Fang, and S-C. Lee. A compensator to advance gyro-free INS precision. *International Journal of Control, Automation, and Systems*, 4(3):351–358, June 2006.

[31] K. Parsa, T.A. Lasky, and B. Ravani. Design and implementation of a mechatronic, all-accelerometer inertial measurement unit. *IEEE/ASME Transactions on Mechatronics*, 12(6):640–650, December 2007.

[32] J-P. Merlet. *Parallel Robots.* Kluwer Academic Publishers, 2000.

[33] T.R. Kane and D.A. Levinson. *Dynamics, Theory and Applications.* McGraw-Hill, 1985.

[34] A. Gelb, editor. *Applied Optimal Estimation.* MIT Press, 1974.

[35] M.D. Shuster. A survey of attitude representations. *Journal of the Astronautical Sciences*, 41(4):439–517, 1993.

[36] Y. Wu, X. Hu, D. Hu, T. Li, and J. Lian. Strapdown inertial navigation system algorithms based on dual quaternions. *IEEE Transactions on Aerospace and Electronic Systems*, 41(1):110–132, January 2005.

[37] A.T. Yang. *Basic Questions of Design Theory*, chapter Calculus of Screws, pages 265–281. North-Holland/American Elsevier, 1974.

[38] I.Y. Bar-Itzhack. Navigation compuation in terrestrial strapdown inertial navigation systems. *IEEE Transactions on Aerospace and Electronic Systems*, 13(6):679–689, November 1977.

[39] P.G. Savage. A unified mathematical framework for strapdown algorithm design. *Journal of Guidance, Control, and Dynamics*, 29(2):237–249, March-April 2006.

[40] C.C. Chou and S.C. Sinha. On the kinematics of the head using linear acceleration measurements. *Journal of Biomechanics*, 9:607–613, 1976.

[41] C-W. Tan and S. Park. Design of accelerometer-based inertial navigation systems. *IEEE Transactions on Instrumentation and Measurement*, 54(6):2520–2530, December 2005.

[42] M. Ding, Q. Wang, G. Shen, and P. Zhao. A novel non-gyro inertial measurement unit. *Key Engineering Materials*, 295-296:583–588, 2005.

[43] K. Parsa, J. Angeles, and A.K. Misra. Attitude calibration of an accelerometer array. *Proceedings of the 2002 IEEE International Conference on Robotics & Automation*, pages 129–134, May 2002.

[44] B.M. Bell and F.W. Cathey. The iterated Kalman filter update as a gauss-newton method. *IEEE Transactions on Automatic Control*, 38(2):294–297, February 1993.

[45] J. Wang, Q. Wang, and S. Sun. Optimum techonology for non-gyro micro inertial measuring unit. *Journal of Harbin Institute of Technology*, 34(5):632–635, September-October 2002.

[46] W. Qi D. Mingli, Weiwei. Design of a nine-accelerometer non-gyro inertial measurement unit. In Yun-Jiang Rao, editor, *Advanced Sensor Systems and Applications II*. SPIE, 2005.

[47] T.R. Williams and K.R. Fyfe. Planar accelerometer configurations. *Journal of Applied Mechanics*, 71:10–14, 2004.

[48] H. Anton. *Elementary Linear Algebra*. John Wiley & Sons, 7th edition, 1994.

[49] M. Audin. *Geometry.* Springer, 2003.

[50] J.G. Semple and G.T. Kneebone. *Algebraic Projective Geometry.* Oxford, 1963.

[51] S. Barnett. *Matrices, Methods and Applications.* Clarendon Press, Oxford, 1990.

[52] G.H. Golub and C.F. Van Loan. *Matrix Computations.* John Hopkins, 1989.

[53] J.W. Eaton. *GNU Octave Manual.* Newtork Theory Limited, 2002.

[54] O. Bottema and B. Roth. *Theoretical Kinematics.* Dover, 1990.

[55] J.M. Selig. *Geometrical Methods in Robotics.* Springer, 1996.

[56] K.H. Hunt. *Kinematic Geometry of Mechanisms.* Oxford University Press, 1978.

[57] C.G. Gibson and K.H. Hunt. Geometry of screw systems-I. *Mechanism and Machine Theory,* 25(1):1–10, 1990.

[58] C.G. Gibson and K.H. Hunt. Geometry of screw systems-II. *Mechanism and Machine Theory,* 25(1):11–27, 1990.

[59] O. Veblen and J.W. Young. *Projective Geometry,* volume 1. Ginn and Company, 1938.

[60] M. Ding, Q. Zhou, Q. Wang, and C. Wang. Feasibility analysis of accelerometer configuration of non-gyro micro inertial measurement unit. In *Power Electronics and Motion Control Conference, IPEMC '06,* volume 3. CES/IEEE, 2006.

[61] J.M. McCarthy. *Geometric Design of Linkages.* Springer-Verlag, 2000.

[62] H. Pottmann and J. Wallner. *Compuational Line Geometry.* Springer, 2001.

[63] J. Phillips. *Freedom in Machinery, Volume 2, Screw theory exemplified.* Cambridge University Press, 1990.

[64] A. Dandurand. The rigidity of compound spatial grids. *Structural Topology,* 10:41–55, 1984.

[65] K. Britting. *Inertial Navigation Systems Analysis.* John Wily & Sons, 1972.

[66] Analog Devices. *Low Cost +/-10g Dual-Axis Accelerometer with Duty Cycle, AXDL210E*, 2002.

[67] J.R. Hubbard. *Schaum's Outline of Fundamentals of Computing with C++*. McGraw-Hill, 1998.

[68] J. Wittenburg. *Dynamics of Systems of Rigid Bodies*. B.G. Teubner Stuttgart, 1977.

[69] R.L. Burden and J.D. Faires. *Numerical Analysis*. PWS, 5^{th} edition, 1993.

[70] C-Y. Hung and S-C. Lee. A calibration method for six-accelerometer INS. *International Journal of Control, Automation, and Systems*, 4(5):615–623, October 2006.

[71] IEEE. *IEEE Standard Specification Format Guide and Test Procedure for Linear, Single-Axis, Nongyroscopic Accelerometers*, 1999.

[72] B. Dasgupta and T.S. Mruthyunjaya. The Stewart platform manipulator: a review. *Mechanism and Machine Theory*, 35:15–40, 2000.

[73] M.L. Husty. An algorithm for solving the direct kinematics of general Stewart-Gough platforms. *Mechanism and Machine Theory*, 31(4):365–380, 1996.

[74] K. Sugimoto. Kinematic and dynamic analysis of parallel manipulators by means of motor algebra. *Journal of Mechanisms, Transmission, and Automation in Design*, 109:3–7, March 1987.

[75] J.-P. Merlet. Direct kinematics of parallel manipulators. *IEEE Transactions on Robotics and Automation*, 9(6):842–846, December 1993.

[76] X. Zhao and S. Peng. A successive approximation algorithm for the direct position analysis of parallel manipulators. *Mechanism and Machine Theory*, 35:1095–1101, 2000.

[77] Y. Wang. A direct numerical solution to forward kinematics of general Stewart-Gough platforms. *Robotica*, 25(1):121–128, January 2006.

[78] C. Innocenti and V. Parenti-Castelli. A novel numerical approach to the closure of the 6-6 Stewart platform mechanism. In *ICAR, Fifth International Conference on Advanced Rotobics*, pages 851–855, June 1991. Pise, Italy.

[79] S. Egner. Semi-numerical solution to the 6/6-Stewart-platform kinematics based on symmetry. *Applicable Algebra in Engineering, Communication and Computing*, 7(6):449–468, 1996.

[80] L-C. T. Wang and C.C. Chen. On the numerical kinematic analysis of general parallel robotic manipulators. *IEEE Transactions on Robotics and Automation*, 9(3):272–285, June 1993.

[81] L-C. T. Wang and K-T. Oen. Numerical direct kinematic analysis of fully parallel linearly actuated platform type manipulators. *Journal of Robotic Systems*, 19(8):391–400, 2002.

[82] G.H. Jung and K.I. Lee. Real-time estimation of the Stewart platform forward kinematics solution. In *SICE*, pages 1239–1244, August 4-6 1993.

[83] J-Y. Kang, D.H. Kim, and K-I. Lee. Robust estimator design for forward kinematics solution of a Stewart platform. *Journal of Robotic Systems*, 15(1):29–42, 1998.

[84] E.D. Fasse and A.J. Wavering. Configuration estimation of Gough-Stewart platforms using Extended Kalman Filtering. In *Proceedings of the DETC'00*. ASME, September 2000.

[85] Y-J. Chiu and M-H Perng. Forward kinematics of a general fully parallel manipulator with auxiliary sensors. *The International Journal of Robotics Research*, 20(5):401–414, May 2001.

[86] K.C. Cheok, J.L. Overholt, and R.R. Beck. Exact methods for determining the kinematics of a Stewart platform using additional displacement sensors. *Journal of Robotic Systems*, 10(5):689–707, 1993.

[87] V. Parenti-Castelli and R. Di Gregorio. A new algorithm based on two extra-sensors for real-time computation of the actual configuration of the generalized Stewart-Gough manipulator. *Journal of Mechanical Design*, 122:294–298, September 2000.

[88] L. Baron and J. Angeles. The direct kinematics of parallel manipulators under joint-sensor redundancy. *IEEE Transactions on Robotics and Automation*, 16(1):12–19, February 2000.

[89] L. Baron and J. Angeles. The kinematic decoupling of parallel manipulators using joint-sensor data. *IEEE Transactions on Robotics and Automation*, 16(6):644–651, December 2000.

[90] J. Gao, P. Webb, and N. Gindy. Error reduction for an inertial-sensor-based dynamic parallel kinematic machine positioning system. *Measurement Science and Techonology*, 14:543–550, 2003.

[91] J. Gao, P. Webb, and N. Gindy. Investigation of an inertial-sensor-based dynamic position measurement system for a parallel kinematic machine.

Transactions of the Institute of Measurement and Control, 26(4):293–310, 2004.

[92] J. Gao, P. Webb, and N. Gindy. Research on an inertial positioning system for a parallel kinematic machine. *Mechatronics*, 15:1–22, 2005.

[93] K. Wohlhart. Mises derivatives of motors and motor tensors. *Romansy 14, Theory and Practice of Robots and Manipulators, Proceedings of the Fourteenth CISM-IFToMM Symposium*, pages 87–98, 2001.

[94] B. Dasgupta and T.S. Mruthyunjaya. A constructive predictor-corrector algorithm for the direct position kinematics problem for a general 6-6 Stewart platform. *Mechanisms and Machine Theory*, 31(6):799–811, 1996.

[95] D. Jakobović and L. Budin. Forward kinematics of Stewart platform mechanism. In *Proceedings of the* 6^{th} *International Conference on Intelligent Engineering Systems INES 2002,*, pages 149–154, Opatija, May 2002.

[96] P.C. Hughes. *Spacecaft Attitude Dynamics.* Wiley, 1986.

[97] W-H. Steeb. *Matrix Calculus and the Kronecker Product with Applications and C++ Programs.* World Scientific, 1997.

[98] A. Graham. *Kronecker Products and Matrix Calculus with Applications.* Ellis Horwood, 1981.